



**INSTITUT FÜR KERNCHEMIE
UNIVERSITÄT MAINZ**

**JAHRESBERICHT
2004**

Herausgeber: Jens Volker Kratz
Mainz, im März 2005

IKMz 2005 - 1
ISSN 0932-7622

INSTITUT FÜR KERNCHEMIE
UNIVERSITÄT MAINZ

**JAHRESBERICHT
2004**



März 2005

Kernchemie im Internet

Das Institut für Kernchemie der Universität Mainz ist mit einer Homepage im World Wide Web vertreten. Unter der Adresse:

<http://www.kernchemie.uni-mainz.de>

finden Sie aktuelle Informationen zum Institut, seinen Mitarbeitern, den Lehrveranstaltungen und den Forschungsaktivitäten.

Die in diesem Bericht vorgelegten Ergebnisse stammen zum Teil aus noch nicht abgeschlossenen Arbeiten und sind daher als vorläufige Mitteilung zu bewerten.

Vorwort

Der vorliegende Jahresbericht 2004, den die Mitarbeiter des Instituts vorlegen, gibt einen Überblick über die wissenschaftlichen Aktivitäten der Arbeitsgruppen des Instituts für Kernchemie. Er soll gleichzeitig all denen, die uns in ideeller und finanzieller Weise gefördert haben, Rechenschaft ablegen über die Verwendung nicht unerheblicher öffentlicher Mittel.

Der Bericht umfasst wieder drei Forschungs-Schwerpunkte:

- Kernchemie im Sinne grundlegender Fragestellungen,
- Radiopharmazeutische Chemie und Anwendung radiochemischer Methoden mit medizinischer Zielsetzung, und
- Hochempfindliche und –selektive Analytik für umweltrelevante, technische und biologische Probleme.

Außerdem beschreibt der Bericht den Status der Technischen Einrichtungen des Instituts und technische Neu-entwicklungen. Schließlich gibt er Rechenschaft über die Leistungen des Instituts in Form von Publikationen, Konferenzbeiträgen, Dissertationen, Diplomarbeiten und Staatsexamensarbeiten, sowie über die Beiträge seiner Hochschullehrer in der Lehre und Weiterbildung.

Die Arbeiten wurden wiederum vielfältig finanziell gefördert. Schwerpunkte der Förderung kamen vom Land Rheinland-Pfalz über die Johannes Gutenberg-Universität, durch die Zentren für Umweltforschung und physikalisch-chemische Verbundforschung, vom Bundesministerium für Bildung und Forschung, vom Bundesministerium für Wirtschaft und Arbeit, von der Deutschen Forschungsgemeinschaft, von der Gesellschaft für Schwerionenforschung in Darmstadt, von der Stiftung Rheinland-Pfalz für Innovation und durch die Helmholtz-Gemeinschaft über das Virtuelle Institut „Struktur der Kerne und nukleare Astrophysik“ VISTARS. Weitere Förderungen erfolgten im Rahmen der JINA-VISTARS-Kooperation durch die University of Notre Dame und die Michigan State University. Förderungen durch die Europäische Gemeinschaft erfolgten im Rahmen der Vorhaben EMIL und ACTINET. Die Hochschullehrer erfreuten sich auch weiterhin der Unterstützung durch den Fonds der Chemischen Industrie. Den Fördernden sei an dieser Stelle herzlich gedankt.

Für Mitglieder des Instituts gab es auch im Jahr 2004 ehrenvolle Auszeichnungen. J.V. Kratz wurde von der International Union of Pure and Applied Chemistry zum IUPAC Fellow ernannt. K.-L. Kratz erhielt den GSI Exotic Nuclei Community Membership (GENCO) Award für „Basic Experiments in Nuclear Structure and Nuclear Astrophysics“.

Dieser Bericht wird vollständig im Internet unter der „Homepage“ des Instituts (<http://www.kernchemie.uni-mainz.de>) bereitgestellt. Gedruckte Versionen gehen unaufgefordert nur an Bibliotheken und fördernde Institutionen. Interessenten können, falls der Wunsch besteht, eine gedruckte Version anfordern.

Mainz, den 23.03.2005

Prof. Dr. Jens Volker Kratz

Zusammenfassung

A. Grundlagenforschung

- Driftzeit-Messungen in einer Puffer-Gas-Zelle
- Chemie der schwersten Elemente
- Struktur extrem neutronenreicher Kerne
- R-Prozess Chronometer
- Thermochromatographie
- N-Einfang
- Siderophile Elemente in Xenolithen
- Radiochemische Trennungen
- Detektoren zum μ -Imaging
- Ultrakalte Neutronen am TRIGA Mainz

B. Radiopharmazeutische Chemie

- Targetentwicklung und Isotopenproduktion
- Synthese von ^{68}Ga - und ^{18}F -Markierungssynthons
- Synthese von $^{18,19}\text{F}$ - und ^{11}C -markierten Verbindungen
- Synthese von $^{72,74,77}\text{As}$ -, ^{123}I - und ^{131}In -Verbindungen
- Evaluierung von Radiodiagnostika und –therapeutika
- Nuklearmedizinische Studien

C. Analytik für Umwelt und Technik

- Batch- und EXAFS-Experimente zur Sorption von U(VI) und Np(V) an Kaolinit
- Nachweis aquatischer Kolloide mit LIBD
- Neue CE-Systeme für Speziationsuntersuchungen
- Ultraspurenanalyse mit RIMS
- Komplexierung von Pu(IV) mit Huminsäure
- Weiterentwicklung LASER-analytischer Verfahren

D. Technische Einrichtungen

- Betrieb des Forschungsreaktors TRIGA Mainz
- Personendosisüberwachung

E. Veröffentlichungen, Vorträge, Lehrveranstaltungen

- Diplomarbeiten und Dissertationen
- Veröffentlichungen und Vorträge
- Vorträge in den Seminaren des Instituts
- Beiträge der Dozenten des Instituts zu den Lehrveranstaltungen des Fachbereichs sowie zur Weiterbildung

Summary

A. Fundamental Problems

- Drift-time measurements in a buffer-gas cell
- Chemistry of the heaviest elements
- Structure of extremely neutron-rich nuclei
- R-process chronometers
- Thermochromatography
- N-Capture
- Siderophile elements in Xenolithes
- Radiochemical Separation
- Detectors for μ -imaging
- Ultra cold neutrons at the TRIGA Mainz

B. Radiopharmaceutical Chemistry

- Target developments and isotope production
- Synthesis of ^{68}Ga - and ^{18}F -labelling synthons
- Synthesis of $^{18,19}\text{F}$ -and ^{11}C -labelled compounds
- Synthesis of $^{72,74,77}\text{As}$ -, ^{123}I - and ^{131}I -labelled compounds
- Evaluation of radiodiagnostics and –therapeutics
- Nuclear medical studies

C. Analytics for Environment and Technology

- Batch and EXAFS studies of U(VI) and Np(V) sorption on kaolinite
- Detection of aquatic colloids with LIBD
- New CE systems for element speciation
- Ultra-trace analysis with RIMS
- Complexation of Pu(IV) with humic substances
- Further development of LASER-analytical techniques

D. Technical Facilities

- Operation of the research reactor TRIGA Mainz
- Personal dose monitoring

E. Publications and Teaching Activities

- Diploma theses and dissertations
- Publications in journals and contributions to conferences
- Guest contributions to the seminars of the institute
- Contributions of the staff to lectures and lab-courses of the Department of Chemistry and Pharmacy and to professional training in health physics

III

Wissenschaftliche Mitarbeiter

Amayri	S.	Keller	H.	Reich	T.
Denschlag (pensioniert)	J.O.	Kiselev	O.	Rösch	F.
Eberhardt	K.	Kratz	J. V.	Schirrmacher	E.
Erdmann	N.	Kuczewski	K.-L.	Schirrmacher	R.
Hampel	G.	Mühlhausen	B.	Schmidt	G.
Herrmann (emeritiert)	G.	Pfeiffer	U.	Trautmann	N.
		Piel	B.	Wiehl	N.
			M.		

Diplmanden, Doktoranden und Staatsexamenskandidaten

Arndt	O.	Hennrich	S.	Riß	P.
Banik	N.	Humrich	H.	Schertz	F.
Bauman	A.	Jennewein	M.	Stark	D.
Beck	C.	Jermolajev	A.	Sulignano	B.
Buda	R.	Jost	C.	Wängler	B.
Bürger	S.	Kessler	R.	Wolf	B.
Comagic	S.	Korobeinikov	K.	Zhernosekov	A.
Farouqi	K.	Kuczewski	B.		
Getahun	G.	Mühlhausen	U.		
Griesel	T.	Reich	Ta.		
Heinzmann	U.	Rieth	U.		

Angestellte

Breuel	J.	Keim	H. J.	Onasch	I.
Donart	S.	Keller	O.	Peil	A.
Drebert	J.	Kling	H. O.	Praast	B.
Handwerker	C.	Krille	U.	Sach	P.
Heimann	R.	Lehr	G.	Schmidt	A.
Heiser	A.	Liebe	D.	Schmidt	H.-M.
Höhnemann	S.	Marx	B.	Tharun	U.
Hubrath	J.	Maus	S.	Thörle	P.
Janzen	V.	Mendel	M.	Zauner	S.
Jera	R.	Nähler	A.		

Gäste 2004

Auer, D.	Framatome ANP, Erlangen
Ayala-Guardia, F.	Institut für Physik Mainz
Bäßler, St.	Institut für Physik Mainz
Bethig, A.	Framatome ANP, Erlangen
Burgkhardt, B.	Forschungszentrum Karlsruhe
Cetin, F.	Istanbul Technical University, Türkei
Christlieb, N.	Hamburger Sternwarte
Cowan, J.J.	University of Oklahoma (USA)
Ding, Yu Shin	Brookhaven National Laboratory (USA)
Filossofov, D. V.	Joint Institute of Nuclear Research Dubna (Russland)
Frey, A.	Technische Universität München
Gaudefroy, L.	IPN Orsay (Frankreich)
Gutsmiedl, E.	Technische Universität München
Hartmann, J.	Technische Universität München
Heil, W.	Institut für Physik Mainz
Horn, B.	IMM Mainz
Hosmer, P.	MSU (USA)
Hung, T.K.	Atomenergiebehörde (Vietnam)
Korolov, N. A.	Joint Institute of Nuclear Research Dubna (Russland)
Lebedev, N.A.	Joint Institute of Nuclear Research Dubna (Russland)
Lecher, B.	MFD Diagnostics, Mainz
Lhersonneau, G.	INFN, Legnaro (Italien)
Lizon, A.	Medizinische Hochschule Hannover
Mansel, A.	Institut für Interdisziplinäre Isotopenforschung, Leipzig
Marosits, E.	MPI für Chemie Mainz
Möller, P.	LANL (USA)
Montes, F.	MSU (USA)
Müller, A.	IMM Mainz
Munoz, R.	Institut für Physik Mainz
Naidu, G.R.	Sri Venkateswara University Tirupati (Indien)
Nielsson, M.	Chalmers University of Technology Göteborg (Schweden)
Novgorodov, A.F.	Joint Institute of Nuclear Research Dubna (Russland)
Novikov, Y.	University of St. Petersburg (Russland)
Odegaard-Jensen, A.	Chalmers University of Technology Göteborg (Schweden)
Ostrowski, A.N.	Universität Heidelberg
Paul, S.	Technische Universität München
Pfleger, S.	Framatome ANP, Erlangen
Pokotilovsky, Yu.	Joint Institute of Nuclear Research Dubna (Russland)
Rödel, M.	Framatome ANP, Erlangen
Scheidenberger, C.	GSI Darmstadt
Schmied, W.	Technische Universität München
Shergur, J.	University of Maryland (USA)
Shtanko, V.I.	Technologisches Institut, St. Petersburg (Russland)
Skarnemark, G.	Chalmers University of Technology Göteborg (Schweden)
Sobolev, I.	Institut für Physik Mainz
Soldati, A.	Institut für Physikalische Chemie Mainz
Sorlin, O.	IPN Orsay (Frankreich)
Thews, O.	Institut für Pathophysiologie, Mainz
Tillmanns, J.	Institut für Pathophysiologie, Mainz
Truran, J.W.	University of Chicago (USA)
Vincente, V.	Institut für Physikalische Chemie Mainz
Walther, C.	Forschungszentrum Karlsruhe
Wies, K.	Institut für Physik Mainz
Wöhr, A.	University of Notre Dame (USA)

Inhaltsverzeichnis***A. Grundlagenforschung**

- A1 Optical Spectroscopy of Trans-Fermium Elements at SHIPTRAP¹
H. Backe, A. Dretke, R. Horn, T. Kolb, P. Kunz, W. Lauth, P. Thörle, N. Trautmann
- A2 Separation of ²¹¹Pb with ALOHA and subsequent electrochemical deposition^{3,7}
H. Hummrich, F. Freist, D. Liebe, J.V. Kratz
- A3 Separation of fission products with ALOHA and subsequent electrochemical deposition³
H. Hummrich, J.V. Kratz, D. Liebe
- A4 The electrochemical deposition of Hg on various metal electrodes³
H. Hummrich, F. Feist, J.V. Kratz
- A5 Extraction of Gd, Hf, and Tc with the fast continuous liquid-liquid-extraction System MicroSISAK^{3,5}
K. Eberhardt, S. Andersson, C. Ekberg, B. Horn, J.V. Kratz, P. Löb, M. Nilsson, G. Skarnemark, N. Trautmann
- A6 Theoretical Investigation of the Reactivity of MO₄ and the Electronic Structure of Na₂[MO₄(OH)₂], where M = Ru, Os, and Hs (element 108)³
V. Pershina and J.V. Kratz
- A7 Search for the “missing” α-decay branch in ²³⁹Cm³
Z. Qin, D. Ackermann, W. Brückle, F.P. Hessberger, E. Jäger, P. Kuusiniemi, G. Münzenberg, D. Nayak, E. Schimpf, M. Schädel, B. Schausten, A. Semchenkov, B. Sulignano, K. Eberhardt, J.V. Kratz, D. Liebe, P. Thörle, Yu.N. Novikov
- A8 Further investigations on target preparation for heavy element studies⁴
D. Liebe, P. Thörle, J.V. Kratz
- A9 Pygmy and Giant Dipole-Resonances in ¹³⁰⁻¹³²Sn³
P. Adrich, T. Aumann, K. Boretzky, D. Cortina-Gif, U. Datta Pramanik, Th.W. Elze, H. Emling, M. Fallot, H. Geissel, M. Hellström, K.L. Jones, A. Klimkiewicz, J.V. Kratz, R. Kulessa, Y. Leifels, C. Nociforo, R. Palit, H. Simon, G. Surowka, K. Süümmerer, and W. Walus
- A10 Breakup of relativistic halo nuclei (i)³
P. Adrich, T. Aumann, O. Bochkarev, M.J.G. Borge, L.V. Chulkov, D. Cortina, Th.W. Elze, J. Fernandez-Vazquez, U. Datta-Pramanik, H. Emling, H. Fynbo, H. Geissel, L.V. Grigorenko, M. Hellström, H. Johansson, A. Klimkiewicz, K. Jones, B. Jonson, J.V. Kratz, R. Kulessa, Le Hong Khiem, E. Lubkiewicz, K. Markenroth, M. Meister, G. Münzenberg, F. Nickel, T. Nilsson, G. Nyman, M. Pantea, R. Palit, V. Pribora, W. Prokopowic, A. Richter, K. Riisager, C. Scheidenberger, G. Schrieder, H. Simon, K. Süümmerer, O. Tengblad, I.J. Thomson, W. Walus, and M.V. Zhukov

* Auf eine Förderung durch Drittmittel wird durch Indizes an den Titeln der einzelnen Arbeiten hingewiesen, deren Bedeutung am Ende des Inhaltsverzeichnisses erläutert ist.

VI

- A11 Breakup of relativistic halo nuclei (ii)³
 P. Adrich, T. Aumann, O. Bochkarev, M.J.G. Borge, L.V. Chulkov, D. Cortina, Th.W. Elze, J. Fernandez-Vazquez, U. Datta-Pramanik, H. Emling, H. Fynbo, H. Geissel, L.V. Grigorenko, M. Hellström, H. Johansson, A. Klimkiewicz, K. Jones, B. Jonson, J.V. Kratz, R. Kulessa, Le Hong Khiem, E. Lubkiewicz, K. Markenroth, M. Meister, G. Münzenberg, F. Nickel, T. Nilsson, G. Nyman, M. Pantea, R. Palit, V. Pribora, W. Prokopowic, A. Richter, K. Riisager, C. Scheidenberger, G. Schrieder, H. Simon, K. Sümmerer, O. Tengblad, I.J. Thomson, W. Walus, and M.V. Zhukov
- A12 The r-process in the high-entropy bubble scenario^{2,4,31}
 K. Farouqi, K.-L. Kratz, B. Pfeiffer, C. Freiburghaus, F.-K. Thielemann and T. Rauscher
- A13 Neutron captures and the r-process^{4,31}
 K. Farouqi, K.-L. Kratz, B. Pfeiffer, F.-K. Thielemann and T. Rauscher
- A14 Influence of thermally excited isomers on r-process abundances^{2,19}
 B. Pfeiffer and K.-L. Kratz
- A15 How doubly-magic is the nucleus $^{78}_{28}\text{Ni}_{50}$?^{2,31,4}
 B. Pfeiffer, K.-L. Kratz, and the ESR-FSR Collaboration
- A16 N = 82 shell gap above $^{132}_{50}\text{Sn}_{82}$ ^{2,31,4}
 B. Pfeiffer, K.-L. Kratz, and the FRS/ESR Collaboration
- A17 Prediction for the Pb abundance in ultra-metal-poor Halo stars¹⁹
 B. Pfeiffer and K.-L. Kratz
- A18 Gas thermochromatography for ion source development¹⁹
 C. Jost, O. Arndt, K.-L. Kratz, U. Köster, A. Kronenberg
- A19 The $^{44,46}\text{Ar}(n, \gamma)^{45,47}\text{Ar}$ reaction rates studied by (d,p) transfer reactions^{19,31}
 L. Gaudefroy, O. Sorlin, Y. Blumenfeld, K.-L. Kratz, A.N. Ostrowski and the MuST-Collaboration
- A20 High-temperature fractionations in the solar nebula^{31,32}
 G. Schmidt and K.-L. Kratz
- A21 Kosmochemische Fingerabdrücke im Erdmantel: Ein Beitrag zur Herkunft der chemischen Elemente Os, Ir, Ru, Pt, Rh und Pd (Platinmetalle)^{31,32}
 G. Schmidt und K.-L. Kratz
- A22 Pre-concentration and purification of generator-produced ^{68}Ga ¹⁶
 K.P. Zhernosekov, D.V. Filosofov, M. Jahn, M. Jennewein and F. Rösch
- A23 Resolution Studies of a New Small Animal PET System based on Scintillating Fibers^{14,24}
 M. Jennewein, N. Slavine, S. Seliouine, F. Rösch, E. Tsyanov, R.P. Mason
- A24 Calculation of ultracold neutron production at the TRIGA Mainz Reactor²⁸
 Yu.N. Pokotilovski, K. Eberhardt, W. Heil, V. Janzen, J.V. Kratz, U. Tharun, N. Trautmann, Y. Sobolev, N. Wiehl

- A25 A solid Deuterium UCN Source at the research reactor TRIGA Mainz²⁸
 S. Paul, W. Heil, J.V. Kratz, I. Altarev, K. Eberhardt, A. Frei, E. Gutsmiedl, G. Hampel,
 J. Hartmann, N. Trautmann, W. Schmid, Y. Sobolev, D. Tortorella, N. Wiehl

B. Radiopharmazeutische Chemie

- B1 Labelling of DOTA-DPhe¹-Tyr³-octreotide with generator-produced ⁶⁸Ga¹⁶
 K.P. Zhernosekov, D.V. Filosofov, M. Jahn, M. Jennewein, F. Rösch
- B2 Systematische Überprüfung verschiedener Reaktionsparameter bei der Markierung einer
 einfachen Modellverbindung mit [¹⁸F]FETos/Lil
 A. Bauman, M. Piel, S. Höhnemann, M. Kölzer, F. Rösch
- B3 Synthese und Markierung zweier NMDA-Liganden zur Visualisierung des
 Rezeptorstatus^{17,18}
 A. Bauman, M. Piel, S. Höhnemann, M. Jansen, G. Dannhardt, F. Rösch
- B4 Synthese und ¹³¹I-Radioiodierung von Benzamidderivaten zur Visualisierung von D2-
 artigen Dopaminrezeptoren¹⁷
 D. Stark, M. Piel, D. Bier, M.H. Holschbach, F. Rösch
- B5 Improved automated synthesis of [¹⁸F]FECh as a radiotracer for prostate cancer imaging¹⁵
 M. Piel, A. Bauman, I. Klette, S. Höhnemann, R. Wortmann, R.P. Baum, F. Rösch
- B6 ¹³¹I-Radioiodierung neuer MGMT-Inhibitoren und ihrer Glucose-konjugierten Analoga
 U. Mühlhausen, R. Schirrmacher, M. Piel, D. Bier, M.H. Holschbach, B. Kaina, F. Rösch
- B7 Synthesis and evaluation of a sugar-conjugated glibenclamide derivative
 A. Korobeynikov, R. Schirrmacher, M. Schwanstecher, F. Rösch
- B8 *In vivo* Evaluation and PET Imaging of [¹¹C]Harmine in Baboon Brains²³
 T. Capito, Y.-S. Ding, J. Fowler, C. Shea, Youwen Xu
- B9 PK 11195 as radiotracer for peripheral benzodiazepine binding sites (PK binding sites)²³
 Y.-S. Ding, K.-S. Lin, G. Quandt, T. Bretzel, F. Rösch, J. Fowler
- B10 Synthesis of the Phytohormone [¹¹C]Methyl Jasmonate via Methylation on a C₁₈ Sep
 PakTM Cartridge²³
 M.M. Herth, M.R. Thorpe, F. Rösch, R. A. Ferrieri
- B11 Transport and Fixation of Methyljasmonate in Tabacco Plants²³
 M.M. Herth, M.R. Thorpe, F. Rösch, R.A. Ferrieri
- B12 *In vitro* Stability and Immunoreactivity of ⁷⁴As[SATA] Vatuximab[®] ^{14,24}
 M. Jennewein, D. Zhao, J. He, A. Hermanne, S.M. Qaim, R.P. Mason, P.E. Thorpe, F.
 Rösch

VIII

- B13 New PET/MRI Fusion Images of ^{74}As labelled Vatuximab[®] in Prostate Cancer bearing Rats^{14,24}
M. Jennewein, N. Slavine, S. Seliouine, E. Tsyganov, V. Kodibagkar, A. Hermanne, S.M. Qaim, R.P. Mason, P.E. Thorpe, F. Rösch
- B14 *In vitro-* und erste *in vivo*-Untersuchungen mit ^{131}I -radioiodierten MGMT-Inhibitoren
U. Mühlhausen, D. Stark, B. Lecher, A. Piee-Staffa, M. Briegert, G. Nagel, R. Schirrmacher, M. Piel, B. Kaina, F. Rösch
- B15 *In vitro*-Affinitäten von halogenierten D2-artigen Dopaminrezeptorenliganden¹⁷
D. Stark, M. Piel, H. Hübner, P. Gmeiner, F. Rösch
- B16 *Ex vivo*-Biodistributionen des D₂-Antagonisten Desmethoxyfallypride¹⁷
M. Piel, S. Höhnemann, D. Stark, U. Schmitt, F. Rösch
- B17 *Ex vivo*-Biodistributionen des D₂-Antagonisten Fallypride¹⁷
M. Piel, S. Höhnemann, D. Stark, U. Schmitt, F. Rösch
- B18 Evaluation ^{131}I -markierter Dopaminrezeptorliganden *in vitro*¹⁷
H. Lüddens, D. Stark, M. Piel, F. Rösch
- B19 Receptor-PET/CZ of neuroendocrine tumors using the gallium-68 labelled somatostatin analog DOTA-NOC: First clinical results¹⁵
R.P. Baum, M. Schmücking, A. Niesen, K.P. Zhernosekov, F. Rösch
- B20 Somatostatin receptor expressing tumors: Imaging with ^{68}Ga -DOTATOC-PET/CT versus ^{111}In -DTPAOC-SPECT/CT¹⁵
P. Aschoff, M. Oeksuez, B. Kemke, K. Zhernosekov, M. Jennewein, F. Rösch, H. Bihl
- B21 Enhanced visualization of disseminated bone metastases of primary neuroendocrine tumors using ^{68}Ga -DOTATOC¹⁵
P. Aschoff, M. Oeksuez, B. Kemke, K. Zhernosekov, M. Jennewein, F. Rösch, H. Bihl
- B22 [^{18}F]FECholin is a promising radiotracer for PET/CT imaging of prostate cancer¹⁵
R.P. Baum, M. Piel, A. Bauman, I. Klette, S. Höhnemann, R. Wortmann, F. Rösch
- B23 High Striatal Occupancy of D₂-like Dopamine Receptors by Amisulpride in Brain of Patients with Schizophrenia¹⁷
I. Vernaleken, T. Siessmeier, H.-G. Buchholz, S. Härtter, Ch. Hiemke, P. Stoeter, F. Rösch, P. Bartenstein, G. Gründer
- B24 Decreased temporal dopamine D₂/D₃ receptor binding in temporal lobe epilepsy: an ^{18}F -Fallypride PET study¹⁷
K.J. Werhan, Ch. Landvogt, S. Klimpe, H.-G. Buchholz, W. Müller-Forell, I. Yakushev, M. Piel, F. Rösch, M. Schreckenberger, P. Bartenstein
- B25 Alcohol craving correlates with striatal dopamine receptor density and dopamine synthesis capacity¹⁷
T. Siessmeier, A. Heinz, H.G. Buchholz, J. Wräse, C. Landvogt, R. Schirrmacher, M. Piel, F. Rösch, M. Schreckenberger, P. Cumming, G. Gründer, P. Bartenstein

IX

- B26 Funktionelle Charakterisierung somatosensorischer Areale im parasympatischen Kortex des Menschen¹⁷
U. Baumgärtner, M. Schreckenberger, W. Magerl, F. Rösch, P. Bartenstein, P. Stoeter, R.-D. Treede
- B27 Vergleich unterschiedlicher Quantifizierungsmethoden des Bindungspotenzials für den unspezifischen Opiatrezeptorliganden ¹⁸F-Fluor-Ethyl-Diprenorphin¹⁷
Th. Siessmeier, H.-G. Buchholz, H.-J. Wester, G. Hendrickson, M. Piel, F. Rösch, M. Schreckenberger, P. Bartenstein

C. Analytik für Umwelt und Technik

- C1 Structure of Uranium(VI) Surface Complexes on Kaolinite⁸
S. Amayri, T. Reich, A. Jermolajev, Ta. Reich, J. Drebert, S. Boulyga
- C2 Neptunium(V) Sorption onto Kaolinite in the Presence and Absence of CO₂⁸
S. Amayri, T. Reich, J. Drebert
- C3 Feasibility of EXAFS experiments at the Np L-edge to investigate neptunium sorption on kaolinite⁸
T. Reich, S. Amayri, Ta. Reich, J. Drebert, A. Jermolajev, P. Thörle, N. Trautmann, C. Hennig, S. Sachs
- C4 Application of the Tikhonov regularization method to the detection of U-Si neighbours in soddyite using EXAFS spectroscopy
Ta. Reich, T. Reich, A.L. Ageev, M. Korshunov
- C5 Investigation of Zr(IV)-hydroxide Solubility with LIBD and EXAFS²⁹
C. Walther, H.R. Cho, M.A. Denecke, Th. Fanghänel, J.V. Kratz, V. Neck, J. Rothe
- C6 Neue Möglichkeiten der Kapillarelektrophorese durch Verwendung eines Dioden-Array-Detektors (DAD)^{8,25}
B. Kuczewski, S. Bürger, J.V. Kratz, N. Trautmann
- C7 Off-line Kopplung der Resonanzions-Massenspektrometrie an die Kapillarelektrophorese zur Speziation der leichten Actiniden im Ultraspurenbereich^{8,25,29}
S. Bürger, N.L. Banik, R.A. Buda, J.V. Kratz, B. Kuczewski, N. Trautmann
- C8 Dreifach-resonante Ionisation von Uran-Isotopen für den isotopenselektiven Spurennachweis von ²³⁶U²⁵
P.G. Schumann, B.A. Bushaw, S. Boulyga, G. Passler, N. Trautmann, K. Wendt
- C9 Spurenanalytische Bestimmung von ⁹⁹Tc mit einem Ti:Sa Lasersystem²⁵
K. Wies, N. Erdmann, G. Passler, N. Trautmann, K. Wendt
- C10 Complexation of ²¹²Pb with Humic Acids⁸
A. Mansel, B. Kuczewski, H. Hummrich, N. Trautmann, J.V. Kratz, H. Kupsch
- C11 Interaction of Pu with Humic Substances^{8,25}
R.A. Buda, N.L. Banik, S. Bürger, B. Kuczewski, J.V. Kratz, N. Trautmann

X

- C12 Limitation of the Ultrafiltration Method for the Determination of Complexation Constants of Pu(IV) with Humic Substances^{8,25}
N.L. Banik, R.A. Buda, S. Bürger, J.V. Kratz, B. Kuczewski, N. Trautmann
- C13 Precipitation of Aldrich Humic Acid in Dependence of pH^{8,25}
N.L. Banik, S. Bürger, J.V. Kratz, N. Trautmann
- C14 Untersuchungen zur Ultrafiltration von Huminsäure und Fulvinsäure für die Bestimmung von Komplexbildungskonstanten mit Metallionen^{8,25}
S. Bürger, N.L. Banik, J.V. Kratz, N. Trautmann
- C15 Kopplung von Ionenstrahl-Sputtern und Resonanzionsmassenspektrometrie zur ortsaufgelösten Analyse von Actiniden^{10,30}
N. Erdmann, J.V. Kratz, N. Trautmann, G. Passler, P. Lievens, R.E. Silverans, E. Vandeweert
- C16 Spurenanalyse von gammastrahlenden Radionukliden in der bodennahen Luft
H. Keller, R. Heimann, B. Praast

D. Technische Einrichtungen

- D1 Betrieb des Forschungsreaktors TRIGA Mainz im Jahre 2004
N. Trautmann
- D2 Personendosisüberwachung
B. Praast, I. Onasch

E. Veröffentlichungen und Vorträge

- E1 Diplomarbeiten und Dissertationen
- E2 Veröffentlichungen und Vorträge der Mitarbeiter der berichterstattenden Arbeitsgruppen
- E3 Vorträge im Seminar für Kern- und Radiochemie und im Seminar über aktuelle Themen aus Kosmochemie und Astrophysik
- E4 Beiträge der Dozenten des Instituts zu den Lehrveranstaltungen des Fachbereichs Chemie und Pharmazie (SS 04 und WS 04/05) sowie zur Weiterbildung

- (1) Gefördert durch das Bundesministerium für Bildung und Forschung (BMBF) im Rahmen des Vorhabens „Optische Spektroskopie an schweren Elementen“
- (2) Gefördert durch das Bundesministerium für Bildung und Forschung (BMBF) im Rahmen des Vorhabens „Kernchemische Untersuchungen von Kernreaktionen und Kernzerfall“
- (3) Gefördert durch das Bundesministerium für Bildung und Forschung (BMBF) im Rahmen des Vorhabens „Kernchemische Untersuchungen schwerster Elemente und Kernstruktur“
- (4) Gefördert durch die Gesellschaft für Schwerionenforschung, Darmstadt, im Rahmen der Zusammenarbeitsvereinbarungen zwischen Wissenschaftlern von Hochschulen und der GSI
- (5) Gefördert vom Fonds der Chemischen Industrie (FCI)
- (6) Gefördert durch die Deutsche Forschungsgemeinschaft im Rahmen des Vorhabens „Chemische Eigenschaften des Elements 106“
- (7) Gefördert durch das Zentrum für physikalisch-chemische Verbundforschung der Johannes Gutenberg-Universität Mainz
- (8) Gefördert durch das Bundesministerium für Wirtschaft und Arbeit im Rahmen des Vorhabens „Migration von Actiniden im System Ton, Huminstoff, Aquifer – Wechselwirkung von Neptunium und Plutonium mit Huminstoffen und Kaolinit“
- (9) Gefördert durch das Zentrum für Umweltforschung der Johannes Gutenberg-Universität Mainz
- (10) Gefördert durch den Forschungsfonds der Johannes Gutenberg-Universität Mainz
- (11) Gefördert durch das Kompetenzzentrum „Spurenanalytik“ des Landes Rheinland-Pfalz
- (12) Gefördert durch das Medizinisch-Naturwissenschaftliche Forschungszentrum der Johannes Gutenberg-Universität Mainz
- (13) Gefördert durch die Deutsche Forschungsgemeinschaft im Rahmen des Vorhabens „Einführung des Auger-Elektronen-Emitters ^{140}Nd zur Synthese von Neodym-Chelat-Peptid- oder Neodym-Chelat-Antikörper-Verbindungen für die Endoradiotherapie kleiner Tumore“
- (14) Gefördert durch die Deutsche Forschungsgemeinschaft im Rahmen des Vorhabens „Entwicklung einer neuen Klasse von Radiopharmaka für die Positronen-Emissions-Tomographie: $^{70,72}\text{As}$ -markierte Verbindungen“
- (15) Gefördert durch die Europäische Gemeinschaft im Rahmen des Vorhabens „European Molecular Imaging Laboratoires“
- (16) Gefördert durch die Deutsche Forschungsgemeinschaft im Rahmen des Vorhabens „Wissenschaftleraustausch mit Russland – Metall-Chelat-Peptid-Systeme“
- (17) Gefördert durch das Kompetenzzentrum „Neuro-PET“ des Landes Rheinland-Pfalz
- (18) Gefördert durch die Deutsche Forschungsgemeinschaft im Rahmen des Vorhabens „Synthese von hochaffinen ^{18}F -markierten Liganden zur Untersuchung von NMDA-Rezeptoren mittels Positronen-Emissions-Tomographie (PET)“
- (19) Gefördert durch die Deutsche Forschungsgemeinschaft im Rahmen des Vorhabens „Kernstrukturuntersuchungen an r-Prozeß-Schlüsselnukliden“
- (20) Gefördert durch EURISOL – European Isotope Separation On-line Radioactive Nuclear Beam Facility
- (21) Gefördert durch die Stiftung Rheinland-Pfalz für Innovation
- (22) Gefördert durch MAIFOR
- (23) Gefördert durch den DAAD im Rahmen des Internationalen Studentenaustausch-Programms zwischen der „Johannes Gutenberg-Universität Mainz und der State University of New York at Stony Brook/dem Brookhaven National Laboratory“
- (24) Gefördert durch die Boehringer-Ingelheim-Stiftung
- (25) Gefördert durch das Graduiertenkolleg „Spurenanalytik von Elementspezies: Methodenentwicklungen und Anwendungen“

XII

- (26) Gefördert durch die Deutsche Forschungsgemeinschaft im Rahmen des Vorhabens „Determination of ^{236}U in Environmental Samples by High Resolution Resonance Ionization Mass Spectrometry“
- (27) Gefördert durch die EU im Rahmen des EMERGE-Projekts
- (28) Gefördert durch die Deutsche Forschungsgemeinschaft im Rahmen des Vorhabens „Installation und Optimierung eines Systems zur Erzeugung von ultrakalten Neutronen (UCN) am TRIGA-Reaktor sowie Studien mit UCN“
- (29) Gefördert durch die Europäische Gemeinschaft im Rahmen des Network of Excellence „ACTINET“
- (30) Gefördert durch die Deutsche Forschungsgemeinschaft im Rahmen des Vorhabens „Determination of the isotopic composition of trace amounts of actinides in environmental micro-particles by Resonance Ionisation Mass Spectrometry (RIMS) of Sputtered Neutrals (SN)“
- (31) Gefördert durch die Helmholtz Gemeinschaft im Rahmen des „Virtuellen Instituts für Struktur der Kerne und Nukleare Atrophysik“ (VISTARS)
- (32) Gefördert durch Max-Planck-Institut für Chemie, Kosmochemie, Mainz

A. Grundlagenforschung

- Driftzeit-Messungen in einer Puffer-Gas-Zelle
- Chemie der schwersten Elemente
- Struktur extrem neutronenreicher Kerne
- R-Prozess Chronometer
- Thermochromatographie
- N-Einfang
- Siderophile Elemente in Xenolithen
- Radiochemische Trennungen
- Detektoren zum μ -Imaging
- Ultrakalte Neutronen am TRIGA Mainz

A. Fundamental Problems

- Drift-time measurements in a buffer-gas cell
- Chemistry of the heaviest elements
- Structure of extremely neutron-rich nuclei
- R-process chronometers
- Thermochromatography
- N-Capture
- Siderophile elements in Xenolithes
- Radiochemical Separation
- Detectors for μ -imaging
- Ultra cold neutrons at the TRIGA Mainz

Optical Spectroscopy of Trans-Fermium Elements at SHIPTRAP

H. Backe¹, A. Dretzke¹, R. Horn¹, T. Kollb¹, P. Kunz¹, W. Lauth¹, P. Thörle², and N. Trautmann²

¹Institut für Kernphysik, Universität Mainz, Germany; ²Institut für Kernchemie, Universität Mainz, Germany

An ultra sensitive laser spectroscopic method is being developed for the investigation of the completely unknown atomic structure of the elements No and Lr. Such experiments aim in the investigation of relativistic effects. These, roughly speaking, originate from a shrinkage of the wave functions of inner shell electrons which, in turn, influence the binding energy of the valence electrons and thus the chemical properties. A direct approach to investigate relativistic effects may be to study first ionization potentials (IP) or even better, the atomic level schemes [1].

First experiments will be performed within the SHIPTRAP collaboration at No which will be produced via the fusion reaction $^{208}\text{Pb}(^{48}\text{Ca},2\text{n})^{254}\text{No}$. The reaction products, separated by SHIP, will be stopped in a buffer gas cell in which Resonance Ionization Spectroscopy (RIS) is performed with detection of the ionization process by the α -decay of ^{254}No . The technique is similar to that developed for RIS at fission isomers [2]. The experimental setup is shown in Fig. 1. The reaction products with an energy of 40 MeV are injected into the argon buffer gas trap and stopped in the gas at an pressure of 100-300 mbar. The neutral part of about 15% will be ionized resonantly and guided by electric fields onto a detector which registers the α -decay radiation. After each detuning of the laser frequency of the first excitation step one has to wait for the decay of the accumulated ions. The symmetric construction offers the opportunity to collect on one detector ions, that are resonantly ionized while counting with the other one the activity collected at a different wavelength.

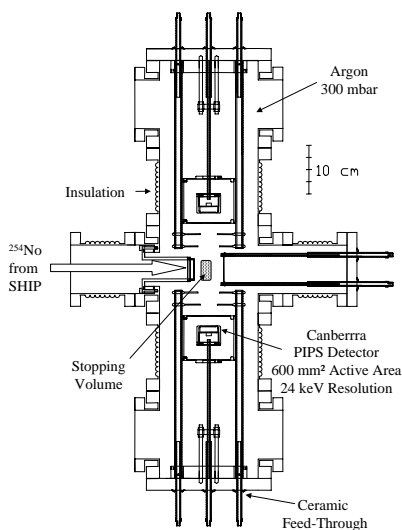


Figure 1: Experimental set-up. The separated fusion product from SHIP is injected into a buffer gas trap. About 10% of these ions neutralize in the slowing down process and are thus available for laser spectroscopic investigations.

A first on-line test experiment at GSI was carried through with the radioactive isotopes $^{152,153}\text{Er}$ (half-lives of 10.3 s and 37.1 s, α -decay) which were produced by the nuclear reaction $^{40}\text{Ar}(^{116}\text{Sn},\text{xn})^{152,153}\text{Er}$ with the relatively large reaction cross sections of about 100 mb. The

atomic level scheme of erbium is well known, and this reaction thus provides an ideal test case. The longitudinal and transversal distribution of the recoils has been measured with the aid of a semiconductor strip detector. For the resonance ionization spectroscopy experiments a mixture of approx. 150 mbar Ar and approx. 40 mbar N₂ was chosen. The pressure was optimized in such a way that the stopping distribution was located in the middle of the cell, where the overlap with the laser beams ($\lambda_1 = 472$ nm, 100 μJ and $\lambda_2 = 351$ nm, 2 mJ) is maximal. A slight but significant increase of the α -events in the detector was observed. A dependency on the laser frequency λ_1 could not be observed, meaning that the ionization is a non-resonant process. A possible reason for the non-resonant low ion signal could be that erbium compounds, such as ErN, are formed.

The second on-line experiment was performed on ytterbium, the chemical homolog of nobelium. It was produced by the fusion reaction $^{40}\text{Ca}(^{118}\text{Sn},\text{xn})^{154,155}\text{Yb}$. The gas cell was filled with 150 - 250 mbar argon. Wave lengths $\lambda_1 = 398.9$ nm and $\lambda_2 = 399.6$ nm were chosen for the first and second level, respectively. The second level is a Rydberg state, which should provide a higher efficiency as excitation into the continuum. Results of these measurements are shown in Fig. 2. Although the apparatus could be proven in this experiment to be operational, the efficiency for resonance ionization turned out to be only $2\text{-}4 \cdot 10^{-5}$. An increase of the efficiency by a large gain factor may be obtained if the 85% fraction of the thermalized ions are collected by and reevaporated from a filament as atoms by a high temperature pulse. The atom cloud, localized in this way, would also improve the overlap with the laser beams.

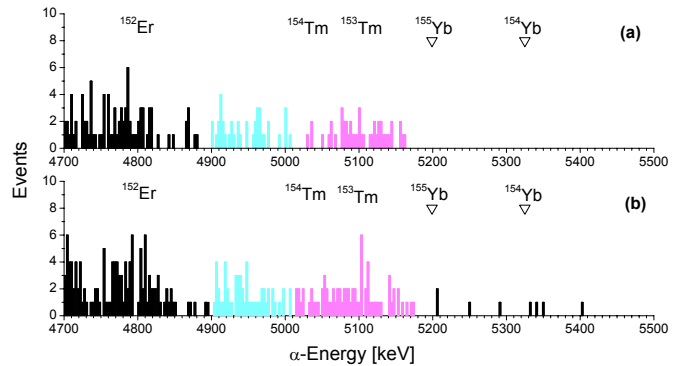


Figure 2: Resonance ionization signals of ^{154}Yb and ^{155}Yb . (a) α -energy spectrum off-resonant and (b) at resonance ($\bar{\nu}_1 = 25068.24 \text{ cm}^{-1}$, $\bar{\nu}_2 = 25025.84 \text{ cm}^{-1}$). The α -lines of the $^{154,155}\text{Yb}$ decay are marked with ∇ .

Work supported by the Bundesministerium für Bildung und Forschung under contract 06 MZ 959I.

References

- [1] M. Sewitz et al., Phys. Rev. Lett. 90, 163002-1 (2003)
- [2] H. Backe et al., Phys. Rev. Lett. 80, 920 (1998)

Separation of ^{211}Pb with ALOHA and subsequent electrochemical deposition

H. Hummrich, F. Feist, D. Liebe, J.V. Kratz

Institut für Kernchemie, Johannes Gutenberg-Universität Mainz, Germany

To achieve a fast and (quasi)-continuous transfer of recoil atoms from the recoil chamber into the liquid phase, the ALOHA system was constructed and successfully used in chromatography experiments [1].

To prepare liquid phase experiments with element 114, the separation of its homolog Pb with ALOHA and its subsequent electrochemical deposition was investigated. A ^{219}Rn -emanating source was prepared by co-precipitation of ^{227}Ac with $\text{Fe}(\text{OH})_3$. The source was placed in a 300 ml glass chamber where the 3,96s ^{219}Rn was allowed to decay. The daughter nuclides ^{211}Pb and ^{211}Bi were attached to KCl-clusters and transferred with a He flow of 2 l/min to ALOHA and deposited by impaction on a Ta disc. After impaction, the activity was stepped to the dissolution position and transferred to the electrolytic cell by continuously cyclic pumping of the electrolyte (0.1M HCl) with a low dead-volume HPLC pump. Fig. 1 shows the experimental set-up.

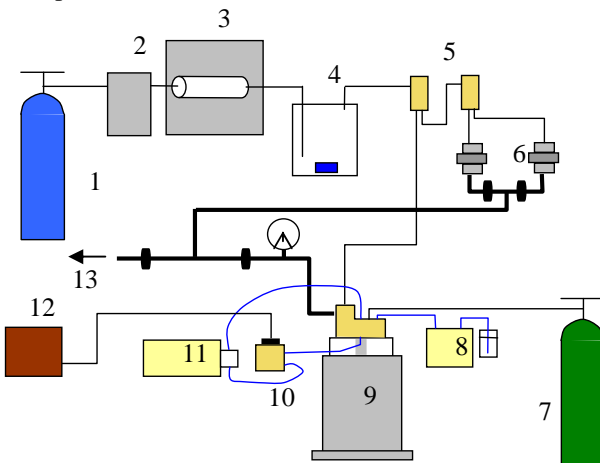


Fig.1: Experimental set-up. 1 Helium, 2 mass-flow-controller, 3 KCl cluster oven, 4 ^{227}Ac emanating source, 5 gas-jet switches, 6 direct catch and waste unit, 7 Nitrogen, 8 Acetone pump, 9 ALOHA, 10 electrodeposition cell, 11 electrolyte pump, 12 potentiostat, 13 to the ventilation system. Gas jet flow: black line, vacuum system: thick black line, liquid flow: blue line

The yield of impaction and dissolution in ALOHA (compared to a direct catch on a glassfiber filter) was measured via γ -spectrometry at different stepping times. Fig.2 shows that about 75 to 90% of the activity was successfully transferred from the gas-jet into the liquid phase using stepping times of 5s and longer. At lower stepping times, activity is lost due to the low dissolution volume.

For electrodeposition experiments with ^{211}Pb , a heatable electrolytic cell was attached to the ALOHA system. Pd was chosen as electrode material, 0.1M HCl as electrolyte. The deposition potential was -500 mV vs. Ag/AgCl.

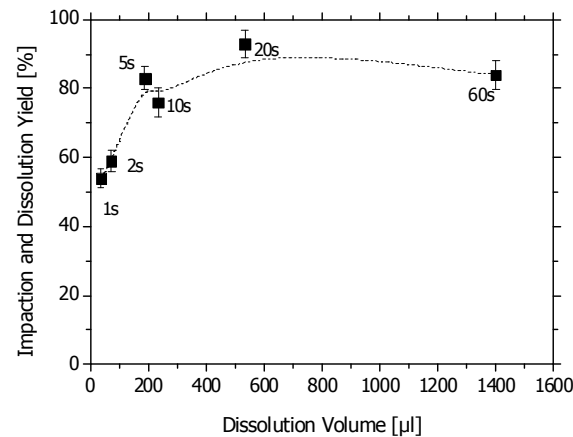


Fig.2: Impaction and dissolution yield for $^{211}\text{Pb}/^{211}\text{Bi}$ vs. dissolution volume (stepping time) with the ALOHA system, solvent 0.1M HCl

The activity was impacted for 10 min in the collection position, transferred to the dissolution position and dissolved. The deposition experiments were carried out at a temperature of ca. 75° and under vigorous stirring. At $t_{50\%}=20\text{s}$, 50% of the activity was deposited, as can be seen in Fig.3.

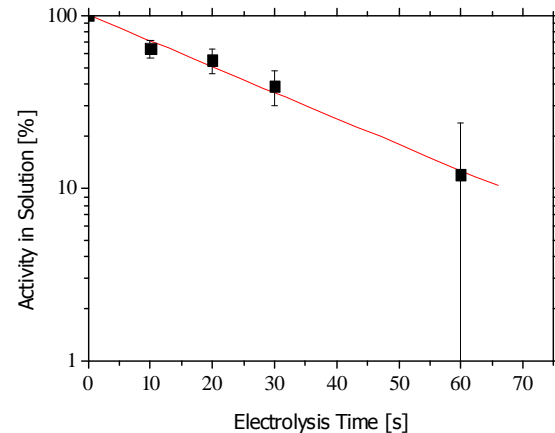


Fig.3: Electrodeposition of ^{211}Pb on Pd electrodes from 0.1M HCl at -500mV vs. electrolysis time.

The deposited activity could also be measured via α -spectrometry after the radioactive equilibrium between ^{211}Pb and ^{211}Bi was reached. Here, a 0.1 μm polycarbonate filter was used for the direct catch. In both cases, a FWHM of 60 keV for the 6,2 MeV line of ^{211}Bi was achieved

The presented system will be tested in a beam time at GSI with short lived Pb-isotopes in the reaction ^{40}Ar on Gd.

References

- [1] A. Kronenberg et al., Annual Report, Institut für Kernchemie, Universität Mainz 2001, A4

Separation of fission products with ALOHA and subsequent electrochemical deposition

H. Hummrich, J.V. Kratz , D. Liebe,

Institut für Kernchemie, Johannes Gutenberg-Universität Mainz, Germany

The separation of fission products was studied with a coupling of the ALOHA system [1] and an electrochemical deposition device. A ^{235}U -Target (see fig. 1), which was covered with 15 μm Al to suppress the heavy-mass fission products, was irradiated at the TRIGA reactor. The light mass fission products recoiling from the target, were stopped in He and transported with a KCl-cluster gasjet to the ALOHA system. After impaction onto a Ta-disc, the disc was stepped into the dissolution position and the fission products were dissolved in 0.1M HClO_4 and transferred into the electrochemical cell by continuously cyclic pumping at a flow rate of 1-2 ml/min.

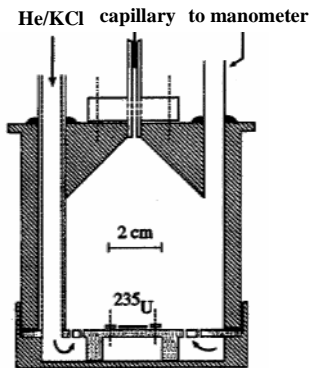


Fig.1: Set-up of the ^{235}U -target and recoil chamber used for fission product production

The overall impaction and dissolution yield in ALOHA compared to a direct catch on a glassfiber filter (measured via the gross γ -activity) was about 80%, if the Ta-disc was stepped in intervals of 5s and longer. For shorter stepping times, the dissolution volume was low compared to the dead volume of the dissolution position, thus leading to a decrease in yield to about 60%. The impaction and dissolution yield for a specific fission product can be determined, if the fractional and the cumulative fission yield are in the same dimension. For ^{84}Se (fractional yield: 0,66%, cumulative yield: 0,99%), 55 \pm 10% of the activity was recovered from the gas-jet.

The potential dependence of the electrodeposition yield was investigated. Pd working electrodes and a Pt counter electrode were used. The potential was controlled potentiostatically vs. a Ag/AgCl reference electrode. The fission-products were collected for 5 min., then the electrodeposition was performed for 5 min. at a given potential under vigorous stirring. After that, the deposited activity was measured. The experiment was carried out for various electrode potentials.

Even at -1000mV, only $^{101/104}\text{Tc}$ and ^{84}Se were deposited. ^{101}Mo , ^{93}Sr , ^{90}Rb and ^{94}Y remained in solution. Fig. 2 shows the potentials, at which the electrodeposition of Tc and Se start (critical potential).

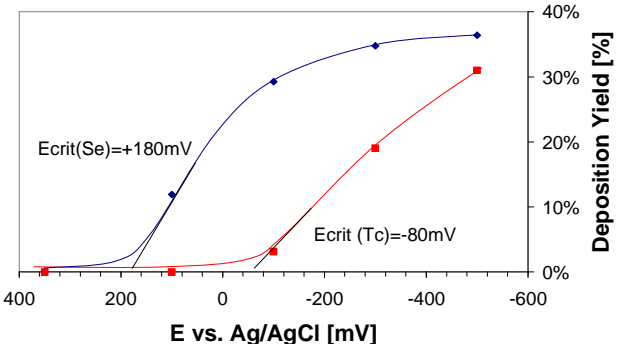


Fig. 2: Critical potentials for the electrochemical deposition of Tc and Se from 0.1M HClO_4 on Pd electrodes

In experiments with fission products with a longer half-life, ^{103}Ru and ^{99m}Tc could also be electrodeposited onto Pd. At -500 mV, $^{97/95}\text{Zr}$, ^{96}Nb and ^{99}Mo remained in solution. Fig. 3 shows the critical potential for the deposition of Ru.

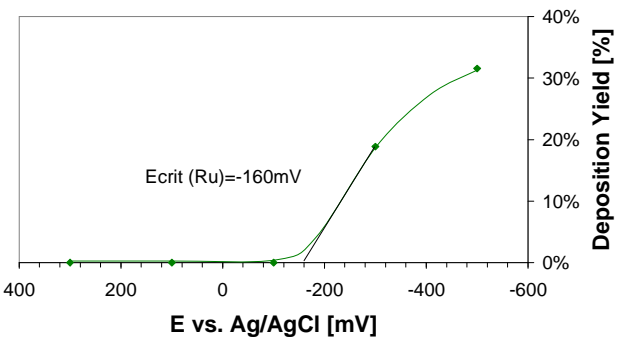


Fig. 3: Critical potential for the electrochemical deposition of Ru from 0.1M HClO_4 on Pd electrodes

In superheavy element chemistry, the coupling of ALOHA with an electrochemical deposition device may be suitable for experiments with Bh (homolog of Tc) and Hs (homolog of Ru). Further experiments with Re and Os, the heavier homologs of Bh and Hs, are necessary to confirm this assumption.

References

- [1] H. Hummrich et al., this report

The electrochemical deposition of Hg on various metal electrodes

H. Hummrich, F. Feist, J.V. Kratz

Institut für Kernchemie, Johannes Gutenberg-Universität Mainz, Germany

Recently, attempts were undertaken to chemically characterize element 112 in gas phase experiments [1].

A different approach involves experiments in the liquid phase. If we assume that element 112 is a noble metal (like its homolog Hg), a separation by electrochemical deposition on a metal electrode should be possible. Furthermore, this would result in an ideal sample for α -spectrometry.

In our experiments, we investigated the electrochemical deposition of Hg on various metal electrodes. A solution of $\text{Hg}(\text{NO}_3)_2$ in 0.1M HNO_3 was irradiated at the TRIGA reactor of the Mainz for 6h at a neutron flux of $7 \cdot 10^{11} \text{ n/s/cm}^2$. The isotope ^{197}gHg with a half live of 64.1h was produced with a specific activity of 70 kBq/mg, and its γ -line at 77 keV was evaluated in the experiments.

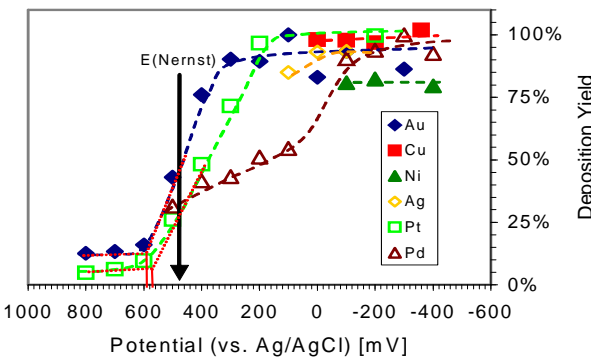


Fig.1: Electrodeposition yield vs. electrode potential for the deposition of ^{197}gHg on various metal electrodes. In the experiments with Ag, Au, and Cu, 0.1M HNO_3 and with Pt, Pd, and Ni, 0.1M HCl was used as electrolyte

A heatable electrolysis cell with two working electrodes (total area 2 cm^2), a Pt counter electrode and a Ag/AgCl reference electrode was used. The electrolyte volume of 1-2 ml was stirred with a high volume magnetic stirrer at 1000-1400 rpm. The total Hg concentration in each experiment was $5 \cdot 10^{-6} \text{ mol/l}$. This was low enough, so that the deposition still took place in the sub-monolayer region. 0.1 M HCl and 0.1 M HNO_3 were used as the electrolyte. The electrolysis time was 10 min. This should result in the maximum possible deposition for the given potential.

The electrodeposition yield was measured vs. the electrode potential (Fig. 1). The experiments, in which Ag, Cu, and Ni electrodes were used, were started at the potential that occurred when the electrode is immersed into the solution (rest potential). At the rest potential, no current is applied. An increase of the potential beyond this rest potential would lead to a dissolution of the electrodes. For the deposition of Hg on Pt and Au, a critical potential at which a significant deposition starts, was deduced. For Pd, no well defined critical potential was found. For Cu, Ni, and Ag, the deposition is already nearly complete at the rest potential (spontaneous deposition).

In table 1, the critical potentials are compared with $E_{50\%}$ -values, which were calculated with a microscopic-macroscopic model proposed by Eichler and Kratz [2] using thermodynamic properties of Hg and of the electrode material.

Table 1: Critical potentials for the deposition of Hg on various metal electrodes compared with theroretically predicted $E_{50\%}$ -values (all potentials vs. Ag/AgCl)

Electrode	E_{crit} [mV]	$E_{50\%}$ calc.
Au	+ 600	+ 710
Ni	> +50	+ 660
Ag	> +100	+ 620
Cu	> -100	+ 630
Pt	+ 580	+ 970
Pd	-	+ 1140

The electrodeposition speed was investigated for the deposition on Pd (20° and 80°) and Cu electrodes. Fig. 2 shows the decrease in activity vs. the electrolysis time. The $t_{50\%}$ -value is the time at which 50% of the activity is deposited. The electrodeposition seems to be faster on Cu electrodes than on Pd electrodes at room temperature. An increase in temperature lead to an increase in electrodeposition speed, in analogy to previous experiments with Pb [3].

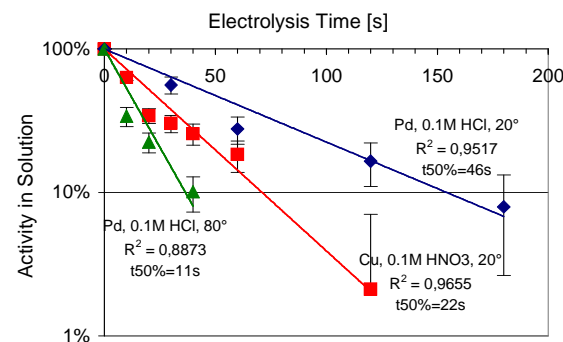


Fig.2: Electrodeposition speed vs. electrolysis time for the deposition of ^{197}gHg on Pd and Cu. Electrolytic systems: Pd / 0.1M HCl / 20° / -500mV; Cu / 0.1M HNO_3 / 20° / -300mV; Pd / 0.1M HCl / 80° / -500mV

The obtained results will be taken into account in a beam time at GSI, where carrier-free Hg isotopes are produced via the reaction of ^{40}Ar with Sm. The transport of Hg with a KCl gas jet, the transfer into the liquid phase with the ALOHA system [4] and a subsequent electrodeposition will be investigated.

References

- [1] S. Soverna et al, GSI, *Scientific Report 2003*, p. 187
- [2] B. Eichler, J.V. Kratz, *Radiochimica Acta* **88**, 475 (2000)
- [3] H. Hummrich et al., GSI, *Scientific Report 2003*, p. 199
- [4] H. Hummrich et al, *this report*

Extraction of Gd, Hf, and Tc with the fast and continuous liquid-liquid-extraction System MicroSISAK

K. Eberhardt¹, S. Andersson², C. Ekberg², B. Horn³, J.V. Kratz¹,
P. Löb³, M. Nilsson², G. Skarnemark², N. Trautmann¹

¹ Institut für Kernchemie, Universität Mainz, D-55099 Mainz, Germany; ² Chalmers University of Technology, S-41296 Göteborg, Sweden; ³ Institut für Mikrotechnik Mainz, D-55133 Mainz

MicroSISAK is a miniaturized apparatus developed for performing fast and continuous liquid-liquid separations. It is designed to provide a separation time of about 1 s at a flow rate of 60 ml/h (≤ 0.02 ml/s), as required, e.g., for chemical studies of the heaviest elements or for process studies with new types of ligands that are only available in very small amounts. MicroSISAK consists of a stack of microstructured [1] discs with a diameter of 8 mm made of Ti and sealed in a Ti-housing. The main components are:

1. a micromixer (Fig. 1a) with interdigital channels for intense mixing of the phases. Here, small droplets are formed with typical diameters in the range of the channel dimension (see Table 1 for details) yielding an emulsion. The emulsion is subsequently fed into
2. up to three filter units (teflon membrane, 0.5 μm pore size) for phase separation, as shown in Fig. 1b. A differential pressure Δp (10-50 mbar) regulated via a valve must be applied across the membrane in order to ensure proper phase separation [2].

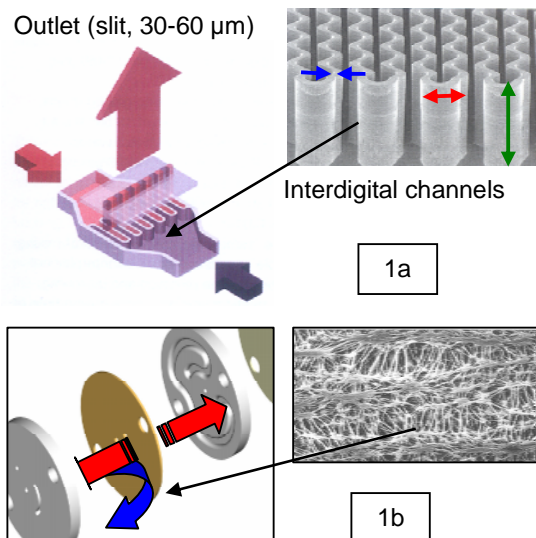


Figure 1: Mixer (Fig. 1a) and filter unit (Fig. 1b) for MicroSISAK. Different mixer types are used (see table 1).

The MicroSISAK set-up has been applied for extraction studies with Gd, Hf, and Tc. Here, different types of mixers have been used in order to optimize the extraction efficiency. Table 1

gives the dimensions of the different types of mixers.

Table 1: Dimensions of the mixer units as used for MicroSISAK (see also Fig. 1a)

Type	Channels	Width	Height	Wall
A	2 x 16	45 μm	100 μm	60 μm
B	2 x 15	30 μm	100 μm	60 μm
C	2 + 1	30 μm	100 μm	60 μm

Figure 2 comprises the results for the extraction of Gd, Hf, and Tc with MicroSISAK. Extraction yields and phase purities have been determined by means of γ -ray spectroscopy. For this, aliquots of the outgoing phases were measured after neutron activation at the TRIGA Mainz. $^{99\text{m}}\text{Tc}$ -activity was obtained by milking a commercial Mo-generator. To monitor phase purity, Na_2CO_3 was added to the aqueous phase prior to extraction. The yield depends on the extraction kinetics, the flow rate (hold-up time), and the mixer structure (droplet size).

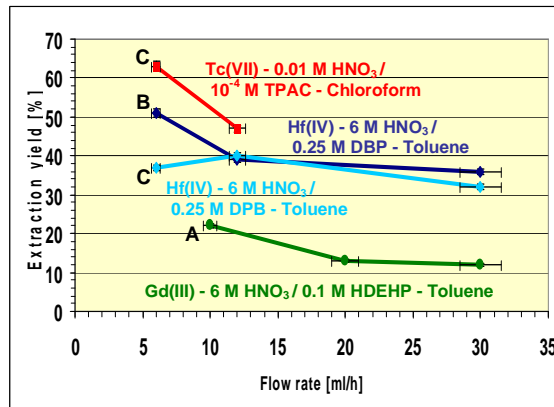


Figure 2: Extraction of Gd, Hf, and Tc with MicroSISAK. A, B, and C indicate the mixer type.

Further experiments are planned to measure the total hold-up time of the system and to optimize the extraction yield for flow rates ≤ 60 ml/h (≤ 0.02 ml/s). For this, different combinations of mixer- and filter units will be investigated.

References

- [1] W. Ehrfeld et al., *Microreactors*, Wiley-VCH Weinheim (2000)
- [2] K. Eberhardt et al., Institut für Kernchemie Annual Report (2003)

Theoretical Investigations of the Reactivity of MO_4 and the Electronic Structure of $\text{Na}_2[\text{MO}_4(\text{OH})_2]$, where M = Ru, Os, and Hs (element 108)

V. Pershina* and J. V. Kratz**

*GSI, Darmstadt

**Institut für Kernchemie, Universität Mainz

Recent experiments on the chemical identification of element 108, Hs, have delivered straightforward evidence that it belongs to group 8 of the Periodic Table [1]. In the presence of oxygen, Hs formed HsO_4 which was deposited in a gas-phase chromatography column at a temperature somewhat higher than that of OsO_4 , thus confirming its chemical similarity with the latter and the high volatility. In more recent experiments [2] with volatile tetroxides, HsO_4 was shown to react with moisturized NaOH forming very probably the sodium hassate (VIII), $\text{Na}_2[\text{HsO}_4(\text{OH})_2]$, by analogy with $\text{Na}_2[\text{OsO}_4(\text{OH})_2]$ according to the reaction



In the present work, we study the reactivity of RuO_4 , OsO_4 , and HsO_4 with NaOH on the basis of results of the fully relativistic calculations for the components of the reaction of type (1) using the 4-component Density-Functional Theory method [3]. A model [4] was used to determine the free energy change ΔG^\ddagger of a reaction via changes in the ionic (ΔE^{C}) and covalent (ΔE^{OP}) contributions to the total binding energy. The latter are calculated using Mulliken effective charges Q_M and overlap populations, OP. It was shown that relative values of ΔG^\ddagger could be reliably predicted via the ΔE^{C} . The bond lengths (R_e) of the Os complex were taken from the experiment [5], and those of the Ru and Hs complexes were estimated using R_e for RuO_4 and HsO_4 with respect to $R_e(\text{OsO}_4)$ [6].

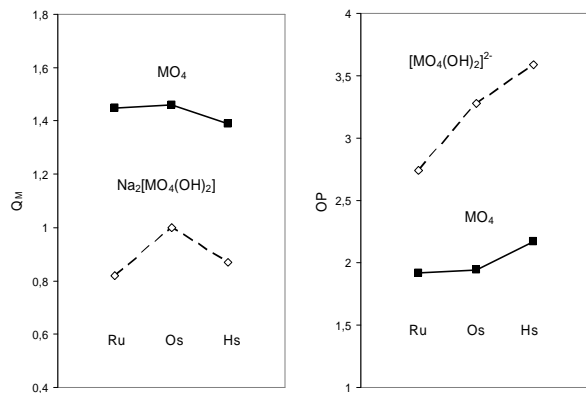


Fig. 1. Effective metal charges, Q_M , and overlap populations, OP, in MO_4 [6] and $[\text{MO}_4(\text{OH})_2]^{2-}$ [this work] ($\text{M} = \text{Ru}, \text{Os}, \text{and Hs}$).

The values of Q_M and OP obtained for $[\text{MO}_4(\text{OH})_2]^{2-}$ and MO_4 are depicted in Fig. 1. They show $[\text{HsO}_4(\text{OH})_2]^{2-}$ to be more covalent than the Os homolog, similarly to MO_4 . Both Q_M and OP in $[\text{RuO}_4(\text{OH})_2]^{2-}$ are significantly smaller than Q_M and OP of the Os and Hs anions, which is indicative for

the fact that the Ru anion is not stable due to the weak ionic and covalent constituents of the bond strength. This is not the case with MO_4 , where Q_M and OP of RuO_4 are very similar to those of OsO_4 (Fig. 1).

Table 1. Coulomb binding energies, E^{C} , for complexes of Ru, Os, and Hs and their differences, ΔE^{C} (in eV), for reactions of the complex formation

Complex/reaction	Ru	Os	Hs	Ref.
$E^{\text{C}}: \text{MO}_4$	-13.74	-13.86	-12.04	6
$E^{\text{C}}: [\text{MO}_4(\text{OH})_2]^{2-}$	-3.58	-7.64	-5.26	this
$E^{\text{C}}: \text{Na}_2[\text{MO}_4(\text{OH})_2]$	-5.70	-8.77	-6.41	this
$\Delta E^{\text{C}}: \text{MO}_4 \rightleftharpoons [\text{MO}_4(\text{OH})_2]^{2-}$	10.16	6.23	6.78	this
$\Delta E^{\text{C}}: \text{MO}_4 \rightleftharpoons \text{Na}_2[\text{MO}_4(\text{OH})_2]$	8.04	5.09	5.63	this

The obtained E^{C} for the species and ΔE^{C} for the complex formation reactions are given in Table 1. The values are similar for reactions of HsO_4 and OsO_4 ; HsO_4 should be slightly less reactive than OsO_4 . We can give the upper limit of the difference in ΔG^\ddagger between HsO_4 and OsO_4 of 52 kJ/mol defined by the difference in their ΔE^{C} . (The slightly larger $\Delta \text{OP}=1.42$ for the Hs reaction than $\Delta \text{OP}=1.34$ for the Os reaction should slightly decrease this value). The values of ΔE^{C} for the reactions of RuO_4 are about 300 kJ/mol more positive than ΔE^{C} of the OsO_4 and HsO_4 reactions. The reason for that is the too low stability of the Ru complex anion manifested in its low E^{C} (low Q_M) and low E^{OP} (low OP) (Fig. 1). Thus, the so much more positive ΔG^\ddagger of the complex formation reaction of Ru compared to those of Os and Hs explains why $[\text{RuO}_4(\text{OH})_2]^{2-}$ is not known. Finally, on the basis of these calculations, we predict the following trend for the formation of $[\text{MO}_4(\text{OH})_2]^{2-}$, or $\text{Na}_2[\text{MO}_4(\text{OH})_2]$ in group 8:



The predicted slightly lower reactivity of HsO_4 as compared to that of OsO_4 has so far not clearly been revealed experimentally [2].

References

- [1] C. Düllmann *et al.* Nature (Letters) **418**, 859 (2002).
- [2] A. von Zweidorff, *et al.* A. Radiochim. Acta **92**, 855 (2004).
- [3] S. Varga *et al.* Phys. Rev. A **59**, 4288 (1999).
- [4] V. Pershina, Radiochim. Acta **92**, 455 (2004).
- [5] N. N. Nevskii, *et al.* Dokl. Akad. Nauk. **266**, 628 (1982).
- [6] V. Pershina, *et al.* J. Chem. Phys. **115**, 792 (2001).

Search for the "missing" α -decay branch in ^{239}Cm

Z. Qin^{1,2}, D. Ackermann^{1,3}, W. Brückle¹, F.P. Hessberger¹, E. Jäger¹, P. Kuusiniemi¹, G. Münzenberg¹, D. Nayak^{1,4}, E. Schimpf¹, M. Schädel¹, B. Schausten¹, A. Semchenkov^{1,6}, B. Sulignano^{1,3}, K. Eberhardt³, J.V. Kratz³, D. Liebe³, P. Thörle³, Yu.N. Novikov^{1,5}

¹GSI, Darmstadt, Germany, ²Institute of Modern Physics, Chinese Academy of Science, Lanzhou, P.R. China,

³Johannes Gutenberg-Universität, Mainz, Germany, ⁴Saha Institute of Nuclear Physics, Kolkata, India,

⁵Petersburg Nuclear Physics Institute, Gatchina, Russia, ⁶Technical University of Munich, Germany

It is of special interest to search for those unknown α -emitters in the transuranium region which (i) are located along the path of α -decay chains that start in the super-heavy element region, and (ii) establish a link to nuclides with known masses. The knowledge of all Q_α values in an α -decay chain provides direct information on strongly desired mass values of SHE [1]. A search for the α -decay of ^{239}Cm was carried out at JAERI applying nuclear chemistry techniques [2]. Three α -events with an energy of 6.43 ± 0.14 MeV were assigned to ^{239}Cm and the α/EC branching ratio was estimated as $(6.2 \pm 1.4) \times 10^{-5}$. However, due to this poor statistics, not only the α -energy was determined with an insufficient precision but also the isotope assignment remained questionable.

In our experiment, curium isotopes were produced in the reaction $^{232}\text{Th}(\text{C}_{12},\text{xn})^{244-\text{x}}\text{Cm}$. Banana-shaped ^{232}Th targets were prepared by molecular plating at the University of Mainz. As a backing material, 5 μm thick Ti and 15 μm thick Be foils were used. Th target thicknesses were $\approx 700 \mu\text{g/cm}^2$ on Ti and $\approx 900 \mu\text{g/cm}^2$ on Be. $^{12}\text{C}^{2+}$ beams from the UNILAC were chosen such that after passing through a 20 μm Be vacuum window, He cooling gas of 200 mbar, and the backing material, the ^{12}C projectile energy was 74 MeV in the middle of the target. According to HIVAP calculations, this energy corresponds to the maximum of the excitation function for the reaction $^{232}\text{Th}(\text{C}_{12},\text{5n})^{239}\text{Cm}$. Irradiations were performed with the rotating target wheel ARTESIA. Reaction products recoiling out of the target were implanted into 3.9 μm Cu catcher foils mounted 4 mm behind the rotating target wheel. Most fission fragments passed through the catcher because of their high TKE. To avoid overheating of the target and catcher material by the intensive ion beam, irradiations were carried out in a He atmosphere at 200 mbar. Each irradiation lasted ≈ 6 to 8 hours, and typical (particle) beam intensities varied between 0.3 μA during daytime and 0.85 μA at night. After irradiation, the copper catcher wheel was dismounted and was transported to a chemistry laboratory. The radiochemical separation procedure to prepare a purified Cm sample for α -spectroscopy was finished within 1.5 h or less. This procedure is described in a separate contribution to this report [3].

Two separate runs were carried out at the beginning and end of November. During the first run, targets with Th on Ti were used. They failed because of massive losses of target material from the Ti backing during the irradiation. Furthermore, $^{48,49,51}\text{Cr}$, $^{43,44,46-48}\text{Sc}$, and $^{55,56}\text{Co}$ were produced from ^{12}C on Ti reactions with very high β -

and γ -activities masking complementary γ -spectroscopic measurements. During the second run, targets with Th on Be foil were used which did not show significant Th losses. β and γ activities were about ten times lower than in the first run, and the nuclides mentioned above were not present.

In attempts to identify ^{239}Cm by γ -spectroscopic measurements, some samples were measured with a γ -x-detector and with a Ge-clover detector. γ -ray spectra dominantly showed lines from the decay of ^{153}Sm , $^{150,151}\text{Pm}$ and ^{147}Nd originating from fission of the compound nucleus. Cross sections for these isotopes are about 5 mb [4]. These activities from chemically not separated homologous rare earth elements did not allow identifying ^{239}Cm in the (single) γ -spectra or any Cm by characteristic x-rays. A further evaluation of coincidences is under way.

Samples were assayed for α -activities by 450 mm^2 PIPS detectors. The energy resolution of the evaporated samples was 60 keV. The α -events together with detector numbers and associated times were recorded and stored in list mode. Fig. 1 shows, for the first 10 h measuring time, the sum spectrum of five samples. As expected, ^{240}Cm (4n-channel, $\approx 100\%$ α -decay) with α -energies of 6.29 and 6.24 MeV is dominant. Interestingly, there are some events around 6.5 MeV, close to the energy of ^{238}Cm (6n-channel). Data analysis and search for ^{239}Cm with a reported energy of 6.43 MeV [2] are in progress.

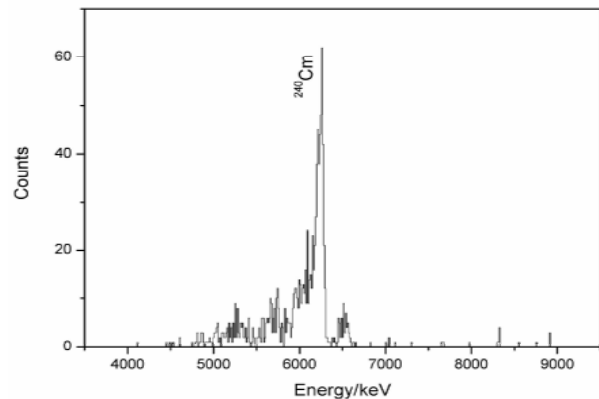


Fig.1 Sum α -spectrum of five samples ($t_m=10$ h each).

- [1] G. Münzenberg. FRS Berichte, GSI (1995) (unpublished)
- [2] N. Shinohara et al., JAERI-Review 2002-029, p. 45
- [3] Z. Qin et al., GSI Scientific Report 2004
- [4] A. Ramaswami et al., J. Radiochem. Nucl. Chem. 246 (2000) 225

Further investigations on target preparation for heavy element studies.

D.Liebe, P.Thörle, J.V. Kratz

Institut für Kernchemie, Universität Mainz, D-55099 Mainz, Germany

For heavy element studies at GSI, again lanthanide and actinide target segments for the rotating wheel assembly were prepared by molecular plating. ^{232}Th targets were used during two ^{12}C beamtimes to investigate the decay of ^{239}Cm [1]. Er has been again by ^{12}C to perform Multi-Column Experiments with Tungsten. The procedures for molecular plating have been applied basically as approved before [2]. Ti with a thickness of $5\mu\text{m}$ has been used as backing for both, Th and Er. Additionally, one target wheel with three segments of Th on an $15\mu\text{m}$ Be-Backing had to be prepared as well since the Th on the Ti-backing was lost almost completely from the rotating wheel during the first beamtime in september 2004. See Table 1.

Table 1: Segments for rotating wheel at GSI

Isotope	Backing	Thickn. [$\mu\text{g}/\text{cm}^2$]
Th	Ti / $5\mu\text{m}$	700
Th	Ti / $5\mu\text{m}$	710
Th	Ti / $5\mu\text{m}$	410
Er	Ti / $5\mu\text{m}$	550
Er	Ti / $5\mu\text{m}$	570
Er	Ti / $5\mu\text{m}$	560
Th	Be / $15\mu\text{m}$	1000*
Th	Be / $15\mu\text{m}$	900
Th	Be / $15\mu\text{m}$	950*

* plated twice

In order to improve the yield and the surface quality of all of those targets numerous tests have been done prior to and after the actual GSI -targets. The use of an ultrasonic probe for cleaning the backing foil prior to deposition seemed to be promising. The optimized parameters are listed below:

Pretreatment:

- washing the already mounted backing with acetone, HCl , H_2O , isopropanol.
- ultrasonic cleaning in isopropanol
- 14 ml fresh and water free isopropanol

Electrodeposition of Th

- 1.0-1.5 ml Th in isopropanol (corresponding to 2mg/ml)
- $10\mu\text{l}$ 0,1n HNO_3
- Voltage 10 min at 0.5 kV, 50min at 1.0kV

Electrodeposition of Er

- $3-5\mu\text{l}$ Er in 0.1n HNO_3 (corresponding to 200mg/ml)
- Voltage 1.0 kV constantly for 60min

Deposition yields are calculated from neutron activated aliquots of the plating solution prior to and after the procedure.

With ultrasonic treatment, which lasted up to 120min, the foil surfaces looked more structured than without this pretreatment. However, so far, there is no linear dependence of surface stability and deposition yield on the duration of the ultrasonic pretreatment of the Ti or Be backings.

A second issue was to achieve the required target thickness, surface stability and uniformity by two or three subsequent plating procedures. The quantity of Th used for each plating was decreased from 1.5ml to 0.5ml isopropanolic Th-Solution because higher deposition yields at lower concentration seem to be achieved. All other conditions remained as before. In general, the surfaces of all so prepared targets seemed to be more uniform and stable than for targets prepared at once. The densities of multi-plated targets varied between 814–1170 $\mu\text{g}/\text{cm}^2$ what corresponds to a deposition yield of 55–78 %. See table 2.

Table 2: Multi plated targets

Target	1	2	3	4
$1.\text{pl.}[\mu\text{g}/\text{cm}^2]$	329	131	285	212
$2.\text{pl.}[\mu\text{g}/\text{cm}^2]$	377	233	430	264
$3.\text{pl.}[\mu\text{g}/\text{cm}^2]$	310	474	455	338
sum $[\mu\text{g}/\text{cm}^2]$	1016	707	885	602

Backing: Ti $25\mu\text{m}$, other conditions see text.

Besides the target preparation recent work focuses also on requirements of the newly formed TASCA project. Some basic investigations are already in progress since december 2004. Especially the usability of very thin aluminium ($2-10\mu\text{m}$) as backing material for uranium deposition takes priority.

References:

- [1] Z. Quin et al., "Search for the 'missing' α -decay branch in ^{239}Cm ", GSI Scientific Report 2005
- [2] K.Eberhardt et al., "Preparation of Targets by electrodeposition for heavy element studies", Nuclear Instruments and Methods in Physics Research A 521 (2004), 208-213

Pygmy and Giant Dipole Resonances in $^{130-132}\text{Sn}$

P. Adrich^{a,d}, T. Aumann^a, K. Boretzky^b, D. Cortina-Gil^f, U. Datta Pramanik^a, Th.W. Elze^c, H. Emling^a, M. Fallot^a, H. Geissel^a, M. Hellström^a, K.L. Jones^a, A. Klimkiewicz^{a,d}, J.V. Kratz^b, R. Kulessa^d, Y. Leifels^a, C. Nociforo^b, R. Palit^c, H. Simon^e, G. Surowka^d, K. Sümmerer^a, and W. Walus^d

^aGSI Darmstadt; ^bUniv. Mainz; ^cUniv. Frankfurt; ^dUniv. Kraków, Poland; ^eTU Darmstadt; ^fUniv. Santiago de Compostela, Spain

We report on first results from the experiment aimed on dipole strength measurements in the region of ^{132}Sn . The motivation and experimental technique were already presented in the last year status report [1]. In brief, such a studies are motivated by the theoretical predictions of much different distributions of the multipole strength in exotic nuclei compared to the stable ones, which in turn provides a source of information on the isospin dependence of the effective nuclear interactions [2] and brings pronounced consequences for astrophysical models of the r-process nucleosynthesis [3]. One of the most exciting prediction concerns a new mode of collective excitation of medium and heavy neutron-rich nuclei at energies below the GDR region. This so called Pygmy or Soft Dipole mode (PDR), being interpreted as an oscillation of the neutron skin against the core of the nucleus, is at the moment lively discussed [4, 5, 6].

Measurements of the dipole strength in ^{132}Sn and about 20 other isotopes of similar A/Z ratio have been performed with the LAND-FRS facility. The secondary, radioactive beam was produced via in-flight fission of primary ^{238}U beam at 550 MeV/u. Isotopes of interest were selected with the FRS and identified on event-by-event basis. After delivering to Cave B they were electromagnetically excited in a secondary 0.5 g/cm² Pb target. Energy differential cross section spectra were obtained by means of the invariant mass analysis. To allow for the reconstruction of the invariant mass momenta of all the decay products (neutron(s), γ -rays and a heavy fragment remaining after dissociation in the target) were measured.

Left panels in the figure 1 show the measured cross sections in ^{130}Sn and ^{132}Sn . In the corresponding right panels the photoneutron cross section spectra deduced by means of the semiclassical method of virtual photons are presented. The enhancement of the cross section at energies close to 10 MeV is evident in both isotopes.

In order to extract quantitative information a function being sum of a lorentzian (to account for the GDR) and a gaussian (to account for the enhancement at low energy) was adopted to describe the shape of the photoneutron cross section. This function was then translated into energy differential cross section (by means of virtual photon method) and folded with the detector response obtained from an elaborated Monte Carlo simulation. Finally parameters of both components were found by means of a χ^2 minimization against the experimental data. The solid red line in the figure indicates the fitted function. The lorentzian and gaussian contributions are showed separated as green dash-dotted and blue dashed lines respectively.

The low energy peak is found at $10.1_{-0.3}^{+1.1}$ MeV in ^{130}Sn

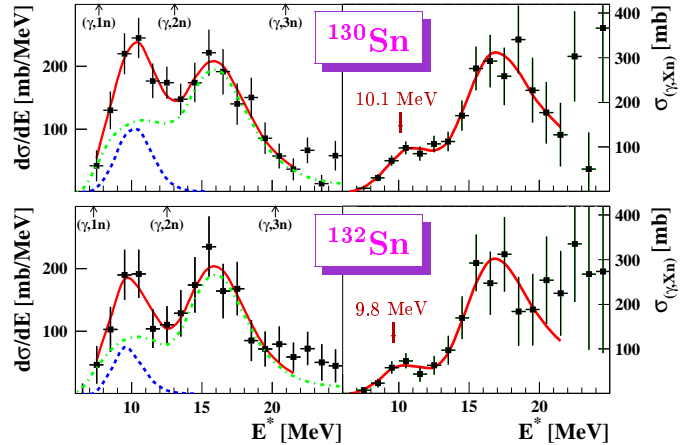


Figure 1: Experimental cross sections.

and at 9.8 ± 0.7 MeV in case of ^{132}Sn . The integrated cross sections attributed to those peaks amount to 130_{-50}^{+60} and 75_{-55}^{+60} mb·MeV accordingly, what exhausts 7% and 4% of the respective values of the Thomas-Reiche-Kuhn sum rule ($S_{TRK} = 60 \frac{N-Z}{A}$ mb·MeV). Such amount of strength is certainly too large to be interpreted in terms of single particle transitions but is consistent with the picture of the collective excitation.

Maxima of the GDR peaks are located at 15.9 ± 0.5 MeV in ^{130}Sn and at $16.1_{-0.6}^{+0.9}$ MeV in ^{132}Sn . In both cases the width was found to be 4.7 MeV with uncertainty of the order of 2 MeV.

The cross section integrated in an interval ranging from the neutron separation threshold up to 25 MeV amounts to 126% of the S_{TRK} in case of ^{130}Sn and 107% in case of ^{132}Sn .

A more complete report of the experimental findings obtained so far is being prepared for a publication in one of the scientific journals. At the same time the analysis of remaining data collected for neutron rich isotopes of In, Sb and Te is in progress and will be reported elsewhere.

References

- [1] P. Adrich and the LAND Collaboration, GSI Scientific Report 2003, ISSN 0174-0814, p. 26
- [2] P.-G. Reinhard, Nucl. Phys. **A649** (1999) 305c-314c
- [3] S. Goriely, Phys. Lett. **B436** (1998) 10-18
- [4] D. Sarchi, P. F. Bortignon and G. Colò, Phys. Lett. **B601** (2004) 27-33
- [5] N. Paar, et al., Phys. Rev. **C67** (2003) 34312
- [6] N. Tsoneva, H. Lenske and Ch. Stoyanov, Phys. Lett. **B586** (2004) 213-218

Breakup of relativistic halo nuclei (i)

P. Adrich^{a,h}, T. Aumann^{a,e}, O. Bochkarev^b, M.J.G. Borge^f, L.V. Chulkov^{a,b}, D. Cortina^a, Th.W. Elze^g, J. Fernandez-Vazquez^a, U. Datta-Pramanik^a, H. Emling^a, H. Fynbo^j, H. Geissel^a, L.V. Grigorenko^{a,b}, M. Hellström^a, H. Johansson^{a,d}, A. Klimkiewicz^{a,h}, K. Jones^a, B. Jonson^d, J.V. Kratz^e, R. Kulessa^h, Le Hong Khiem^a, E. Lubkiewicz^h, K. Markenroth^d, M. Meister^{a,d}, G. Münenberg^a, F. Nickel^a, T. Nilsson^{i,k}, G. Nyman^d, M. Pantea^{a,k}, R. Palit^a, V. Pribora^b, W. Prokopowic^h, A. Richter^k, K. Riisager^j, C. Scheidenberger^a, G. Schrieder^k, H. Simon^a, K. Sümmeler^a, O. Tengblad^f, I.J. Thomson^c, W. Walus^h, and M.V. Zhukov^d

^aGSI Darmstadt; ^bKurchatov Institute, Moscow; ^cUniversity of Surrey, Guilford; ^dChalmers Tekniska Högskola, Göteborg; ^eJohannes-Gutenberg-Universität, Mainz; ^fCSIC, Madrid; ^gJohann-Wolfgang-Goethe-Universität, Frankfurt; ^hUniversytet Jagiellonski, Krakow; ⁱCERN, Geneva; ^jAarhus Universitet, Aarhus; ^kTechnische Universität, Darmstadt

In the studies of the breakup of relativistic halo nuclei, the complete kinematics data as well as the energy and angular correlations have given new insight concerning the ground-state structure of the Borromean nuclei.

For the analysis of experimental data, we propose an effective method based on a series expansion of the transition amplitude into hyperspherical functions. The expansion coefficients are determined from the fit to the experimental distributions. The method makes possible the determination of the relative contribution of different partial waves. The comparison with the theoretical partial amplitudes allows either to choose between different models or to specify changes in the model that would be needed to describe the experimental data.

This was demonstrated with the example of ${}^6\text{He}$. The dissociation of ${}^6\text{He}$ on a lead target, where the main contribution is expected from the electromagnetic dissociation, has been studied at 240 MeV/u.

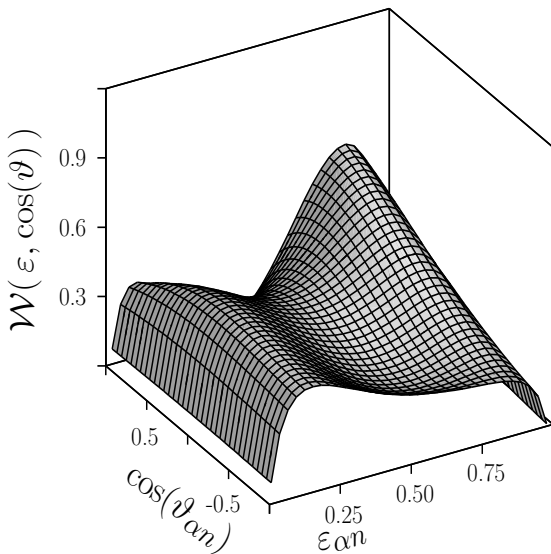


Figure 1: Two-dimensional correlation spectrum reconstructed from the fit to the experimental distributions in the continuum energy region 3-6 MeV.

The experimental continuum energy spectrum and the angular distributions for breakup of the 240 MeV/u ${}^6\text{He}$ nucleus on a lead target are well described under the assumption of pure electromagnetic dipole dissociation without involving any other reaction mechanisms, while using

different theoretical approaches (see Refs. [1, 2]). The inclusion in the analysis of the three-body correlation distributions results in more strict and quantitative conclusions.

The three-body correlation distributions have, for the first time, been used in the analysis. The distributions have been directly compared with the results of calculations using the hyperspherical harmonics method while assuming a dipole mode for the electromagnetic dissociation [1]. The experimental data have also been analyzed by using a series expansion of the final transition amplitude into hyperspherical functions.

Besides the orientation of the whole system, the three-body configuration is determined by the angle $\vartheta_{\alpha n}$ between Jacobi momenta $\mathbf{q}_{\alpha n}$ and $\mathbf{q}_{n-\alpha n}$, by the total energy of the three-body system E , and by the energy shared in a selected pair of particles, e.g. fractional energy in the subsystem $\alpha-n$, $\varepsilon_{\alpha n} = q_{\alpha n}^2/E$. The dependence of $\vartheta_{\alpha n}$ on $\varepsilon_{\alpha n}$ reconstructed from experimental data in the region $3 < E < 6$ is shown in Fig. 1. Two distinct ridges of the distribution in Fig. 1 correspond to the αn interaction forming the ${}^5\text{He}(3/2^-)$ resonance. The role of this resonance is more important than expected from the hyperspherical harmonics method [1], but is in line with the results of the calculations made in the framework of the complex scaling method [2]. The analysis has shown that the transition of one neutron from the p -shell to the s -shell dominates. This statement is consistent with the calculations [1, 2] at low energies, but in the energy region 3-6 MeV, theoretical considerations predict a larger contribution from the p - to d -shell transition. The analysis points out the existence of a ${}^6\text{He}$ resonant state with a $p_{3/2}s_{1/2}$ structure at continuum energy 3 - 6 MeV.

Thus, the new experimental observables pose new questions to the theoretical models for the dissociation of the Borromean nucleus ${}^6\text{He}$ at high energy, and give interesting insight in the development of the theory.

References

- [1] B.V. Danilin *et al.*, Nucl. Phys. **A 632** (1998) 383
- [2] T. Myo *et al.*, Phys. Rev. **C63** (2001) 054313

Breakup of relativistic halo nuclei (ii)

P. Adrich^{a,h}, T. Aumann^{a,e}, O. Bochkarev^b, M.J.G. Borge^f, L.V. Chulkov^{a,b}, D. Cortina^a, Th.W. Elze^g, J. Fernandez-Vazquez^a, U. Datta-Pramanik^a, H. Emling^a, H. Fynbo^j, H. Geissel^a, L.V. Grigorenko^{a,b}, M. Hellström^a, H. Johansson^{a,d}, A. Klimkiewicz^{a,h}, K. Jones^a, B. Jonson^d, J.V. Kratz^e, R. Kulessa^h, Le Hong Khiem^a, E. Lubkiewicz^h, K. Markenroth^d, M. Meister^{a,d}, G. Münenberg^a, F. Nickel^a, T. Nilsson^{i,k}, G. Nyman^d, M. Pantea^{a,k}, R. Palit^a, V. Pribora^b, W. Prokopowic^h, A. Richter^k, K. Riisager^j, C. Scheidenberger^a, G. Schrieder^k, H. Simon^a, K. Sümmeler^a, O. Tengblad^f, I.J. Thomson^c, W. Walus^h, and M.V. Zhukov^d

^aGSI Darmstadt; ^bKurchatov Institute, Moscow; ^cUniversity of Surrey, Guilford; ^dChalmers Tekniska Högskola, Göteborg; ^eJohannes-Gutenberg-Universität, Mainz; ^fCSIC, Madrid; ^gJohann-Wolfgang-Goethe-Universität, Frankfurt; ^hUniversytet Jagiellonski, Krakow; ⁱCERN, Geneva; ^jAarhus Universitet, Aarhus; ^kTechnische Universität, Darmstadt

The quasi-free scattering (QFS) is the dominant reaction mechanism in the nuclear breakup at several hundred MeV/nucleon and provide quite precise information concerning clustering effects in nuclei. In QFS, a probe particle scatters off a bound cluster inside a nucleus. The process leads to a separation of the cluster from the nucleus, the rest of the nucleus acts as a spectator. The transition amplitude may be separated into a reaction term and a nuclear structure term, this property is a prerequisite for nuclear-structure investigations. In the past, QFS studies have provided a wealth of nuclear structure information for stable nuclei. The application of this method to experiments with radioactive beams is very promising. The QFS method has been used in investigations of the cluster structure of drip-line nuclei Refs. [1, 2]. However, these experiments were restricted mainly to the valence-neutron knockout by a complex particle (⁹Be or ¹²C). Here we describe a complete-kinematics experiment with

of the recoil proton allows the separation of different QFS channels [3], while a registration of neutrons in coincidence with fragments makes possible the usage of an invariant-mass method.

Table 1: Preliminary cross sections (mb) for different reaction channels.

Channel	⁸ He	¹¹ Li	¹⁴ Be
-2n	20.6 ⁶ He	42.4 ⁹ Li	56.4 ¹² Be
-3n	-	28.5 ⁸ Li	24.1 ¹¹ Be
-4n	6.5 ⁴ He	15.6 ⁷ Li	-
-p2n	-	4.9 ⁸ He	5.9 ¹¹ Li
-p3n	-	-	-
-p4n	0.5 ³ H	10.4 ⁶ He	8.7 ⁹ Li
-p5n	-	-	7.8 ⁸ Li
-p6n	-	9.2 ⁴ He	7.1 ⁷ Li

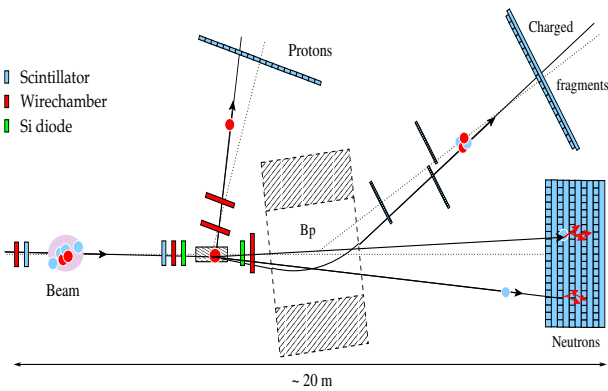


Figure 1: Experimental setup.

a proton as a probe particle and present preliminary results. The experiment was performed at GSI, Darmstadt, where radioactive beams were produced by fragmentation of ¹⁸O (308 MeV/nucleon and 362 MeV/nucleon) beams from the heavy-ion synchrotron, SIS, on a beryllium production target. The secondary ⁸He, ¹¹Li and ¹⁴Be beams with energies of 230 MeV/nucleon, 265 MeV/nucleon and 290 MeV/nucleon, respectively, were selected by magnetic analysis in the fragment separator, FRS, and directed towards the liquid-hydrogen target which was placed in front of the large-gap magnetic dipole spectrometer, ALADIN. The experimental setup is shown in Fig. 1. A detection

Estimated cross sections for the breakup of ⁸He, ¹¹Li and ¹⁴Be resulting in different fragments in the final state are shown in Table 1. The neutron knockout has largest cross section. Note, that for Borromean nuclei this channel leads to neutron unstable states. Large cross section is observed for channels which might be associated with the proton knockout. Proton knockout channels will lead to the nuclear-unstable resonances ⁷H, ¹⁰He and ^{12,13}Li. The α -particle knockout from ⁸He is of special interest in connection with recently renewed discussions of a bound tetra-neutron nucleus [4]. Besides, the spectroscopic factors for neutrons, protons α clusters, and momentum distributions of knocked-out particles and of the spectators are among the main goals of the present experiment.

References

- [1] B. Jonson, Phys. Rep. **389** (2004) 1.
- [2] B.A. Brown, P.G. Hansen, B.M. Sherrill, J.A. Tostevin, Phys. Rev. **C 65** (2001) 061601(R).
- [3] L.V. Chulkov *et al.*, submitted to Nucl. Phys. A.
- [4] F.M. Marquéset *et al.*, Phys. Rev. **C 65** (2002) 044006.

The r-process in the high-entropy bubble scenario

K. Farouqi^{1,2}, K.-L. Kratz^{1,2}, B. Pfeiffer^{1,2}, C. Freiburghaus³, F.-K. Thielemann³ and T. Rauscher³

¹Institut für Kernchemie, Universität Mainz, Germany; ²HGF Virtual Institute for Nuclear structure and Astrophysics, Mainz, Germany; ³Departement für Physik und Astronomie, Universität Basel, Switzerland

Using dynamical r-process network calculations based on the high-entropy bubble scenario as a possible site for the r-process we were able to investigate some quite important features of the nucleosynthesis in the above mentioned astrophysical model.

A brief summary of the high-entropy bubble scenario is as follows. During the final stages of the evolution of a massive ($8 - 25 M_{\odot}$) star, an “iron” core forms in its central region and subsequently undergoes gravitational collapse. When the central density reaches nuclear matter density, the collapse stops abruptly to cause a “core bounce”. A shock wave is created and starts to propagate outward. According to hydrodynamical calculations [1], this shock wave loses its entire kinetic energy within a few milliseconds to stall well inside the outer edge of the initial iron core, and no immediate disruption (a “prompt” explosion) of the star occurs. On a timescale from several tens of milliseconds to about half a second, the neutrinos streaming out from the new-born neutron star can deposit energy behind the standing accretion shock at a rate high enough to revive its outward motion and initiate the final explosion of the star. This is the neutrino-driven “delayed” explosion mechanism originally suggested by Wilson [2].

The main parameters in this model are the entropy S , the electron abundance Y_e and the expansion speed of the bubble V_{exp} . The relation between those three parameters is given by the simple formula

$$\frac{Y_n}{Y_{seed}} = k_{SN} V_{exp} \left(\frac{S}{Y_e} \right)^3, \quad k_{SN} \approx 8,05835 \times 10^{-11}.$$

In fact, the entropy S is not constant in the whole expanding bubble. In a realistic approach to this problem, one divides the occurring high-entropy bubble in several mass regions, and then with a detailed hydrodynamical simulation one can determine for each mass region the corresponding entropy. Since we do not do hydrodynamical simulations, we used a simple fit function like

$$g_i = g(S_i) = X_1 e^{X_2 S_i}, \quad i = 1, \dots, n.$$

g_i is the weight factor of the i th component which we mix in, X_2 determines the slope of the weight function and X_1 is a global value showing the superposition to the experimental measured curve of the isotopic solar abundances.

In fact, it is really hard to fit the whole range between $A=120$ and $A=209$ because of the lack of the neutron capture rates for the nuclei with $Z \geq 84$ and the occurrence of spontaneous and n-induced fission of the nuclei with $A \geq 250$.

The figure 1 shows an example of a superposition by using the ETFSI-Q formula. It was shown that the idea of an instantaneous freeze-out is only approved if the neutron-to-seed ratio is about the unity. Nevertheless, in that case an effective r-process cannot take place.

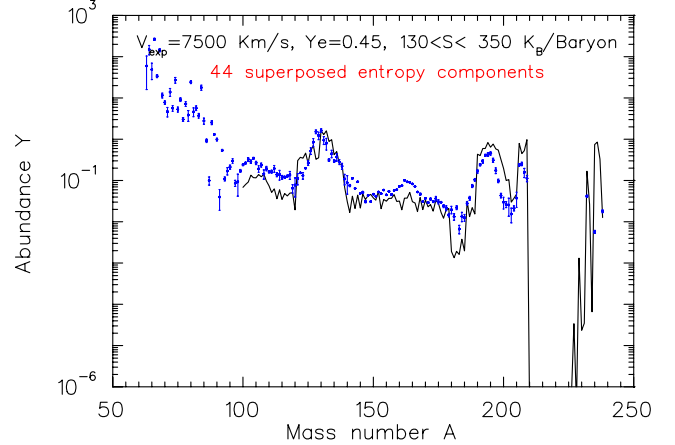


Figure 1: Superposition of abundances from 44 components to reproduce the solar r-abundances beyond $A \simeq 120$

Therefore the canonical approach of the r-process can be seen as a snapshot of the dynamical approach in a certain time t before the total disappearance of the neutrons.

Among other things we determine the odd-to-even ratio of the three barium isotopes ($A=135, 137$ and 138) which are synthesised by the s- and r-process.

The odd-to-even ratio for the solar r-abundances is

$$\text{Ratio} = \frac{Y^{(135)\text{Ba}} + Y^{(137)\text{Ba}}}{Y^{(135)\text{Ba}} + Y^{(137)\text{Ba}} + Y^{(138)\text{Ba}}} = 0,72.$$

The table below shows the obtained results for a fixed expansion speed and variable Y_e and S .

Mass model	V_{exp} (km/s)	Entropy (k_B /Baryon)	Y_e	Ratio
ETFSI-Q	7500	210	0.49	0.764
		185	0.47	0.758
		165	0.45	0.742
		145	0.43	0.767
		125	0.41	0.818
FRDM	7500	225	0.49	0.804
		205	0.47	0.713
		185	0.45	0.740
		160	0.43	0.788
		145	0.41	0.810

References

- [1] Myra & Bludman, 1989, ApJ 340, 384
- [2] Wilson, J. R., 1985, in Numerical Astrophysics

Neutron captures and the r-process

K. Farouqi^{1,2}, K.-L. Kratz^{1,2}, B. Pfeiffer^{1,2}, F.-K. Thielemann³, and T. Rauscher³

¹Institut für Kernchemie, Universität Mainz, Germany; ²HGF Virtual Institute for Nuclear Structure and Astrophysics, Mainz, Germany; ³Departement für Physik und Astronomie, Universität Basel, Switzerland

Based on the early description of the electric dipole (E1) strength function of Kadmenkii et al. [1], in a more recent paper Goriely [2] has studied the possible relevance of the existence of a "pygmy" dipole resonance (PDR) in the low-energy tail of the giant dipole resonance (GDR) for neutron-capture cross-section ($\sigma_{n,\gamma}$) calculations. Under certain conditions, i.e. for nuclei where the PDR lies close to the neutron separation energy (S_n), the author predicts local enhancements of the Hauser-Feshbach cross sections by more than a factor 100. If confirmed experimentally, this would result in pronounced consequences for the r-abundance distribution.

To our knowledge, for the first time results from an experiment aimed on the determination of the GDR and the low-lying E1 PDR on medium-heavy, neutron-rich isotopes have been obtained at the LAND-FRS facility of GSI [3]. With respect to possible astrophysical consequences, the measured position of the PDR in ^{130}Sn and ^{132}Sn is of major interest, because some earlier models have predicted considerably lower energies of the PDR in neutron-rich nuclei, in the vicinity of their S_n values. With the known $E(\text{PDR})=9.8$ MeV and $S_n=7.3$ MeV in ^{132}Sn , we now can conclude that at least for this isotope, and presumably for the whole $A\simeq 130$ mass region of astrophysical interest, there will be no significant enhancement of the $\sigma_{n,\gamma}$ value due to the PDR. This is in contrast to what one would extract from e.g. Fig. 3 of [2]. Moreover, we are unable to reproduce the r-abundance calculations shown in Fig. 6a of [2] by any combination of realistic nuclear and astrophysical parameters.

In order to investigate the actual impact of altered $\sigma_{n,\gamma}$

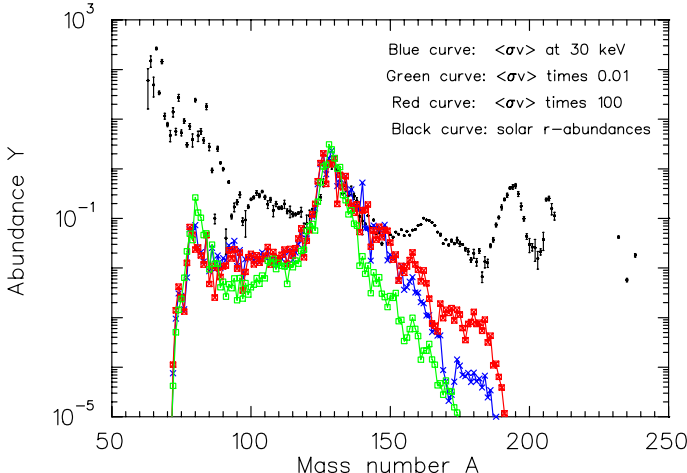


Figure 1: Decayed final abundances of the $S=196$ -entropy component. The neutron capture rates are changed in a range of 4 orders of magnitude.

values of r-process nuclei, we have performed a series of full dynamic network r-process calculations in the model of an adiabatically expanding hot entropy bubble [4, 5]. For the calculations shown below, the seed abundances for

the r-process were obtained from an α -rich freeze-out of a charged-particle network. For the subsequent r-process, an almost instantaneous (n,γ) – (γ,n) equilibrium is established at the onset of the r-process. Therefore, only late-time neutron captures are important, which are then expected to mainly modify the abundances around the r-process peaks at $A\simeq 130$ and 195.

Fig. 1 shows a snapshot for a parameter combination of $Y_e=0.45$, $S=196$ and an expansion time scale of 35 ms, which is representative for the formation of the $A\simeq 130$ r-abundance peak. In order to take into account considerable uncertainties in the $\sigma_{n,\gamma}$ values, we have scaled the "standard" rates of [6] up and down by a factor 100. Fig. 2 shows the corresponding curves for the development of the neutron number densities as a function of time, again for the above three assumptions on the capture rates. As is clearly evident from Fig. 1, even these large variations in the $\sigma_{n,\gamma}$ values do not affect the final r-abundances in the $A\simeq 130$ peak region, despite the different – but still "fast" – freeze-out behavior shown in Fig. 2. However, components with high entropies, which synthesize heavier r-process nuclei ($A>140$), tend to freeze out slower. Here, late-time neutron captures on nuclei near stability – and not on isotopes in the initial r-process path – can modify the final abundance pattern, in particular around the $A\simeq 195$ peak [5].

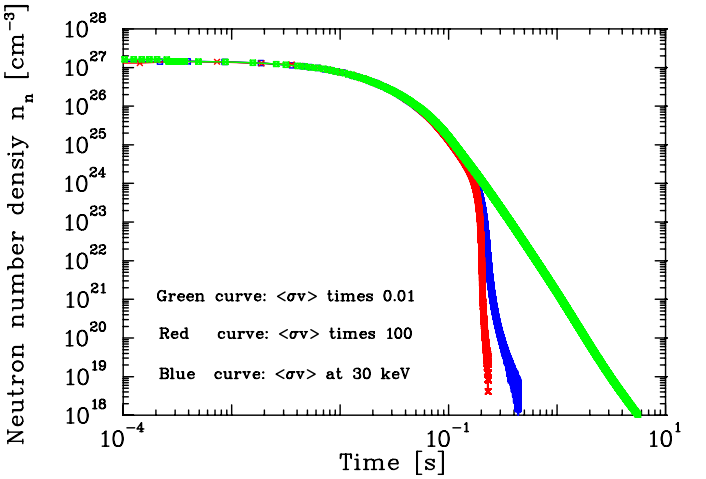


Figure 2: Time evolution of the neutron number density. For $n_n \leq 10^{17}$ ($<\sigma v>$) and $n_n \leq 10^{18}$ ($<\sigma v> \times 100$), the available neutrons are completely exhausted.

References

- [1] S.G. Kadmenkii et al., Sov. J. Nucl. Phys. 37, 165 (1983)
- [2] S. Goriely, Phys. Lett. B 436, 10 (1998)
- [3] P. Adrich et al., Annual Report, Mainz 2004
- [4] C. Freiburghaus et al., Ap. J. 516, 381 (1999)
- [5] K. Farouqi, PhD Thesis, Mainz 2005
- [6] T. Rauscher & F.-K. Thielemann, ADNDT 75, 1 (2000)

Influence of thermally excited isomers on r-process abundances?

B. Pfeiffer^{1,2} and K.-L. Kratz^{1,2}

¹Institut für Kernchemie, Universität Mainz, Germany; ²HGF VISTARS

The influence of nuclear physics input as well as astrophysical parameters on the abundances of r-process nucleosynthesis can be studied systematically within the “waiting-point” concept [1]. Calculations applying theoretical nuclear masses and $T_{1/2}$ and P_n values from the FRDM or the ETFSI-Q mass models allow a satisfactory reproduction of the global isotopic abundances ($N_{r,\odot}$). Nevertheless, there still exist deviations in limited mass regions as the left wing of the $A \approx 130$ peak (see black line in Fig. 1). Even replacing the theoretical values with experimental ones (as far as available) does not solve the problem (see Ref. [3]).

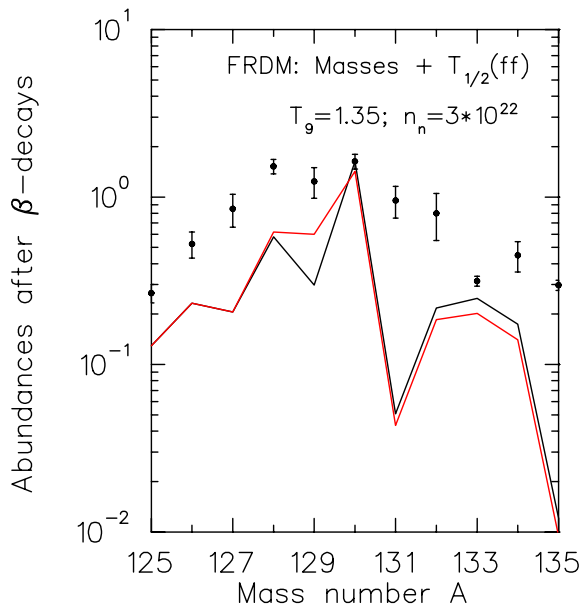


Figure 1: Solar r-process abundances calculated with masses and half-lives from the FRDM mass model [2]. The half-life of ^{129}Ag is either taken as the $\pi g_{9/2}$ g.-s. [black line] or as $T_{1/2}=180$ ms [red line] (see text).

As the abundances are proportional to the half-lives of the precursor nuclei in the r-process boulevard, longer half-lives for the $N=82$ nuclei with $Z \leq 47$ could be a solution. The r-process nucleosynthesis takes place in a heat bath with temperatures in excess of $1 T_9$. In the case of ^{129}Ag we have observed indications to the existence of an isomeric β -decaying $\pi p_{1/2}$ state with $T_{1/2}=160$ ms in addition to the $\pi g_{9/2}$ ground-state (g.-s.) decay with $T_{1/2}=46$ ms [4]. The excitation energy of the isomeric state is not known experimentally. QRPA calculations yield 500 keV. The stellar half-life of ^{129}Ag is shown in Fig. 2 as a function of the equilibrium temperature in units of 10^9 K (T_9). At the freeze-out temperature of $1.35 T_9$, the stellar half-life is only marginally enhanced due to the high excitation energy, not influencing the abundance at $A=129$.

If one follows the γ -decay of unbound states populated

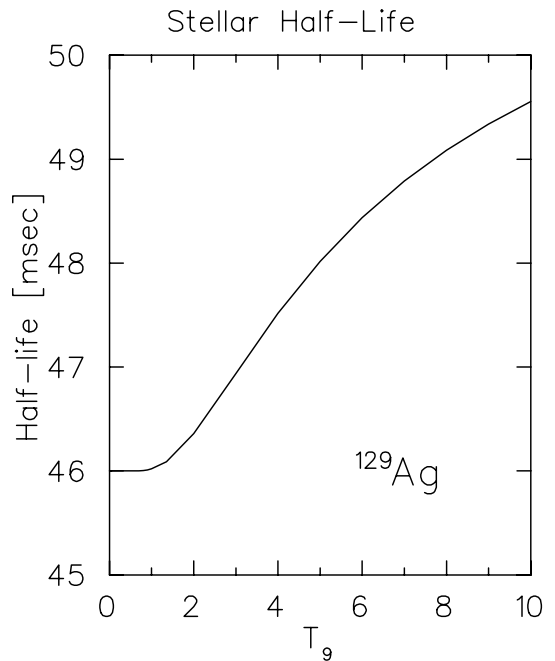


Figure 2: Stellar half-life of ^{129}Ag as a function of temperature. $T_{1/2}$ for the $\pi g_{9/2}$ g.-s. is 46 ms and 160 ms for the $\pi p_{1/2}$ β -isomeric state, respectively. The excitation energy of the isomeric state is assumed as 500 keV according to QRPA calculations.

in neutron capture on ^{128}Ag under non-equilibrium conditions, about one third of the rays populate the isomeric state [5]. From this a stellar half-life of about 80 ms can be deduced, much longer than in the case of the thermal excitation under equilibrium condition. The isotopic abundances obtained in replacing the short g.-s. half-life of ^{129}Ag with this longer value are displayed in Fig. 1 [red line]. The abundance for $A=129$ is now closer to the observed value.

The general solution for the calculated underabundances in the left wing of the $A=130$ peak has to be sought in nuclear structure different from the assumptions underlying the global mass models. Applying single-particle energies which reproduce the surprisingly high-lying 1^+ state in ^{130}Cd in Nilsson model calculations of β -decay half-lives of nuclides in the left wing, longer half-lives were obtained [3].

References

- [1] K.-L. Kratz et al., Ap. J. **403**, 216 (1993).
- [2] P. Möller et al., Phys. Rev. **C67**, 055802 (2003).
- [3] B. Pfeiffer, <http://www.jinaweb.org/events/process/Pfeiffernd05a-d.pdf>
- [4] <http://www.kernchemie.uni-mainz.de/~pfeiffer/khf/>
- [5] T. Rauscher, priv. communication.

How doubly-magic is the nucleus $^{78}_{28}\text{Ni}_{50}$?

B. Pfeiffer^{1,2} and K.-L. Kratz^{1,2}

¹Institut für Kernchemie, Universität Mainz, Germany; ²HGF VISTARS

Doubly-magic nuclei play an important role in nuclear structure theory as testbeds for shell model calculations. Data on neutron-rich nuclei in the regions of doubly-magic nuclei such as $^{78}_{28}\text{Ni}_{50}$ and $^{132}_{50}\text{Sn}_{82}$ have a decisive influence on nucleosynthesis calculations. These “longer-lived” waiting-point nuclei determine the duration of the r-process and the matter flow through the abundance maxima at the magic neutron numbers [1]. Remaining deficiencies prior to the abundance maxima in r-process calculations have been interpreted as signatures of new nuclear structure effects near the neutron drip-line, for example overestimation of the shell strength far from stability in global mass models such as FRDM and ETFSI-1. A

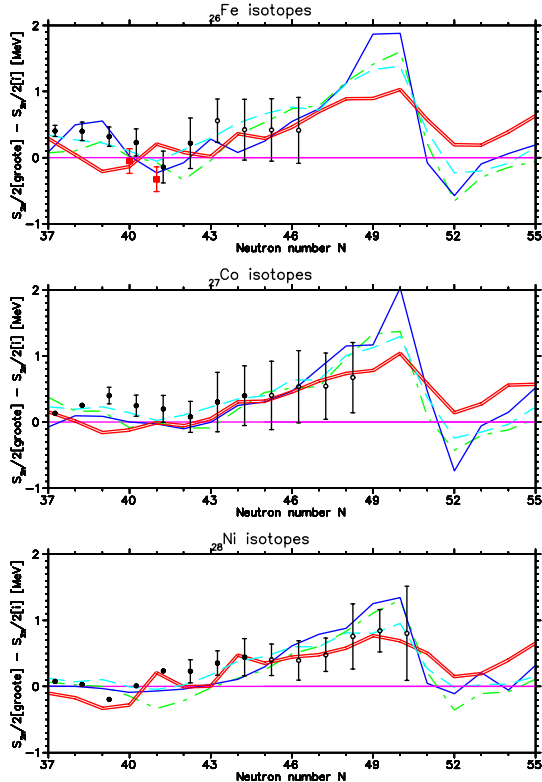


Figure 1: Deviations of experimental [black dots: 2003 mass evaluation [7], red squares: FRS/ESR measurements [8]] and theoretical S_{2n} values from the smoothly varying Groote mass formula [2] across the shell gap at $N=50$ are shown for ^{26}Fe (upper part), ^{27}Co (middle part) and ^{28}Ni (lower part) isotopes. [Theoretical masses: Groote: magenta, FRDM: red [3], ETFSI-1: cyan [4], HFB-2: green [5], HFB-8: blue [6]]

weakening (“quenching”) of spherical shells with increasing isospin, resulting in a gradual setting in of collectivity, has been predicted by recent HFB calculations, and is well established for the lower neutron-magic numbers $N=20$ and $N=28$.

In this context, it is of interest to determine the mutual influence of the proton and neutron magic numbers far from stability. The shell strength can be derived from the dif-

ferences of the two-neutron separation energies S_{2n} prior and behind a magic neutron number. Fig. 1 displays differences between experimental and theoretical S_{2n} values relative to the smoothly varying mass formula of Groote et al. [2] for Fe, Co and Ni isotopes.

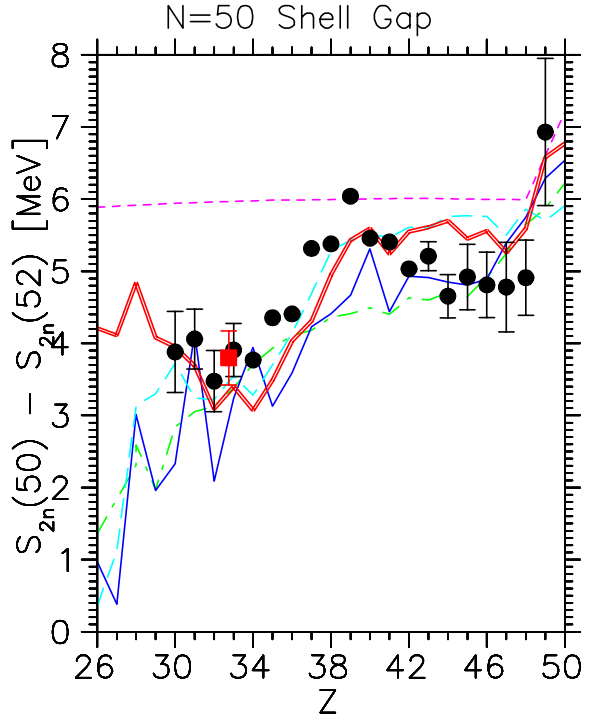


Figure 2: The $N=50$ shell gap as a function of Z . Experimental and extrapolated values from the 2003 mass evaluation [7] (black circles) and experimental values from direct mass measurements at ESR/FSR [red square] are compared to theoretical mass models. [Same colour coding for the mass models as in Fig. 1.]

Fig. 2 shows the $N=50$ shell gap over a wide Z range. Most global mass models predict a local maximum for doubly-magic ^{78}Ni . So far, below $Z=30$ no experimental masses have been determined, so that this prediction cannot be verified. With upgraded U-beams, direct mass measurements at the FRS-ESR of GSI will in future extend the range of experimental masses in this region to more neutron-rich isotopes.

References

- [1] K.-L. Kratz et al., Ap. J. **403**, 216 (1993).
- [2] H. von Groote et al., ADNDT **17**, 418 (1976).
- [3] P. Möller et al., ADNDT **66**, 131 (1997).
- [4] Y. Aboussir et al., ADNDT **61**, 127 (1995).
- [5] S. Goriely et al., ADNDT **77**, 311 (2001).
- [6] M. Samyn et al., Phys. Rev. **70**, 044309 (2004).
- [7] G. Audi et al., Nucl. Phys. **A729**, 3 (2003).
- [8] M. Matos, PhD thesis, Giessen (2004).

N=82 shell gap above $^{132}_{50}\text{Sn}_{82}$

B. Pfeiffer^{1,2} and K.-L. Kratz^{1,2}

¹Institut für Kernchemie, Universität Mainz, Germany; ²HGF VISTARS

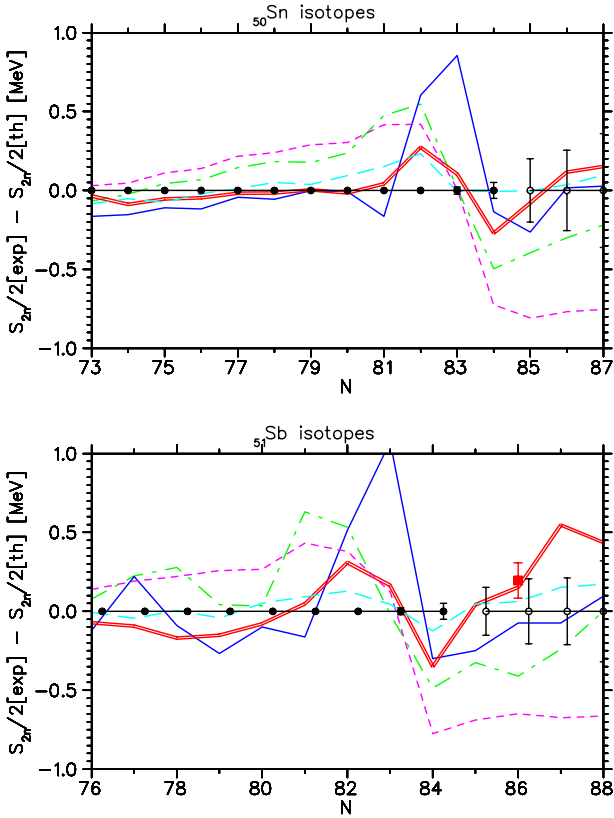


Figure 1: Differences between experimental two-neutron separation energies (S_{2n}) [black dots: 2003 mass evaluation [3], red squares: FRS/ESR measurements [4]] and theoretical values across the shell gap at $N=82$ are shown for ^{50}Sn (upper part) and ^{51}Sb isotopes (lower part). [Theoretical masses: Groote: magenta, FRDM: red, ETFSI-Q: cyan, HFB-2: green, HFB-8: blue]

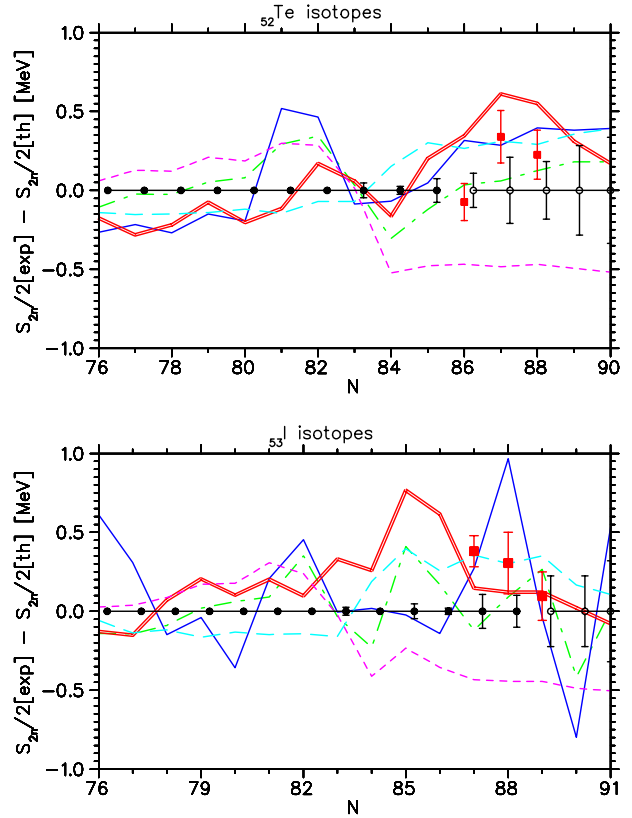


Figure 2: Same notation as for Fig. 1 for ^{52}Te (upper part) and ^{53}I isotopes (lower part).

The influence of nuclear structure on the r-process nucleosynthesis can be studied within the “waiting-point” concept [1]. The successful reproduction of the global isotopic abundances ($N_{r,\odot}$) as well as remaining deficiencies have been interpreted by our group as signatures for new nuclear structure patterns for unstable nuclei [1]. One such effect is an overestimation of the $N=82$ and 126 shell strength in global mass models such as FRDM and ETFSI-1. A weakening (“quenching”) of spherical shells with increasing isospin, resulting in a gradual setting in of collectivity, is well established for the lower neutron-magic numbers and has been predicted by HFB calculations for the spherical shells at $N=82$ and 126 [2].

Signatures for a “quenching” of the shell strength can be derived from two-neutron separation energies (S_{2n}) across a magic neutron number. Studies of the $N=82$ nuclide ^{130}Cd at CERN-ISOLDE yielded a surprisingly high Q_β value, which is only in agreement with recent mass models that include the phenomenon of $N=82$ shell “quenching” [5, 6]. First direct mass measurements on neutron-

rich isotopes at FRS-ESR yielded data on isotopes beyond the double-magic nucleus ^{132}Sn . Together with the experimental and short-range extrapolated masses from the 2003 mass evaluation [3], a meaningful comparison with theoretical approaches is now possible. As an example, Figs. 1 and 2 display S_{2n} values for ^{50}Sn , ^{51}Sb , ^{52}Te and ^{53}I isotopes. Surprisingly, the “old” models ETFSI-Q and FRDM perform better than recent self-consistent HFB approaches as the HFB-2 and especially HFB-8 from the Brussels-Montreal group. But, the discrepancies increase with distance to the magic proton number $Z=50$ for all models.

Direct mass measurements with upgraded U-beams at FRS-ESR will extend the range of experimental masses at $N=50$, 82 and 126 closer to the r-process “boulevard”.

References

- [1] K.-L. Kratz et al., Ap. J. **403**, 216 (1993).
- [2] B. Pfeiffer et al., Acta Physica Polonica **27**, 475 (1996).
- [3] G. Audi et al., Nucl. Phys. **A729**, 3 (2003).
- [4] M. Matos, PhD thesis, Giessen (2004).
- [5] I. Dillmann et al., Phys. Rev. Lett. **91**, 162503 (2003).
- [6] B. Pfeiffer and K.-L. Kratz, Ann. Rep. 2003, Inst. f. Kernchemie, A13.

Prediction for the Pb abundance in ultra-metal-poor Halo stars

B. Pfeiffer^{1,2} and K.-L. Kratz^{1,2}

¹Institut für Kernchemie, Universität Mainz, Germany; ²HGF VISTARS

Age determinations of geological or meteoritical samples can be performed by comparing the content of Th and/or U with their respective α -decay daughters $^{206-208}\text{Pb}$. Due to their long half-lives, ^{232}Th [14.05 Ga] and ^{238}U [4.468 Ga] are ideal cosmochronometers [1]. In the very early phases of nucleosynthesis, only r-process contributions from core-collapse supernova explosions of massive short-lived stars have to be taken into account. But, there are a number of problems to be solved. The old stars are found in the Galactic Halo quite distant from the Earth. In order to take high-resolution optical spectra, big telescopes are needed. Th and U are radioactive; hence since their production about one half of Th, all ^{235}U and 90% of ^{238}U have been decayed. The Pb isotopes at the end of the decay chains are stable, but optical transitions are in the UV which is strongly absorbed in the Earth's atmosphere. It is an advantage that the content of "metals" as Fe in these stars is typically a factor 10^3 lower than in the Sun, thus reducing blending by strong Fe absorption lines. Th can only be observed in the class of neutron-capture element enhanced ultra-metal-poor stars such as CS22892-052. For U and Pb, only upper limits of the abundances could be determined. Comparing the observed Th/Eu ratio with the production ratio derived from our r-process nucleosynthesis calculations, an age of (14.2 ± 3) Ga was determined [3]. The firm determination of a U abundance in a Halo star has been reported for CS31082-001 [4].

Recently, two groups of astronomers (with whom we collaborate since several years) have obtained long observation times on the Hubble Space Telescope in order to detect Pb in CS31082-001 and CS22892-052, respectively. The STIS spectrometer was specially adapted to UV observations not possible from the ground. Within this collaboration, we were asked to predict the Pb abundances in these stars. Tab. 1 lists abundances of $^{206-208}\text{Pb}$, ^{209}Bi , ^{232}Th and $^{235,238}\text{U}$: 1) directly after the nucleosynthesis event and after β -decay of the extremely neutron-rich precursors in the r-process boulevard; 2) after the α -decays with $T_{1/2}$ in the order of several 10 Ma; and 3) after 13.5 Ga.

Tab. 2 lists predicted and observed values for elemental abundances. The isotopic abundances of Tab. 1 were scaled down to the metallicity of the stars by fitting the rare-earth elements. In the case of CS31082-001, the "actinide boost" [4, 5] was determined from ^{72}Hf . All predicted abundances for $Z \geq 72$ were multiplied by a factor 2.4. With this scaling, there is nearly perfect agreement between the predicted and observed values for Th and U. The situation for Pb is, however, less satisfactory. The observed value of (-0.03 ± 0.15) dex [6] for CS22982-052 is slightly above our prediction. On the other hand, Plez et al. reported a Pb abundance for CS32081-001 of (-0.55 ± 0.15) dex [7], much lower than our predictions. Their value is even lower than the fraction of

Table 1: Isotopic abundances from r-process nucleosynthesis calculations [2] in units of $\text{Si} \equiv 10^6$. In the first column are listed abundances after β -decays directly following the explosion. Abundances after α -decays of "short-lived" nuclei as the ones in the Np-chain are tabulated in the second column, and after 13.5 Ga in the third one.

Isotopes	Abundances after		
	β -decays	"short-lived"	13.5 Ga
Pb-206	0.0217	0.1426	0.1637
Pb-207	0.0182	0.1075	0.1447
Pb-208	0.0287	0.1245	0.1443
$\Sigma \text{ PB}$	0.1122	0.3746	0.4527
Bi-209	0.0152	0.1013	0.1013
Th-232	0.0183	0.0415	0.0217
U-235	0.0091	0.0368	
U-238	0.0075	0.0230	0.0019

Table 2: Predicted and observed elemental abundances for two Halo stars in [dex] units. The observed values except for Pb are taken from [3] for CS22892-052 and [4] for CS31082-001. The Pb values are from [6] and [7], respectively.

Element	CS22892-052		CS31082-001	
	pred.	obs.	pred.	obs.
Hf	-1.21	-0.98	-0.61	-0.59
Os	-0.26	0.06	0.33	0.43
Ir	-0.23	0.00	0.36	0.20
Pb	-0.23	-0.03	0.36	-0.55
Bi	-0.88		-0.29	
Th	-1.55	-1.57	-0.96	-0.98
U	-2.61	<-2.3	-2.02	-1.92

the lead synthesized directly in the SN explosion (-0.25 dex). Therefore, one may ask where is the Pb from the α -decay chains (-0.36 dex) from Th and U observed in this star? Abundances similar to those shown in Tab. 1 have been reported in [8]. We therefore conclude that the strong discrepancy between predicted and observed Pb abundances in CS32081-001 cannot be caused by the underlying assumptions on nuclear structure.

References

- [1] K.-L. Kratz et al., NewAR **48**, 105 (2004).
- [2] J.J. Cowan et al., ApJ **521**, 194 (1999).
- [3] C. Sneden et al., ApJ **591**, 936 (2003).
- [4] V. Hill et al., A & A **387**, 560 (2002).
- [5] H. Schatz et al., ApJ **579**, 626 (2002).
- [6] J.J. Cowan, priv. comm.
- [7] B. Plez et al., A & A **428**, L9 (2004).
- [8] S. Goriely and M. Arnould, A & A **379**, 1113 (2001).

GAS THERMOCHROMATOGRAPHY FOR ION SOURCE DEVELOPMENT

C. Jost, O. Arndt, K.-L. Kratz (Institut für Kernchemie, Mainz), U. Köster (CERN), A. Kronenberg (ORNL)

The adsorption behaviour of Zn, Rb, As, Ag, In, Cd and Cs on quartz glass surfaces was studied at the new ISOLDE (CERN) gas thermochromatography setup. A high retention of alkali metals and a high volatility of Cd were observed and will be utilised for improved quality of Cd beams at ISOLDE experiments in 2005.

1 INTRODUCTION

In recent years very neutron-rich isotopes of silver (Ag [1]), cadmium (Cd [2]) and indium (In [3]) have been identified by resonant laser ionization at ISOLDE and their half-lives were measured by detection of beta-delayed neutrons. However, detailed $\beta\gamma$ spectroscopy is still hampered by the omnipresent background of huge amounts of surface ionized cesium and indium (in the case of Ag and Cd) isobars. In the present study we concentrated on the suitability of fused silica surfaces to retain these elements, which could supplement the selectivity of the resonant laser ionisation by a chemical pre-separation. Earlier studies [4] proposed quartz surfaces for this purpose.

2 EXPERIMENTAL

A new thermochromatographic (TC) setup has been installed at the offline experimental hall at ISOLDE. The setup can be used for gas or vacuum thermochromatography. The addition of a reactive second gas is also possible.

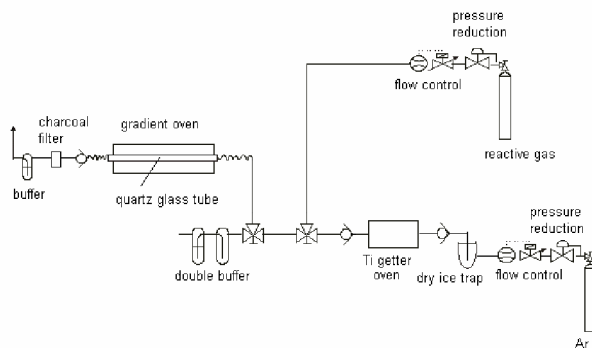


Fig. 1: Setup of the TC experiment at ISOLDE (CERN)

The radiotracers (^{65}Zn , ^{74}As , ^{84}Rb , ^{105}Ag , ^{114m}In , ^{115m}Cd and $^{134,136}\text{Cs}$) were produced at ISOLDE and implanted into Ta foils. For investigation of non-carrier free Cs, CsNO_2 was irradiated at TRIGA Mainz and also applied to Ta foils. The samples were inserted into a quartz glass thermochromatography column of 150 cm length with 6 mm inner diameter. The column was placed into a 10 zone gradient oven with a maximum temperature of 1200 °C. The temperature gradient was approximately linear with 1200 °C/m. The applied gas flow (Ar) varied between 20 and 100 ml/min. The samples were exposed to the temperature gradient for 1h. After cooling, the tubes were scanned with an HPGe detector in steps of 2 cm by use of a Pb collimator. The activity distribution was determined by γ -spectroscopy.

3 RESULTS

All radiotracers except As were released from the sample foils. The alkali metals (Rb and Cs) show a high adsorption enthalpy, probably due to chemical reaction [5]. For Cs, both chemisorption and physisorption occur, and thus several peaks can be observed. As expected, cadmium was barely retained on the quartz glass surface, but remained volatile even below 100 °C. Indium was found to be slightly less volatile on the used surface. Often a second indium peak was observed at lower temperatures, probably corresponding to indium oxide produced from oxygen impurities. Silver shows a medium retention on the quartz glass surface.

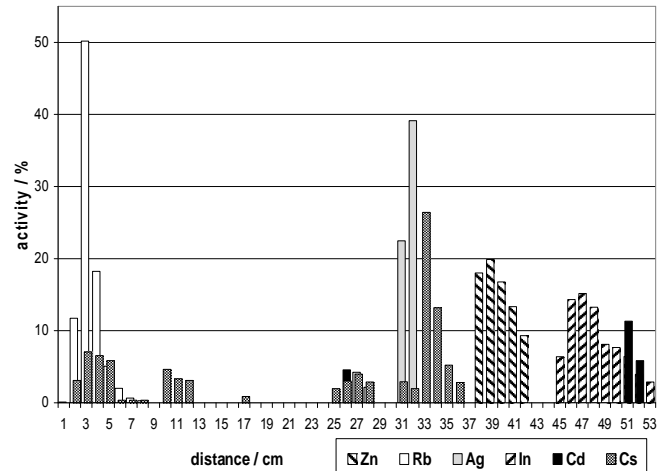


Fig. 2: The deposition of Zn, Rb, As, Ag, In, Cd and Cs on quartz surfaces.

4 OUTLOOK

Due to the obtained results the use of a quartz glass transfer line connecting the target to the resonance ionization laser ion source will be tested at ISOLDE experiments (amongst others at REX-ISOLDE). Hopefully, background from Cs isobars and short-lived In isotopes will be suppressed by a large factor. As silver shows a noticeable adsorption on quartz glass surfaces, other materials for improving the quality of silver beams will be investigated.

5 REFERENCES

- [1] K.L. Kratz et al., Hyperfine Interact. 129 (2000) 185.
- [2] O. Arndt et al., Jahresbericht 2002, IKMz 2003-1, A15.
- [3] I. Dillmann et al., Eur. Phys. J. A13 (2002) 281.
- [4] L. Westgaard et al., J.Inorg.Nucl.Chem. 31 (1969) 3747.
- [5] Roccaforte et al., J. Appl. Phys. 89 (2001) 3611

The $^{44,46}\text{Ar}(n,\gamma)^{45,47}\text{Ar}$ reaction rates studied by (d,p) transfer reactions

L. Gaudefroy¹, O. Sorlin², Y. Blumenfeld¹, K.-L. Kratz³, A.N.Ostrowski⁴ and the MuST-Collaboration

¹ Institut de Physique Nucléaire, F-91406 Orsay Cedex, France; ²GANIL, F-14076 Caen Cedex 5, France; ³ Institut für Kernchemie, Universität Mainz, D-55099 Mainz, Germany; ⁴Fakultät für Physik & Astronomie, Universität Heidelberg, D-69120 Heidelberg, Germany;

The aim of our experiment is to determine the $^{44}\text{Ar}(n,\gamma)^{45}\text{Ar}_{27}$ and $^{46}\text{Ar}(n,\gamma)^{47}\text{Ar}_{29}$ reaction rates by measuring the $^{44}\text{Ar}(\text{d},\text{p})^{45}\text{Ar}$ and $^{46}\text{Ar}(\text{d},\text{p})^{47}\text{Ar}$ transfer reactions in order to evaluate the role of the N=28 closed shell on astrophysical relevant neutron-capture rates and determine the size of the N=28 gap.

The motivation of this study is therefore twofold, one is of astrophysical, the other of nuclear physics interest. In astrophysics, this experiment will help to understand the large $^{48}\text{Ca}/^{46}\text{Ca}$ abundance ratio (60 - 250) in certain refractory meteoritic inclusions, e.g. the EK 1-4-1 sample from the Allende meteorite. The ^{46}Ar is thought to be the main progenitor of ^{46}Ca and the determination of its neutron capture cross section provides a constraint for astro-phycists on the neutron densities which should be present in explosive stellar environments to account for the large isotopic ratio found.

In nuclear physics, neither the size of the N=28 shell gap (between $f_{7/2}$ and $p_{3/2}$), nor the occupation of these orbitals have been determined in any of these nuclei yet. The study of ^{44}Ar and ^{46}Ar transfer reaction experiments will determine the size of the N=28 gap, and the occupation probabilities of the two orbitals $f_{7/2}$ and $p_{3/2}$. These results will firmly establish an erosion or persistence of the N=28 closed-shell below ^{48}Ca .

The transfer $^{44,46}\text{Ar}(\text{d},\text{p})$ reactions have been performed at 10 MeV per nucleon incident energy at the GANIL/SPIRAL1 facility in reverse kinematics A deuterated polythene target of 0.3 mg/cm² area density was used. Beam intensities of 2×10^5 and 2×10^4 incident ions per second have been obtained for the radioactive ^{44}Ar and ^{46}Ar beams, respectively. The target was surrounded by 8 modules of the MuST silicon strip detector array located between 110 and 170 degrees in the laboratory frame. The beam profile was monitored by a gas filled tracking detector in order to reconstruct the reactions' locations in the target.

The transfer-like products were detected in the focal plane of the magnetic spectrometer SPEG using a combination of drift chambers and a plastic scintillator. Energy-loss and time of flight information were recorded. The use of the high segmentation of the MuST detector as well as the high position resolution of the beam tracking detector was found to be essential for the reconstruction of the kinematics of the reaction. This was

necessary in order to infer the levels which were involved in the transfer leading to the A+1 nuclei.

The $^{41}\text{Ar}(\text{d},\text{p})$ reaction was utilized in order to calibrate our set up, and we were able to measure the population of the known levels of ^{41}Ar and determine the corresponding spectroscopic factors. Analysis in the case of the ^{44}Ar induced transfer is in progress and already at least 7 excited states are clearly identifiable - among them half exhibit an $\ell=1$ angular pattern (cf. Figs.1 and 2). The other half have rather an $\ell=3$ behaviour. Spectroscopic factors for these levels will enable us to determine the size of the N=28 gaps and henceforth the strength of the $f_{7/2}-f_{5/2}$ spin orbit splitting south of the doubly magic ^{48}Ca nucleus. The analysis of ^{46}Ar transfer has just been started.

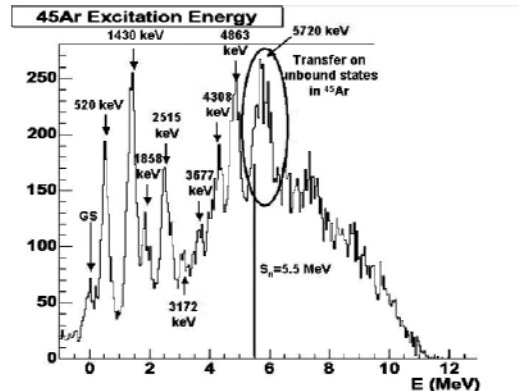


Figure 1: Preliminary proton spectrum of the $^{44}\text{Ar}(\text{d},\text{p})^{45}\text{Ar}$ reaction at 10 A.MeV. The energy scale is calibrated on ^{45}Ar revealing known states in this nucleus.

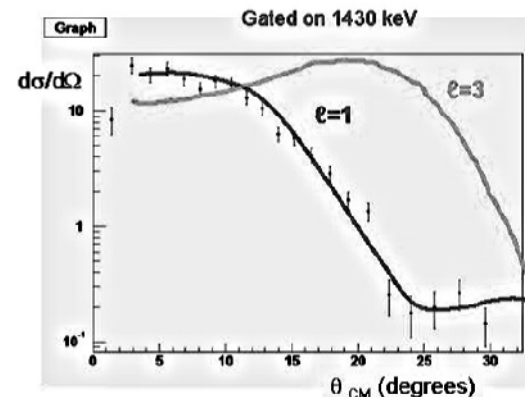


Figure 2: Preliminary angular distribution of the $^{44}\text{Ar}(\text{d},\text{p})^{45}\text{Ar}(E_x=1430\text{ keV})$ transfer reaction.

High-temperature fractionations in the solar nebula

Gerhard Schmidt^{1,2} and Karl-Ludwig Kratz^{1,2}

¹Institut für Kernchemie, Universität Mainz

²Helmholtz Gemeinschaft Deutscher Forschungszentren (HGF)

Virtuelles Institut für Struktur der Kerne und Nukleare Astrophysik

Of particular interest in geochemistry and cosmochemistry is the question of whether the elements Os, Ir, Ru, Pt, Rh, and Pd (HSE = highly siderophile elements) are fractionated in the Earth's mantle [1]. In Fig. 1 the Cl-normalized abundances of siderophiles in the Earth's upper mantle as measured by instrumental neutron activation on large homogenized samples and aliquots of 10 to 20 g rock powders, are shown in order of decreasing volatility in a solar gas. The relative abundances of HSE are shown in first order to be nearly Cl-chondritic. However, the abundance pattern is inversely correlated with the volatility of the elements [2]. The excess of the non-refractory element Pd and depletions in the ultra-refractory elements Ir and Os appear to be consistent with a high-temperature gas-condensation fractionation process [3]. Continuous loss of ultra-refractory nebular condensates from the late-veneer formation region during condensation could be suggested to account for the depletion and fractionation of refractory elements in the Earth's late accreted component.

The process of condensation along with isolation of metal grains is likely to be responsible for the element pattern of the Earth's mantle. Based on a condensation model, in which metals condense first out of a hot nebular gas, followed by silicates, the highly siderophile components of the Earth's mantle may have formed in the nebular region during gradual removal of solids from the location where these „late material“ formed during condensation. It is well known that gas-solid fractionation during condensation from a solar gas is one of the most important processes leading to fractionations in primitive objects of our solar system.

Formation Location of the Late Veneer Material

It is also known that enstatite chondrites were depleted in refractory siderophiles. The carbonaceous, ordinary and enstatite chondrites exhibit successively greater degrees of reduction in combination with successively lower contents of refractory elements. These features are most likely associated with formation at successively smaller radial distances from the Sun in hotter portions of the solar nebula. Many authors favored an enstatite formation location in the innermost solar system (perhaps even less than 1 AU from the Sun: possibly in the Mercury-Venus region). Based on the assumption that the observed gradient in the abundance of the radiogenic ^{53}Cr between the Earth-Moon system, Mars and the asteroid Vesta is considered as a function of the heliocentric distance. The ^{53}Cr excess of the enstatite chondrites would point to a formation location of about 1.4 AU or somewhat closer to the Sun (i.e. >1.0-1.4 AU [4]).

The HSE systematics of upper mantle samples resembles materials more closely to highly reduced EH or EL-chondrites than carbonaceous chondrites. In fact, the HSE in the Earth's mantle are even more fractionated than the enstatite chondrites. This may serve as an indication that some inner solar system materials were more highly fractionated than the latter.

Materials from formation regions closer to the Sun (Mercury-Venus region), as is supposed for enstatite chondrites, might be found in the future. Of course,

planetary processes can also affect the distribution of HSE in the mantle. But, an igneous and/or an aquatic process that can exactly mimic the detailed volatility element pattern as shown in Fig. 1 seems unlikely (e.g. [5]).

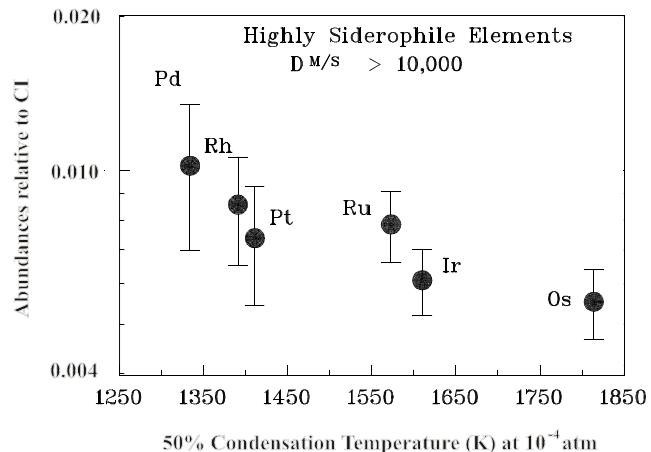


Fig. 1. Abundance pattern of HSE in the Earth's mantle.

Conclusion

The abundances of HSE in the depleted mantle differ from those in CI-chondrites. The abundance distribution of the HSE is remarkably uniform with increasing Cl-normalized abundances, and with decreasing 50% condensation temperatures from Os to Pd. A possible interpretation is that the present upper-mantle noble-metal ratios could have been established in the solar nebula by fractionation processes that resulted in the loss of refractory components. The last material to contribute to the growing Earth is likely to have been derived from the innermost solar system.

The database for the elements Sb, Ag, As, W and Mo and some other elements has to be improved for the Earth's mantle and for Rh in the chondrite groups in order to make final decisions about the nature of the late veneer. In future studies, HSE as well as moderately siderophile element-based models might contribute to our understanding of the origin of the solar system and the processes involved to form planetary bodies, and giving the Earth their unique composition.

Acknowledgments

The authors acknowledges financial support from the Max Planck Institut für Chemie in Mainz (Cosmochemistry Department, G. W. Lugmair).

References: [1] Morgan J.W. et al. (2001) Meteoritics & Planetary Science 36, 1257-1275. [2] Schmidt G. (2004) Meteoritics & Planetary Science 39. [3] Wasson J. T. (1985) Meteorites: Their Record of Early Solar-System History, Freeman, New York, USA. 267 pp. [4] Shukolyukov A. and Lugmair G. W. (2004) Geochim. Cosmochim. Acta 68, 2875-2888. [5] Schmidt G., Witt-Eickschen G., Palme H., Seck H., Spettel B. and Kratz K.-L. (2003) Chem. Geol. 196, 77-105.

Kosmochemische Fingerabdrücke im Erdmantel: Ein Beitrag zur Herkunft der chemischen Elemente Os, Ir, Ru, Pt, Rh, und Pd

Gerhard Schmidt^{1,2} und Karl-Ludwig Kratz^{1,2}

¹Institut für Kernchemie, Universität Mainz

²Helmholtz Gemeinschaft Deutscher Forschungszentren (HGF)

Virtuelles Institut für Struktur der Kerne und Nukleare Astrophysik

Unser Sonnensystem ist aus einer präsolaren Gas- und Staubwolke entstanden, die unter der eigenen Gravitation, bzw. dem Einfluß von Schockwellen einer nahen Supernova, kollabierte. Bei der Abkühlung des solaren Gasnebels bildeten sich Körner durch Kondensation, die sich zusammenballten und durch gegenseitige Akkretion größere Körper, die Planeten, Monde, Asteroiden und Meteorite bildeten. Die Erde erhielt sich soweit, dass die Silikate aufschmolzen und so ein differenzierter Körper entstand. Bestimmte Gruppen von Meteoriten stellen primitive Solarmaterie dar aus denen sich Informationen über frühe Prozesse in der Entwicklung des Sonnensystems gewinnen lassen. Die meisten der undifferenzierten Meteorite werden als Chondrite bezeichnet. Sie setzen sich aus Metallphasen, Silikaten und Sulfiden zusammen und enthalten die nicht flüchtigen Elemente nahezu in solaren Verhältnissen. Für die Erde wird ein den Meteoriten analoger Ursprung (Akkretionsprodukt des solaren Nebels) und ein ähnliches Alter, wie für undifferenzierte Meteorite von ~4,6 Ga angenommen. Die Bildung des metallischen Erdkerns fand in den ersten 30 Ma (Ende der Hauptphase der Akkretion) statt. Die ursprünglich vorhandenen hochsiderophilen Platinmetalle sind bei der Mantel-Kern-Bildung quantitativ in den Kern gewandert. Nach der Segregation des Erdkerns war der Silikatmantel der Erde praktisch frei von Platinmetallen. Trotzdem liegen heute diese Elemente im Erdmantel in „relativ hohen (ng/g-Bereich“ und fast solaren Häufigkeitsverhältnissen vor [1]. Wie lässt sich dies erklären? Die Erde war wie der Mond in den ersten ~500 Ma einem intensiven Meteoritenbombardement ausgesetzt, wodurch diese Elemente dem Erdmantel nach der Mantel-Kern-Bildung wieder durch kosmische Materie zugeführt wurden. Es ist daher anzunehmen, dass der heutige Erdmantel diese Gruppe von Elementen noch in ihren ursprünglichen kosmischen Elementverhältnissen dieser letzten Zumischung(en) („late veneer“) enthält.

Hinweise auf Kondensationsprozesse im solaren Nebel – „eingefroren“ in Gesteinen des Erdmantels

Bei der Kondensation des solaren Nebels in die primitiven Bausteine des Sonnensystems findet ein Übergang von einer Gasphase geringer

Dichte (10 atm) in die feste Phase statt. Kondensationsmodelle gehen davon aus, dass

ursprünglich alle Elemente in der Gasphase vorlagen und der Nebel eine solare Zusammensetzung hatte. Betrachtet man die einzelnen Metalle so kondensierten zunächst Os (1814 K), gefolgt von Ir (1610 K), Ru (1573 K), Pt (1411 K), Rh (1391 K) und Pd (1334 K) entsprechend ihrer relativen Flüchtigkeiten im solaren Nebel.

Ca- und Al-reiche Hochtemperatur Einschlüsse (CAI) von Chondriten werden als frühe Kondensate des solaren Nebels interpretiert. In den meisten Einschlüssen findet man eine starke Anreicherung der hochschmelzenden Elemente entsprechend ihrer relativen Flüchtigkeiten im solaren Nebel.

Die Verteilung der hochschmelzenden Platinmetalle im Erdmantel ist jedoch komplex. Im Erdmantel beobachtet man genau den umgekehrten Trend (Abb. 1 in [2]). Da Os und Ir gegenüber Pd und Rh verarmt sind, muß ein Teil des Os und Ir während der Kondensationsphase als Kondensat entfernt worden sein, bevor die Elemente Pd und Rh vollständig kondensiert waren. Die Kondensation der weniger refraktären Platinmetalle Pd und Rh erfolgte offenbar an einem Ort im solaren Nebel aus dem zuvor Hochtemperaturkondensate weggeführt wurden. Eine Ausnahme bildet Ru (positive Ru-Anomalie!), dessen Ursache noch unklar ist.

Diese Vorstellung von der Einstellung der Platinmetallverhältnisse im heutigen Erdmantel erfordert die vorherige Bildung einer komplementären Komponente als Erstkondensate des solaren Nebels mit einer entsprechenden Os und Ir-Anreicherung. Solche Anreicherungen sind aus ultrarefraktären Einschlüssen von Chondriten auch bekannt. Anreicherungen der Elemente Pd und Rh, wie sie im Erdmantel nachgewiesen sind, sind bei einer Gas/Fest-Kondensationen unter Fortführung der refraktären Elemente Os und Ir zu erwarten, nicht aber bei magmatischen Fraktionierungsprozessen. Die heutigen Häufigkeitsverhältnisse der Platinmetalle im Erdmantel könnten somit kosmochemische Fingerabdrücke von Prozessen darstellen, die im solaren Nebel stattgefunden haben.

[1] Schmidt G. (2004) Meteoritics & Planetary Science 39. [2] Schmidt G., Kratz K.-L. (2005) Jahresbericht.

Pre-concentration and purification of generator-produced ^{68}Ga

K.P. Zhernosekov¹, D.V. Filosofov², M. Jahn¹, M. Jennewein¹ and F. Rösch¹

¹Institut für Kernchemie, Johannes Gutenberg-Universität, D-55128 Mainz, Germany

²Joint Institute of Nuclear Research, LNP, 141980 Dubna

Introduction: The $^{68}\text{Ge}/^{68}\text{Ga}$ generator (^{68}Ge : $T_{1/2} = 270.8$ d) provides a cyclotron-independent source of positron-emitting ^{68}Ga ($T_{1/2} = 68$ min, β^+ branching = 89%), which can be used for labelling of biomolecules via bifunctional chelators. It is thus of great interest for clinical PET and PET/CT [1].

Commercially available $^{68}\text{Ge}/^{68}\text{Ga}$ generators based on TiO_2 (Cyclotron Co., Obninsk, Russia) allow to elute > 50% of ^{68}Ga in 5-7 ml 0.1 M HCl solution. However, the eluate normally is contaminated with long-lived ^{68}Ge and contains small amounts of Zn(II), Ti(IV), Fe(III) and residuals of construction materials used. For labelling, ^{68}Ga must thus be treated following several principles (i) pre-concentration; (ii) purification; (iii) transfer of ^{68}Ga into a form useful for labelling (volume, pH). The aim of this work was to develop a system for pre-concentration and purification of ^{68}Ga from 0.1 M HCl solutions and to obtain ^{68}Ga in solutions of small volume and acceptable H^+ concentration. Analysis of cation exchange distribution coefficients with Bio-Rad AG 50W-X8 in hydrochloric acid / acetone media [2] showed, that Ga(III) can be eluted from the resin using low acid concentration. Furthermore, it is possible to separate Ga(III) from Ge(IV), Zn(II), Ti(IV) and Fe(III).

Experimental: A micro-chromatography column was prepared using 53 mg of Bio-Rad AG 50W-X8 cation exchanger. A 20 mCi $^{68}\text{Ge}/^{68}\text{Ga}$ generator (~12 months old) was used to obtain about 110 MBq of ^{68}Ga in 7 ml of 0.1 M HCl. The activity of ^{68}Ge in the eluate was 170-200 kBq (determined 48 h after generator elution using γ -spectroscopy on HPGe detector).

^{59}Fe was produced in a neutron capture reaction on natural iron. 198 mg of iron oxide Fe_2O_3 were irradiated for 50 days at the HMI neutron source BER II at $1.6 \cdot 10^{14} \text{ n cm}^{-2} \text{ s}^{-1}$, resulting in 440 MBq ^{59}Fe . ^{54}Mn was co-obtained with an activity 0.25 MBq per 1 MBq of ^{59}Fe . ^{69}Zn was produced with specific activity of ~700 kBq/mg by

irradiation of 380 μg of >98% enriched ^{68}Zn for 6 h at the TRIGA reactor Mainz at a neutron flux of $4 \cdot 10^{12} \text{ cm}^{-2} \text{ s}^{-1}$.

^{68}Ga in 7 ml of 0.1 M HCl was loaded dynamically on the chromatography column. For purification from ^{68}Ge , Zn(II) and Fe(III) an 80% acetone / 0.15 M HCl solution was selected. ^{68}Ga itself was subsequently eluted with 400 μl of a 97.6% acetone / 0.05 M HCl solution. The chromatography column was purified with 1 ml 4 M HCl and 1 ml H_2O .

Distribution of radionuclides ^{59}Fe , ^{54}Mn and ^{69}Zn , containing 83 μg and 130 μg of Fe(III) and Zn(II), respectively, was measured in solutions, using an HPGe detector. The distribution of about 20 μg Ti(IV) was studied by an Elan 5000 ICP-MS (Perkin-Elmer).

Results: More than 97% of ^{68}Ga could be obtained finally in 400 μl of the 97.6% acetone / 0.05 M HCl solution (Tab.1) containing < 0.1% of ^{68}Ge . About 0.1% of Ti(IV) and 10% of Mn(II) were detected in the eluted solution. The purification step using 80% acetone / 0.15 M HCl solution allows to reduce the amount of Zn(II) up to 10^{-3} % and of Fe(III) up to 11% (Tab.1).

The presented system allows to concentrate ^{68}Ga from 0.1 M HCl solutions and to obtain it with high specific activity and contamination of ^{68}Ge less than 0.1% in a small volume with low HCl amount ($2 \cdot 10^{-5}$ mol). Cation exchanger with hydrochloric acid-acetone media seem to be a useful tool also for the preparation of other gallium isotopes such as cyclotron-produced $^{66,67}\text{Ga}$.

Acknowledgements: Thanks to Bernhard Kuczewski for the ICP-MS measurements.

References

- [1] Mäcke, H. R., Good, S.: "Radiometals (non-Tc, non-Re) and bifunctional labeling chemistry"; Handbook of Nuclear Chemistry, volume 4, Amsterdam, (2003)
- [2] Sterlow, F. W. E., et. al., Anal. Chem. **43**, 870, (1971)

Table 1. Relative distribution [%] of ^{68}Ga (III), ^{68}Ge (IV), Zn(II), Ti(IV), Fe(III) and Mn(II) on a micro-chromatography column (53mg Bio-Rad AG 50W-X8 cation exchanger) using a) 0.6 ml and b) 5 ml of 80% acetone / 0.05 M HCl solutions for purification

Volume a)	Step / concentration	Relative distribution [%]					
		Ga(III)	Ge(IV)	Zn(II)	Ti(IV)	Fe(III)	Mn(II)
7 ml	Generator elution: 0.1 M HCl	0.16	97.08	0.77	7.30	0.13	4.41
0.6 ml	Purification: 80% acetone / 0.15 M HCl	1.43	2.92	98.15	0.68	37.86	0.49
0.4 ml	Ga(III) elution: 97.6% acetone / 0.05 M HCl	97.82	$3 \cdot 10^{-2}$	1.08	$7 \cdot 10^{-2}$	49.78	11.10
1 ml	Washing: 4 M HCl	0.41	$5 \cdot 10^{-3}$	$5 \cdot 10^{-3}$	72.15	11.61	69.38
1 ml	Washing: H_2O	0.18	$3 \cdot 10^{-3}$	< 10^{-3}	19.80	0.62	14.62
b)							
7 ml	Generator elution: 0.1 M HCl	0.11	97.68	0.43	7.18	0.73	5.20
5 ml	Purification: 80% acetone / 0.15 M HCl	6.29	2.32	99.57	3.99	87.37	1.71
0.4 ml	Ga(III) elution: 97.6 % acetone / 0.05 M HCl	92.73	$5 \cdot 10^{-3}$	<10^{-3}	0.11	11.10	9.79
1 ml	Washing: 4 M HCl	0.77	$2 \cdot 10^{-3}$	< 10^{-3}	86.54	0.71	83.09
1 ml	Washing: H_2O	0.10	$2 \cdot 10^{-3}$	< 10^{-3}	2.18	0.09	0.21

Resolution Studies of a New Small Animal PET System based on Scintillating Fibers

^{1,2}M. Jennewein, ²N. Slavine, ²S. Seliouine, ¹F. Rösch, ²E. Tsyganov, ²R.P. Mason,
¹Institute for Nuclear Chemistry, Johannes Gutenberg-University of Mainz, Fritz Strassmann-Weg 2, 55128 Mainz, Germany
²University of Texas Southwestern Medical Center, Dallas, TX 75390, USA

Single Photon Emission Computed Tomography (SPECT) and Positron Emission Tomography (PET) are widely used in the clinic and in the laboratory. The technique detects radiolabeled agents quantitatively at the picomolar level and detects normal and disturbed biochemical and physiological functions noninvasively and quantitatively that are not available otherwise. PET in animal models is a powerful technique capable of answering basic and applied questions in biology and pharmacology.

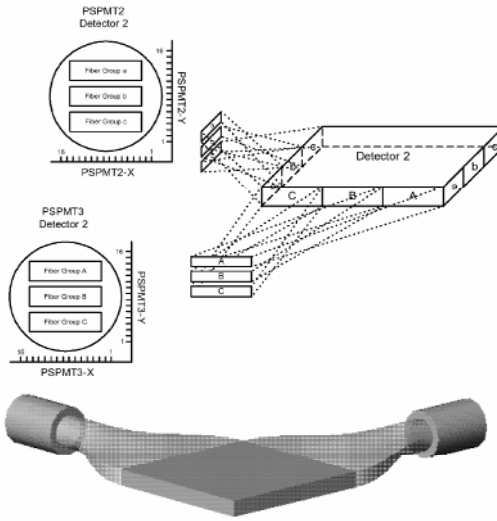


Figure 1: Scheme of PSPMT-to-Fiber Detector Layout.

The newly developed system [1,2,3] comprises two plastic fiber scintillator detectors, the position sensitive photo multiplier tube (PSPMT) light sensors, PET coincidence trigger electronics, and a custom-built FADC crate to digitize detector signals. The current Data Acquisition (DAQ) system is based on a multistandard platform: a custom back plane for the Analog-to-Digital Convertor (ADC) modules and a PXI (the Compact PCI standard from National Instruments) enclosure for the data readout from the ADCs. Two interface modules (PXI-6508 for slow control, and PXI-6533 for the fast data transfer) are included in this enclosure. The current data transfer rate is about 6 MB/s (~40 K events per second), with the possibility to attain a final data transfer rate of 40 MB/s. Small animal scans usually are performed with activities of 1-3 mCi and take from 20 to 40 minutes. The detectors were fabricated using BCF-10 (Bicron Corp, Newbury, Ohio) scintillating plastic fibers. The fiber core is polystyrene ($C_8 H_8$)_n doped with butyl-PBD and dPOPOP. The fibers are clad in a non-scintillating Lucite cladding. Generally, the scintillation mechanism is via excitation of π -electrons in the butyl-PBD benzene ring. These ~365 nm photons penetrate through a plastic scintillator by a distance of ~1 mm and produce a so-called X-Y “conferencing” effect firing the neighboring fibers due to

wave-shifting mechanism with the dPOPOP to ~420 nm. This wavelength provides high fiber transparency and is also more compatible with the optimal spectral response of standard photo multiplier cathodes. The photo electron fraction is small and Compton scatter interactions dominate in the photon energy distribution in a plastic scintillator at 511 keV. The scatter electrons give up their energy well within a 1 mm range.

The detectors consist of an epoxied stack of 28 layers each containing 135 fibers. The criss-crossed overlap region forms a 13.5x13.5x2.8 cm³ detector volume. Fig. 1 shows schematics of the PSPMT-to-detector fiber layout.

As local resolution of the imaging also depends on the mean and respectively, the maximum kinetic energy of the positron emitted, in this study, the spatial resolution of the scanner for various positron emitting isotopes [4] was studied. Point sources of 1mm diameter were prepared, measured in the center of the field of view and FWHM values were calculated. Isotopes used were: ²²Na, ¹⁸F, ⁷⁴As, ¹²⁴I and ⁷²As.

The results are illustrated in Fig. 2, showing a linear dependency between mean positron energy and spatial resolution of the scanner system within reasonable errors.

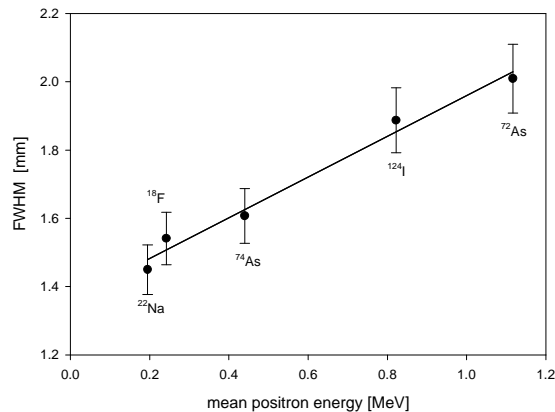


Figure 2: Spatial resolution for different positron emitting isotopes versus their mean positron energy. Measurements were done at the Small Animal PET of the UTSW Medical Center at Dallas using equal-sized point sources, $\varnothing = 1$ mm.

References:

- [1] Kulkarni, P.V. et al., *Nuclear Instruments and Methods in Physics Research B79* (1993) 921-925.
- [2] Anderson J., et al., *Scintillating Fiber Technology and Applications, Proc. SPIE*, 2007 (1993) 125-131.
- [3] Tsyganov, E. et al., *Performance of the Dallas PET Imager*, IEEE Transactions in Nuclear Science, submitted
- [4] National Nuclear Data Center, Brookhaven National Laboratory (2004)
<http://www.nndc.bnl.gov/nudat2/index.jsp>.

Financial Support of the Böhringer Ingelheim Foundation is grateful acknowledged.

Calculation of ultracold neutron production at the TRIGA Mainz Reactor

Yu. N. Pokotilovski¹, K. Eberhardt², W. Heil³, V. Janzen², J. V. Kratz², U. Tharun², N. Trautmann², Y. Sobolev³, N. Wiehl²

¹Joint Institute for Nuclear Research, Dubna, Moscow Region, 141980, Russia; ²Institut für Kernchemie, Universität Mainz, D-55099 Mainz, Germany; ³Institut für Physik, Universität Mainz, D-55099, Germany

Ultracold neutrons (UCN) are, by definition, neutrons with energies below the reflecting potential of most materials. This means, the kinetic energy of UCN is below ~ 250 neV. Therefore, UCN can be stored in traps enabling experiments at very low energies. The most significant experiments in this field are searches for a static electric dipole moment of the neutron (EDM) and measurements of the free neutron lifetime [1,2].

UCN can be produced by inelastic down-scattering of higher energy neutrons creating excitations in a moderator material. In thermal equilibrium, the rates of up- and down-scattering are equal and the temperature of the neutrons becomes that of the moderator. However, up-scattering depends strongly on the moderator temperature. Below a certain temperature, up-scattering is negligible. A moderator where no thermal equilibrium can be reached is called a converter. One possible converter material is solid deuterium at 5 K.

The expected UCN production and the energy release for solid deuterium as a converter was calculated for the TRIGA Mainz reactor. A UCN source of this type was recently installed at the beam tube C [3]. The neutron fluxes averaged over the converter volume were calculated by Monte Carlo N- Particle simulations with the program MCNP [4]. As input to MCNP, a detailed model of the reactor core was used including exact positions of all fuel elements, regulation rods and their claddings. Based on these fluxes, the UCN production was calculated in the one phonon incoherent approximation for the scattering cross section and with a dynamic Debye model of the moderator material [5]. In this model, the down-scattering cross section of a room temperature thermal neutron flux down to the energy range 50 neV to 250 neV in very low temperature deuterium is 10^{-8} b. The most optimal neutron temperature was found to be ~ 30 K. In this case, the cross section is 14 times larger.

The thermal neutron flux in the tangential beam tube C averaged over a 5 cm thick deuterium cell is 1.1×10^{11} n/cm²·s at a reactor power of 100 kW. Neglecting multi-phonon down-scattering which increases the UCN production, the calculation results in a UCN production rate of 60 UCN/cm³·s. During a 6 MJ pulse the total UCN production will be 3.5×10^3 UCN/cm³.

As mentioned above, premoderation of the incident neutron flux will increase the UCN production. A premoderator of 1.0 – 1.2 cm thickness of solid or liquid methane at the temperature of 10 K to 20 K decreases the neutron temperature down to 30 K to 40 K. In this case, the cold neutron flux at 100 kW reactor power will be 7×10^{10} n/cm²·s. With this, the predicted UCN production rate at beam tube C is 4.5×10^2 UCN/cm³·s, the total UCN production during a reactor pulse of 6 MJ is 2.7×10^4 UCN/cm³.

At the radial beam channel D, a graphite shield of 10 cm – 12 cm thickness was found to be necessary to reduce the heating of the converter. In this case, the thermal neutron flux is 5.4×10^{11} n/cm²·s at 100 kW. With this shield and a methane premoderator, the predicted UCN production rate at beam tube D is 3.5×10^3 UCN/cm³·s at 100 kW and 2×10^5 UCN/cm³ per 6 MJ pulse.

As experimental check of the MCNP calculations, heating of different substances in the central thimble of the TRIGA Mainz during a 6 MJ pulse was measured and compared with the calculations (Table 1). For all materials, a constant ratio of ~ 1.5 was found between measured and calculated values, indicating that the used model of the reactor was still not exact, but it shows also that the calculated values of the UCN production rates are close to reality.

Material	$\Delta T_{\text{exp}} [\text{K}]$ (measured)	$\Delta T_{\text{calc}} [\text{K}]$ (calculated)	$\Delta T_{\text{exp}} / \Delta T_{\text{calc}}$
Al	3.5	2.27	1.54
PE	6.0	3.55	1.69
Graphite	5.4	3.55	1.52
PMMA	5.4	3.53	1.53

Table 1: Comparison of calculated and measured heating of different materials in the central thimble of the TRIGA Mainz

References

- [1] P.G.Harris et al., PRL 82 (1999) 904.
- [2] S. Arzumanov et al., NIM A 440 (2000) 511.
- [3] S. Paul et al., this report.
- [4] J. F. Briesmeister, Ed., LA-13709-M (April 2000)
- [5] V. Turchin, "Slow Neutrons", Atomizdat, Moscow,1963.

A solid Deuterium UCN Source at the research reactor TRIGA Mainz

S. Paul¹, W. Heil², J.V. Kratz³, I. Altarev¹, K. Eberhardt³, A. Frei¹, E. Gutsmiedl¹, G. Hampel³, J. Hartmann¹, N. Trautmann³, W. Schmid¹, Y. Sobolev², D. Tortorella¹, N. Wiehl³

¹ Technische Universität München, Physik Department E18, D-85748 Garching, Germany;

² Institut für Physik, Universität Mainz, D-55099 Mainz, Germany; ³ Institut für Kernchemie, Universität Mainz, D-55099 Mainz, Germany;

A strong source for ultracold neutrons (UCN) [1] shall be built for the research reactor FRM-II. This source, called Mini-D2, will be installed at the beam tube SR4, that is horizontally pointing directly to the already existing cold neutron source. For converting cold neutrons to UCN a solid D₂ converter with 200 cm³ volume at a temperature of 5K is frozen out at the beginning of this beam tube, near to the cold source. The inner part of the beam tube (diameter 6 cm, (length 8 m) is cooled to 30 K and covered with beryllium in order to store and accumulate UCN and to bring them to different experiments. Simulations indicate, that with this setup, UCN densities up to 10⁴ cm⁻³ can be reached.

For a test of this conversion mechanism, a smaller setup has been built (see figure 1) and is currently operated at the pulsed TRIGA reactor in Mainz. This test setup contains all essential parts that will later be used for the FRM-II UCN-source, such as the converter, the storage tube, the D₂-gas system and the software programmable control (SPC) -system. For this configuration, a UCN density of 3.5x10³ UCN/cm³ per 6MJ pulse is expected [2].

The solid Deuterium UCN Source (SDUCNS) was installed at the TRIGA Mainz in late autumn 2004 . First cool down tests (freezing out the deuterium gas at 5 – 8 K) where made successfully in December 2004. A first

measurement with neutrons from the TRIGA reactor in the pulse mode was also performed in December 2004. This measurement indicated some problems with the UCN Silicon detectors, which are covered with a converter foil (Ti foil with ⁶Li/⁶²Ni-multilayer) [3], and the data acquisition electronics.

After the disassembling of the cryostat, the UCN detector system was checked. It turned out, that the converter foil of the Si detector was broken. Also the data acquisition electronics was checked with a Si-detector and an α -source and has been re-adjusted.

A new bigger UCN detector will be supplied with a new converter aluminium foil, which is covered by a pure ⁶Li layer. This detector will be installed outside of the cryostat, connected with a UCN guide (1.5 – 2 meter away form the cryostat), in order to reduce the thermal and epithermal neutron background.

References

- [1] S. Paul et. al., The 3rd UCN Workshop, Pushkin, St. Petersburg, Russia, June 18-22, 2001
- [2] Yu. N. Pokotilovski et. al., this report
- [3] G. Petzold et. al., The 3rd UCN Workshop, Pushkin, St. Petersburg, Russia, June 18-22, 2001

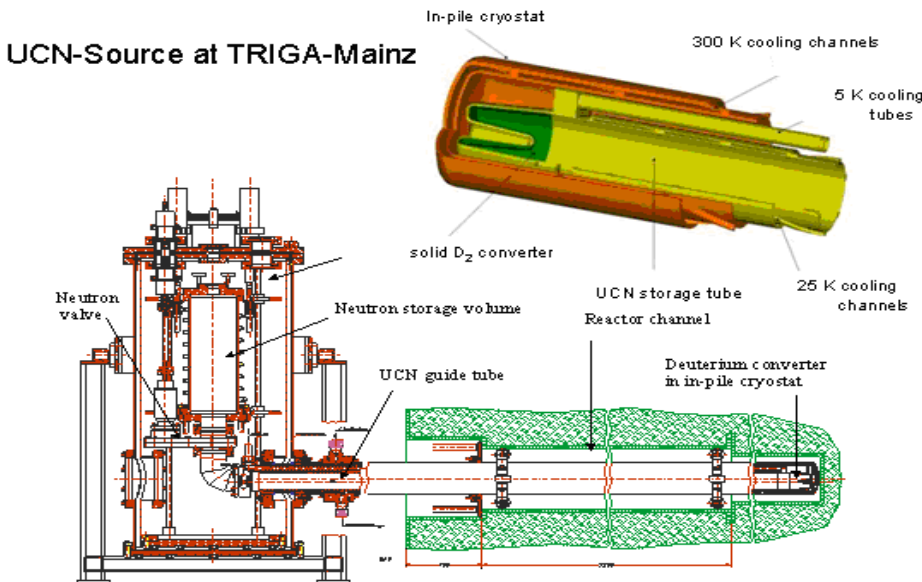


Figure 1: Vertical cross section of the test facility

B. Radiopharmazeutische Chemie

- Targetentwicklung und Isotopenproduktion
- Synthese von ^{68}Ga - und ^{18}F -Markierungssynthons
- Synthese von $^{18,19}\text{F}$ - und ^{11}C -markierten Verbindungen
- Synthese von $^{72,74,77}\text{As}$ -, ^{123}I - und ^{131}I -Verbindungen
- Evaluierung von Radiodiagnostika und –therapeutika
- Nuklearmedizinische Studien

B. Radiopharmaceutical Chemistry

- Target developments and isotope production
- Synthesis of ^{68}Ga - and ^{18}F -labelling synthons
- Synthesis of $^{18,19}\text{F}$ -and ^{11}C -labelled compounds
- Synthesis of $^{72,74,77}\text{As}$ -, ^{123}I - and ^{131}I -labelled compounds
- Evaluation of radiodiagnostics and –therapeutics
- Nuclear medical studies

Labelling of DOTA-DPhe¹-Tyr³-octreotide with generator-produced ⁶⁸Ga

K.P. Zhernosekov¹, D.V. Filosofov², M. Jahn¹, M. Jennewein¹ and F. Rösch¹

¹Institut für Kernchemie, Johannes Gutenberg-Universität, D-55128 Mainz, Germany

²Joint Institute of Nuclear Research, LNP, 141980 Dubna

Introduction: Bifunctional chelators labelled with ⁶⁸Ga ($T_{1/2} = 68$ min, β^+ branching = 89%) are of great interest for clinical PET. In particular the somatostatin analogue [⁶⁸Ga]DOTA-DPhe¹-Tyr³-octreotide ([⁶⁸Ga]DOTATOC) shows great potential for diagnosis of somatostatin receptor expressing tumours [1].

Commercially available ⁶⁸Ge/⁶⁸Ga generators based on TiO₂ (Cyclotron Co., Obninsk, Russia) provide a cyclotron-independent source of ⁶⁸Ga. More than 50% of the activity can be eluted with 5-7 ml 0.1 M HCl. However, the eluate contains the long-lived ⁶⁸Ge and small amounts of Zn(II), Ti(IV), Fe(III) and cannot be used directly for labelling of DOTATOC.

Pre-concentration and purification of ⁶⁸Ga from the eluate can be performed on a cation exchanger in HCl / acetone media [2]. The ⁶⁸Ga activity can be obtained in a small volume with low HCl concentration.

The aim of this work was to develop a system for simple and efficient handling of the ⁶⁸Ge/⁶⁸Ga generator eluate for labelling of nanomolar amounts of DOTATOC. The main component of the system is a micro-chromatography column (Fig.1) filled with 53 mg of Bio-Rad AG 50W-X8 resin.

Experimental: The generator is connected to the column with tube (1) (Fig.1). PEEK capillary tubing (4) is directed to reagents vials. The column can be also eluted using a standard single-used syringe (3) and is connected to the waste vials with tube (2).

For pre-concentration and purification of ⁶⁸Ga the following protocol is used: (i) elution of the generator (1-2) and separation of more than 99% of ⁶⁸Ga from the eluate; (ii) purification of ⁶⁸Ga (3-2) using 1 ml 80% acetone / 0.15 M HCl solution (loss of activity < 5%); (iii) elution of ⁶⁸Ga directly into the reaction vial (3-4) with 400 μ l of 98% acetone / 0.05 M HCl solution. The procedure takes 4 minutes. Finally, the column is purified with 1 ml 4 M HCl and 1ml H₂O (3-2).

With its relatively small ionic radius of 0.62 Å, trivalent gallium evidently hydrolyses over pH 2–3 [3] and has a high tendency to adsorb on surfaces (glass, plastic), especially in no-carrier-added form. Ga³⁺ precipitates easily as insoluble Ga(OH)₃(am) with $\lg K_s \approx -37$. Thus, 500 MBq of ⁶⁸Ga precipitate already at pH = 4.4 (Fig. 2).

For labelling of biomolecules via bifunctional chelators such as DOTATOC, due to the slow kinetics of complexation and due to the complex aqua chemistry of the cation, selecting of optimum reaction conditions is essential.

For labelling, the ⁶⁸Ga eluate (400 μ l 98% acetone /0.05 M HCl) is added to 4 ml of heated water solution (~ 98°C), which contains 20 μ g (14 nmol) of DOTATOC. 2·10⁻⁵ mol of acid provide a pH value of 2.30±0.05. This condition

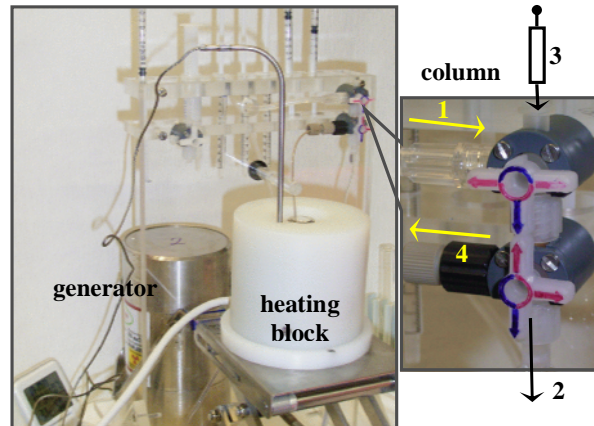


Fig. 1. Equipment for labelling of DOTATOC with generator-produced ⁶⁸Ga; to the right the micro-chromatography column.

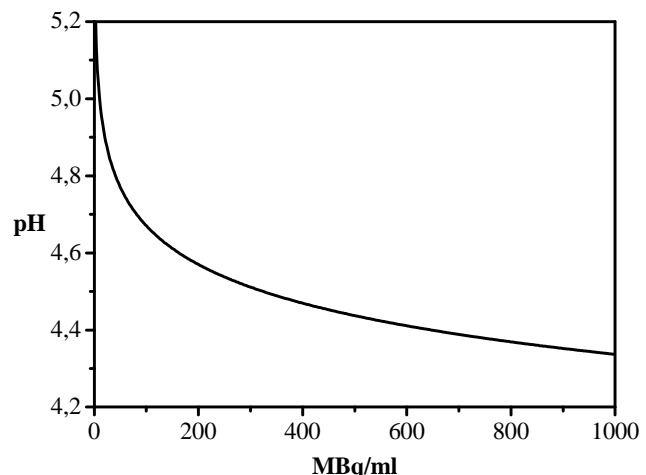


Figure 2. Solubility curve of ⁶⁸Ga

suppresses the hydrolysis and allows complexation in about 10 min. Finally, ⁶⁸Ga-DOTATOC is purified on a C-18 cartridge and can be obtained in 0.2-0.4 ml ethanol with a final specific activity of ~18 MBq per μ g peptide.

The developed system represents a simple and efficient way for labelling of DOTATOC with ⁶⁸Ga and preparation of an injectable radiopharmaceutical within 20-25 min.

References

- [1] Mäcke, H. R., Good, S.: “Radiometals (non-Tc, non-Re) and bifunctional labeling chemistry”; Handbook of Nuclear Chemistry, volume 4, Amsterdam, (2003)
- [2] Zhernosekov et al., this report
- [3] Baes, C. F., Mesmer, R. E. The Hydrolysis of Cations, Krieger Publisher Company, Inc., Florida (1986)

Systematische Überprüfung verschiedener Reaktionsparameter bei der Markierung einer einfachen Modellverbindung mit [¹⁸F]FETos/LiI

A.Bauman, M. Piel, S. Höhnemann, M. Kölzer, F. Rösch

Institut für Kernchemie, Johannes Gutenberg - Universität Fritz Straßmann Weg 2, 55128 Mainz

Durch geringen Zusatz an Alkalimetalliodiden zu einer Lösung, die den Markierungsvorläufer enthält und Starten der Reaktion durch Zugabe des sekundären Markierungsvorläufers [¹⁸F]BFE lässt sich auf einfache und effiziente Weise die Markierungsausbeute drastisch steigern: In einem Finkelstein-Austausch entsteht *in situ* [¹⁸F]IFE, das stärker alkylierende Eigenschaften besitzt [1]. Insbesondere die Wahl des Lösungsmittels und des Alkalimetalliodides haben großen Einfluß auf die radiochemische Ausbeute. In weiteren Experimenten an Verbindungen mit nuklearmedizinischer Relevanz konnte außerdem gezeigt werden, dass durch Zugabe von [¹⁸F]FETos in analoger Weise [¹⁸F]IFE gebildet wird und so die Markierungsausbeute teilweise um den Faktor 2 gesteigert wird [2]. In einer aktuellen Veröffentlichung von Zhang et al. [3] wurde berichtet, dass der Zusatz von NaI zum sekundären Markierungsvorläufer [¹⁸F]BFE einen deutlichen Effekt auf die radiochemische Ausbeute hat, dieser aber unabhängig von der Konzentration des NaI ist.

Im Rahmen dieser Arbeit sollte daher überprüft werden, inwiefern sich die Reaktionsparameter Temperatur, Iodsalz- und Markierungsvorläufer-Konzentration auf die radiochemische Ausbeute auswirken. Zum Zweck einer systematischen Untersuchung wurde für die Reaktionen als Iodsalz LiI ausgewählt. Die Reaktionen wurden ohne Verwendung einer Base, bei 100 °C im Lösungsmittel DMSO hinsichtlich ihrer Kinetik mit 4-Phenylpiperazin untersucht.

Bei der Verwendung unterschiedlicher Ausgangskonzentrationen von LiI zeigte sich eine deutliche Abhängigkeit der radiochemischen Ausbeute von der eingesetzten Menge des Salzes. Bei Verwendung der Konzentrationen 0, 15, 49, 75 und 150 µmol konnte eine deutliche Erhöhung der radiochemischen Ausbeute erreicht werden (Abb. 1).

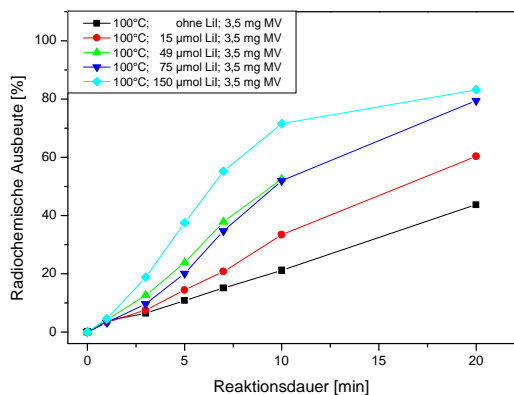


Abbildung 1: Abhängigkeit der radiochemischen Ausbeute bei der Markierung von 4-Phenylpiperazin im System [¹⁸F]FETos/LiI/DMSO/100°C bei verschiedenen Iodkonzentrationen

Zur Abschätzung der Temperaturabhängigkeit wurde LiI in einer Konzentration von 150 µmol in DMSO mit dem Substrat bei 80°C, 100°C und 120°C umgesetzt.

Erwartungsgemäß wurde die radiochemische Ausbeute sehr stark durch die Wahl der Temperatur bestimmt. So wurden

nahezu quantitative Ausbeuten bei 120°C erreicht, während bei 80°C lediglich 38% Ausbeute erzielt wurden (Abb. 2).

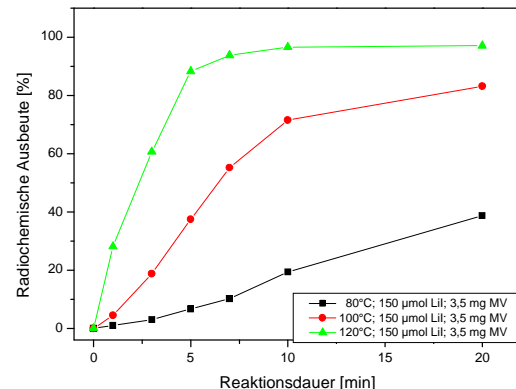


Abbildung 2: Abhängigkeit der radiochemischen Ausbeute bei der Markierung von 4-Phenylpiperazin im System [¹⁸F]FETos/LiI (143 µmol) bei verschiedenen Temperaturen

Die Verwendung verschiedener Konzentration an Markierungsvorläufer führte zu einer signifikanten Änderung der Ausbeuten. Eine Variation von 2 mg über 3,5 mg auf 8 mg bewirkte eine sukzessive Steigerung der Ausbeute bis zu 97% (Abb. 3).

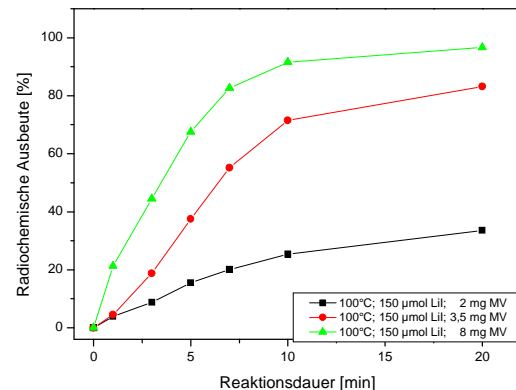


Abbildung 3: Resultate der radiochemischen Markierungen von 4-Phenylpiperazin im System [¹⁸F]FETos/LiI/DMSO/100°C bei unterschiedlicher Markierungsvorläuferkonzentration

Zusammenfassend lässt sich damit feststellen, dass die radiochemische Ausbeute nicht nur von den Parametern Lösungsmittel, Temperatur und Iodsalz abhängt, sondern auch in nicht vernachlässigbarer Weise von der Konzentration des verwendeten Iodsalzes und Markierungsvorläufers.

Literatur:

1. Bauman A., Diplomarbeit, Universität Mainz, **2002**
2. Bauman, A.; Piel, M.; Schirrmacher, R.; Rösch, F.; Tetrahedron Letters, 2003, 44, 9165-9167
3. Zhang, M.-R.; Furutsuka, K.; Yoshida, Y.; Suzuki, K. J. Label. Compd. Radiopharm. 2003, 46, 587-598

Synthese und Markierung zweier NMDA-Liganden zur Visualisierung des Rezeptorstatus

A. Bauman¹, M. Piel¹, S. Höhnemann¹, M. Jansen², G. Dannhardt², F. Rösch¹

Institut für Kernchemie, Johannes Gutenberg–Universität, Fritz Strassmann-Weg 2, 55128 Mainz

Institut für Pharmazie, Johannes Gutenberg–Universität, Staudingerweg 5, 55128 Mainz

Nachdem in früheren Arbeiten [1] erfolgreich die kalte Standardverbindung **11a** synthetisiert wurde und die *in vitro*-Testung mit einem IC₅₀-Wert von 57 nM sehr vielversprechend war, wurde in weiteren Versuchen eine ¹⁸F-Fluorethylierung durchgeführt.

Die Synthese [2,3,4] des Indol-2-carbonsäure-derivates **9**, **10** wurde ausgehend von 4,6-Dichlorphenylhydrazin **1** durchgeführt. In einer Reaktion mit Ethylpyruvat wurde das entsprechende 3,5-Dichlorphenylhydrazon **2** erhalten. Die Überführung des Hydrazons in das entsprechende Indol erfolgte nach Fischer, die Einführung der Aldehydgruppe in einer Vilsmeier-Synthese mittels N-Methylformanilid und Phosphorychlorsäure. Nach reduktiver Aminierung in Anwesenheit von Natriumacetoxymethyldihydrid wurde **5** erhalten, das mit Triphosgen und anschließender Zugabe von 4-(benzyloxy)anilin zum Harnstoffderivat **6** umgesetzt wurde. Der Ringschluss zum Hydantoin **7** erfolgte mittels Natriummethanolat in ethanolischer Lösung.

Zur Darstellung des Markierungsvorläufers **9**, wurde ausgehend von Verbindung **7** die Benzylschutzgruppe unter Katalyse mit Palladium auf Aktivkohle reduktiv entfernt, während die Darstellung von Markierungsvorläufer **10** eine vorausgehende Verseifung des Carbonsäureesters **7** und anschließende reduktive Entfernung der Benzylschutzgruppe erfordert.

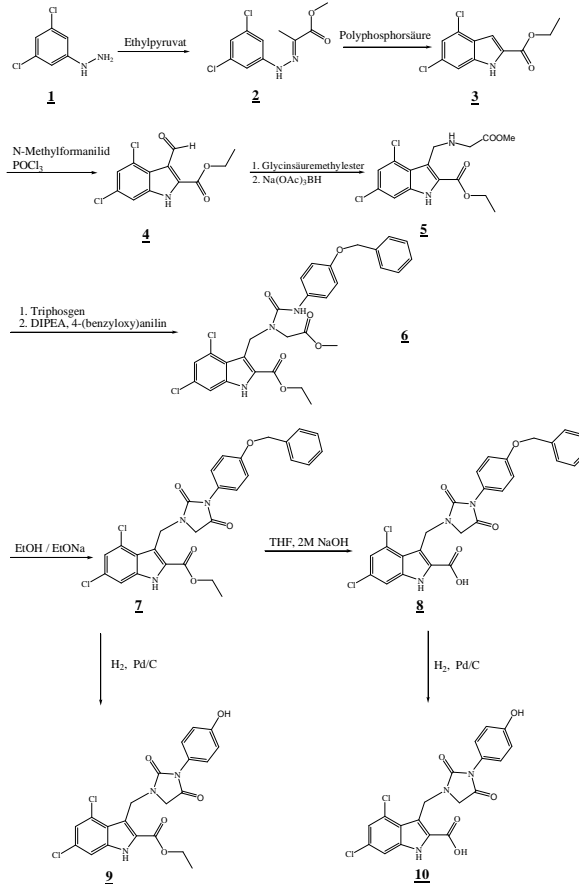


Abb. 1: Syntheseschema zur Darstellung der Markierungsvorläufer

In ersten Markierungsversuchen wurde **8** in DMF bei 100°C unter Verwendung von 5 N NaOH mit [¹⁸F]FETos, bzw. [¹⁸F]FETos/LiI umgesetzt. Hierbei konnte das gewünschte Produkt **11** zu 7% (^{[18]F}FETos) bzw. 21% (^{[18]F}FETos/LiI) erhalten werden. Im Fall von [¹⁸F]FETos wurde, neben marginalen Mengen von Zersetzungreaktionen, ein unbekanntes Nebenprodukt zu 76%, im Fall von [¹⁸F]FETos/LiI zu 21% detektiert. Weiterhin wurde in diesem Fall eine beträchtliche Menge an nicht umgesetzten [¹⁸F]IFE identifiziert. Aufgrund des Vorhandenseins einer weiteren reaktiven funktionellen Gruppe, neben der phenolischen Funktion, kann davon ausgegangen werden, dass es sich bei dem unbekannten Nebenprodukt um **12** handelt.

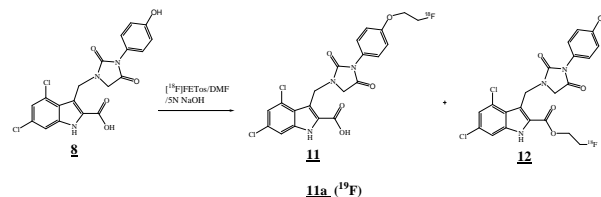


Abb. 2: Radioaktive Markierung von **8** im System FETos/DMF, 100 °C, bzw. FETos/LiI/DMF, 100 °C

Zur Vermeidung dieser Nebenreaktion wurde die Markierung in weiteren Versuchen ausgehend von **7** durchgeführt. Im Anschluss an die Markierung erfolgte die Abtrennung mittels präparativer HPLC und schließlich die Verseifung mit 1 N NaOH. Dieser Ansatz zeigte sich erfolgversprechender. Nach einer Reaktionszeit von 5 min. konnte **11** mit einer Ausbeute von 35% erhalten werden, wobei eine Verlängerung der Reaktionszeit zu einer Verminderung der Ausbeute führte, da unter den gegebenen Reaktionsbedingungen eine fortschreitende Verseifung und Nebenprodukten eintraten.

Eine Übertragung auf eine semiautomatisierte Apparatur wurde bereits erfolgreich durchgeführt, so dass für die Zukunft eine Optimierung der Reaktionsparameter sowie weitere Derivatisierungen im Hinblick auf eine ¹¹C-Markierung angestrebt werden.

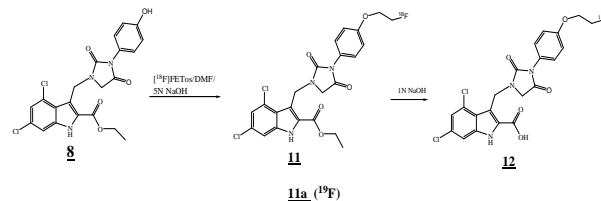


Abb. 3: Radioaktive Markierung von **7** im System FETos/DMF, 100 °C

References

1. Bauman, A. et al.; Jahresbericht **2003**,
2. Micheli, F.; Di Fabio, R.; et al. *Arch. Pharm. Pharm. Med. Chem.* **1999**, 332, 271-278
3. Jansen, M.; Dissertation; Universität Mainz **2001**
4. Jansen, M.; Potschka, H.; Brandt, C.; Löschner, W.; Dannhardt G.; *J. Med. Chem.* **2003**, 46, 64-73

Synthese und ^{131}I -Radioiodierung von Benzamidlderivaten zur Visualisierung von D2-artigen Dopaminrezeptoren

D. Stark¹, M. Piel¹, D. Bier², M. H. Holschbach², F. Rösch¹

¹⁾ Institut für Kernchemie, Johannes Gutenberg-Universität, Fritz-Straßmann-Weg 2, 55128 Mainz

²⁾ Institut für Kernchemie, Forschungszentrum Jülich GmbH, 52452 Jülich

Einleitung: In vorausgegangenen Arbeiten wurden iodierte Analoga der bereits etablierten D2-selektiven PET-Radioliganden [^{18}F]Fallypride ([^{18}F]FP) und [^{18}F]Desmethoxyfallypride ([^{18}F]DMFP) synthetisiert [1 - 6]. Diese zur Klasse der Benzamide gehörenden Verbindungen besitzen günstige Eigenschaften, die mittels der iodierten Derivate, [^{131}I]IFP und [^{131}I]IDMFP, für die SPECT nutzbar gemacht werden sollen, um eine Alternative zu [^{123}I]IBZM zu bieten (Abb. 1).

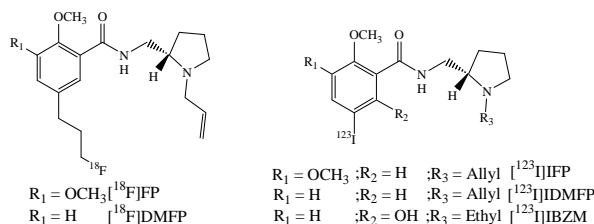


Abb. 1: Struktur von [^{18}F]FP, [^{18}F]DMFP, [^{131}I]IFP, [^{131}I]IDMFP und [^{123}I]IBZM.

Zielstellung: Ebenfalls wurden Brom- und Stannyl-Markierungsvorläufer synthetisiert sowie erste Radioiodierungsversuche mit [^{131}I]NaI durchgeführt [6].

Die Radioiodierung der Brom-Markierungsvorläufer verlief mit Ausbeuten von 60 – 85 %. Die Radioiodierung des Stannyl-Markierungsvorläufers gelang zunächst nicht [6] (Abb. 2).

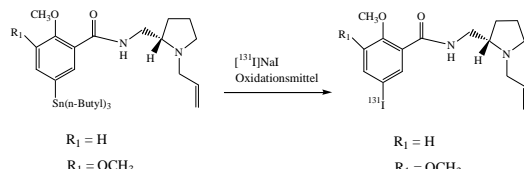


Abb. 2: Radioiodierung der Stannyl-Vorläufer

Es galt nun, die Durchführung dieser Markierungsreaktion zu modifizieren. In einem Ethanol/Phosphatpuffergemisch mit Chloramin T (CAT) als Oxidationsmittel verliefen die Radioiodierungen des Stannyl-Markierungsvorläufers erfolgreich. Die verschiedenen Reaktionsbedingungen sind in Tabelle 1 aufgelistet.

Methode	Aktivität	Vorläufer**	2 N HCl	Puffer pH 7,5	CAT***	
					in Wasser	in Puffer
Methode A	10 μl	25 μl	---	25 μl	10 μl	---
Methode B	10 μl	25 μl	3 μl	---	10 μl	---
Methode C	10 μl	25 μl	---	25 μl	---	10 μl
Methode D	10 μl	25 μl	---	10 μl	---	10 μl
Methode E	10 μl	25 $\mu\text{l}^{\#}$	---	25 μl	---	10 μl
Methode F	10 μl	25 $\mu\text{l}^{\#}$	---	10 μl	---	10 μl
Methode G	10 μl	25 $\mu\text{l}^{\#}$	3 μl	---	10 μl	---

**= 7,7 MBq in 100 μl Wasser

**= 50 μg Vorläufer gelöst in 50 μl abs. Ethanol

***= 15 mg in 10 μl Wasser bzw. Phosphatpuffer pH 7,5

= 50 μg Vorläufer gelöst in 75 μl abs. Ethanol

Tab. 1: Reaktionsbedingungen der Radioiodierungen mit [^{131}I]NaI und Chloramin T als Oxidationsmittel

Die Radiochemischen Ausbeuten für die Iodierung von SnFP beliefen sich auf ca. 20 - 60 % (Abb. 3).

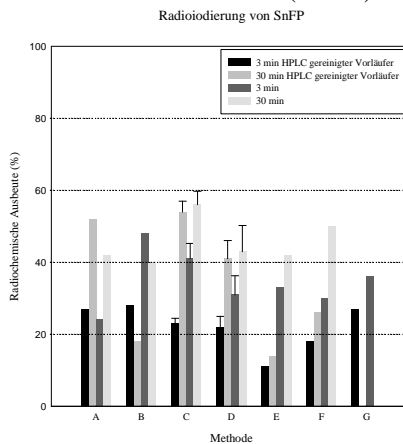


Abb. 3: Radioiodierung von SnFP mit CAT (Mittelwerte, n = 1-6)

Die radiochemischen Ausbeuten für die Radioiodierung von SnDMFP mit CAT lagen im Bereich von 50 % bis 70 % (Abb. 4).

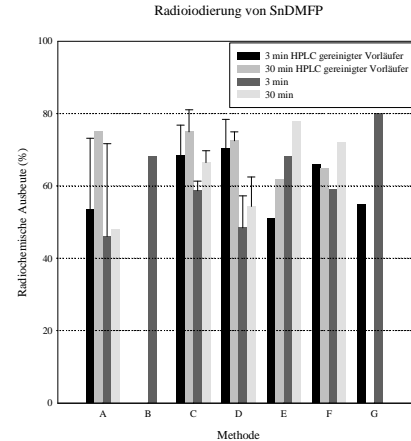


Abb. 4: Radioiodierung von SnDMFP mit CAT (Mittelwerte, n = 1-6)

Eine Aufreinigung des Vorläufers mittels HPLC ergab nur in Einzelfällen bessere radiochemische Ausbeuten. Methode C erwies sich als optimale Radioiodierungsmethode.

Ausblick: Untersuchungen zur Biodistribution in Ratten sind in Vorbereitung

- [1] M. Piel, Diplomarbeit, Institut für Kernchemie, Johannes Gutenberg-Universität Mainz, 1997
- [2] M. Piel et. al., Jahresbericht 1997, B 3, S. 22, Institut für Kernchemie, Johannes Gutenberg-Universität Mainz, 1998
- [3] T. Höglberg et al., Acta Chemica Scandinavica 43 (1989), 660-664
- [4] S. Chumpradit et al., J. Med. Chem. 36 (1993), 221-228
- [5] D. Stark et al., Jahresbericht 2001, C 11, Institut für Kernchemie, Johannes Gutenberg-Universität Mainz, 2002
- [6] D. Stark, Diplomarbeit, Institut für Kernchemie, Johannes Gutenberg-Universität Mainz, 2002

Improved automated synthesis of [¹⁸F]FECh as a radiotracer for prostate cancer imaging

M. Piel¹, A. Bauman¹, I. Klette¹, S. Höhnemann¹, R. Wortmann², R. P. Baum², F. Rösch¹

¹Institute of Nuclear Chemistry, Johannes Gutenberg-Universität Mainz; ²Department of Nuclear Medicine, Zentralklinik Bad Berka

Introduction: Many tumours are characterized by an enhanced cell proliferation. This is normally associated with an elevated uptake and phosphorylation of choline to form phosphoryl choline, which is used in the synthesis of membrane phospholipids.

Therefore [¹¹C]choline was developed and has shown its potential by evaluation of brain tumours, esophageal carcinoma and prostate carcinoma.¹⁻³ Because of the short half-life of ¹¹C ($T_{1/2} = 20.3$ min), resulting in a limited usefulness for clinical routine, different ¹⁸F-labelled ($T_{1/2} = 109.7$ min) analogues were synthesized to overcome this problem. Shown in figure 1 are the most prominent choline derivatives:

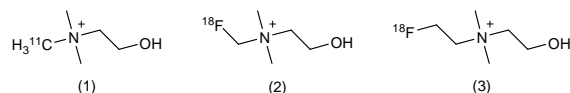


Fig. 1:
Structure of [¹¹C]choline (1) and the fluorinated analogues [¹⁸F]fluorocholine (2,) and [¹⁸F]fluoroethylcholine (3, FECh)

GE Medical System. Because of the different labelling techniques of ¹¹C and ¹⁸F the module had to be modified. Hence the cooling, the heating and some valves and tubes had to be rearranged, resulting in the module shown in figure 2.

[¹⁸F]FECh was prepared in a two step synthesis, via a ¹⁸F-fluoroethylation using [¹⁸F]FETos. In the first step [¹⁸F]fluoride was dried and reacted with ethylenglycol-1,2-ditosylate to yield [¹⁸F]FETos. The crude product then was diluted with water, loaded on a Lichrolut EN column and eluted using DMSO. Afterwards this solution was reacted with N,N-dimethylaminoethanol for 20 minutes using alkali iodide catalysis, then diluted with water and purified with a LiChrolut SCX column and HPLC to yield the [¹⁸F]FECh.

This synthesis results in a total radiochemical yield of 20-25 % within 50 min. The identity of [¹⁸F]FECh was confirmed by gradient HPLC, by comparing the radiochromatograms with chromatograms of the unlabelled FECh, showing a radiochemical purity of over 95%.

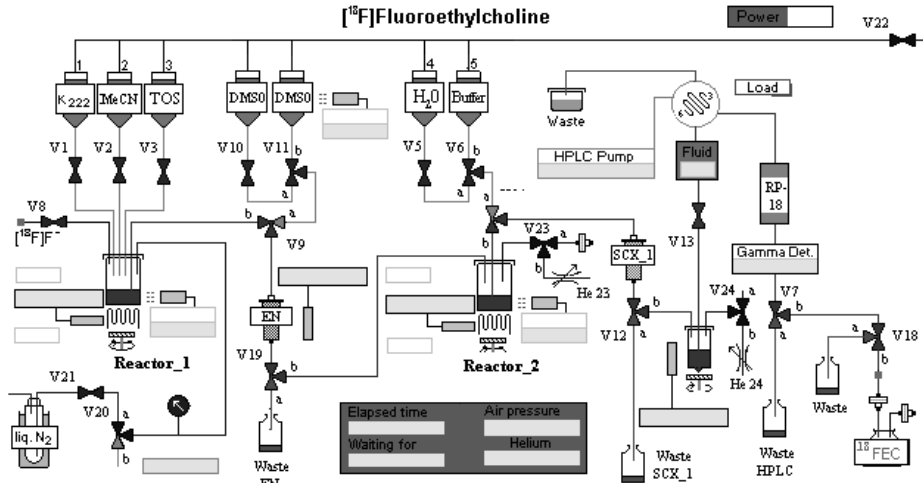


Fig. 2: Diagram of the automated synthesis module for the production of [¹⁸F]FECh

Considering the isotope properties, complexity of synthesis and biochemical behaviour of the derivatives, [¹⁸F]FECh seems to be the most promising candidate for clinical PET studies. Hence there is a high interest in a reliable, fully automated synthesis for the production of [¹⁸F]FECh.

Recently we reported that the addition of alkali iodides to 2-[¹⁸F]fluoroethyltosylate ([¹⁸F]FETos) and 1-bromo-2-[¹⁸F]fluoroethane led to drastically increased radiochemical yields most probably due to the *in situ* formation of 1-iodo-2-[¹⁸F]fluoroethane.⁴ We therefore developed a new approach for a fully automated synthesis for the production of [¹⁸F]FECh, using the iodide promoted alkylation, which circumvents the problems of the one-pot strategy.

Results: The automated radiosynthesis of [¹⁸F]FECh was performed by using a module for ¹¹C-methylation from

Conclusion: After optimization and automation of this iodide promoted ¹⁸F-fluoroalkylation of N,N-dimethylaminoethanol, a fast and reliable high-yield synthesis of [¹⁸F]fluoroethylcholine was developed, which can be accomplished by a modified commercial available module. This is especially important when large amounts of [¹⁸F]fluoroethylcholine, for example in PET studies, are needed.

References:

- [1] Hara T, Kosaka N, Shinoura N, Kondo T, J Nucl Med 1997; **38**: 842-847
- [2] Larson SM, J Nucl Med 1994; **35**: 1653-1655
- [3] Hara T, Kosaka N, Kishi H, J Nucl Med 1998; **39**: 990-995
- [4] Bauman A, Piel M, Schirrmacher R, Rösch F, Tetrahedron Lett 44 (2003) 9165-9167

¹³¹I-Radioiodierung neuer MGMT-Inhibitoren und ihrer Glucose-konjuguierten Analoga

U. Mühlhausen¹, R. Schirrmacher¹, M. Piel¹, D. Bier², M. H. Holschbach², B. Kaina³, F. Rösch¹

1) Institut für Kernchemie, Johannes Gutenberg-Universität, Fritz-Straßmann-Weg 2, 55128 Mainz

2) Institut für Kernchemie, Forschungszentrum Jülich GmbH, 52452 Jülich

3) Institut für Toxikologie, Johannes Gutenberg-Universität, Obere Zahlbacher Str. 67, 55131 Mainz

Einleitung: Bestimmte Tumorarten produzieren ein Enzym, das die Therapie mit alkylierenden bzw. chloralkylierenden Chemotherapeutika erschwert. Die Wirkung dieser Cytostatika beruht auf einer Blockierung der Replikation der Tumor-DNA durch Alkylierung von Guanin (Thymin), die im günstigsten Fall einen Rückgang des Tumorwachstums zur Folge hat. Das Enzym O⁶-Methylguanin-DNA-methyltransferase (MGMT) ist in der Lage, diese Blockierung der DNA effektiv rückgängig zu machen. Als Folge dieses Reparatur schrittes sind die Tumorzellen wieder in der Lage, sich zu vermehren.

Schon seit einiger Zeit ist bekannt, dass MGMT eine hohe Affinität zu bestimmten O⁶-substituierten Guaninen aufweist. Unter diesen zeigen das O⁶-5-Bromothenylguanin ($IC_{50} = 0,005 \mu\text{M}$) und das O⁶-Benzylguanin ($IC_{50} = 0,62 \mu\text{M}$) die höchsten Affinitäten [1]. Durch Konjugation dieser Inhibitoren mit einer Glucoseeinheit soll eine selektivere Aufnahme dieser Verbindungen in Tumorzellen gegenüber gesunden Zellen ermöglicht und so mögliche Nebenwirkungen minimiert werden [2]. Mit einem geeigneten radioaktiv markierten Substrat kann dieses Konzept des besseren Tumor-Targetings und auch die Anreicherung im Tumorgewebe überprüft werden.

Zielstellung: In der Hoffnung, die Pharmakokinetik der MGMT-Substrate für das Tumorgewebe zu erhöhen, wurden die O⁶-substituierten Guanine ITG (O⁶-(5-Iodothenyl)guanin) und IBG (O⁶-(3-Iodbenzyl)guanin) in 9-Position über einen Alkylspacer mit einer β-Glucoseeinheit konjugiert und ihre IC_{50} -Werte zur MGMT untersucht [3]. Für *in vitro*- und *in vivo*-Untersuchungen sollten die Glucose-Konjugate mit ¹³¹I radioiodiert und mit den entsprechenden radioiodierten nichtglycosylierten Verbindungen verglichen werden.

Für die Radioiodierung wurden die korrespondierenden Stannylvorläufer SnBGG, SnBGSi, SnTGG und SnTGGSi dargestellt (Abb. 1).

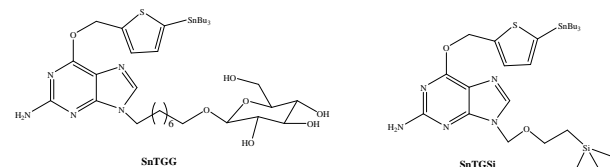


Abbildung 1: Markierungsvorläufer SnTGG und SnTGGSi

Die Radioiodierungen erfolgten in einem Phosphatpuffer/Ethanol-System bei einem pH-Wert von 7,0 mit Chloramin-T (CAT) als Oxidationsmittel. Die Reaktionsbedingungen wurden hinsichtlich der Reaktionszeit, der Markierungsvorläuferkonzentration und der CAT-Konzentration optimiert. Als Reaktionszeit erwies sich für alle Verbindungen 5 Minuten als ideal. Während bei den Glucosekonjugaten keine verstärkte Abspaltung des Alkohols an O⁶ mit zunehmender CAT-Konzentration beobachtet werden kon-

nnte, war die RCA bei den silygeschützten Guaninen stark von der CAT-Konzentration abhängig.

Im Anschluss an die Radioiodierung mussten diese Derivate noch an N⁹ entschützt werden. Dies erfolgte nach einer Literaturvorschrift [4] mit Tetrabutylammoniumfluorid in THF (Abb. 2).

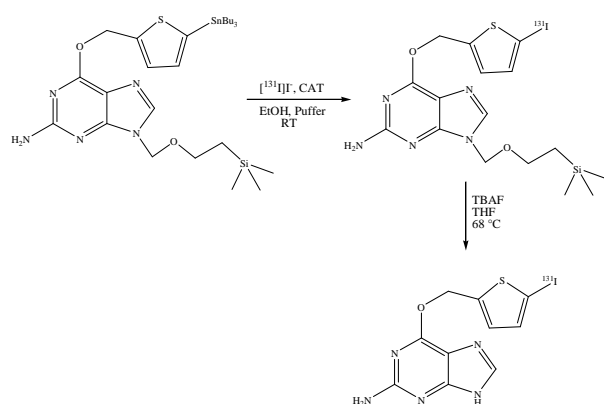


Abbildung 2: Darstellung von ^[131]IITG

Die Entschützung dauert etwa 30 Minuten, was bei einer Halbwertszeit von 8 d bei ¹³¹I kein Problem darstellt. Unter den für die jeweilige Verbindung optimalen Bedingungen konnten sehr gute radiochemische Ausbeuten (RCA) zwischen 72 und 94 % erreicht werden (Tabelle 1).

Tabelle 1: Optimierte RCA der MGMT-Verbindungen

	[¹³¹ I]ITG	[¹³¹ I]ITGG	[¹³¹ I]IBG	[¹³¹ I]IBGG
RCA / %	71,5 ± 5,0	93,6 ± 0,8	82,0 ± 6,9	89,1 ± 0,9

Für weitere Untersuchungen wurden die Verbindungen mittels HPLC aufgereinigt und in einem für den jeweiligen Zweck geeigneten Lösungsmittel aufgenommen. Für eine längere Lagerung der radioiodierten Verbindungen eignete sich absolutes Ethanol bei 4°C am besten. Unter diesen Bedingungen waren alle Verbindungen länger als 30 Tage stabil.

Ausblick:

- Durchführung von Aufnahmestudien mit den radioiodierten Verbindungen zur Validierung des Konzeptes des besseren Tumor-Targetings durch Glucosekonjugation
- Übertragungsstudien auf MGMT mit den radioiodierten Verbindungen
- *in vivo*-Studien an tumortragenden Nacktmäusen

[1] R. S. McElhinney et al., J. Med. Chem.; **41**, 5265-5271 (1998)

[2] J. Reinhardt et al., J. Med. Chem.; **44**, 4050-4061 (2001)

[3] B. Kaina et al., J. Pharmacol. Exp. Therap.; **311**, 585-593 (2004)

[4] G. Vaidyanathan et al., Bioconjugate Chem; **11**, 868-875 (2000)

Synthesis and evaluation of a sugar-conjugated glibenclamide derivative

A. Korobeynikov^a, R. Schirrmacher^a, M. Schwanstecher^b, F. Rösch^a

^aInstitut für Kernchemie, Johannes Gutenberg – Universität, Fritz-Straßmann-Weg 2, 55128 Mainz;

^bInstitut für Pharmakologie und Toxikologie, Universität, Beethovenstr. 55, 38106 Braunschweig

Diabetes mellitus, better known as “diabetes”, is a chronic disease associated with abnormally high levels of the sugar glucose in the blood. There are two main types of the disease: insulin-dependent diabetes mellitus (IDDM, type 1), and non-insulin-dependent diabetes mellitus (NIDDM, type 2). IDDM is an autoimmune disease characterized by destruction of pancreatic β -cells being responsible for insulin secretion. It causes absolute insulin deficiency. NIDDM is associated with defects of insulin action (insulin resistance) and insulin secretion although pancreatic β -cells remain intact [1-3]. In this case, some pharmacological agents including sulfonylurea derivatives are commonly used to stimulate insulin secretion by binding to sulfonylurea receptors (SUR1) of β -cells.

Glibenclamide, one of the sulfonylurea derivatives, has a high binding affinity to human SUR1 [4]. This might allow using its ^{18}F -labelled analogues for visualizing and quantifying β -cells concentrations *in vivo* via positron emission tomography (PET).

Unfortunately glibenclamide has relatively high lipophilicity resulting in unspecific accumulation of a glibenclamide PET ligand in other organs. Thus, conjugation with a sugar moiety should decrease lipophilic properties of glibenclamide to an acceptable value not changing dramatically the binding affinity.

The synthesis of α -glucose-conjugated glibenclamide was carried out in eight reaction steps (Fig. 1) starting with the removing the acetyl group from the anomeric hydroxyl group of glucose pentaacetate (**1**) by means of benzylamine. Resulting tetraacetyl-D-glucose (**2**) was reacted with tert-butyl bromoacetate to yield the protected α -glucose-linker (**3**). Following deprotection with trifluoroacetic acid and chlorination in thionyl chloride gave the product (**5**), which was coupled with 4-amino-5-chloro-2-methoxybenzoic acid to yield the conjugate (**6**). This compound was then reacted with p-(2-aminoethyl)benzenesulfonamide through the formation of mixed anhydride by using ethylchloroformate and the product (**7**) was obtained. Reaction with cyclohexyl isocyanate in presence of copper chloride (**I**) gave the protected α -glucose-glibenclamide conjugate (**8**). The following deprotection with sodium methoxide yielded

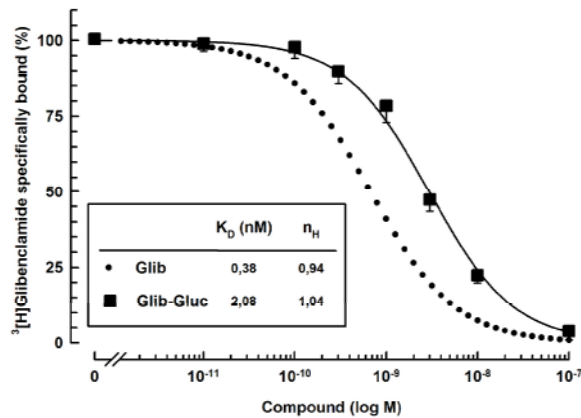


Fig.2

the final 4-[2-(α -D-glucopyranoside)-*O*-acetyl]amino-*N*{2-[4-({[(cyclohexylamino)carbonyl]amino}sulfonyl)-phenyl]ethyl}-5-chloro-2-methoxybenzamide (**9**). Competition binding experiments *in vitro* were performed as described [5] to assess the affinity of the glibenclamide-glucose conjugate for binding to human SUR1 (Fig. 2). The substance induced a complete monophasic inhibition curve (■) with a Hill coefficient (n_H) close to 1 (1.04) yielding a dissociation constant (K_D) of 2.08 nM. In parallel control displacement by unlabelled glibenclamide was assessed (K_D = 0.38 nM, n_H = 0.94, dotted line).

This result allows to go continue this study, the next step of which is the synthesis of glucose-conjugated glibenclamide precursor and its labeling with Fluor-18.

- [1] Ronner P. et al. Diabetes, 42: 1760-1772 (1993).
- [2] Schatz H. Diabetologie kompakt.- Berlin: Blackwell Wiss.- 2001.
- [3] Balabolkin M. I. Diabetologia.- Moskau: Medizina.-2000.
- [4] Ashcroft S., Ashcroft F. Biochimica et Biophysica Acta, 1175: 45-59 (1992).
- [5] Schwanstecher M. et al. Br J Pharmacol, 106: 295-301 (1992).

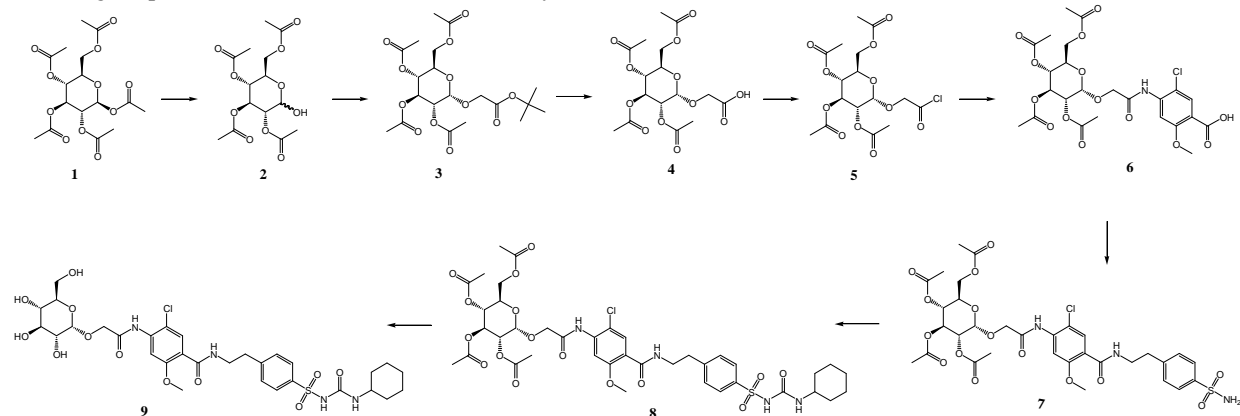


Fig. 1.

In vivo Evaluation and PET Imaging of [¹¹C]Harmine in Baboon Brains

T.Capito¹, Y.-S.Ding², J.Fowler², C.Shea², Youwen Xu²

¹Institut für Kernchemie, Johannes Gutenberg – Universität, Fritz Straßmann Weg 2, 55128 Mainz

²Chemistry Department, Brookhaven National Laboratory, NY

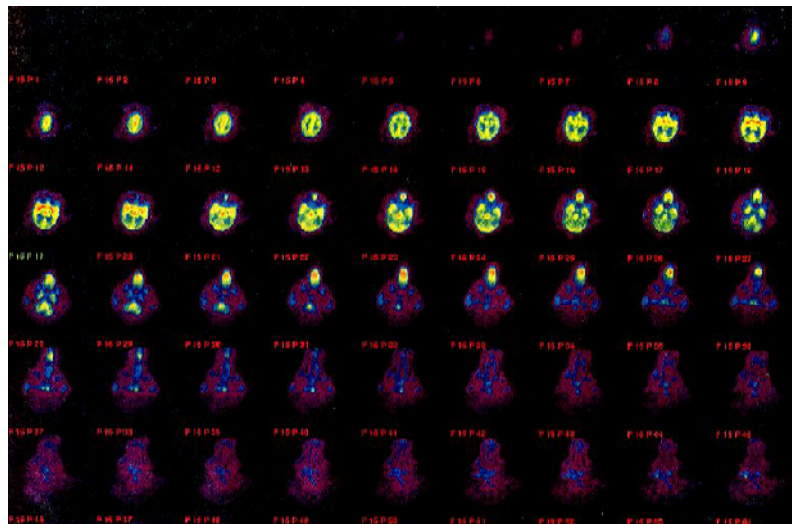


Fig. 1: Uptake of [¹¹C]harmine in a baboon showing specific and heterogeneous uptake in various brain areas

Introduction:

MAO (Monoamine-oxidases) are enzymes which participate in the oxidative deamination of monoamines. They exist in two different forms. Each form (MAO A and MAO B) is characterized by its substrate selectivity, specificity and its sensitivity to inhibitor substances.

Positron Emissions Tomography (PET) is a molecular imaging tool which allows the non-invasive and detailed observation of tracer kinetics *in vivo*. One of the requirements for the metabolic evaluation of drugs is the development of analogue radiotracers which are able to show quantitatively the distribution in tracer amounts inside the body.

For MAO B various radiopharmaceutical tracers are existing. L-[¹¹C]deprenyl and L-[¹¹C]deprenyl-D2 are used in PET-studies with high sensitivity in regions of high MAO B concentration. L-deprenyl is highly selective for MAO B but leaving MAO A intact. It is used in the treatment of Parkinson's disease, Alzheimer's disease, Schizophrenia and cocaine- and smoking-addiction [1].

However, in contrary to the large amount of MAO B-tracers used for PET, there are only few radiotracers for MAO A available to date. Although for example [¹¹C]chlordgyline is able to bind to MAO A in the human body, there is a lack of specific binding in rhesus monkeys. A group at the Uppsala University, Sweden has already developed another radiotracer, [¹¹C]harmine, with which they could get images of the *in vivo* uptake in rhesus monkeys [2].

In this report, the synthesis of [¹¹C]harmine is described and first *in vivo* images of baboon brains are illustrated.

Synthesis of [¹¹C]harmine:

0.471mmol harmine was dissolved in glacial acetic acid and heated subsequently to the addition of 48% hydrobromic acid overnight under refluxing. The evaporated residue was suspended in water and dissolved by addition of diluted potassium hydroxide. The aqueous

solution was washed with methylene chloride and diethyl ether. The product was precipitated with ammonium chloride and gave, after drying under reduced pressure, 77.2 mg (82%) precursor (desmethylated harmine) (1).

[¹¹C]methyl iodide was added to a mixture of 1.5 mg precursor (1) in 200 µl DMF and 3 equivalents of sodium hydroxide (4.5 µl). The reaction mixture was heated at T = 80°C for 5 minutes and then diluted with 500 µl 50 mM ammonium formate/acetonitrile (70:30).

Purification and Analysis:

Semi-preparative HPLC: Luna C₁₈ ODS 2, 5 µm, 250x10.00 mm); eluted with 50 mM ammonium formate/acetonitrile (70:30); flow 6 ml/min; UV-detection at 254 nm; retention time 13 min;

Analytical HPLC: Phenosphere C18 ODS 2, 5 µm, 250x4.60 mm) eluted with 50 mM ammonium formate/acetonitrile (60:40); flow 2.2 ml/min; UV-detection at 254 nm; retention time 8.2 min.

TLC (methylene chloride / ethylacetate / methanol / ammonium hydroxide [3 M] (20:20:10:1), Rf-value 0.75.

Conclusion:

The precursor for the production of [¹¹C]-harmine was synthesized with 82% yield using [¹¹C]methyl iodide. The compound was injected to a baboon and imaged using PET. [¹¹C]-harmine is a useful tracer for the observation of MAO A metabolism *in vivo*.

References:

- [1] MacGregor R.R et al., J. Label. Compd. Radiopharm. (1988), **25**, 1
[2] Bergström M et al., Nuc. Med. Biol. (1997), **24**, 381-389.

Acknowledgement:

This work was part of an ISAP exchange between the University of Mainz and the State University of New York at Stony Brook, 2003. Support by the DAAD is gratefully acknowledged.

PK 11195 as radiotracer for peripheral benzodiazepine binding sites (PK binding sites)

Yu-Shin Ding¹, Kuo-Shyan Lin¹, G Quandt², T Betzel², F Rösch², J Fowler¹

¹Brookhaven National Laboratory, ²Johannes Gutenberg-Universität Mainz

The isoquinoline carboxamide PK 11195 is a compound that binds specifically to the so-called “peripheral benzodiazepine binding sites” (PK binding sites). Although they are found at low levels in whole brain homogenates they are not neurotransmitter receptors. They are widespread and found in the kidney, adrenal gland, testicles, ovaries, lung and heart, where they are localized in the outer mitochondrial membrane; yet, their exact function is unclear.

It was found that the levels of PK binding sites in rat brains significantly increase in case of neuronal damage; for example after intrastratal or systemic injections of neuronal excitotoxins. This is associated with a macrophage invasion that occurs after the brain insult. Macrophages are known to be rich in PK binding sites. Therefore, [N-methyl-¹¹C]PK 11195 has a potential to be used as a tracer to study stroke, tumours, and diseases involving cell loss, e.g. Parkinson’s disease.

This project was focused on developing HPLC conditions for the semi-prep and the analytical column, and then doing a practice run. These have been our first steps towards a PET study with [N-methyl-¹¹C]-PK11195.

The precursor is N-desmethyl-PK 11195, obtained from ABX. It is labelled at the nitrogen position with a ¹¹C-methyl group derived from ¹¹C-methyliodide. The reaction vessel was preloaded with 1 mg N-desmethyl-PK 11195, which was dissolved in 0.4 mL DMSO and 10 mg finely powdered KOH. The whole reaction mixture was heated for 1.5 min at 90°C and then purified by semi-prep HPLC (Water μ-Bondapak-C18, 300 x 7.8 mm, 10 μm particle size; flow: 6 mL/min; solvent: 60% 0.01 M H₃PO₄, 40% acetonitrile). The retention time of the product was 10.8 min and that of the precursor was about 16 min. The solvent was removed by rotary evaporation, and the product was taken up in about 3 mL sterile saline.

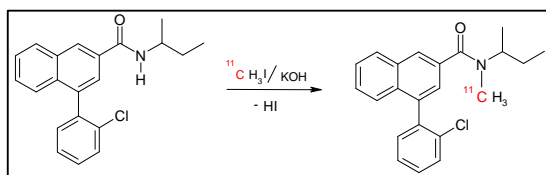


Fig.1: Labelling of PK 11195

For quality control, an aliquot of the product was analyzed by analytical HPLC and by radio-TLC. The analytical column for this purpose was Water μ-Bondapak-C18, 300 x 7.8 mm, 10 μm particle size, the flow was 1 mL/min and the solvent was the

same as that used for the semi-prep (60 % 0.01 M H₃PO₄, 40% acetonitrile). The product had a retention time of 11.6 min. For the radio-TLC 50% cyclohexane and 50% ethyl acetate was used as a solvent. The R_f of PK 11195 was 0.2 (see fig.2).

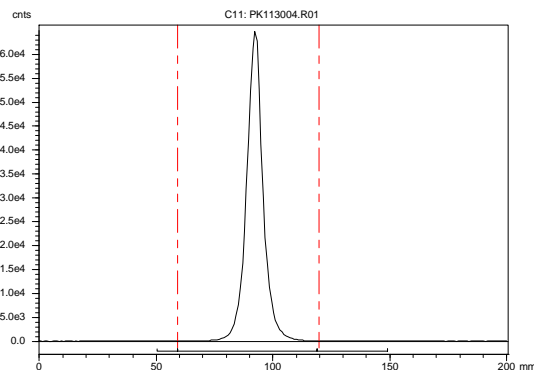


Fig.2: Radio-TLC, 99.85 % radiochemical purity

The practice run showed that N-desmethyl-PK 11195 can be labelled very easily with carbon-11. The radiochemical yield for this reaction was very high (about 78%). Unfortunately, much of the activity was trapped in the millipore filter; therefore, a smaller millipore filter will be used for the next run to avoid this problem. Also, the pH of the saline-product-solution was too low (~ 1.0), so 0.1 mL sodium bicarbonate solution had to be added to obtain a pH of about 5.5. The radiochemical purity of the product was 99.85%. The PPB was low, suggesting that most of the tracer doesn’t bind to the protein and can therefore reach the brain (not sure about this).

More studies with this tracer are being planned.

References

V.W. Pike et al., Radioligand for PET Studies of Central Benzodiazepine Receptors and PK Binding Sites, Nucl. Med. Biol., Vol. 20, No. 4, 503-525, 1993

Acknowledgement:

This work was part of an ISAP exchange between the University of Mainz and the State University of New York at Stony Brook, 2004. Support by the DAAD is gratefully acknowledged.

Synthesis of the Phytohormone [¹¹C]Methyl Jasmonate via Methylation on a C₁₈ Sep Pak™ Cartridge

Matthias M. Herth¹, Michael R. Thorpe², Frank Rösch³, Richard A. Ferrieri²

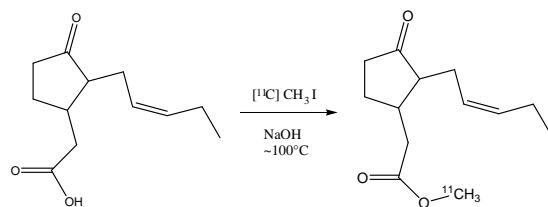
¹Johannes Gutenberg–Universität, Fachbereich Chemie, D –55099 Mainz, Germany

²Brookhaven National Laboratory, Chemistry Department, Upton, NY 11973-5000, USA

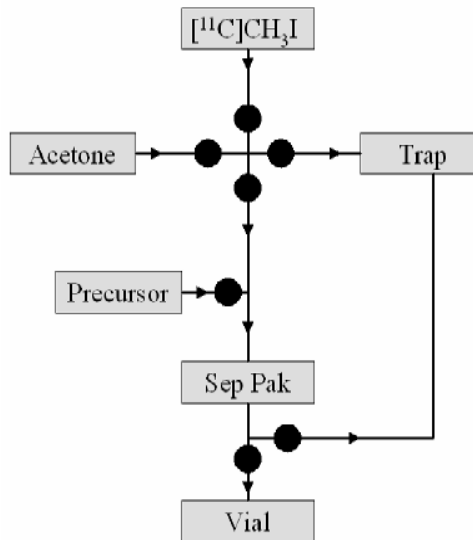
³Institute of Nuclear Chemistry, Johannes Gutenberg–Universität, D –55099 Mainz, Germany

Introduction: Exposure of plants to jasmonates, a class of plant hormones, has been shown to increase growth rate,¹ production of defensive secondary chemicals² and lignins.³ Recently, we have shown that jasmonates will increase leaf ¹¹C-sugar intermediates,⁴ with subsequent increase in phloem loading and ¹¹C-sucrose partitioning to roots. Hence, we believe a role of jasmonates in resource partitioning and chemical fractionation may come from their regulation of sugar-transport proteins that mediate the long-distance transport of carbohydrates within the plant vasculature. The purpose of the present work was to develop a rapid method for introducing carbon-11 ($t_{1/2}$ 20.4 min) into methyl jasmonate (MeJA). A key advantage for using this short-lived β^+ -emitting radionuclide in plant biology is that tracer can be quantified *in vivo*, so that the same plant can be tested repeatedly over time. Additionally, the high specific activity achievable with ¹¹C allows us to administer non-physiological doses of tracer for observations of *in vivo* transporter binding. These measurements cannot be made with ¹⁴C, ¹³C or ³H as tracers. The approach described in this work makes use of a solid-supported ¹¹C-methylation reaction.⁵ This approach holds significant appeal for ease of experimental setup, and minimal effort to purify the final product.

Results and Discussion: [¹¹C]Labeled (\pm)-methyl jasmonate was synthesized using a C₁₈ Sep Pak™ at ~100°C to sustain a solid-supported ¹¹C-methylation reaction of sodium (\pm)-jasmonate using [¹¹C]methyl iodide. After reaction, the Sep Pak was rinsed with acetone to elute the labeled product, and the solvent evaporated rendering [¹¹C]-(\pm)-methyl jasmonate at 96% radiochemical purity. The substrate, (\pm)-jasmonic acid, was retained on the Sep Pak so further chromatography was unnecessary. Total synthesis time was 25 min from the end of bombardment (EOB) which included 15 min to generate [¹¹C]methyl iodide using the GE Medical Systems PET Trace MeI system, 5 min for reaction and extraction from the cartridge, and 5 min to reformulate the product for plant administration. An overall radiochemical yield (at EOB) of 17 ± 4.3 % was obtained by this process, typically producing 10 mCi of purified radiotracer. A specific activity of 0.5 Ci/ μ mol was achieved using a short 3 min cyclotron beam to produce the starting ¹¹C.



Conclusions: (\pm)-[¹¹C]Methyl jasmonate was successfully produced in a short time, with high radiochemical purity of 96%, and in sufficient quantities that will allow for topical administration of tracer to intact leaves of plants. Although tracer specific activity was low, using larger starting amounts of ¹¹C might be expected to improve on this. The method described—using a disposable C₁₈ Sep Pak—has great appeal due to the ease of setup. The approach is amenable to automation, or at least remote operation, in order to minimize personnel exposure to radiation hazards. This is essential if we are to use tracer for receptor imaging.



Schematic diagram of the reaction system

References:

1. van Kleunen M., Ramponi G., Schmid B. -Basic and Applied Ecology 5(2): 173-181 (2004)
2. Arnold T.M., Appel H., Patel V., Stocum E., Kavalier A., Schultz J. -New Phytologist 164 (1): 157-164 (2004)
3. Lee J.E., Vogt T., House B., Lobler M. -Plant and Cell Physiology 38(7): 851-862 (1997)
4. Ferrieri R.A., Gray D.W., Babst B.A., Schueller M.J., Schlyer D.J., Thorpe M.R., Orians C.M., Lerdau M. - Plant, Cell & Environment (in press)
5. Pascali C., Bogni A., Iwata R., Cambiè M., Bombardieri E. -J. Labelled Cpd. Radiopharm. 43: 195–203 (2000)

Acknowledgement:

This work was part of an ISAP exchange between the University of Mainz and the State University of New York at Stony Brook, 2004. Support by the DAAD is gratefully acknowledged.

Transport and Fixation of Methyljasmonate in Tobacco Plants

Matthias M. Herth¹, Michael R. Thorpe², Frank Rösch³, Richard A. Ferrieri²

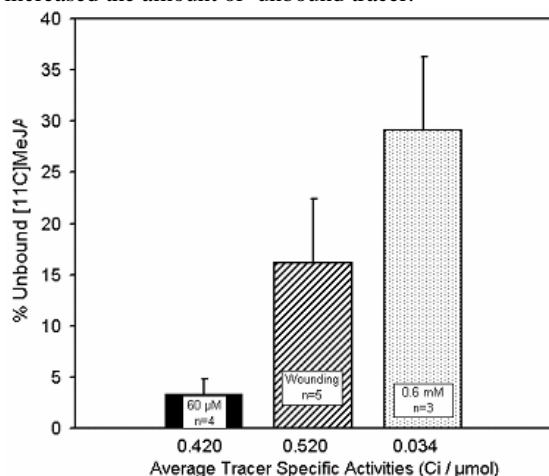
¹Johannes Gutenberg–Universität, Fachbereich Chemie, D –55099 Mainz, Germany

²Brookhaven National Laboratory, Chemistry Department, Upton, NY 11973-5000, USA

³Institute of Nuclear Chemistry, Johannes Gutenberg–Universität, D –55099 Mainz, Germany

Introduction: Jasmonates, a class of plant hormones, has been shown to increase production of defensive secondary chemicals after exposure to biological stress.¹ Those defense responses can be observed at the administration site as well as on other plant regions. But it is totally unclear if jasmonates, by themselves, or other messenger molecules are responsible for those systemic effects. Besides, we have shown that jasmonates will increase leaf ¹¹C-sugar intermediates,² with subsequent increase in phloem loading and ¹¹C-sucrose partitioning to roots. Hence, we believe a role of jasmonates in resource partitioning and chemical fractionation may come from their regulation of sugar-transport proteins that mediate the long-distance transport of carbohydrates within the plant vasculature. Recently, we developed a rapid method for introducing carbon-11 ($t_{1/2}$ 20.4 min) into methyl jasmonate (MeJA).³ This is a key advantage because it enables us to quantify the distribution of MeJA in vivo.

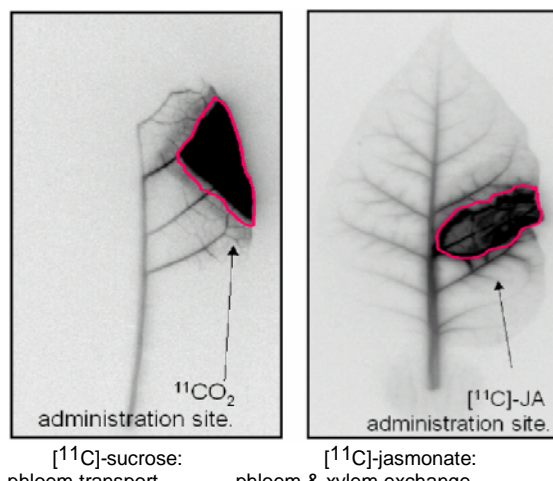
Results and Discussion: Transport of (\pm)-[¹¹C]Methyl jasmonate in Tabacco plants was determined by phosphor plate images 90 min after treatment. The radiographic images showed evidence of heavy tracer fixation within vascular tissue of administration site even though unbound tracer averaged $2.4 \pm 1.6\%$ ($n=4$). Wounding or treating the leaves with unlabeled MeJA prior to the administration increased the amount of unbound tracer.



Treatment with unlabeled MeJA 90 min after tracer administration also increased the total amount of unbound tracer. The results suggest a reversible binding of MeJA to receptors. Recently, we have shown that jasmonates will increase leaf ¹¹C-sugar

intermediates,² with subsequent increase in phloem loading and ¹¹C-sucrose partitioning to roots. Therefore MeJA could interact with sucrose transporters. A pretreatment with MeJA prevents the inhibition of sucrose transporters by pcmbs ((p-Chloromercuribenzene)-Sulfonic Acid) and underpin the former statement. In a further study we determined the binding affinity of MeJA for sucrose transporters to $2.5 \mu\text{M}$.

However, the distribution of MeJA is fundamentally different from that of sucrose. Sucrose is exclusively transported by the phloem whereas a xylem-phloem exchange could be observed from MeJA transport.



[¹¹C]-sucrose: phloem transport [¹¹C]-jasmonate: phloem & xylem exchange

Conclusions: We have shown heavy reversible fixation , phloem- xylem exchange and a prevention of sucrose transporters inhibition by pcmbs that suggests an interaction of MeJa with those transporters.

References:

1. Arnold T.M., Appel H., Patel V., Stocum E., Kavalier A., Schultz J. -New Phytologist **164** (1): 157-164 (2004)
2. Ferrieri R.A., Gray D.W., Babst B.A., Schueller M.J., Schlyer D.J., Thorpe M.R., Orians C.M., Lerdau M. - Plant, Cell & Environment (in press)
3. Herth M., Thorpe M., Ferrieri R. – Journal of labelled compounds, (in press)

Acknowledgement: This work was part of an ISAP exchange between the University of Mainz and the State University of New York at Stony Brook, 2004. Support by the DAAD is grateful acknowledged.

In vitro Stability and Immunoreactivity of ^{74}As [SATA]Vatuximab[®]

^{1,2}M. Jennewein, ²D. Zhao, ²J. He, ³A. Hermanne, ⁴S.M. Qaim, ²R.P. Mason, ²P.E. Thorpe, ¹F. Rösch

¹Institute for Nuclear Chemistry, Johannes Gutenberg-University of Mainz, Fritz-Strassmann-Weg 2, 55128 Mainz

²University of Texas Southwestern Medical Center, Dallas, TX 75390, USA

³Cyclotron Department, Vrije Universiteit Brussel, Laarbeeklaan 103, 1090 Brussels, Belgium

⁴Institute of Nuclear Chemistry, Research Centre Jülich, D-52425 Jülich,

Introduction: Vascular phosphatidylserine (PS) exposure is observed in solid tumors as a result of exposure to stress conditions in the tumor microenvironment [1,2]. Therefore antibodies against PS should be ideal for tumor targeting, especially for the targeting of tumor vasculature endothelium [2]. The Vatuximab[®] anti-PS antibody (AB) was labelled with the PET isotope ^{74}As ($T_{1/2}=17.77$ d, 29% β^+) as described in [3] and tested for its *in vitro* long term stability and immunoreactivity after labelling. Purpose of this study was the evaluation of the developed labelling method for ABs with radioactive arsenic isotopes, using Vatuximab[®] as an example.

Experimental: The antibody was SATA-modified and labelled as described in [3]. The deprotection of the sulphydryl groups was performed directly before the labelling. 100 μg of SATA-modified antibody in 3 ml PBS at pH=7.5 then were combined with nca [^{74}As]AsI₃ solution at 37°C for 30 minutes. Quality control was performed with HPLC, using an Agilent 1100 Series HPLC system, with an LDC/Milton Roy UV-Monitor III at 254 nm and a ‘Gabi’ NaI-radiation Monitor from Raytest. The column was a Bio-Silic Sec 250-5, 300x7.8 mm and PBS + 0.01M NaN₃ was used as solvent.

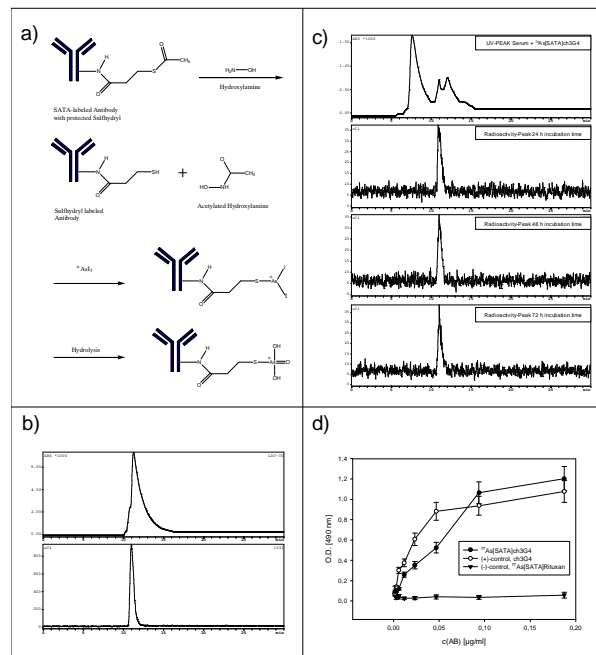
In vitro stability of the radioarsenic labeled ch3G4 was tested via incubation in fetal bovine serum (FBS) and HPLC measurements at various timepoints up to 72 h. 10 μg of radioarsenic labeled ch3G4 in 50 μl PBS were combined with 500 μl FBS and incubated at T= 37°C. Aliquots of 50 μl were taken at t=30 min, 24, 48, and 72 h, diluted with 200 μl water and 20 μl were applied to HPLC under the conditions described above.

The immunoreactivity of the [^{74}As]SATA-Vatuximab[®] was tested using ELISA, with unlabelled anti-PS as positive control and [^{74}As]SATA-Rituxan[®] as negative control.

Results and Discussion: The quality control showed labelling yields after 30 min labelling time in general were above 99.9 %. The *in vitro* stability of the radioarsenic label was evaluated by incubation in serum, followed by HPLC. No degradation of the label was observed for incubation times up to 72 h. This reflects the covalent bound of the arsenic to the antibody. Attempts by other groups to bind arsenic via complexation to biomolecules always failed because of the low *in vitro* stability due to exchange with free thiols in the blood. The immunoreactivity of the labelled ch3G4 could be demonstrated using ELISA and no inhibition of immunoreactivity through SATA-modification and subsequent labelling with nca ^{74}As I₃ could be observed.

Fig. 1.

a) Reaction scheme for the labelling of SATA-modified antibodies with radioactive arsenic isotopes. The ^{74}As I₃ couples to one SH under elimination of HI, which can be caught by salts in the buffer solution. The 2 iodines remaining at the arsenic are getting hydrolysed and we assume that As is oxidized to +V.



b) Quality control of the labelling of ch3G4. After a labelling time of 30 min, an aliquot of 20 μl of the ^{74}As [SATA]ch3G4-solution was given over a size-exclusion column for radio-HPLC. The upper graph shows the UV-spectrum, the lower the corresponding radioactivity progression. No free ^{74}As was detectable.

c) *In vitro* stability of ^{74}As SATA-ch3G4. The upper graph shows the UV spectrum. Because of the low concentration of AB versus serum-proteins, we detected a typical serum profile. The lower graph shows the corresponding radioactivity peak remaining unchanged in position and peak area.

d) Immunoreactivity. Immunoreactivity was tested with an ELISA of ^{77}As [SATA]ch3G4, using unlabelled and unmodified ch3G4 as positive control and ^{77}As [SATA]Rituxan as negative control. No reduction of immunoreactivity through the applied SATA-modification with subsequent radioarsenic labeling was detectable.

Conclusion: The new method of labelling antibodies with radioactive arsenic isotopes was exemplified using the anti-PS AB Vatuximab[®]. Conditions for standard testing systems were established and evaluated. Labelling reactions were quantitatively and the label was stable attached to the AB, even though incubated in serum for 72 hours. The SATA modification and the used labelling method did not change the ABs immunoreactivity. This *in vitro* results very much encourage future *in vivo* evaluations of radioarsenic labelled antibodies.

References:

[1] Ran, S. et al., Cancer Research 62, 6132-6140, 2002

[2] Ran, S. et al., Int. J. Rad. Oncol. **54**, 1479, 2002

[3] Jennewein, M. et al., Annual Report, this issue.

Financial Support of the Böhringer Ingelheim Foundation is grateful acknowledged

New PET/MRI Fusion Images of ^{74}As labelled Vatuximab[®] in Prostate Cancer bearing Rats

^{1,2}M. Jennewein, ²N. Slavine, ²S. Seliouine, ²E. Tsyganov, ²V. Kodibagkar, ³A. Hermanne, ⁴S.M. Qaim, , ²R.P. Mason, ²P.E. Thorpe ¹F. Rösch

¹Institute for Nuclear Chemistry, Johannes Gutenberg-University of Mainz, 55128 Mainz; ²University of Texas Southwestern Medical Center, Dallas, TX 75390, USA; ³Cyclotron Department, Vrije Universiteit Brussel, 1090 Brussels, Belgium; ⁴Institute of Nuclear Chemistry, Research Centre Jülich, D-52425 Jülich

Introduction: Anionic phospholipids, principally phosphatidylserine, become exposed on the external surface of viable vascular endothelial cells in tumors, possibly in response to oxidative stresses present in the tumor microenvironment [1,2]. A new chimeric IgG₃ monoclonal antibody, Vatuximab[®], directed against anionic phospholipids was raised. A method for the labelling of antibodies with radioactive arsenic isotopes was developed [3] and the antibody was tested for its ability to localize to tumor vessels and imaging qualities with PET.

Experimental: Four R3227 Dunning prostate AT1 tumor bearing rats were injected with 10 MBq of $^{74}\text{As}[\text{SATA}]ch3G4$ in 500 μl of PBS (pH 7.4, 1 mMol EDTA) in the tail vein. The animals were sedated using Isoflurane and imaged with a self-developed Small

Animal PET camera at 24, 48 and 72 h after injection. Coincident data were collected for the 511 keV gamma rays with a 250-750 keV window for 2 h. The images were reconstructed using a self-programmed 3D-reconstruction algorithm.

Results and Conclusion: Vatuximab[®] localizes specifically to anionic phospholipids on the surface of vascular endothelial cells in Dunning rat prostate tumors. The biomedical use of radioactive arsenic isotopes was demonstrated for the first time in a multi-modality molecular imaging approach *in vivo*.

References:

- [1] Ran, S. et al., Cancer Research 62, 6132-6140, 2002
- [2] Ran, S. et al., Int. J. Rad. Oncol. **54**, 1479, 2002
- [3] Jennewein, M. et al., Annual Report, 2003.

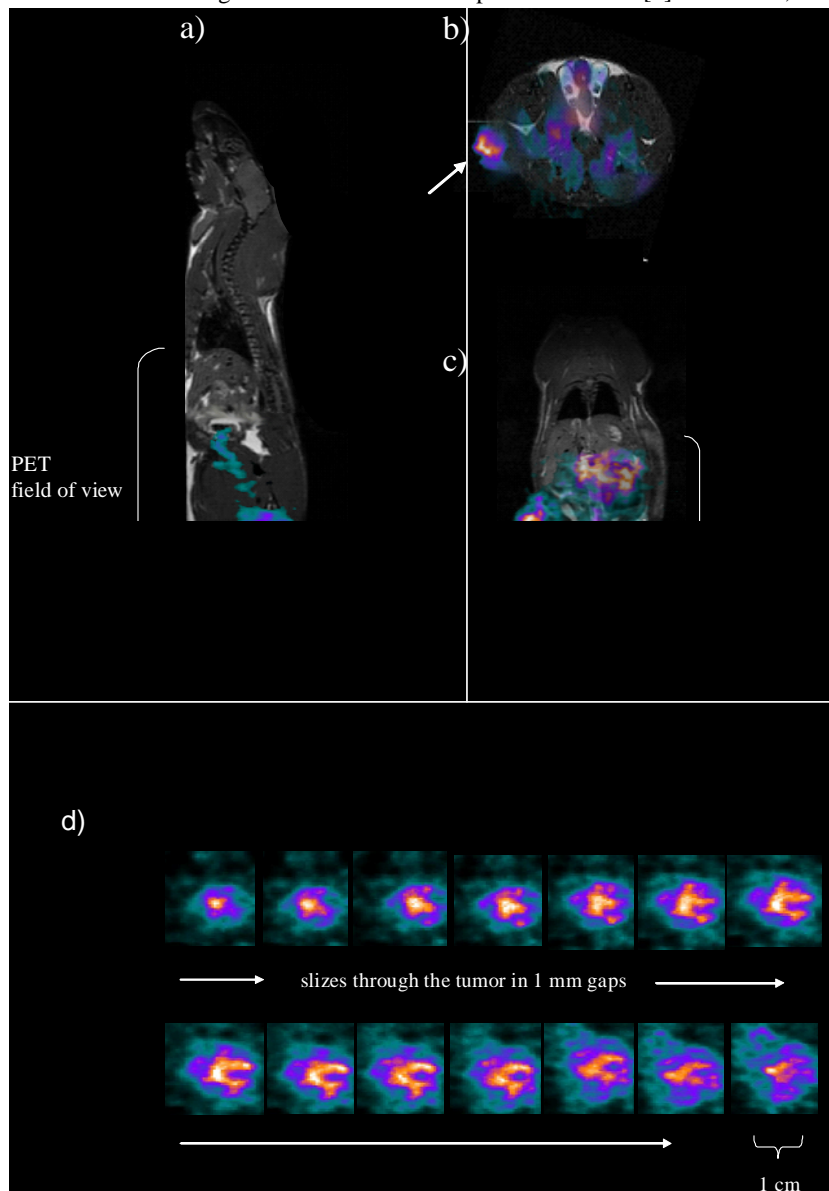


Fig. 1:
Representative images obtained with a Small Animal PET camera 48 h after injection of 10 MBq of $^{74}\text{As}[\text{SATA}]Vatuximab^{\circledast}$ in frontal, sagittal, and transversal orientation (a-c) and 1 mm slices through the tumor capsule (d)

Financial Support of the Böhringer Ingelheim Foundation is grateful acknowledged

In vitro- und erste *in vivo*-Untersuchungen mit ^{131}I -radioiodierten MGMT-Inhibitoren

U. Mühlhausen¹, D. Stark¹, B. Lecher², A. Piee-Staffa³, M. Briegert³, G. Nagel³,
R. Schirrmacher¹, M. Piel¹, B. Kaina³, F. Rösch¹

1) Institut für Kernchemie, Johannes Gutenberg-Universität, Fritz-Straßmann-Weg 2, 55128 Mainz

2) MFD Diagnostics, Mainz

3) Institut für Toxikologie, Johannes Gutenberg-Universität, Obere Zahlbacher Str. 67, 55131 Mainz

Einleitung: Exprimiert ein Tumor große Konzentrationen an O⁶-Methylguanin-DNA-methyltransferase, einem Reparaturenzym, so ist eine Chemotherapie durch Alkylantien kontraindiziert. Das Ziel einer radioaktiven Markierung von MGMT-Inhibitoren ist die nichtinvasive Bestimmung des MGMT-Status von Tumoren *in vivo*. Eine wesentliche Voraussetzung für einen solchen Einsatz der Inhibitoren ist, dass der radioaktiv markierte Alkoholrest am O⁶ des Guanins tatsächlich auf die MGMT übertragen wird. Dies wurde in der Literatur zwar für den MGMT-Inhibitor [^{131}I]IBG beschrieben [1], jedoch für die von uns neu dargestellten Verbindungen [^{131}I]IBGG, [^{131}I]ITG und [^{131}I]ITGG gab es keine vergleichbaren Daten. Kürzlich wurde auch eine Biodistributionsstudie von [^{131}I]IBG in Tumor-tragenden Nacktmäusen publiziert [2]. Die Autoren kamen zu dem Schluss, dass eine Untersuchung mit [^{131}I]IBG als Tracer prinzipiell möglich sei, es aber wünschenswert wäre, eine weniger lipophile Verbindung zu solchen Untersuchungen heranzuziehen, die bessere pharmakokinetische Eigenschaften *in vivo* besitzt. Durch die Glucoskonjugation der MGMT-Inhibitoren am N⁹ des Guanins sollten unsere Verbindungen weniger lipophil sein und es sollte eine selektivere Aufnahme in die Tumorzellen erfolgen [3]. Mit den ^{131}I -radioiodierten MGMT-Inhibitoren [^{131}I]IBG und [^{131}I]IBGG wurden vergleichende *ex vivo*-Biodistributionsstudien an Tumor-tragenden Nacktmäusen durchgeführt.

Ergebnisse und Diskussion: Mit den radioiodierten MGMT-Inhibitoren [^{131}I]ITG und [^{131}I]IBG und ihren Glucoskonjugierten Analoga [^{131}I]ITGG und [^{131}I]IBGG wurden Übertragungsstudien auf die gereinigte MGMT durchgeführt. Bei allen vier Verbindungen wurde der radioiodierte Alkoholrest am O⁶ des Guanins spezifisch auf die MGMT übertragen. In negativen Kontrollversuchen wurde kaum Bindung an BSA, einem unspezifischen Protein, beobachtet (Abb. 1).

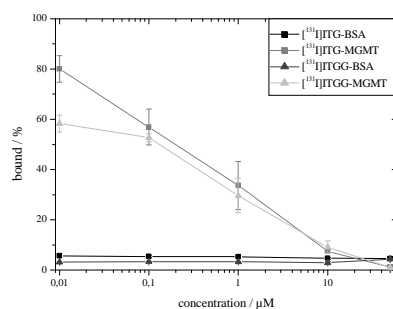


Abbildung 1:

Bindung von [^{131}I]ITG und [^{131}I]ITGG an gereinigte MGMT als Funktion der Konzentration von kaltem ITG und ITGG

In ersten *ex vivo*-Studien an Nacktmäusen mit MEX(+)-Tumoren (HeLa S3) wurden die Organ- und Tumorverteilungen von [^{131}I]IBG und [^{131}I]IBGG miteinander verglichen. Wichtig für einen potentiellen Einsatz der Verbindungen als Tracer

zur Quantifizierung des MGMT-Status in Tumoren ist ein günstiges Tumor/Blut-Verhältnis. Ein Vergleich der beiden Verbindungen zeigte, dass das Tumor/Blut-Verhältnis für das Glucoskonjugat [^{131}I]IBGG 0,5 h p.i. deutlich günstiger ist als für das nichtglycosyierte Derivat [^{131}I]IBG (Tabelle 1).

Tabelle 1: Tumor/Blut-Verhältnis in Nacktmäusen mit MEX(+) Tumor nach Injektion von [^{131}I]IBG bzw. [^{131}I]IBGG

	Tumor/Blut-Verhältnis			
	0,5 h	1 h	4 h	8 h
[^{131}I]IBGG	0,76	0,38	0,20	0,47
[^{131}I]IBG	0,24	0,46	0,45	-

Ein weiterer wichtiger Punkt ist die Deiodierung der Verbindungen im Organismus, die nicht erwünscht ist, da die Übertragung des radioiodierten Alkohols auf die MGMT gemessen werden soll. Bei [^{131}I]IBG ist die Aufnahme von [^{131}I]I in die Schilddrüse wesentlich höher (Abb. 2) als bei dem Glucoskonjugat.

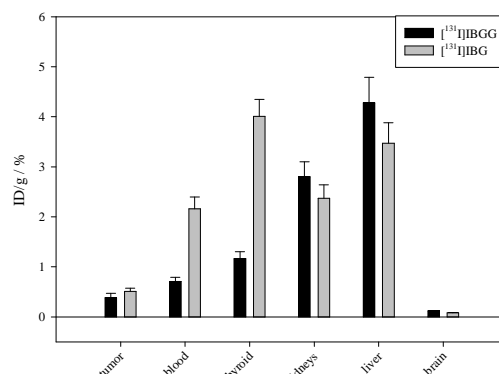


Abbildung 2:

Vergleich der ^{131}I -Aufnahme in ausgewählten Geweben bei Nacktmäusen mit MEX(+) Tumoren 0,5 h p.i. von [^{131}I]IBG und [^{131}I]IBGG

Aufgrund dieser ersten Ergebnisse scheint das Glucoskonjugat [^{131}I]IBGG als potentieller Tracer für die Quantifizierung des MGMT-Status *in vivo* geeigneter zu sein.

Ausblick:

- *ex vivo*-Studien an Nacktmäusen mit anderen Tumortypen
- *ex vivo*-Studien an tumortragenden Nacktmäusen mit [^{131}I]ITG und [^{131}I]ITGG
- Tier-SPECT-Studien mit [^{131}I]IBG und [^{131}I]IBGG an tumortragenden Nacktmäusen

[1] G. Vaidyanathan et al., Bioconj Chem.; **11**, 868-875 (2000)

[2] G. Vaidyanathan et al., Bioconj Chem.; **15**, 402-408 (2004)

[3] J. Reinhardt et al., J. Med. Chem.; **44**, 4050-4061 (2001)

In vitro-Affinitäten von halogenierten D2-artigen Dopaminrezeptorenliganden

D. Stark¹, M. Piel¹, H. Hübler², P. Gmeiner², F. Rösch¹

¹⁾ Institut für Kernchemie, Johannes Gutenberg-Universität, Fritz-Straßmann-Weg 2, 55128 Mainz

²⁾ Institut für Pharmazie und Lebensmittelchemie, Friedrich Alexander Universität, 91052 Erlangen

Name	Struktur	pD1 [³ H]SCH23390	hD2 _{short} [³ H]Spiperone	hD2 _{long} [³ H]Spiperone	hD3 [³ H]Spiperone	hD4.4 [³ H]Spiperone	p5-HT _{1A} [³ H]8-OH-DPAT	p5-HT ₂ [³ H]Ketan.	pα1 [³ H]Prazosin
DMFP		29500±1500	30±4	30±5	32,8±7,8	3000±400	2250±750	4450±50	1900±100
FP		18000±2000	2,2±0,1	2,2±0,1	1,7±0,3	1300±250	1080±120	3700±300	970±330
NADE		13000±1000	19±1	15±1	11±1	630±19	170±100	2400±1200	1950±150
NAE		17500±500	0,7±0,7	0,7±0,2	0,5±0,1	250±30	145±15	485±65	1130±170
NABrDE		17000	23±12	26,5±2,5	21,5±2,5	1700±100	225±10	2100±800	2000
NABrE		13000	0,9±0,2	0,9±0,1	0,6±0,2	210±10	140±40	1060±640	1600±100
IBZM		11500±1500	4,2±0,5	4,2±0,8	4,2±1,4	570±1,9	1050±50	2000±900	1850±50
FLB 457		15000	1,6±0,5	0,65±0,01	0,42±0,06	210±5	2200±50	1200	830±95
Raclopridetartrat		37000	31±3,1	17±2,4	15±2,1	3100±205	4400±600	3500±500	3000±100

Tab. 1: Struktur und Affinitäten (K_i in nM) von FP, DMFP, NAE, NADE, NABrE, NABrDE, IBZM, FLB 457 und Racloprid-Tartrat.

Einleitung: Halogenierte Analoga der bereits etablierten D₂-selektiven PET-Radioliganden [¹⁸F]Fallyprid ([¹⁸F]FP) und [¹⁸F]Des-methoxyfallyprid ([¹⁸F]DMFP) wurden in vorrausgegangenen Arbeiten synthetisiert [1-6]. Diese zur Klasse der Benzamide gehörenden Verbindungen wurden in einem Assay auf ihre Affinitäten zu verschiedenen Subtypen des Dopaminrezeptors untersucht. Die Strukturen der evaluierten Verbindungen und die ermittelten K_i -Werte sind in Tab.: 1 dargestellt.

Experimentelles: Rezeptorbindungseigenschaften wurden gemäß Literatur in Kompetitionsexperimenten mit hochaffinen Radioliganden und entsprechenden rezeptorsubtypselektiven Membranpräparationen durchgeführt [7,8]. Dabei wurden Homogenate mit den humanen Rezeptoren D2_{long}, D2_{short}, D3 und D4 aus stabil transfizierten CHO-Zelllinien gewonnen und mit [³H]Spiperon inkubiert. Versuche mit dem D1-Rezeptor sowie mit den serotoninergen Rezeptoren 5-HT_{1A} und 5-HT₂ und den adrenergen α1-Rezeptor wurden mit nativen Rezeptoren aus Präparationen des Schweinehirns durchgeführt. Striatale Membranen wurden dazu mit [³H]SCH23390 für D1-Bindung und corticale Homogenate mit [³H]8-OH-DPAT (5-HT_{1A}), [³H]Ketanserin (5-HT₂) oder [³H]Prazosin (α1) inkubiert. Die K_i -Werte in Tabelle 1 stellen Durchschnittswerte aus zwei bis vier unabhängigen Versuchen dar, die jeweils mit acht unterschiedlichen Konzentrationen im Bereich von

0,01-100 000 nM ermittelt wurden. Die aus den erhaltenen Dosis-Wirkungskurven abgeleiteten EC₅₀-Werte wurden gemäß der Umrechnung nach Cheng und Prusoff in K_i -Werte transformiert [9].

Ergebnis: Beste Affinitäten zu den D2-Rezeptoren ist zu erkennen, wenn die Verbindungen eine 2,3-Dimethoxybenzamidstruktur aufweisen, was für NAE, NABrE und FP zu K_i -Werten von 0,7 nM/0,7 nM (D2short/D2long), 0,9 nM/0,9 nM und 2,2 nM/2,2 nM führt. Gleiches gilt für FLB. Dagegen toleriert der D2-Rezeptor verschiedene Substitutionen in Position 5, wie es in obigen Verbindungen mit Iod, Brom oder auch 3-Fluorpropan realisiert ist. Die um den Faktor drei höhere Affinität zum D2-Rezeptor von NAE ($K_i = 0,7$ nM) im Vergleich zu FP ($K_i = 2,2$ nM) und die um das 1,5fach höhere Affinität von NADE ($K_i = 19$ nM) im Vergleich zu DMFP ($K_i = 30$ nM) lassen für die iodierten Analoga gute Eigenschaften für die molekulare Bildgebung erwarten.

[1] M. Piel, Diplomarbeit, Universität Mainz, 1997

[2] M. Piel et al., Jahresbericht 1997, B 3, S. 22, Institut für Kernchemie, Universität Mainz, 1998

[3] T. Höglberg et al., Acta Chemica Scandinavica 43 (1989), 660-664

[4] S. Chumpradit et al., J. Med. Chem. 36 (1993), 221-228

[5] D. Stark et al., Jahresbericht 2001, C 11, Institut für Kernchemie, Universität Mainz, 2002

[6] D. Stark, Diplomarbeit, Universität Mainz, 2002

Ex vivo-Biodistributionen des D₂-Antagonisten Desmethoxyfallypride

M. Piel¹, S. Höhnemann¹, D. Stark, U. Schmitt², F. Rösch¹

¹Institut für Kernchemie, ²Klinik für Psychiatrie, Johannes Gutenberg-Universität Mainz

In Zusammenarbeit mit der Klinik für Psychiatrie wurden die Synthese [1], die Markierung [2] und die *in vitro*-Affinität [3] des selektiven D₂-Antagonisten Desmethoxyfallypride evaluiert, Abb.1:

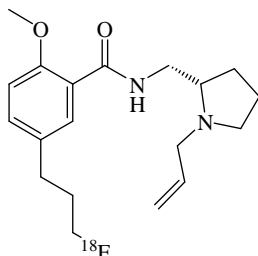


Abb.1: N-(((S)-1-Allylpyrrolidin-2-yl)methyl)-5-(3-[¹⁸F]fluorpropyl)-2-methoxybenzamid ([¹⁸F]Desmethoxyfallypride, [¹⁸F]DMFP)

Im Rahmen dieser *ex vivo*-Biodistributionsstudie sollte die Organverteilung des Liganden für verschiedene, für die PET relevante Organe untersucht werden.

Experimentelles: Zur Darstellung von [¹⁸F]DMFP wurde der Markierungsvorläufer (5 mg, 10 µmol) in 1 mL MeCN gelöst und für 5 Minuten mit 5 mg K₂CO₃ behandelt. Anschließend wurde diese Lösung bei 85°C für 20 Minuten mit [¹⁸F]Fluorid umgesetzt:

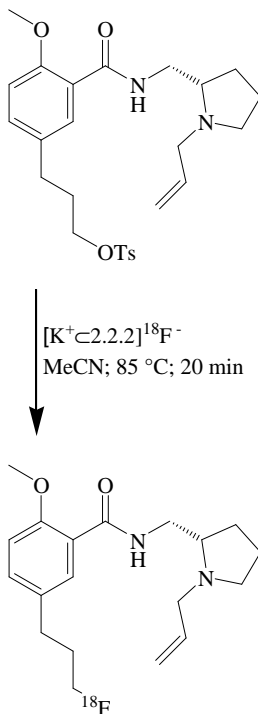


Abb.2: Reaktionsschema der ¹⁸F-Fluorierung des Markierungsvorläufers des [¹⁸F]DMFP

Die Reaktionslösung wurde anschließend in Wasser aufgenommen, mittels HPLC gereinigt, auf einer Strata X Kartusche fixiert und mit wenig Ethanol eluiert. Das Lö-

sungsmittel wurde im Vakuum entfernt und das Produkt in isotonischer Kochsalzlösung aufgenommen. 100 µL dieser Lösung wurden in Sprague-Dawley Ratten (200-250 g, n = 12) injiziert, diese nach festgelegten Zeitpunkten t (5, 10, 30, 60 und 90 Minuten) getötet und die Verteilung der Verbindung in den verschiedenen Organen untersucht, Abb. 3 & 4:

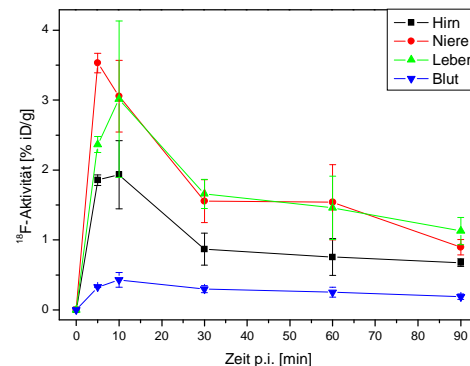


Abb.3: Biodistribution von [¹⁸F]DMFP in Hirn, Niere, Leber und Blut

Dabei zeigte sich für Leber und Niere eine relativ identische Anreicherungskinetik mit einer maximalen Aktivität von 3,0 – 3,5 %ID/g. Die Anreicherung der Verbindung im Gehirn ergab eine hohe Hirnaufnahme von ca. 2 %ID/g, die für einen hirngängigen PET-Liganden sehr gut ist. Die Aktivitätsanreicherung im Blut dagegen betrug maximal 0,5 %ID/g, was ein gutes Aktivitätsverhältnis Hirn/Blut erwarten lässt.

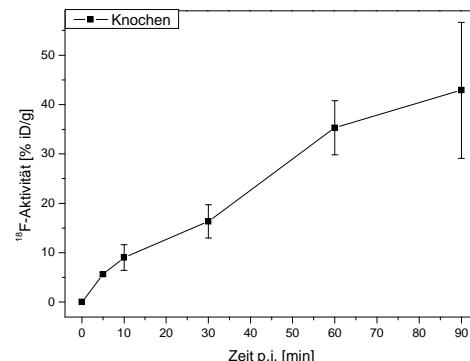


Abb.4: Biodistribution von [¹⁸F]DMFP im Knochen

Die Aktivitätsanreicherung im Knochen dagegen stieg stetig an bis auf ein Maximum von 40 %ID/g, was auf eine Freisetzung des ¹⁸F-Fluors in Form von [¹⁸F]Fluorid hindeutet:

Literatur:

- [1] M. Piel et al., Jahresbericht 1997, Artikel B3
- [2] M. Piel et al., Jahresbericht 1997, Artikel B4
- [3] D. Stark et al., Jahresbericht 2003, Artikel B5

Ex vivo-Biodistributionen des D₂-Antagonisten Fallypride

M. Piel¹, S. Höhnemann¹, D. Stark, U. Schmitt², F. Rösch¹

¹Institut für Kernchemie, ²Klinik für Psychiatrie, Johannes Gutenberg-Universität Mainz

In Zusammenarbeit mit der Klinik für Psychiatrie wurden die Synthese, die Markierung [1] und die *in vitro*-Affinität [2] des selektiven D₂-Antagonisten Fallypride evaluiert, Abb.1:

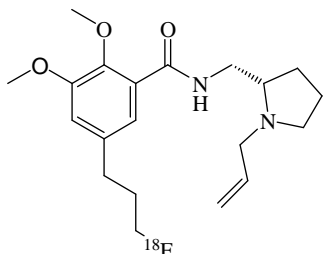


Abb.1: N-((S)-1-Allylpyrrolidin-2-yl)methyl)-5-(3-[¹⁸F]fluorpropyl)-2,3-dimethoxybenzamid (^{[18}F]Fallypride, ^{[18}F]FP)

Im Rahmen dieser *ex vivo*-Biodistributionsstudie sollte die Organverteilung des Liganden für verschiedene, für die PET relevante Organe untersucht werden.

Experimentelles: Zur Darstellung von ^[18]F]FP wurde der Markierungsvorläufer (5 mg, 10 µmol) in 1 mL MeCN gelöst und für 5 Minuten mit 5 mg K₂CO₃ behandelt. Anschließend wurde diese Lösung bei 85°C für 20 Minuten mit ^[18]F]Fluorid umgesetzt:

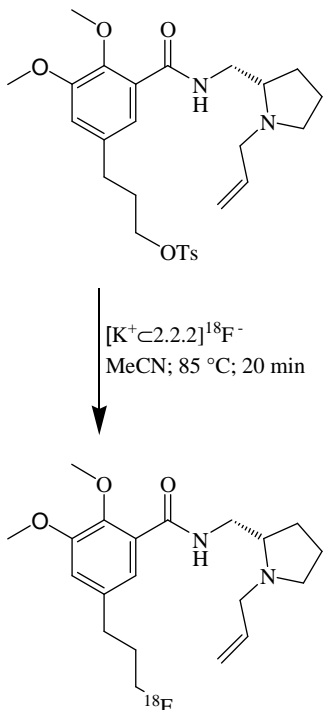


Abb.2: Reaktionsschema der ¹⁸F-Fluorierung des Markierungsvorläufers des ^{[18]F]FP}

Die Reaktionslösung wurde anschließend in Wasser aufgenommen, mittels HPLC gereinigt, auf einer Strata X Kartusche fixiert und mit wenig Ethanol eluiert. Das Lö-

sungsmittel wurde im Vakuum entfernt und das Produkt in isotonischer Kochsalzlösung aufgenommen. 100 µl dieser Lösung wurden in Sprague-Dawley Ratten (250-350 g, n = 12) injiziert, diese nach festgelegten Zeitpunkten t (5, 10, 30 60 und 90 Minuten) getötet und die Verteilung der Verbindung in den verschiedenen Organen untersucht, Abb. 3 & 4:

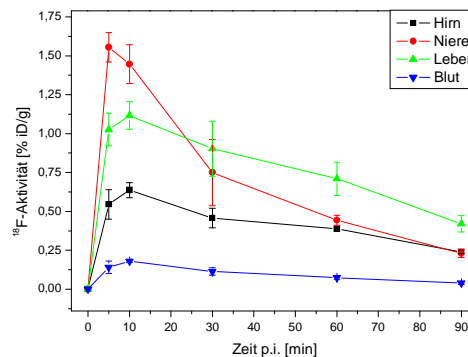


Abb.3: Biodistribution von ^{[18]F]FP} in Hirn, Niere, Leber und Blut

Dabei zeigte sich für Leber und Niere eine ähnliche Anreicherungskinetik mit einer maximalen Aktivität von 1,0 - 1,5 %ID/g. Die Anreicherung der Verbindung im Gehirn ergab eine hohe Hirnaufnahme von ca. 0,7 %ID/g, die für einen hirngängigen PET-Liganden gut ist. Die Aktivitätsanreicherung im Blut dagegen betrug maximal 0,2 %ID/g, was ein gutes Aktivitätsverhältnis Hirn/Blut erwarten lässt.

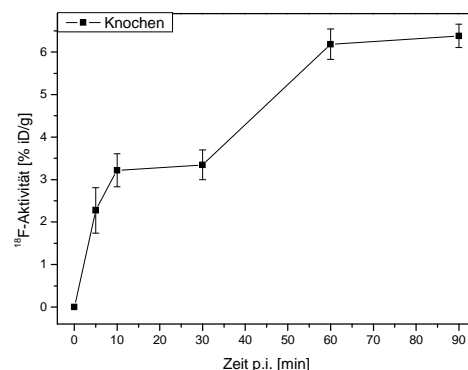


Abb.4: Biodistribution von ^{[18]F]FP} im Knochen

Die Aktivitätsanreicherung im Knochen dagegen stieg stetig an bis auf ein Maximum von 6 %ID/g, was auf eine teilweise Freisetzung des ¹⁸F-Fluors in Form von ^{[18]F]Fluorid} hindeutet:

Literatur:

- [1] Diplomarbeit A. Gleich, Institut für Kernchemie, 2000
- [2] D. Stark et al., Jahresbericht 2003, Artikel B5

Evaluation ^{131}I -markierter Dopaminrezeptorliganden *in vitro*

H. Lüddens¹, D. Stark², M. Piel², F. Rösch²

¹⁾ Psychiatrische Klinik und Poliklinik der Universität Mainz, Untere Zahlbacher Str. 8, 55131 Mainz
²⁾ Institut für Kernchemie, Johannes Gutenberg-Universität, Fritz-Straßmann-Weg 2, 55128 Mainz

Einleitung: Dopaminerge D2-Rezeptoren finden sich im Gehirn vorwiegend postsynaptisch im Corpus striatum, daher ermöglicht eine Untersuchung mit diesen Dopaminrezeptorliganden eine Darstellung der Integrität des postsynaptischen Anteils der dopaminerigen Synapsen im Corpus striatum, insbesondere zur Differentialdiagnose bei Parkinson-Syndromen. Fallypride (FP) und Desmethoxyfallypride (DMFP) sind selektive D2/3-Rezeptorliganden zur Analyse des dopaminerigen Systems mit hoher bzw. mittlerer Affinität zu ihrem Rezeptor. Mit dem ersten Liganden kann *in vivo* die D2-Rezeptorverteilung im Gesamthirn und mit dem zweiten präferentiell die Kompetition am Rezeptor mit natürlichem Dopamin dargestellt werden. Beide Liganden haben sich als ^{18}F -markierte PET-Radioliganden zur Visualisierung von Dopamin-Rezeptoren bewährt. Um ihre Eigenschaften auch für SPECT als Alternative zum $[^{123}\text{I}]$ Iodobenzamid (IBZM) nutzbar zu machen, wurden ihre entsprechenden Iodanaloga, $[^{131}\text{I}]$ IodoFP und $[^{131}\text{I}]$ IodoDMFP, synthetisiert und hier an Schnitten des Rattenhirns evaluiert.

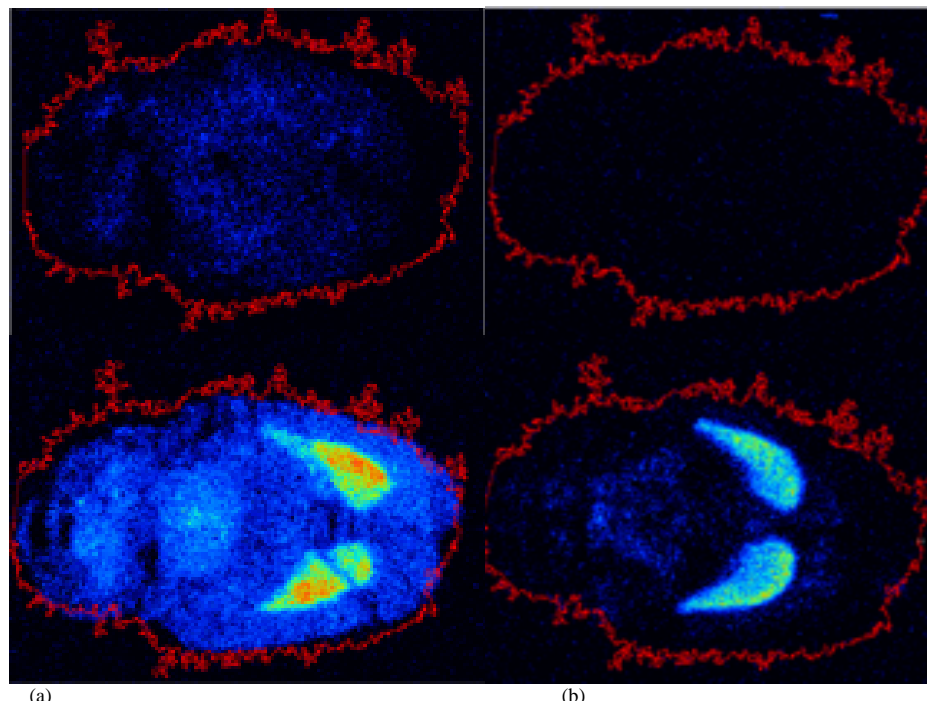
Material und Methoden: Rattenhirne wurden nach der Dekapitation auf Trockeneis eingefroren und bei -80°C aufbewahrt. $20\ \mu\text{m}$ horizontale Schnitte der Hirne wurden luftgetrocknet und bei -80°C bis zum Gebrauch aufbewahrt. Die Schnitte wurden zweimal 12 min in TANKM (50 mM TRIS/HCl, pH 7,5; 0,1% Ascorbinsäure; 120 mM NaCl; 5 mM KCl; 1 mM MgCl₂) präinkubiert und dann mit

$[^{131}\text{I}]$ -IodoDMFP (spez. Aktivität $0,25 \cdot 10^6$ Bq/ nmol; 0,1 bis 5,2 nM) und $[^{131}\text{I}]$ IodoFP (spez. Aktivität $1,0 \cdot 10^6$ Bq/ nmol; 5 bis 182 pM) in An- und Abwesenheit von $10\ \mu\text{M}$ IBZM für 90 min bei Raumtemperatur, jeweils in TANKM, inkubiert. Danach wurden die Schnitte vier Mal für je 2 min in TANKM gewaschen und einmal kurz in H₂O getaut, bevor sie schnell unter einem kalten Luftstrom getrocknet wurden (Methode nach Mansour et al., 1990). Die Bindung an die Schnitte wurden in einem Storm860 (Molecular Dynamics) quantifiziert, nachdem sie über Nacht einen ‚phosphor screen‘ belichtet hatten. Die Quantifizierung wurde nach Auslesen des ‚screens‘ manuell vorgenommen.

Ergebnisse: Beide Liganden eignen sich sehr gut zur Darstellung der D2-Rezeptor-Verteilung *in vitro*. Dabei ist $[^{131}\text{I}]$ IodoFP für diese Anwendung zu bevorzugen, da es in dem hier eingesetzten Konzentrationsbereich das bessere Signal:Rauschen-Verhältnis liefert.

Literatur:

Mansour A, Meador-Woodruff J, Bunzow J, Civelli O, Akil H, Watson S (1990) Localization of dopamine D2 receptor mRNA and D1 and D2 receptor binding in the rat brain and pituitary: an *in situ* hybridization-receptor autoradiographic analysis. J Neurosci 10:2587-2600.



Falschfarbendarstellung von 5,2 nM $[^{131}\text{I}]$ IodoDMFP (a) und 0,18 nM $[^{131}\text{I}]$ IodoFP-Bindung (b) auf Schnitten des Rattenhirns in Anwesenheit (oben) und Abwesenheit (unten) eines Überschusses von IBZM ($10\ \mu\text{M}$)

Receptor-PET/CT of neuroendocrine tumors using the gallium-68 labelled somatostatin analog DOTA-NOC: First clinical results

R. P. Baum¹ M. Schmücking¹, A. Niesen¹, K. P. Zhernosekov² F. Rösch²

¹Dept. of Nuclear Medicine / Center for P.E.T., Zentralklinik Bad Berka, Germany

²Institut für Kernchemie, Johannes Gutenberg-Universität, D-55128 Mainz, Germany

Introduction: Modification of the octapeptide octreotide in position 3 resulted in a compound [DOTA]-1-Nal³-octreotide (DOTA-NOC) which showed an increased somatostatin receptor (sstr) affinity for sstr2, sstr3, and sstr5. After labelling with ¹¹¹Indium- or ⁹⁰Yttrium, DOTA-NOC is superior to all somatostatin-based radiopeptides having this particular type of binding profile, and has three to four times higher binding affinity to sstr2 than In^{III}, Y^{III}-DOTA-Tyr³-octreotide (In^{III}, Y^{III}-DOTA-TOC).

In addition, [¹¹¹In]DOTA-NOC showed a specific and high rate of internalization into tumour cells which was about two times higher than that of [¹¹¹In]DOTA-TOC [1]. These very promising preclinical data prompted us to use this new radiopeptide for somatostatin receptor PET/CT imaging in patients with neuroendocrine tumours (NET) after labelling with Gallium-68, a short-lived positron emitter with a half-life of 68 min.

Experimental: 30 mCi ⁶⁸Ge/⁶⁸Ge-generators based on TiO₂-phase (Cyclotron Co., Obninsk, Russia) were used to obtain 500-750 MBq of ⁶⁸Ga. [⁶⁸Ga]DOTA-NOC was synthesised with specific activities of about 15 MBq / µg peptide as described elsewhere [2].

34 patients with histologically proven NET (mostly carcinoids) and progressive metastases were studied before peptide receptor radiotherapy (PRRT). A mean of 74 MBq (65-140 MBq) ⁶⁸Ga-DOTA-NOC were injected. Simultaneously, furosemide (20 mg) was injected to increase the renal elimination (patients were well hydrated). Acquisition was started 20-110 min p.i. (mean 51 min p.i.) from the femoral shaft to the head (up to 9 bed positions) using the latest generation LSO-based whole body PET/CT (biograph DUO, Siemens). Emission time ranged between 2 to 5 min per bed. Attenuation correction was performed using the low-dose whole-body spiral-CT (Somatom Emotion duo) integrated in the PET/CT scanner. CT images were acquired after injection of 100 cc iodinated contrast material.

Standardized uptake values (SUV) were determined for all tumour lesions and for normal tissue (pituitary gland, thyroid, lung, liver, kidney, spleen, gluteus muscle). Volumetry of the lesions was done using individualized iso-SUV-lines (cut-off levels) for every patient.

PET images were read independently by two experienced nuclear medicine physicians without knowledge of the CT results; the CT scans were read by trained radiologist (knowing the PET results).

Results: In almost all patients more lesions were detected as compared with ¹¹¹In-OctreoScan or ^{99m}Tc-TETOC (especially with regard to small bone

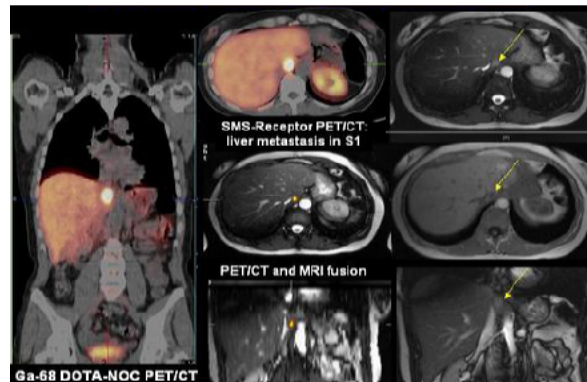


Fig. 1 ⁶⁸Ga-PET/CT and image fusion of PET/CT and MRI for detection of a liver metastasis of a neuroendocrine carcinoma

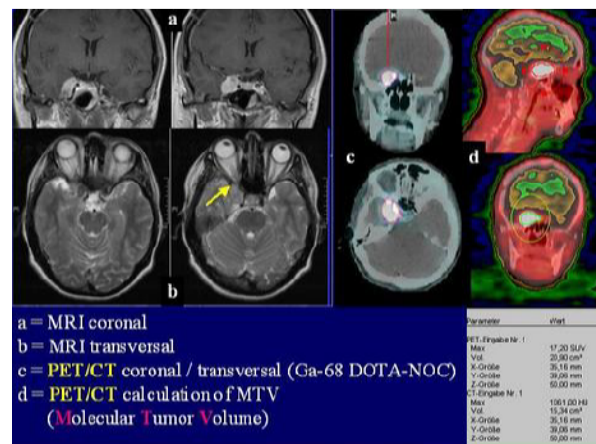


Fig. 2 Inoperable meningioma: ⁶⁸Ga-DOTA-NOC PET/CT of the head and MRI fusion

metastases) or with CT or MRI (especially regarding lymph node metastases). In some patients, small lung nodules were seen on CT which were receptor negative on the PET scan (lung metastases vs. benign lesions).

Brilliant PET/CT images of all known tumour lesions (see Fig. 1-2) and in addition small lymph node metastases of less than 5 mm were easily visualized as early as 20 min p.i. Receptor PET/CT using ⁶⁸Ga-DOTA-NOC advances as the new gold standard for imaging of neuroendocrine tumours possibly allowing also tumour dosimetry.

References

- [1] Wild et al., Eur J Nucl Med Mol Imaging; **30**:1338 (2003)
- [2] Zhernosekov et al., this report

Somatostatin receptor expressing tumors: Imaging with ^{68}Ga -DOTATOC-PET/CT versus ^{111}In -DTPAOC-SPECT/CT

P. Aschoff¹, M. Oeksuez¹, B. Kemke¹, K. Zhernosekov², M. Jennewein², F. Roesch², H. Bihl¹

¹Klinik für Nuklearmedizin und PET-Center, Klinikum Stuttgart, D-70022, Stuttgart

²Institut für Kernchemie, Johannes Gutenberg-Universität, D-55128 Mainz

Introduction: Imaging of somatostatin-receptor (SSTR) expressing tumors using ^{111}In -DTPA-octreotide (^{111}In -DTPAOC) has proven to be helpful in the detection of SSTR-expressing tumors and their metastases. One of the drawbacks of this method - even if performed in SPECT-technique - is its limited sensitivity in detecting small lesions. ^{68}Ga -DOTA-DPhe(1)-Tyr(3)-octreotide (^{68}Ga -DOTATOC) is a new PET-radiotracer with a higher specific binding to SSTR2 compared to ^{111}In -DTPAOC [1].

This study compares the clinical performance of both methods in detecting SSTR2-positive tumor lesions.

Experimental: Thirty-six patients with metastatic neuroendocrine gastroenteropancreatic tumor were evaluated with both ^{111}In -DTPAOC SPECT/CT (185 MBq) and ^{68}Ga -DOTATOC-PET/CT (50-120 MBq). GE Millennium VG Hawkeye gamma camera and GE Discovery LS PET/CT-scanner were used to perform the respective scans.

400-200 MBq of ^{68}Ga were obtained using a 20 mCi $^{68}\text{Ge}/^{68}\text{Ge}$ -generator, based on a TiO_2 -phase (Cyclotron Co., Obninsk, Russia). For syntheses of ^{68}Ga -DOTATOC, ^{68}Ga was pre-concentrated and purified on micro-chromatography column filled with Bio-Rad AG 50W-X8 [2].

Results: Whereas ^{111}In -DTPAOC-scintigraphy was performed in a 2-d protocol, ^{68}Ga -DOTATOC-PET/CT generated decisive images of high quality 20 min after injection. 95% of all lesions were already seen 10 min after injection (Fig.1). All " ^{111}In -DTPAOC-lesions" were detected with ^{68}Ga -DOTATOC-PET/CT as well and additional lesions (bone, lymphnodes) could be identified in 24/36 patients (67%). In all patients, lesion localisation was significantly more precise with PET/CT than with SPECT/CT.

In this study, ^{68}Ga -DOTATOC-PET/CT turned out to be superior to ^{111}In -DTPAOC-SPECT/CT in the detection of SSTR2-positive tumors and metastases. For clinical practice, it is important that ^{68}Ga -DOTATOC-PET/CT can be performed in a 1-d protocol, i.e. scans will start immediately after tracer injection (20 min) and will be achieved in about <30 min.

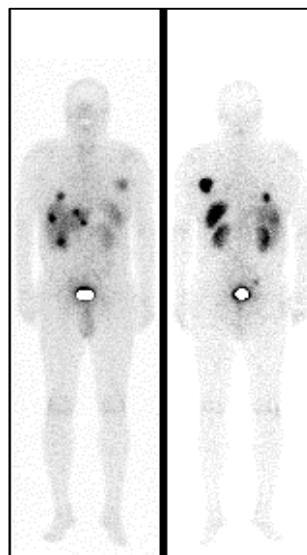
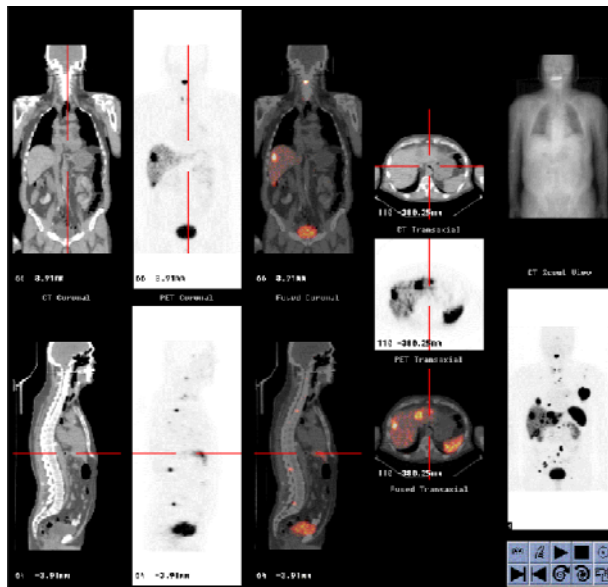


Figure 1



Patient with liver and bone metastasis:

Figure 1) ^{111}In -DTPAOC planar imaging

Figure 2) ^{68}Ga -DOATATOC PET/CT and image fusion of PET/CT

References

- [1] Mäcke, H. R., Good, S.: "Radiometals (non-Tc, non-Re) and bifunctional labeling chemistry"; Handbook of Nuclear Chemistry, volume 4, Amsterdam, (2003)
- [2] Zhernosekov, K.P. et. al., this report

Enhanced visualization of disseminated bone metastases of primary neuroendocrine tumors using ^{68}Ga -DOTATOC

P. Aschoff¹, M. Oeksuez¹, B. Kemke¹, K. Zhernosekov², M. Jennewein², F. Roesch², H. Bihl¹

¹Klinik für Nuklearmedizin und PET-Center, Klinikum Stuttgart, D-70174, Stuttgart

²Institut für Kernchemie, Johannes Gutenberg-Universität, D-55128 Mainz

Introduction: The diagnosis of neuroendocrine tumors (e.g. carcinoides, pancreatic tumors, etc) in terms of Somatostatin-Receptor-Scintigraphy (SRS) so far is performed using the tumor-specific somatostatin-analogue ^{111}In -DTPA-D-Phe¹-octreotide (^{111}In -Octreoscan). However, due to the limitations of gamma camera technology, the implementation of somatostatin-analogues labelled with a positron emitting isotope and the use of PET/CT-technology is challenging because of the following reasons:

1. Spacial resolution dramatically increases from 10-20 mm to 4-6 mm.
2. (Semi-) quantitative examination of the somatostatin-receptor status per ml tumour tissue appears to be possible, which is relevant for therapy choice, prognostic outcome and therapy response control
3. Using PET/CT-technology, an exact morphological correlation is possible

^{68}Ga -DOTATOC (^{68}Ga -DOTA-D-Phe¹-Tyr³-octreotide) represents a biochemically most promising peptidic targeting vector for determination of human somatostatin subtype 2 expressing tumors. The potency of this ligand for molecular imaging of small metastases is currently paralleled by the implementation of PET/CT.

Experimental: ^{68}Ga -DOTATOC images were recorded with a GE DISCOVERY LS PET/CT-Scanner [PET: (GE Advance NXi): 2-D-Modus, CT-based attenuation correction, iterative reconstruction. CT: (GE LightSpeed Plus): Multislice (4-rows) Low-dose-Spiral-CT], 40 min after i.v.-injection of 106 MBq ^{68}Ga -DOTATOC, scan area: vertex to groin. ^{68}Ga -DOTATOC was synthesised using a newly developed procedure providing intrinsic minimisation of the $^{68}\text{Ge}/^{68}\text{Ga}$ generator eluate (volume down to < 0.5 ml), separation of metallic impurities and high-yield (> 95%) labelling in buffer-free media within an overall processing period of about 20 min. [1]

Results and Discussion: The patient illustrated here was examined using FGD, ^{111}In -Octreoscan and ^{68}Ga -DOTATOC. Whereas enhanced visualization of metastases in the whole skeleton via ^{68}Ga -DOTATOC receptor binding is obvious, these bone metastases don't show any increased FDG-uptake. ^{111}In -Octreoscan is more specific for neuroendocrine tumours than FDG, but in the patient studied shows only some metastases in the skull. The subsequent PET/CT-Scan, using ^{68}Ga -DOTATOC, reveals disseminated bone metastases, which could not be observed with any other imaging modality.

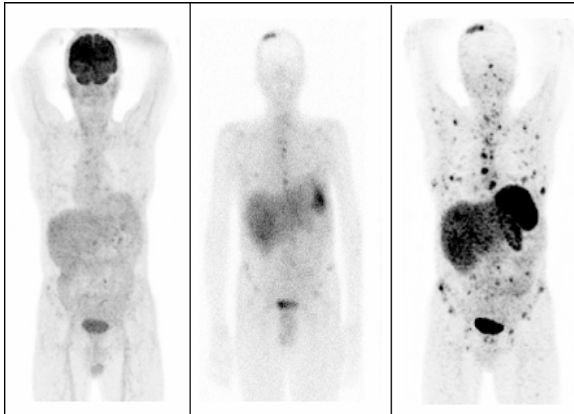


Fig. 1. Comparison of ^{18}F -FDG, ^{111}In -Octreoscan and ^{68}Ga -DOTATOC in the same patient
[Patient: male, *1939, neuroendocrine tumor with unknown primary, multiple liver and bone metastases]

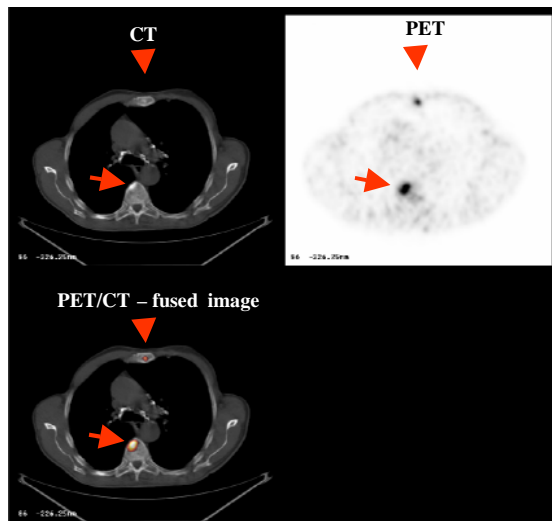


Fig. 2. osteoblastic bone metastases in sternum and spine
 ^{68}Ga -DOTATOC
[same patient as in Fig.1]

Conclusion: First results have been obtained regarding the diagnosis of disseminated bone metastases originating from primary neuroendocrine tumors using ^{68}Ga -DOTATOC. Visualization is dramatically enhanced compared to standard imaging modalities used to date, like e.g. ^{18}F -FDG-PET or ^{111}In -Octreoscan. Further studies with a greater number of patients should be performed.

[¹⁸F]FECholin is a promising radiotracer for PET/CT imaging of prostate cancer

R. P. Baum², M. Piel¹, A. Bauman¹, I. Klette¹, S. Höhnemann¹, R. Wortmann², F. Rösch¹

¹Institute of Nuclear Chemistry, Johannes Gutenberg-Universität Mainz; ²Department of Nuclear Medicine, Zentralklinik Bad Berka

Introduction: Many tumors are characterized by an enhanced cell proliferation. This is usually associated with an increased uptake and phosphorylation of choline to form phosphoryl choline which is used in the synthesis of membrane phospholipids.

[¹¹C]choline has shown potential for the evaluation of brain tumors, esophageal carcinoma and prostate cancer.¹⁻³ Because of the short half-life of ¹¹C ($T_{1/2} = 20.3$ min), resulting in a limited usefulness for clinical routine, different ¹⁸F-labeled ($T_{1/2} = 109.7$ min) analogues were synthesized to overcome this problem.

Recently, we reported that the addition of alkali iodides to 2-[¹⁸F]fluoroethyltosylate ([¹⁸F]FETos) and 1-bromo-2-[¹⁸F]fluoroethane led to drastically increased radiochemical yields, most probably due to the *in situ* formation of 1-iodo-2-[¹⁸F]fluoroethane.⁴

[¹⁸F]FECh was applied clinically for the detection of prostate cancer recurrences (in patients presenting with rising PSA levels) or for staging newly diagnosed patients before planned radiotherapy using PET/CT.

Results: Using PET/CT, [¹⁸F]FECh was shown to clearly localize in primary prostate cancer, lymph node and bone metastases. Occult metastases, not detected by conventional imaging methods (CT scan, MRI, bone scan) as well as local recurrences could be clearly visualized by [¹⁸F]FECh PET/CT (as confirmed by histology or fine needle biopsy).

Primary prostate cancer:

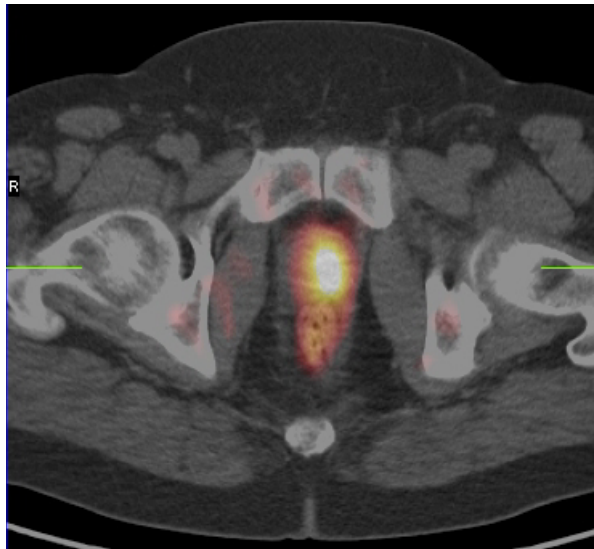


Fig. 1: [¹⁸F]FECh PET/CT for imaging primary prostate cancer: strong uptake in the left lobe.

Lymph node metastases: [¹⁸F]FECh-PET/CT allows for the detection of lymph node metastases as small as 5 – 10 mm in diameter.

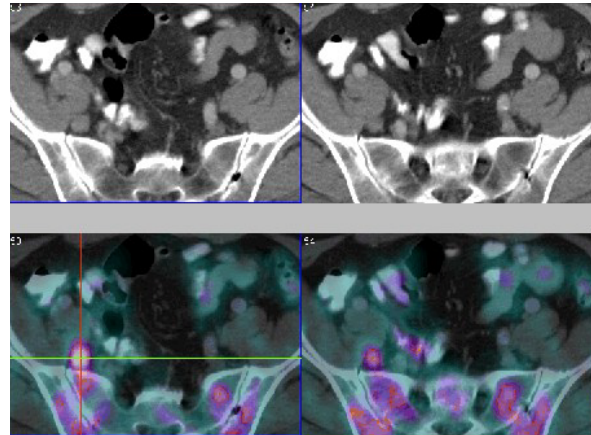


Fig. 2: [¹⁸F]FECh PET/CT: detection of a previously unknown lymph node metastasis in the pelvis.

Bone metastases: Also osseous metastases can be easily visualized by [¹⁸F]FECh-PET/CT.

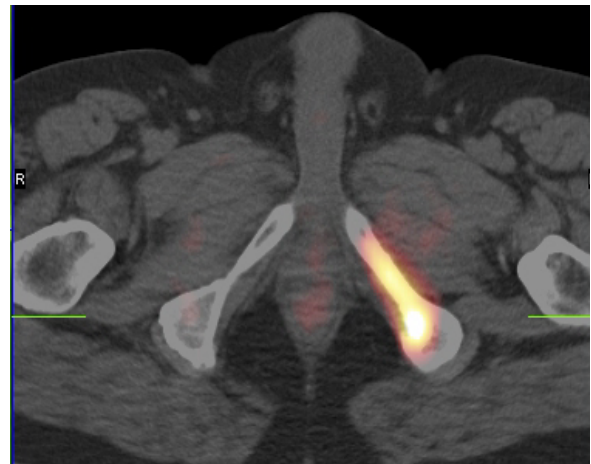


Fig. 3: [¹⁸F]FECh PET/CT: detection of a previously unknown bone metastasis in the pelvis. The patient was originally planned for radical prostatectomy.

Conclusion: [¹⁸F]FECh appears to be a very valuable new tracer for the primary staging and for restaging of prostate carcinoma, in particular when using PET/CT. Due to a more versatile handling it has advantages compared to [¹¹C]Choline diagnostic studies using [¹⁸F]FECh could significantly improve the management of prostate cancer (better staging, esp. detection of lymph node metastases and higher sensitivity for the early detection of recurrences).

References:

- [1] Hara T, Kosaka N, Shinoura N, Kondo T, J Nucl Med 1997; 38: 842-847
- [2] Larson SM, J Nucl Med 1994; 35: 1653-1655
- [3] Hara T, Kosaka N, Kishi H, J Nucl Med 1998; 39: 990-995
- [4] Piel M, Bauman A, Klette I, Höhnemann S, Wortmann R, Baum RP, Rösch F, this annual report

High Striatal Occupancy of D₂-like Dopamine Receptors by Amisulpride in Brain of Patients with Schizophrenia

Ingo Vernaleken¹, Thomas Siessmeier², Hans-Georg Buchholz², Sebastian Härtter³, Christoph Hiemke³, Peter Stoeter⁴, Frank Rösch⁵, Peter Bartenstein², Gerhard Gründer¹

¹Department of Psychiatry and Psychotherapy, RWTH University of Aachen;

²Department of Nuclear Medicine, University of Mainz; ³ Department of Psychiatry; University of Mainz

⁴ Institutes of Neuroradiology, University of Mainz; ⁵ Institute of Nuclear Chemistry; University of Mainz

Introduction: The substituted benzamide amisulpride is of high interest for understanding “atypicality”. It acts specifically on D₂-like receptors and is not binding to receptor being discussed as target for “atypicality”. The atypical features of amisulpride have been attributed to preferential extrastratial binding. Previous neuroimaging studies revealed different extents of striatal amisulpride binding due to varying radiotracers and methods of analysis. Because of these conflicting previous results regarding striatal D₂-occupancies the present PET study wants to relate striatal D₂-receptor occupancy by amisulpride with plasma levels and to compare these findings to previous findings. We use [¹⁸F]desmethoxyfallypride-PET with simplified reference tissue model; previous studies have validated the results of this methodological approach.

Methods: We examined 9 patients suffering from acute schizophrenia or schizoaffective psychosis with predominantly positive symptoms aged 19-53 years (mean \pm SD 35.9 ± 12.5). They received stable amisulpride treatment with daily doses ranging from 200 to 1200 mg (622 ± 323 mg/d). Patients were avoid of dopaminergic or serotonergic co-medication. The mean PANSS score was 76.0.

Amisulpride plasma concentrations were measured at 8 a.m., before drug intake, and during the PET-Scan (4-5h after drug intake). As a control group we examined 12 healthy volunteers aged 24-60 years (mean 35.4 ± 15.9). They underwent dynamic PET scans over a duration of 124 min (30 time frames) after bolus injection of 157-308 MBq DMFP. Scans were performed using a Siemens ECAT EXACT Scanner with FWHM of 5.4 mm.

The analysis was carried out VOI-based (Caudate Nucleus (NC), Putamen; Cerebellum as reference region) using the simplified reference tissue model (SRTM). All

PET scans were motion corrected, coregistered with T1 weighed MRI and normalized to SPM coordinates.

Results: We found 43-85% (putamen) and 67-90% (caudate) D₂-like receptor occupancy. Plasma amisulpride concentrations at time of tracer injection but not administered doses were significantly non-linearly correlated to occupancy levels (putamen: $r_s=0.88$, $p=0.0017$; caudate: $r_s=0.78$, $p=0.0127$). The maximal attainable D₂ receptor occupancy (Emax) in putamen (96%) and caudate (90%) was very similar to the Emax value in temporal cortex (91%) calculated from the data reported by Xiberas et al. (2001), but occupancy levels were lower in caudate at lower amisulpride plasma concentrations. Calculated plasma levels to attain 60 to 80% receptor occupancy range from 119 to 474 ng/ml (caudate) and from 241 to 732 ng/ml (putamen). No linear correlation could be found between D₂-like dopamine receptor occupancy and side effects as assessed by the SAS rating scale

Conclusions: Our data show high striatal D₂-like receptor occupancies at higher plasma levels. Maximal attainable striatal occupancies were similar to previously reported temporal values. However, region-specific different steepness of the concentration/occupancy curve suggests a concentration-dependent preferential extrastratial binding with higher differences at lower amisulpride concentrations. This may partly explain amisulpride’s “atypical” properties. There is a broad range of plasma levels leading to striatal occupancies below the EPS border of 80% although extrastratial occupancies of more than 60% can be expected.

Reference :

Xiberas X, Martinot J-L, Mallet L, Artiges E, Canal M, Loc'h C, Mazière B, Pailleire-Martinot M-L (2001). In vivo extrastratial and striatal D2 dopamine receptor blockade by amisulpride in schizophrenia. Journal of Clinical Psychopharmacology 21: 207-14

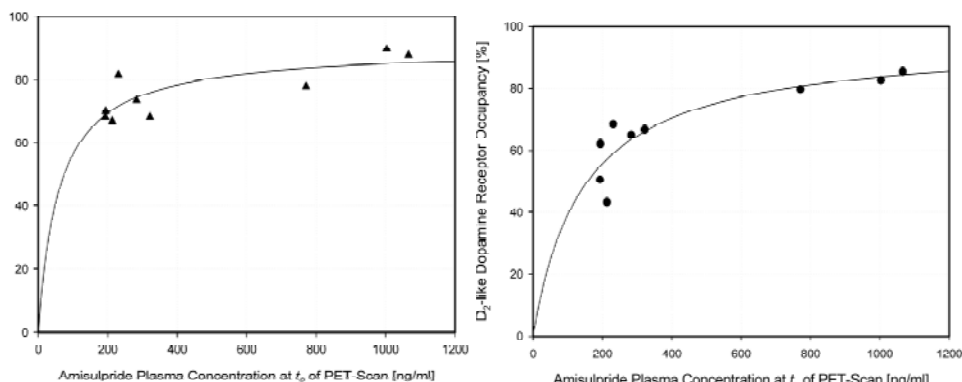


Fig.1:

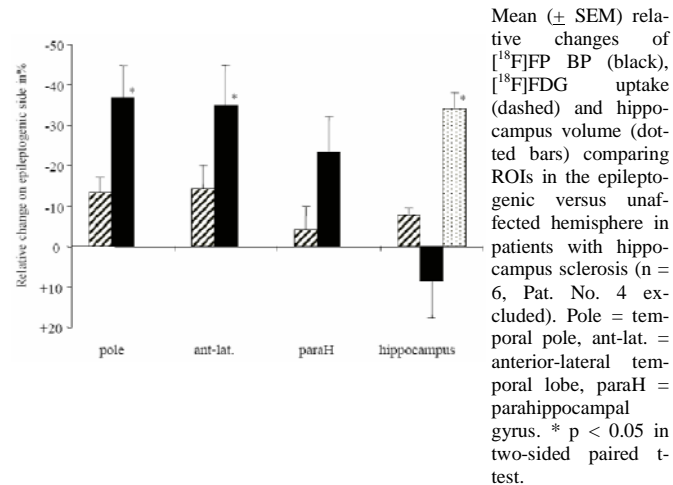
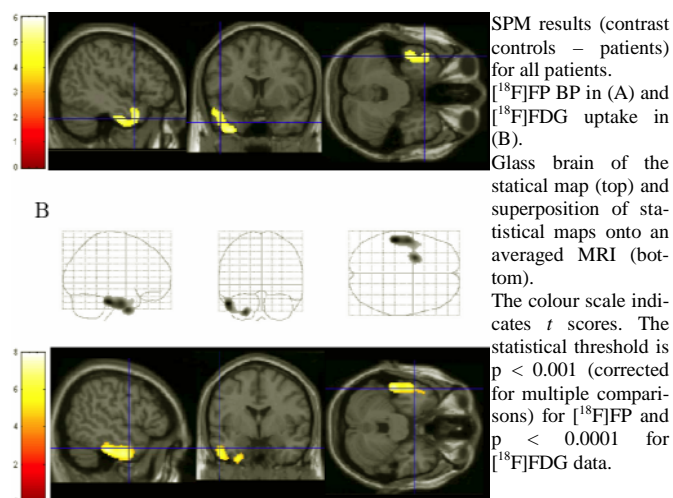
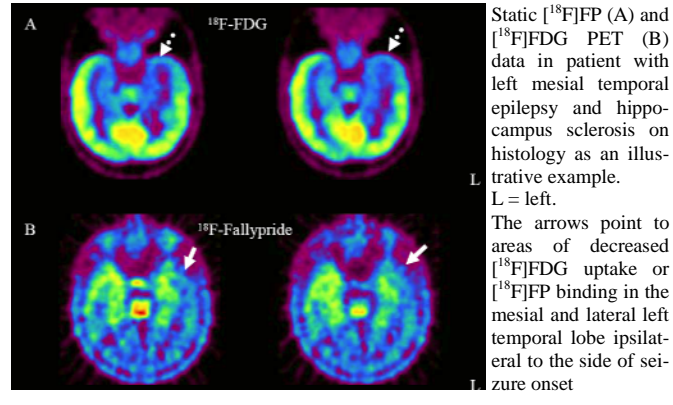
Relationship between amisulpride plasma concentrations and D₂R receptor occupancies in putamen [left] and caudate nucleus [right].

Decreased temporal dopamine D2/D3 receptor binding in temporal lobe epilepsy: an ^{18}F -Fallypride PET study

Konrad J. Werhahn^{1*}, Christian Landvogt², Sven Klimpe¹; Hans-Georg Buchholz², Wibke Müller-Forell³, Igor Yakushev², Markus Piel⁴, Frank Rösch⁴, Mathias Schreckenberger², Peter Bartenstein²

¹Department of Neurology, ²Nuclear Medicine, ³Institute of Neuroradiology and ⁴Institute for Nuclear Chemistry, Johannes Gutenberg-University, Rhineland-Palatinate, Germany

The role of dopamine in focal epilepsy is controversial. In animal models of temporal lobe epilepsy (TLE) activation of D1-receptors has a pro- and of D2-receptors an anticonvulsant effect. Evidence for an alteration of the extrastriatal dopaminergic system in human focal epilepsy is missing. To quantify D2/D3 receptor density we studied seven patients with mesial TLE and 7 aged-matched control subjects by PET using the high affinity dopamine D2/D3 receptor ligand ^{18}F -Fallypride ($[^{18}\text{F}]FP$) suitable for imaging extrastriatal binding. Mesial TLE was defined by interictal and ictal Video-EEG, MRI and ^{18}F -Fluorodesoxyglucose ($[^{18}\text{F}]FDG$) PET and was due to hippocampus sclerosis. Anatomical regions of interest (ROIs) were drawn on MRIs. PET data were quantified using the simplified reference tissue model to assess binding potential (BP) values in each ROI, with cerebellum as reference. For each patient, a normalized percentage BP change was calculated as the relative variation of BP in each ROI on the epileptogenic compared with the unaffected hemisphere. In addition, a voxel-based analysis was performed using statistical parametric mapping (SPM). Results were correlated with $[^{18}\text{F}]FDG$ PET and MR-volumetry data. Compared to the controls, $[^{18}\text{F}]FP$ BP was significantly decreased in the epileptogenic temporal lobe. This reduction was particularly evident in areas surrounding the seizure onset zone in the pole (- 34%) and lateral aspects (- 33%) of the temporal lobe. The decrease of $[^{18}\text{F}]FP$ BP in these areas was significantly greater than the decrease of $[^{18}\text{F}]FDG$ uptake. In contrast, in the hippocampus there was no significant decrease of $[^{18}\text{F}]FP$ binding whereas $[^{18}\text{F}]FDG$ uptake was significantly reduced and correlated with hippocampus atrophy (- 33%). Reduction of $[^{18}\text{F}]FP$ BP did not correlate with seizure or spike frequency, and hippocampal atrophy as measured by MR-volumetry. Our findings are consistent with the hypothesis of reduced D2/D3 binding in the temporal pole and lateral aspects of patients with mesial temporal lobe epilepsy with hippocampus sclerosis.



Alcohol craving correlates with striatal dopamine receptor density and dopamine synthesis capacity

T Siessmeier*, A Heinz[†], HG Buchholz*, J Wräse[†], C Landvogt*, R Schirrmacher[‡] M Piel[‡], F Rösch[‡], M Schreckenberger*, P Cumming[†], G Gründer^{*}, P Bartenstein*

[†]Department of Nuclear Medicine University of Mainz Germany

[‡]Department of Psychiatry Charite University of Berlin Germany

[†]Institute of Nuclear Chemistry University of Mainz Germany

[†]Department of Psychiatry University of Mainz Germany

[†]PET Center Arhus Kommunehospital Arhus Denmark

Aim:

It is known from animal experiments that stimulus-associated dopamine release in the striatum directs attention towards drug associated cues and elicits drug craving. In alcoholics it is expected that alcohol associated cues trigger striatal dopamine release in the reward system and induce or enhance craving for alcohol. It has been shown that alcohol, like other drugs of abuse, stimulates dopamine release and induces down regulation of striatal dopamine receptors. In this study we investigated therefore presynaptic dopamine synthesis capacity and postsynaptic dopamine D2 receptor density in abstinent alcoholics and healthy volunteers to further examine the association between striatal dopaminergic dysfunction and alcohol craving.

Methods:

N=11 male abstinent alcoholics (according to DSM-IV and ICD 10 criteria) (age 35-57) and n=13 age matched healthy volunteers (age 32-60) were scanned with ¹⁸F-Fluorodopa (DOPA) and ¹⁸F-Desmethoxyfallypride (DMFP). After application of 194±27MBq DMFP or 198±37MBq DOPA respectively a dynamic emission scan in 3D mode over 124min was started using a Siemens ECAT EXACT PET-camera. Attenuation correction was done applying measured attenuation correction. Binding potential (BP) was calculated on a voxelwise basis using a simplified reference tissue model with the cerebellum as reference region resulting in parametric BP-images (1). For stereotactical normalization of these images a ligand specific template was used created from mean images of healthy volunteers. DOPA-Influx (Ki) was calculated for each pixel using the Gjedde-Patlak analysis with a cerebellar input function (2). Stereotactical normalization was done normalising early summed frames to a flow weighted PET-template and applying the derived normalisation parameters to the Ki-images. Using statistic parametric imaging software (SPM) we calculated categorical group comparison between patients and volunteers as well as pixelwise correlation analyses between the individual scans

and craving for alcohol measured with the Alcohol Craving Questionnaire (ACQ).

Results:

In the categorical group comparison we found no significant differences between the patients and volunteer at a give significance threshold of $p<0,001$ neither for DOPA nor for DMFP. The correlation analyses showed in the patient group a close negative correlation between the craving scale (ACQ) and the dopamine receptor density (DMFP) exclusively in the bilateral ventral striatum ($r=-0,9$; $x/y/z$ 16/14/-6 respectively -15/14/-6). For DOPA as well a negative correlation was found between craving and the patient group in the bilateral putamen ($r=-0,7$; $x/y/z$ 20/6/-6 -22/8/-10 respectively). For the healthy volunteers no significantly correlating voxels could be detected for DMFP and DOPA.

Conclusions:

These results suggest a dysfunction in the striatal dopaminergic neurotransmission in abstinent alcoholics and support the hypothesis that the reward system plays a key role in the origin or conservation of alcohol craving.

References:

- 1) Gunn RN, Lammertsma AA, Hume SP, Cunningham VJ. Parametric imaging of ligand-receptor binding in PET using a simplified reference region model. Neuroimage. 1997 Nov;6(4):279-87.
- 2) Patlak CS, Blasberg RG. Graphical evaluation of blood-to-brain transfer constants from multiple-time uptake data. Generalizations. J Cereb Blood Flow Metab. 1985 Dec;5(4):584-90.

Funktionelle Charakterisierung somatosensorischer Areale im parasympathischen Kortex des Menschen

U. Baumgärtner¹, M. Schreckenberger², W. Magerl¹, F. Rösch³, P. Bartenstein², P. Stoeter⁴, R.-D. Treede¹

Institut für Physiologie und Pathophysiologie¹, Klinik und Poliklinik für Nuklearmedizin², Institut für Kernchemie³, Institut für Neuroradiologie⁴, Johannes Gutenberg-Universität Mainz

Einleitung und bisherige Ergebnisse: Gegenstand dieses Projektes ist die somatosensorische Signalverarbeitung außerhalb des Gyrus postcentralis des Menschen. Sowohl für den Tastsinn als auch für den Schmerzsinn spielen dabei laterale Hirnareale oberhalb der Fissura Sylvii eine wichtige Rolle. Nozizeptive Areale im parasympathischen Kortex werden teils im frontoparietalen Operkulum (meist als SII bezeichnet), teils in der Inselrinde lokalisiert. Die relative Bedeutung dieser Areale wird kontrovers diskutiert. Erhöhte Schmerzschwellen fanden sich bei Patienten mit kleinen Tumoren im Operkulum, aber nicht bei Patienten mit Tumoren in der Inselrinde (Greenspan et al. 1999). Für eine führende Rolle des Operkulums spricht auch dessen Aktivierung ca. 50 ms vor der Inselrinde, die mit Tiefenableitungen bei Epilep-

siepatienten gezeigt wurde (Frot und Mauguière 2003). Umgekehrt ist die Inselrinde das einzige Kortexareal, dessen elektrische Reizung beim Menschen zuverlässig Schmerzen auslöst (Ostrowsky et al. 2002). Ein neues Konzept zur Interzeption (Craig 2002) besagt, dass nozizeptive, gustatorische und andere viszerale Bahnen auf kortikaler Ebene in der dorsalen Inselrinde konvergieren, wobei die nozizeptiven Bahnen über einen phylogenetisch jungen Thalamuskern (VMpo) dorthin projizieren. Dieses Konzept steht in Einklang mit den Ergebnissen unserer kürzlich publizierten Studie (Schlereth et al. 2003), in der wir mittels EEG-Quellenanalyse Laser-evozierte Potentiale nach schmerzhafter Reizung der Hand Dipollokalisierungen sowohl in der Inselrinde als auch im fronto-parietalen Operkulum fanden (Abb.1).

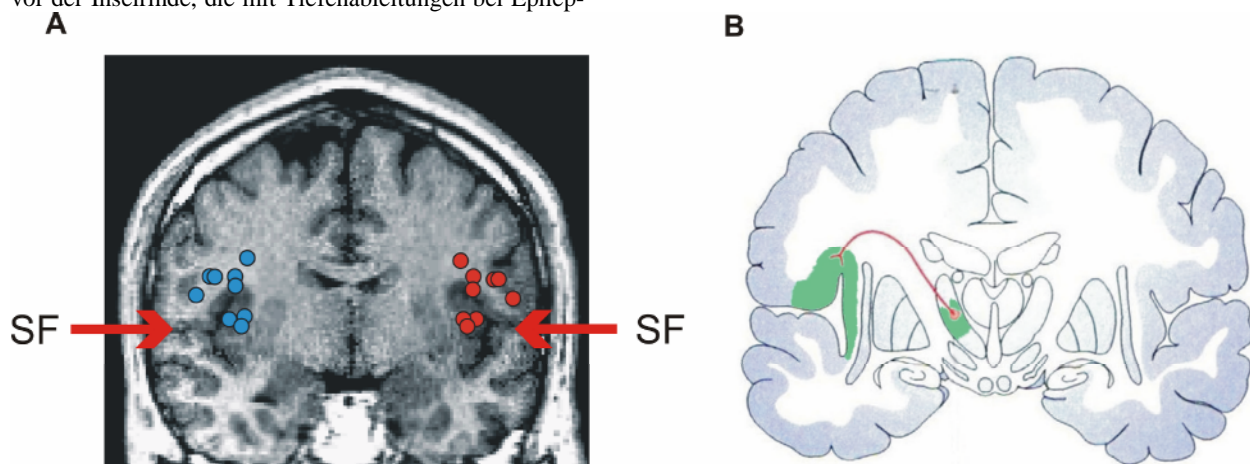


Abb.1: Nozizeptive Areale im parasympathischen Kortex. **A:** Verteilung der individuellen Quellen der frühesten Komponente der Laser-evozierten Potentiale im operculo-insulären Kortex (Schlereth et al. 2003). **B:** Der nozizeptive Thalamuskern VMpo projiziert in die Insel und Teile des frontalen Operkulums (Craig 2002). SF: Sylvische Fissur.

Eine Metaanalyse der PET und fMRI Studien der vergangenen 15 Jahre zeigte eine signifikante Aktivierung der Inselrinde in 94% der Studien, gegenüber 87% für den Gyrus cinguli und je 75% für SI und SII (Apkarian et al. 2005). Auch im direkten Vergleich führen nozizeptive Reize zu einer signifikant stärkeren Aktivierung der Inselrinde als taktile Reize (Coghill et al. 1994, Gelnar et al. 1999, Chen et al. 2002). Schmerzhafte Reizung aktiviert nicht nur SII, sondern auch weiter anterior gelegene Areale im frontalen Operkulum (Frot et al. 1999, Chen et al. 2002, Fabri et al. 2002, Vogel et al. 2003). Diese Areale schließen sich lateral unmittelbar an die dorsale Inselrinde an. Interessanterweise projiziert VMpo in die Inselrinde und ins angrenzende Operkulum (Craig 1995), und VPI (Hauptquelle der nozizeptiven Eingänge von SII) projiziert teilweise in die angrenzende Insel (Jones und Burton 1976). Möglicherweise liegt im operculo-insulären Kortex also ein zusammenhängendes nozizeptives Kortexareal (Peyron et al. 2002, Vogel et al.

2003), das in PET- und fMRI-Studien bei nahezu identischen Koordinaten teils als Insel teils als SII bezeichnet wird (vgl. Brooks et al. 2002 mit Chen et al. 2002). Diese anteriore Lokalisation könnte auch erklären, warum TMS über der klassischen posterioren SII-Region die Schmerzwahrnehmung nicht beeinflusste (wohl aber über SI und ACC; Kanda et al. 2003).

Als weiterer Parameter zur eventuellen Abgrenzung nozizeptiver und taktiler Areale im parasympathischen Kortex wurde die Verteilung der Opiatrezeptoren mittels ¹⁸F-Fluorethyl-Diphrenorphin PET bestimmt. Wir fanden das typische Bindungsmuster (hohe Werte im Gyrus cinguli, den Basalganglien und dem Thalamus, niedrige Werte im sensomotorischen Kortex und in der Sehrinde; Lochmann et al. 2003). Der operculo-insuläre Kortex zeigte eine relativ hohe Opiatrezeptorbinding mit einer Tendenz zu asymmetrischer Verteilung in beiden Hemisphären (Abb.2). Die interindividuelle Variabilität bei inzwischen 8 untersuchten Probanden war relativ hoch.

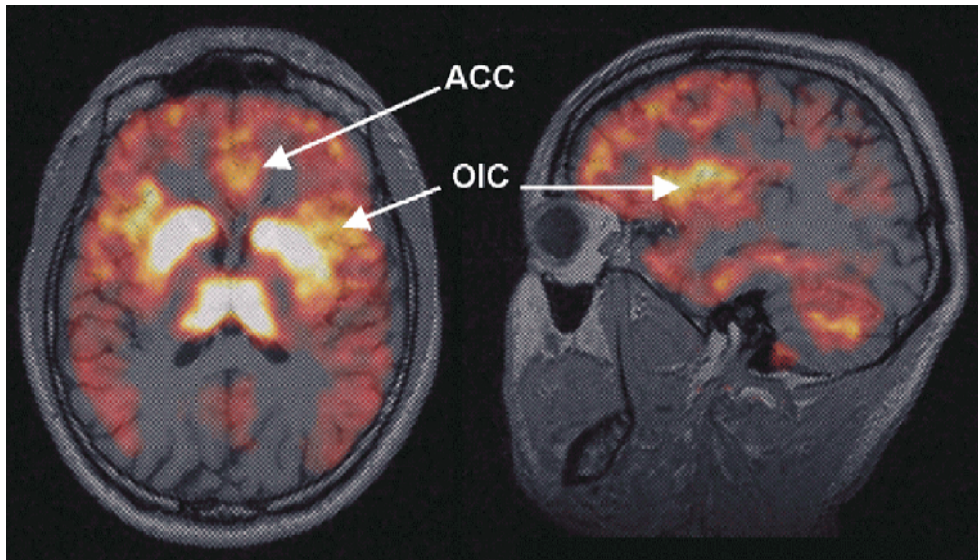


Abb.2: ^{18}F Fluor-Ethyl-Diprenorphin-PET einer Versuchsperson in transversaler und sagittaler Ebene. Neben Thalamus, Basalganglien und anteriorem Gyrus cinguli (ACC) findet sich auch eine hohe Rezeptorbindung in der Insula, die bis zur Innenseite des frontalen Operkulums reicht (OIC: operkulo-insuläre Kortex). Erwartungsgemäß gering ist die Rezeptordichte im primären motorischen, primären somat-sensorischen und im visuellen Kortex.

Weiteres Arbeitsprogramm und Ziele:

Die ausgeprägte Hemisphärenasymmetrie der taktilen und nozizeptiven Repräsentation im parasympatischen Kortex macht es erforderlich, gezielt ein Kollektiv von Linkshändern mit Rechtsphärendominanz zu untersuchen. Um die beobachteten individuellen Unterschiede mit der Variabilität der nozizeptiven Funktionen korrelieren zu können, soll in der nächsten Förderperiode (Tr 236/13-3) u.a. die Verteilung von Opiatrezeptoren an weiteren 12 Versuchspersonen mittels ^{18}F -Fluorethyl-Diprenorphin gemessen werden. Dabei wird Diprenorphin, ein unspezifischer Opiatrezeptor-Antagonist, der in-vivo mit ähnlicher Affinität reversibel an μ -, δ - und κ -Rezeptoren bindet, als Tracer in pharmakologisch unwirksamer Konzentration i.v. verabreicht. Die Versuche werden wie in der ersten Förderperiode in Zusammenarbeit mit Prof. Bartenstein (Nuklearmedizin) und Prof. Rösch (Kernchemie) durchgeführt. Bei jeder VP wird außerdem ein 3D-MRI angefertigt, um die relevanten parasympatischen Kortexareale als Regions-of-interest zu identifizieren. Die Matching-Techniken hierfür stehen im Rahmen der Neuroimaging-Gruppe des Schwerpunkts Neurowissenschaften des FB Medizin in Mainz zur Verfügung. Im Rahmen eines bereits bewilligten Graduiertenkollegs in Kooperation mit der Anatomie (Prof. Reuss, Prof. Konerding; GRK 1044/1, Teilprojekt C3) ist die morphologische Aufarbeitung der operkulo-insulären Region an Hirnschnitten geplant. Zur Untersuchung der Modulierbarkeit der operkulo-insulären Funktion in Bezug auf nozizeptive und taktile Diskriminationsleistungen soll die Auswirkung kortikaler Störimpulse geprüft werden. Mit einem zu diesem Zweck noch zu beschaffenden TMS-Gerät sollen dabei zeitlich an die zu diskriminierenden Reize gekoppelte Magnettpulse über der parasympatischen Region appliziert werden.

Es sollen folgende Fragen beantwortet werden:

- 1) Sind taktil (SII) und nozizeptive Areale (frontales Operkulum, Inselrinde) im parasympatischen Kortex anhand ihrer Somatotopie differenzierbar?
- 2) Welche Konsequenzen hat die Hemisphärenasymmetrie im parasympatischen Kortex für taktil und nozizeptive Sinnesleistungen (sensorisch und/oder affektiv)?
- 3) Durch welche Faktoren (Lernen, deszendierende Hemmung, Ablenkung) kann die taktile und nozizeptive Repräsentation im parasympatischen Kortex moduliert werden?
- 4) Welche Veränderungen zeigen die sensorische Schmerzkomponente und die nozizeptive Repräsentation im parasympatischen Kortex bei paradigmatischen Erkrankungen des Nervensystems?

Drittmittel: Gefördert durch die Deutsche Forschungsgemeinschaft (Tr 236/13-3) und NIH NS 38493

Literatur:

- Apkarian AV, Bushnell C, Treede R-D, Zubieta J-K (2005). Eur J Pain, im Druck
 Brooks JCW, Nurmi TJ, Bimson WE, Singh KD, Roberts N (2002) n. Neuroimage 15:293-301.
 Chen J-I, Ha B, Bushnell MC, Pike B, Duncan GH (2002). J Neurophysiol 88:464-474.
 Coghill RC, Talbot JD, Evans AC, Meyer E, Gjedde A, Bushnell MC, Duncan GH (1994). J Neurosci 14:4095-4108.
 Craig AD (1995) Supraspinal projections of lamina I neurons, in *Forebrain areas involved in pain processing* (Besson JM, Guilbaud G, and Ollat H eds) pp 13-25, John Libbey Eurotext, Paris.
 Craig AD (2002). Nature Reviews 3:655-666.
 Fabri M, Polonara G, Quattrini A, Salvolini U (2002). Cereb Cortex 12:446-451.
 Frot M and Mauguire F (2003) Brain 126:438-450.
 Frot M, Rambaud L, Guénot M, Mauguire F (1999). Clin Neurophysiol 110:133-145.
 Gelman PA, Krauss BR, Sheehe PR, Szeverenyi NM, Apkarian AV (1999). Neuroimage 10:460-482.
 Greenspan JD, Lee RR, Lenz FA (1999). Pain 81:273-282.
 Jones EG and Burton H (1976). J Comp Neurol 168:197-248.
 Kanda M, Mima T, Oga T, Matsuhashi M, Toma K, Hara H, Satow T, Nagamine T, Rothwell JC, Shibasaki H (2003). Clin Neurophysiol 114:860-866.
 Lochmann M, Buchholz HG, Siessmeier T, Schreckenberger M, Rösch F, Bartenstein P (2003). Abstracts of Brain03, Calgary
 Ostrowsky K, Magnin M, Ryvlin P, Isnard J, Guenot M, Mauguire F (2002). Cereb Cortex 12:376-385.
 Peyron R, Frot M, Schneider F, Garcia-Larrea L, Mertens P, Barral FG, Sindou M, Laurent B, Mauguire F (2002). Neuroimage 17:1336-1346.
 Schlereth T, Baumgärtner U, Magerl W, Stoeter P, Treede R-D (2003). NeuroImage 20: 441-454.
 Vogel H, Port JD, Lenz FA, Solaiyappan M, Krauss G, Treede R-D (2003). J Neurophysiol 89:3051-3060.

Vergleich unterschiedlicher Quantifizierungsmethoden des Bindungspotenzials für den unspezifischen Opiatrezeptorliganden ^{18}F -Fluor-Ethyl-Diprenorphin

Th. Siessmeier¹, H.-G. Buchholz¹, H.-J. Wester², G. HendrickSEN², M. Piel³, F. Rösch³, M. Schreckenberger¹, P. Bartenstein¹

¹Department of Nuclear Medicine, University of Mainz, Germany

²Department of Nuclear Medicine, University of Munich, Germany

³Institute of Nuclear Chemistry University of Mainz Germany

Ziel:

F-18-Fluor-Ethyl-Diprenorphin (F-18-DPN) ist ein unspezifischer Opiatrezeptorligand mit vergleichbarer Selektivität und Affinität wie das bekannte C-11-Diprenorphin. Die Markierung mit 18-Fluorid macht seinen Einsatz unabhängig von einem Zyklotron möglich und verspricht Vorteile insbesondere bei Verdrängungsstudien und beim Nachweis endogener Liganden.

Ziel der Studie war aus einem Vergleich unterschiedlicher Quantifizierungsmethoden zur Berechnung des Bindungspotentials (BP) die für Patienten- und Probendienststudien geeignete Methode bezüglich ihrer Genauigkeit und dem Grad ihrer Invasivität zu ermitteln.

Methodik:

6 gesunde männliche Probanden (Alter 20-45) wurden mit ^{18}F -DPN mit einer Siemens ECAT EXACT PET-Kamera untersucht. Nach kalter Transmission erfolgte die Injektion von 188 ± 29 MBq F-18-DPN mit einer dynamischen Emissionsmessung (3D) über 124 min.

Zeitgleich wurde eine metabolitenkorrigierte arterielle Inputfunktion generiert.

Zur Quantifizierung des BP kamen die Spektralanalyse (SA) der Logan Plot (LP) und das simplified reference tissue Modell (SRTM) zur Anwendung, wobei das BP aus für SA und LP indirekt über die Berechnung des Distributionsvolumens (DV) bestimmt wurde. Folgende Regionen wurden anhand des ROI-Templates quantifiziert: occipital (Referenzregion), Thalamus (Th), Putamen (Pu), Nucleus caudatus (NC), frontaler Cortex (FC), Cingulum (GC), temporaler

Cortex (TC), Hypophyse (Hy) und Cerebellum (Ce).

Ergebnisse:

Die Mittelwerte der BP für n=6 Probanden anhand der unterschiedlichen Methoden sind in der Tabelle zusammengefasst. Die absoluten Werte für F-18-DPN waren für alle Regionen etwas niedriger als für C-11-DPN, wobei beim LP eine größere Streuung in Regionen höherer Affinität (Th) festzustellen war.

	Th	Pu	NC	FC	GC	TC	Hy	Ce
SA	2,6	1,7	2,5	1,1	1,4	1,2	2,2	0,6
LP	2,6	1,8	2,5	1,0	1,4	1,2	2,0	0,6
SRTM	2,4	1,5	2,1	1,0	1,2	1,0	2,2	0,6

Schlussfolgerungen:

Die gute Übereinstimmung mit den BP-Werten für ^{11}C -Diprenorphin aus der Literatur (1) weist auf eine äquivalente in vivo Selektivität hin. Das simplified reference tissue Modell (SRTM) scheint auf Grund der geringen Invasivität und vergleichbarer Resultate gut geeignet für die Berechnung des BP.

Literatur:

- (1) Jones AK, Cunningham VJ, Ha-Kawa SK et al. Quantitation of $[^{11}\text{C}]$ diprenorphine cerebral kinetics in man acquired by PET using presaturation, pulse-chase and tracer-only protocols J Neurosci Methods. 1994; 51:123-34.

C. Analytik für Umwelt und Technik

- Batch- und EXAFS-Experimente zur Sorption von U(VI) und Np(V) an Kaolinit
- Nachweis aquatischer Kolloide mit LIBD
- Neue CE-Systeme für Speziationsuntersuchungen
- Ultraspurenanalyse mit RIMS
- Komplexierung von Pb und Pu(IV) mit Huminsäure
- Weiterentwicklung LASER-analytischer Verfahren

C. Analytics for Environment and Technology

- Batch and EXAFS studies of U(VI) and Np(V) sorption on kaolinite
- Detection of aquatic colloids with LIBD
- New CE systems for element speciation
- Ultra-trace analysis with RIMS
- Complexation of Pb and Pu(IV) with humic substances
- Further development of LASER-analytical techniques

STRUCTURE OF URANIUM(VI) SURFACE COMPLEXES ON KAOLINITE

S. Amayri¹, T. Reich¹, A. Jermolajev¹, Ta. Reich¹, J. Drebert¹, S. Boulyga²

¹ Institut für Kernchemie, Universität Mainz, 55099 Mainz, Germany;

² Institut of Inorganic Chemistry and Analytical Chemistry, 55099 Mainz, Germany

The sorption of U(VI) onto the reference kaolinite KGa-1b has been investigated both by batch experiments and EXAFS measurements. Sorption samples were prepared in 0.1 mol/L NaClO₄ at total U concentrations ranging from 1 µmol/L to 20 µmol/L, 4 g/L kaolinite, pH 3.0 to 10.5, presence and absence of ambient CO₂, and 60-h equilibration. The sorption curves for 1 µM U(VI) obtained in presence and absence of CO₂ show that the adsorption edge occurs at pH 5.5. The uptake of U(VI) by kaolinite strongly increased above pH 4.0 and reached its sorption maximum (100 %) in the pH range from 6.0 to 8.0. Above pH 8.0, the amount of U(VI) sorbed onto kaolinite decreased due to the formation of the U(VI) carbonato species in aqueous solution, to 0 % at pH 10.5. In the closed system without CO₂ the sorption of U(VI) was 100 % in the pH range 6.0 to 10.5. At 10 µM total U(VI), the sorption edge is shifted slightly higher to pH 6.0. The uranium uptake also decreased above pH 8.0 in the presence of CO₂ and remains at 100 % in the CO₂-free system. Similar results were found by Sekine, Redden and coworkers [1,2].

The aim of our study was to combine batch experiments with EXAFS spectroscopy to study the speciation of U(VI) at the kaolinite surface in more detail. The samples for the EXAFS measurements were prepared as shown in Table 1. The highest uranium loading of the EXAFS samples was 1200 ppm and the lowest loading was less than 100 ppm, i.e., significantly less than in the previous EXAFS study of Thompson et al. [3]. The uranium L₃-edge EXAFS spectra were recorded in fluorescence mode at room temperature at the Rossendorf Beamlne (ROBL) at the European Synchrotron Radiation Facility (ESRF). The software packages EXAFSPAK and FEFF 8.20 were used for the analysis of the EXAFS data using atomic cluster based on the crystal structure of soddyite [4].

The raw data of the U L₃-edge K^3 -weighted EXAFS spectra of the samples with their corresponding FTs are shown in Fig. 1. The metrical parameters derived from the least-square fits are summarized in Table 1. The U-O_{ax}, U-O_{eq}, and U-Al/Si distances measured by EXAFS suggest that U(VI) forms inner-sphere, monomeric surface complexes with kaolinite in the pH range 5.0 - 8.5. In the presence of atmospheric CO₂, the average U-O_{eq} distance increased from 2.32 to 2.38 Å when the pH was increased from 5.0 to 8.5. This points to the formation of ternary U(VI)-carbonato com-

plexes on kaolinite. A weak and broad feature in the Fourier transform of all samples at approximately 2.3 Å (see Fig. 1) could be fit best with one Si atom at an average U-Si distance of 2.74 ± 0.02 Å. This very short U-Si distance can be rationalized by a corner-sharing model of U(VI) with the [SiO₄] tetrahedrons of kaolinite. However, this possibility needs to be investigated further, for example, by measuring the EXAFS spectra of suitable reference samples.

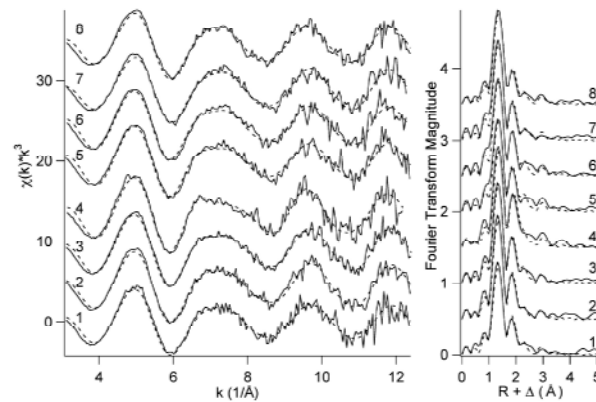


Figure 1: Uranium L₃-edge K^3 -weighted EXAFS spectra (left) and their corresponding FTs (right) for U(VI) adsorbed on kaolinite.

Table 1: EXAFS fit results.

Sample	Conditions [U(VI)](µM)/pH	2xO _{ax} R(Å)	5xO _{eq} R(Å)	1xSi R(Å)
1	10/5.0, air	1.78	2.32	2.71
2	10/6.0, air	1.78	2.33	2.69
3	10/7.0, air	1.78	2.35	2.72
4	10/8.5, air	1.80	2.38	2.71
5	5/7.0, air	1.79	2.35	2.74
6	10/7.0, air	1.79	2.35	2.74
7	20/7.0, air	1.79	2.35	2.88
8	10/8.5, no CO ₂	1.79	2.32	2.71

* $\Delta R = \pm 0.02$ Å

ACKNOWLEDGEMENTS. This work was supported by the BMWA grant No. 02E9653.

REFERENCES

- [1] K. Sekine et al., Int. Alligator Rivers analogue project (18), JAERI Memo 03-036 (1991).
- [2] G. D. Redden et al., in Adsorption of metals by geomedia, in Jenne, E. A., (Ed.), Academic Press, San Diego, 1998, p. 291-314.
- [3] H. A. Thompson et al., ibid, p. 349-370.
- [4] F. Demartin et al., Acta Crystallogr. C48 (1992) 1-4.

NEPTUNIUM(V) SORPTION ONTO KAOLINITE IN THE PRESENCE AND ABSENCE OF CO₂

S. Amayri, T. Reich, J. Drebert
Institut für Kernchemie, Universität Mainz, 55099 Mainz, Germany

Kaolinite, Al₂Si₂O₅(OH)₄, is a clay mineral that has a strong affinity for the sorption of radionuclides and heavy metals. It has been proposed as a backfill material for geologic repositories for nuclear waste. The adsorption of heavy metals on kaolinite is an important process that affects the migration and retardation of neptunium and other actinides in the geosphere. Unfortunately, there is not enough information available on neptunium sorption onto kaolinite. Therefore, detailed studies of the sorption and migration behavior of neptunium from nuclear waste repository are necessary for safety assessments. We investigated the sorption of Np(V) onto the reference clay mineral kaolinite KGa-1b both by batch experiments and EXAFS measurements [1].

The batch experiments were done under relevant environmental Np(V) concentrations of 1.1·10⁻¹¹ and 9.1·10⁻¹³ mol/L and compared to sorption experiments at 2.0·10⁻⁵ and 8.0·10⁻⁶ mol/L Np(V). Sorption samples were prepared in NaClO₄ solution, pH 6.0 to 10.5, presence and absence of ambient CO₂. All experimental conditions of Np(V) sorption on kaolinite are summarized in Table 1.

The sorption curves for 1.1·10⁻¹¹ and 9.1·10⁻¹³ mol/L Np(V) obtained in presence and absence of CO₂, respectively, show that the adsorption edge occurs at pH 8.5. The uptake of Np(V) by kaolinite strongly increased above pH 6.5 and reached its sorption maximum (70 %) at the pH 9.0. Above pH 9.0, the amount of Np(V) sorbed onto kaolinite decreased due to the formation of the Np(V) carbonato species in aqueous solution, to 30 % at pH 10.5.

In the CO₂-free system, the sorption of Np(V) increased continuously with the pH until the sorption maximum of 100 % was reached at pH 10.5. The same sorption behavior was found in batch experiments in the CO₂ equilibrated system with 10 µmol/L Np(V) concentration.

EXAFS experiments on some of these batch samples indicated the formation of Np(V) carbonato species at the kaolinite surface at pH 9.0 where the uptake of Np(V) by kaolinite reached its maximum [1].

Table 1: Experimental conditions of Np(V) sorption on kaolinite

Method: batch experiment
Vessel: 10 ml polypropylene centrifuge tube
Solid/liquid: 4 g/L
Electrolyte: 0.1 mol/L NaClO₄
Np(V) concentration: 2.0·10⁻⁵, 8.0·10⁻⁶, 1.1·10⁻¹¹ and 9.1·10⁻¹³ mol/L
PCO₂: 10^{-3.5} atm, CO₂ free
Temperature: 25 °C
pH-range: 6.0-10.5
Pre-equilibration: 72 h
Separation: centrifugation 5000 rpm for 7 min
Contact time neptunium/kaolinite: 60 h
Agitation: overhead shaking 16 rpm
Chemical analysis: γ-measurement of solid phase and solution (tracer: Np-239 (103 keV, 106 keV)

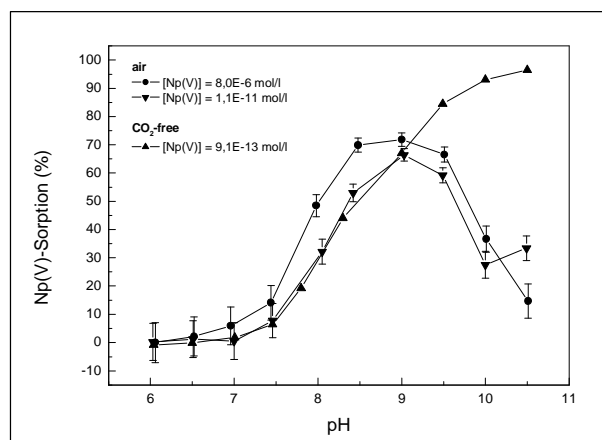


Figure 1: Np(V) adsorbed on kaolinite in the presence and absence of CO₂

ACKNOWLEDGEMENTS. This work was supported by the BMWA grant No. 02E9653.

REFERENCES

- [1] T. Reich, S. Amayri, Ta. Reich, J. Drebert, A. Jermolajev, P. Thörle, N. Trautmann, C. Hennig, S. Sachs, Feasibility of EXAFS experiments at the Np L-edge to investigate neptunium sorption on kaolinite, Institut für Kernchemie, Universität Mainz, This Report 2004.

Feasibility of EXAFS experiments at the Np L-edge to investigate neptunium sorption on kaolinite

T. Reich¹, S. Amayri¹, Ta. Reich¹, J. Drebert¹, A. Jermolajev¹, P. Thörle¹, N. Trautmann¹, C. Hennig², S. Sachs²

¹ Institut für Kernchemie, Universität Mainz, D-55099 Mainz, Germany;

² Institut für Radiochemie, Forschungszentrum Rossendorf, D-01314 Dresden, Germany

Several collaborating groups selected the kaolinite KGa-1b from the Source Clays Repository as reference clay for a broad range of investigations dealing with the interaction of actinides in the system clay, humic substances, and aquifer. During recent EXAFS measurements of uranium(VI) sorption onto kaolinite KGa-1b, we found that this kaolinite contains traces of zirconium. The energy of the Zr K-edge equals 17998 eV. Therefore, we expected a distortion of the Np L₃-edge (17610 eV) EXAFS signal at this energy or at k approximately equal to 9.8 Å⁻¹. In our experiment we wanted to explore the possibilities for avoiding severe distortions in the Np EXAFS signal without limiting the useful k range to 9.8 Å⁻¹.

EXPERIMENTAL. Two samples, 1 and 2, with different amounts of neptunium(V) sorbed on KGa-1b were prepared from a 1.8 mM Np(V) stock solution of Np-237 under the following conditions: 4 g kaolinite/L, pH 9.0, $p(\text{CO}_2) = 10^{-3.5}$ atm, I = 0.1 M NaClO₄. The total neptunium concentration for samples 1 and 2 was $8 \cdot 10^{-6}$ and $2 \cdot 10^{-5}$ mol/L, respectively. The neptunium uptake of samples 1 and 2 as measured by \square -spectroscopy was 300 and 510 ppm, respectively. The solid residue was loaded without drying into the EXAFS sample holder. The neptunium EXAFS spectra were measured at ROBL (ESRF, BM20) [1] at room temperature in the fluorescence mode using a 13-element Ge solid-state detector.

The following measurements were performed on these samples:

1) The Np L₃-radiation at 13.9 keV was recorded as a function of photon energy across the Np L₃-edge EXAFS region using single-channel analyzers (SCA's). The signal was corrected for detector dead time.

2) The EXAFS spectrum was measured at the Np L₂-edge (21600 eV) by setting the SCA's to 17.8 keV to record the Np L₃-radiation. Dead time correction was performed as described above.

RESULTS. Figure 1 shows the Np EXAFS spectra and the corresponding Fourier transforms of sample 1 (300 ppm Np) measured at the L₃- and L₂-edges. Seven sweeps at the Np L₂-edge and six sweeps at the L₃-edge were averaged. The useful k range at the L₃-edge was limited to k_{\max} equal to 9.4 Å⁻¹ due to the Zr K-edge absorption. The Np L₂-edge EXAFS signal could be recorded with good statistics up to k_{\max} equal to 11.4 Å⁻¹. To obtain a higher resolution in the Fourier transform, it is preferable to record the Np EXAFS signal of the kaolinite samples at the Np L₂-edge instead of the L₃-edge.

Table 1 summarizes the EXAFS structural parameters of sample 1 derived from the Np L₃- and L₂-edge k^3 -weighted EXAFS spectra. The detected

neptunium coordination shells and bond distances are consistent with the formation of a neptunium(V) carbonato species at the kaolinite surface. A similar result was obtained for sample 2 (510 ppm, not shown here).

In conclusion, these test experiments showed that it is possible to study the sorption of neptunium onto kaolinite KGa-1b successfully using Np L₂-edge EXAFS spectroscopy. In future EXAFS experiments, it will be possible to study sorption samples with less than 300 ppm neptunium by collecting more than seven sweeps per sample.

ACKNOWLEDGEMENTS. This work was supported by the BMWA grant No. 02E9653.

REFERENCES

- [1] W. Matz et al., J. Synchrotron Rad. **6**, 1076 (1999)

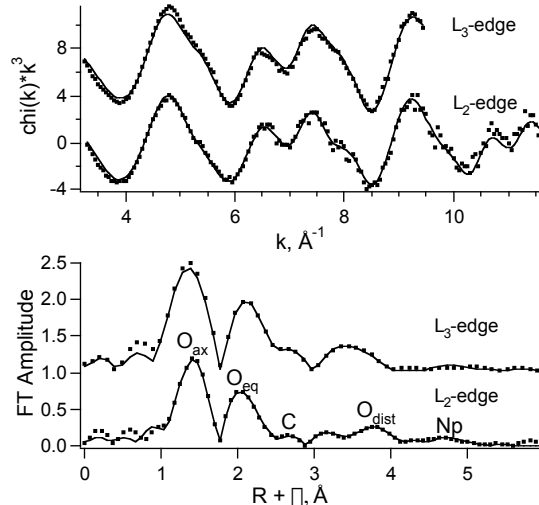


Figure 1: Neptunium L-edge k^3 -weighted EXAFS spectra (top) and corresponding Fourier transforms (bottom) of 300 ppm Np(V) sorbed onto kaolinite at pH 9.0 under ambient conditions. Dots – raw experimental data, solid line - best theoretical fit to the data.

Table 1: EXAFS structural parameters for 300 ppm Np(V) sorbed onto kaolinite at pH 9.0 under ambient conditions. Multiple-scattering paths are not listed. Coordination numbers were held constant during the final fit according to the result of previous fits.

Shell	Np L ₂ -edge R(Å)	Np L ₂ -edge $\square^2(\text{Å}^2)$	Np L ₃ -edge R(Å)	Np L ₃ -edge $\square^2(\text{Å}^2)$
2 x Oax	1.85	0.0021	1.84	0.0010
4 x Oeq	2.55	0.0051	2.55	0.0054
2 x C	2.94	0.0060	2.95	0.0027
2 x Odist	4.24	0.0040	4.25	0.0044
1 x Np	4.86	0.0023	4.89	0.0050

Application of the Tikhonov regularization method to the detection of U-Si neighbours in soddyite using EXAFS spectroscopy

Ta. Reich¹, T. Reich¹, A.L. Ageev², M. Korshunov²

¹ Institut für Kernchemie, Johannes Gutenberg-Universität, Mainz, Germany;

² Institute of Mathematics and Mechanics, Ural Branch of Russian Academy of Sciences, Ekaterinburg, Russia.

Our EXAFS study on U(VI) sorption on kaolinite indicated that U forms inner-sphere complexes with $[\text{SiO}_4]$ tetrahedra [1]. Soddyite, $(\text{UO}_2)_2(\text{SiO}_4)x2\text{H}_2\text{O}$, is a natural mineral with monodentate and bidentate coordination of the UO_2^{2+} moiety to $[\text{SiO}_4]$ with U-Si distances of 3.80 and 3.15 Å, respectively [2]. Before using the Tikhonov regularization method [3] for the EXAFS analysis of the U(VI)/kaolinite samples, we investigated the possibility of detecting U-Si pairs in simulated and experimental U L₃-edge EXAFS spectra of soddyite.

As a first step in our simulation, we calculated three partial radial atomic distribution functions (RDFs) for U-O, U-Si, and U-U in the r -range of 1.5 - 4.6 Å using the crystal structural data of soddyite given in Table 1. The program FEFF8.20 [4] was used to calculate scattering phase and amplitude functions. These functions and the RDFs were used to calculate four theoretical U L₃-edge EXAFS spectra $\chi(k)$. Three $\chi(k)$ were calculated using only the RDF of U-O, U-Si, or U-U. The fourth $\chi(k)$, which simulates the experimental $\chi(k)$, was calculated by combining all three RDFs. Then, four theoretical $\chi(k)$ and one experimental $\chi(k)$, which was measured at 15 K, were analyzed by the Tikhonov regularization method. The regularization parameters were $\alpha = 0.7$ and $\beta = 0.3$ for all calculations. The resulting RDFs (Tikhonov solutions) for the pair U-Si are shown in Fig.1.

We conclude the following based on the results shown in Fig.1:

- 1) The theoretical RDF(U-Si) agrees with the experimental one;
- 2) The pairs U-O, U-Si, and U-U contribute additively to the RDF(U-Si);
- 3) The monodentate U-Si at 3.80 Å cannot be derived from the RDF(U-Si) due to the interference with U-U at 3.85 Å.
- 4) The bidentate U-Si at 3.15 Å can be identified in the theoretical and experimental RDFs.
- 5) For the detection of U-Si in an unknown structure, e.g., U/kaolinite, it is necessary to remove the contributions of U-O and U-U from $\chi(k)$ before calculating the RDF(U-Si) or to perform special calculation experiments with the contributions from U-O and U-Si in $\chi(k)$.

Fig.1.RDF (Tikhonov solution) for the U-Si pair calculated from:

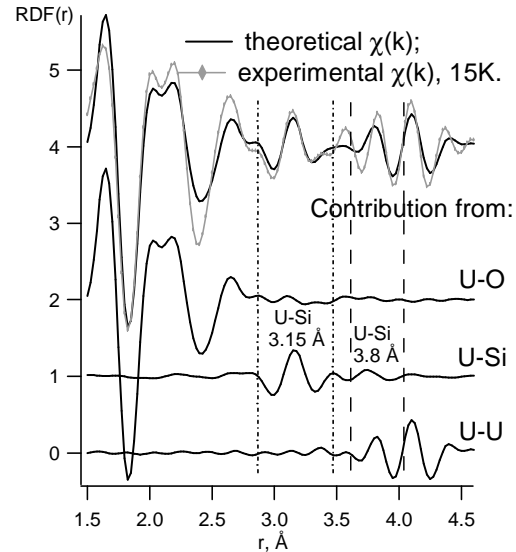


Table1: Structural parameters for the calculation of the model RDFs :

	N	r, Å	$\sigma^2, \text{\AA}^2$
RDF U-O	2	1.78	0.002
	5	2.38	0.010
RDF U-Si	1	3.15	0.004
	2	3.80	0.004
RDF U-U	2	3.85	0.002

References:

- [1] S. Amayri et al., Structure of uranium(VI) surface complexes on kaolinite, Institut für Kernchemie, Universität Mainz, this report 2004.
- [2] F. Demartin, C.M. Gramaccioli, T. Pilati, Acta Cryst. C **48**, 1-4 (1992).
- [3] N.V. Ershov, A.L. Ageev, V.V. Vasin, Yu. A. Babanov, Phys.Stat.Sol.B **108**, 103(1981).
- [4] A. Ankudinov, B. Ravel, J.J. Rehr, S. Conradson, Phys.Rev.B **58**, 7565 (1998).

Investigation of Zr(IV)-hydroxide Solubility with LIBD and EXAFS

C. Walther^{1,2}, H.R. Cho², M.A. Denecke², Th. Fanghänel², J.-V. Kratz¹, V. Neck², J. Rothe²

¹Institut für Kernchemie, Universität Mainz, Fritz Strassmann Weg 2, D-55099 Mainz

²Institut für Nukleare Entsorgung, Forschungszentrum Karlsruhe, Postfach 3640, D-76021 Karlsruhe

Zr(IV) gained increasing attention in recent literature as homologue of Pu(IV), due to its similar hydrolysis and colloid formation [1, 2]. In addition, Zr is an important material in reactor technology and a fission product of high yield and long lifetime (⁹³Zr). In the present work, the solubility of Zr(OH)₄(am) in 0.5M HCl/NaCl solution is determined. Conventionally, solubility data is obtained by measuring the equilibrium amount of solvated species in the presence of a precipitate starting from undersaturation. In the present case, a different approach is chosen, similar to a previous study with Th(IV) [3]. In the acidic range, the "Zr(OH)₄(am)"-solubility decreases with increasing pH. As the pH is increased, eventually the solubility limit is exceeded and some fraction of the Zr will precipitate. However, precipitation is difficult to observe at low concentration. Prior to precipitation, oligomers or colloids form in the solution which remain suspended by Brownian motion due to their small size (10-100nm) and serve as a very sensitive indicator of exceeding the solubility limit. They are detected by laser induced breakdown detection (LIBD) [4, 5]. From a concentrated stock solution ([Zr] = 5 · 10⁻³ M in 0.5 M HCl), 12 starting solutions are prepared below the solubility limit at Zr concentrations between 10⁻³ M and 2.5 · 10⁻⁸ M, at 1 < pH < 3, at constant ionic strength I=0.5 M (addition of NaCl). pH is increased very slowly by coulometric titration. Current control of the CT, pH detection and LIBD measurements are fully automated and operated remote-controlled continuously up to several weeks for one series. The pH is increased by predefined steps (≤ 0.1 pH units). After each step the current is turned off, and after a 30 minute equilibration time, the LIBD measurement is performed and the colloid size distribution is obtained [6]. After the LIBD measurement has finished, the current is switched on again and the pH is increased further. Close to the expected solubility limit, the pH is increased even more slowly by reducing the electric current down to 10 µA ($\sim 3 \cdot 10^{-9}$ mol OH⁻s⁻¹). The onset of colloid formation is depicted in Figure 1 (▲).

In order to calculate the solubility product, hydrolysis has to be taken into account. The first hydrolysis constant for the complex ZrOH³⁺ is taken from potentiometric studies [7] and the other formation constants of Zr(OH)_n⁽⁴⁻ⁿ⁾⁺ ($n = 2-6$) are estimated by using the semi-empirical ligand repulsion model [8]. Based on the assumption of colloid formation from mononuclear species, which is most likely valid for low concentrations, the calculated solubility product, logK_{sp}⁰, is 52.9 ± 0.6 . The data of the present work is in qualitative agreement with a similar method using light scattering for detection (○ from [1]). Deviations at low concentration are due to the low sensitivity of light scattering, as the authors state themselves. The data of Kovalenko

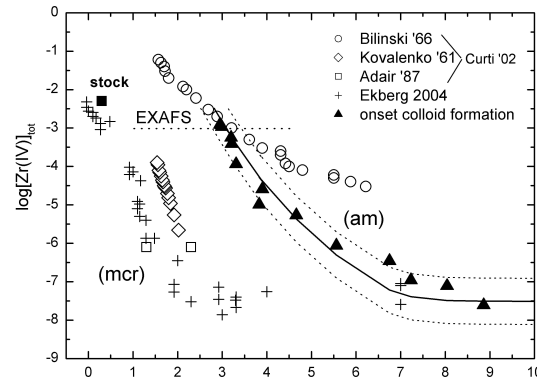


Figure 1: Solubility data for Zr(IV). Present work (▲) and a similar method using light scattering (○) refer to amorphous hydroxide. The data at low pH most likely refer to a microcrystalline phase (mcr)

(◊, from [1]) and Ekberg (+) [2] deviate by six orders of magnitude and seem to refer to microcrystalline ZrO₂ and not to amorphous hydroxide.

The most concentrated solution ([Zr] = 1 · 10⁻³ M) is studied by EXAFS in order to characterize polynuclear species and the structure of the colloids. Polynuclear Zr-species were reported earlier in the literature [9, 10] and confirmed at high concentrations ([Zr] = 1 · 10⁻² M) by strong Zr-Zr interactions even at very acidic conditions pH = 0.3. At [Zr] = 1 · 10⁻³ M no Zr-Zr interaction is found for pH < 2. As the solubility limit is approached close to pH 3, oligomers form. Colloids which form at higher pH are observed to have a higher disorder in their Zr-O coordination shell. The long term stability of these colloids and their agglomeration are also investigated with LIBD and a "single particle counter".

References

- [1] E. Curti and C. Degueldre. Radiochimica Acta 90(9-11), 801-804 (2002).
- [2] C. Ekberg, G. Kallvenius, Y. Albinsson, and P. L. Brown. Journal of Solution Chemistry 33(1), 47-79 (2004).
- [3] T. Bundschuh, R. Knopp, R. Müller, J.I. Kim, V. Neck, and Th. Fanghänel. Radiochim. Acta 88, 625-629 (2000).
- [4] T. Kitamori, K. Yokose, M. Sakagami, and T. Sawada. Japanese J. Appl. Phys. 28(7), 1195-1198 (1989).
- [5] F.J. Scherbaum, R. Knopp, and J.I. Kim. Appl. Phys. B 63, 299-306 (1996).
- [6] C. Walther, H.R. Cho, and Th. Fanghänel. Appl. Phys. Lett. 85(26), 6329-6331 (2004).
- [7] C. Ekberg, P. Brown, J. Comarmond, and Y. Albinsson. On the Hydrolysis of Tetravalent Metal Ions. In Mat. Res. Soc. Symp. volume 663 pages 1091-1099 (2001).
- [8] V. Neck and J. I. Kim. Radiochim. Acta 88(9-11), 815-822 (2000).
- [9] A. Singhal, L. M. Toth, J. S. Lin, and K. Affholter. 118(46), 11529-11534 (1996).
- [10] C. Hagfeldt, V. Kessler, and I. Persson. (14), 2142-2151 (2004).

Neue Möglichkeiten der Kapillarelektrophorese durch Verwendung eines Dioden-Array-Detektors (DAD)

B. Kuczewski, R. Buda, S. Bürger, J. V. Kratz, N. Trautmann

Institut für Kernchemie, Universität Mainz, D-55099 Mainz

Die Detektionsmöglichkeiten der vorhandenen Kapillarelektrophoresesysteme^[1,2] wurden um einen Dioden-Array-Detektor erweitert. Dieser ist unabhängig von den bereits verwendeten Detektoren (Laserinduzierte Fluoreszenz, Kopplung an die ICP-MS) einsetzbar und bietet die Möglichkeit, gleichzeitig den gesamten Wellenlängenbereich vom Ultravioletten (190 nm) bis ins Nahe Infrarot (1024 nm) mit einer Deuterium- und einer Halogenlampe anzuregen. Mit einer Anordnung von 1024 Photodioden wird ein 3-dimensionales Elektropherogramm mit 0,9 nm Auflösung und 1 bzw. 10 Hz Wiederholungsrate gemessen. Dies ermöglicht den gezielten Nachweis von verschiedenen Verbindungen. Abbildung 1 zeigt die Trennung von Huminsäure in 1 M Essigsäure bei -30 kV und 75 mbar Druck. Das erste Signal bei 8 min entspricht dabei der Huminsäure, der Einbruch bei 10 min im Wellenlängenbereich von 200 - 230 nm dem Wasser aus der Probenzone, der gleichzeitige Anstieg von 240 - 280 nm dem der Probe zugesetzten Aceton, das nur durch den elektroosmotischer Fluß (EOF) in der Kapillare transportiert wird. Durch diesen EOF-Marker lässt sich eine geringe Eigenbewegung der Huminsäure im Elektrolyten, und damit ihre negative Ladung in der Essigsäure belegen.

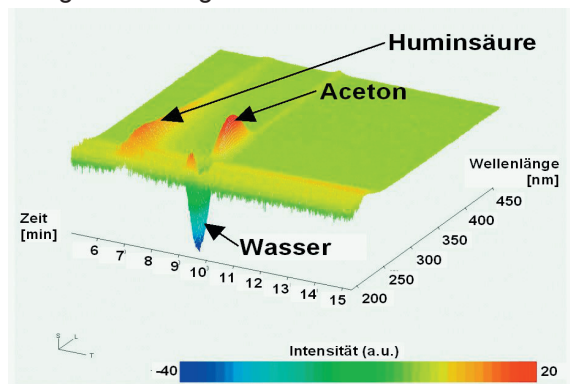


Abb. 1: Elektropherogramm einer Huminsäurelösung (Aldrich HA) mit der CE-DAD-Kopplung
-30 kV, 75 mbar, 1 M Essigsäure als Elektrolyt

Der Nachweis kann dabei sowohl direkt in der CE-Kapillare quer zur Fließrichtung mit einem Lichtweg von 75 µm als auch in einer speziellen z-Zelle mit einem Lichtweg von 1 cm bei allerdings schlechterer chromatographischer Auflösung erfolgen. Den Aufbau der einfachen Meßanordnung zeigt Abbildung 2.

Dabei wird die Messung etwa 5 – 10 cm vor dem Ende der Kapillare durchgeführt, während eine Detektion mit der ICP-MS am Ende der Kapillare erfolgt. Der gemeinsame Einsatz bei-

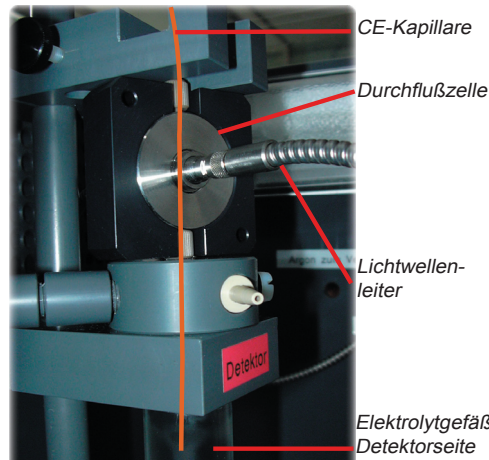


Abb. 2: Durchflußzelle des neuen Dioden-Array-Detektors für die Kapillarelektrophorese

der Detektionsmethoden ist dabei möglich und beabsichtigt. Damit können Metallionen mit der ICP-MS und Huminstoffe mit dem DAD in einem Lauf nachgewiesen werden. Ob 1 M Essigsäure geeignet ist, oder ein anderes Elektrolytsystem noch entwickelt werden muß, bleibt noch zu klären. Besonders interessant ist das Verfahren bei anionischen Trennungen, wie sie Abbildung 3 zeigt. In dieser Grundwasserprobe konnten verschiedene anionische Pu-haltige Spezies nachgewiesen werden^[3,4]. Ob es sich dabei um Humat-Komplexe des Plutoniums oder anorganische Spezies handelt, kann nun untersucht werden.

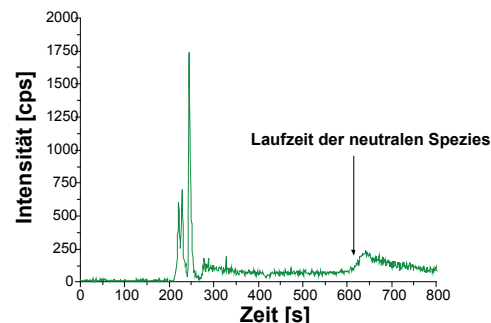


Abb. 3: Elektropherogramm (CE-ICP-MS) einer Grundwasserprobe aus Gorleben
60 min nach der Zugabe von Pu bei pH 7
-30 kV, 100 mbar, 1 M Essigsäure als Elektrolyt

Literatur:

- [1] B. Kuczewski et al.; *Analytical Chemistry*, 2003, 75, 6769-6774.
- [2] B. Kuczewski et al.; *Institut für Kernchemie, Universität, Mainz, Jahresbericht 2003*, C6.
- [3] C. M. Marquardt et al.; *Radiocimica Acta*, 2004, 92, 617-623.
- [4] B. Kuczewski; *Dissertation, Universität Mainz*, 2004.

Off-line Kopplung der Resonanzions-Massenspektrometrie an die Kapillarelektrophorese zur Speziation der leichten Actiniden im Ultraspurenbereich

S. Bürger, N. L. Banik, R. A. Buda, J. V. Kratz, B. Kuczewski, N. Trautmann

Institut für Kernchemie, Johannes Gutenberg-Universität Mainz, D-55099 Mainz, Germany

Das Verhalten der leichten Actiniden in der Umwelt ist in Hinblick auf dieendlagerung hochradioaktiver Abfälle gerade bei sehr niedrigen Konzentrationen von besonderer Bedeutung. Dabei ist die Bestimmung der Oxidationsstufen entscheidend für die Vorhersage der chemisch-physikalischen Wechselwirkungen im jeweiligen geochemischen System und damit auch der Migration der Actiniden von einem möglichen Endlagerstandort bis in die Biosphäre.

Zur Speziation von Plutonium und Neptunium wurde dazu die Kopplung der Kapillarelektrophorese (CE) mit der ICP-MS entwickelt [1]. Die Oxidationszustände des Pu und Np werden in der CE aufgrund ihrer unterschiedlichen Ladungs-/Radius-Verhältnisse im Elektrolyten (1M AcOH) getrennt und die separierten Spezies in einem ICP-MS nachgewiesen. Es können damit die Oxidationszustände III, IV, V und VI des Plutoniums sowie IV und V des Neptuniums separiert werden. Eine Nachweisgrenze von unter 20 ppb oder $10^9 - 10^{10}$ Atome (ICP-QMS Agilent 4500) wird erreicht. Weiterführend wird nun die Kopplung der CE mit der ultrasensitiven Resonanzions-Massenspektrometrie (RIMS) entwickelt. Bei einer Nachweisgrenze von $\leq 10^7$ Atomen (isotopenselektiv) [2] soll so eine Verbesserung um bis zu 2 Größenordnungen gegenüber der CE-ICP-MS möglich sein. Damit wäre sowohl die Bestimmung der Oxidationsstufen sowie der Isotopenzusammensetzung für Plutonium im Ultraspurenbereich möglich.

Über die genaue Bestimmung der Retentionszeiten der verschiedenen Pu-Spezies mit der CE-ICP-MS können durch gezieltes Abschalten der an der Kapillare anliegenden Hochspannung die Vorlagen gewechselt und somit die aus der Kapillare austretenden Elektrolytfaktionen für die verschiedenen Oxidationszustände in separaten Vorlagen gesammelt werden. Das Abschalten der Hochspannung führt zwar zu einer Peakverbreiterung durch Diffusion, verändert aber die mittleren Migrationszeiten für die verschiedenen Oxidationszustände nur unwesentlich, so dass getrennte Fraktionen für Pu(III), Pu(V,VI) und für Pu(IV) genommen werden können (Abb. 1).

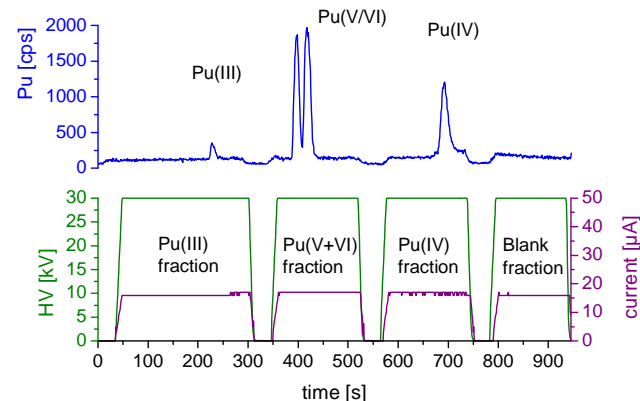


Abb. 1: Elektropherogramm mit den getrennten Pu-Spezies (oben) und zeitlicher Verlauf der Hochspannung (HV) und des Stroms an der Kapillare mit kurzeitigen Unterbrechungen zur Fraktionierung (unten)

Im ersten Schritt wurden für höhere Plutoniumkonzentrationen (ca. 10^{11} Atome) die gesammelten Fraktionen mittels α -Spektroskopie bestimmt und dabei eine relativ gute Übereinstimmung mit Messungen der CE-ICP-MS erhalten: CE-ICP-MS: Pu(III): 30,9%, Pu(V/VI): 5,5%, Pu(IV): 63,6%; α -Spektroskopie: Pu(III): 31,9%, Pu(V/VI): 10,8%, Pu(IV): 57,2%. Des Weiteren wurde die chemische Präparation aus Elektrolytfaktionen auf Tantal-Filamenten durch elektrolytische Abscheidung und Überziehen mit einer Titanschicht durch Sputtern erfolgreich mittels RIMS-Messungen getestet.

Als Nächstes sollen nun die Oxidationsstufenzusammensetzungen anhand von CE-getrennter Fraktionen mit der RIMS (für niedrige Konzentrationen) bestimmt und mit CE-ICP-MS Daten (für höhere Konzentrationen) verglichen werden. Ebenso muss die Bestimmung der Nachweisgrenze sowie der Reproduzierbarkeit von CE-RIMS-Messungen ermittelt werden. Ziel ist eine Anwendung der CE-RIMS-Methode auf Umweltproben unter geogenen Bedingungen.

Literatur:

- [1] Kuczewski, B. et al., Analytical Chemistry **75**, 6769-6774 (2003)
- [2] Grüning, C. et al., International Journal of Mass Spectrometry **235**, 171-178 (2001)

Dreifach-resonante Ionisation von Uran-Isotopen für den isotopenselektiven Spurennachweis von ^{236}U

P.G. Schumann, B.A. Bushaw[#], S. Boulyga^o, G. Passler, N. Trautmann*, K. Wendt

Institut für Physik, *Institut für Kernchemie, ^oInstitut für Anorganische Chemie und Analytische Chemie
Johannes Gutenberg-Universität Mainz
[#]Pacific Northwest National Laboratory, Richland (WA), USA

Das Isotop ^{236}U kommt in der Natur nur mit extrem geringer relativer Häufigkeit von $<10^{-12}$ im Vergleich zu ^{238}U vor. In Kernreaktoren wird ^{236}U durch Neutroneneinfang von ^{235}U -Atomen gebildet. Im Inventar von kerntechnischen Anlagen kann daher das Isotopenverhältnis $^{236}\text{U}/^{238}\text{U}$ um viele Größenordnungen erhöht sein.

Der Nachweis geringster Mengen von ^{236}U ermöglicht es, eine anthropogene Uran-Kontamination aus dem Kernbrennstoff-Kreislauf eindeutig von Natururan zu unterscheiden. Studien der Migration von Kernbrennstoff in der Umwelt wären damit über den Nachweis von ^{236}U realisierbar. Insbesondere kann die Dynamik der Entstehung von löslichen und damit für lebende Organismen zugänglichen U(VI)-Spezies aus anthropogenen Uran-Quellen untersucht werden, wie z.B. in der Umgebung des Tschernobyl-Unfallreaktors.

Für diese Untersuchungen soll das Verfahren der hochauflösenden Resonanzionisations-Massenspektrometrie (HR-RIMS) zur selektiven Bestimmung von ^{236}U angepasst werden. Dafür waren laserspektroskopische Untersuchungen zum Auffinden eines geeigneten Anregungspfades für Uran-Isotope, der einerseits zur effizienten Ionisation führen, andererseits aber selektiv nur ein Isotop ansprechen soll, erforderlich.

Zunächst wurde das atomare Spektrum des Urans auf hochliegende Zustände ungerader Parität im Energiebereich von 36100 cm^{-1} bis 36400 cm^{-1} untersucht. Hierzu wurden Laserstrahlen eines Diodenlasers bei 415 nm als erster Anregungsschritt, eines Titan-Saphir-Lasers bei 820-830 nm als zweiter Anregungsschritt und die 514 nm Linie eines Argon-Ionen-Lasers als Ionisationsschritt eingesetzt. In 17 verschiedenen Anregungsschemata konnten 11 verschiedene Zustände bezüglich genauer Energielagen und Drehimpuls-

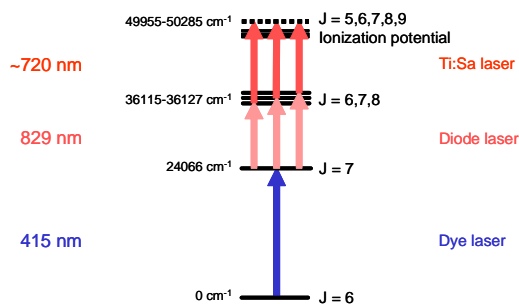


Fig. 1: Anregungsschemata für die dreifach-resonante Autoionisation von Uran

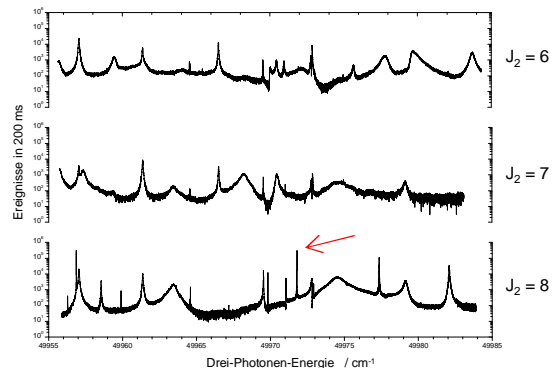


Fig. 2: Spektren autoionisierender Zustände des Urans

Quantenzahlen J spezifiziert werden. Hierbei war es auch möglich, zwei Zustände mit dem für die spätere Autoionisation wichtigen maximal möglichen J -Wert 8 zu identifizieren.

Weitere Untersuchungen, diesmal am Pacific Northwest National Laboratory (USA), betrafen das Spektrum autoionisierender Zustände im Energiebereich direkt oberhalb der Ionisationsgrenze [1]. Hier kamen ein Farbstofflaser bei 415 nm, ein Diodenlaser bei 829 nm und ein Titan-Saphir-Laser bei 720 nm zum Einsatz. Es wurden drei verschiedene Zwischenzustände mit unterschiedlichen J -Werten verwendet (Fig. 1) und jeweils ein Spektrum über fast 30 cm^{-1} der Gesamtenergie aufgenommen (Fig. 2).

Als effizienteste Ionisation wurde eine schmalbandige autoionisierende Resonanz mit einer Breite von 50 MHz bei 49971.8 cm^{-1} und $J=9$ ermittelt. Der dazugehörige Anregungspfad konnte in allen drei Anregungsschritten bezüglich der Hyperfeinstruktur von ^{235}U spezifiziert werden.

Für die Messung der Isotopieverschiebungen von ^{234}U wurde ein Verfahren entwickelt, mit dem durch die Aufnahme dreidimensionaler Laserspektren die spektralen Lagen der Isotope in allen drei Anregungsschritten gleichzeitig gemessen werden können. Dieses Verfahren soll in Kürze auch für die noch ausstehende Messung der Isotopieverschiebungen von ^{236}U angewandt werden.

Weiterführende Untersuchungen werden sich auf die Spezifizierung des analytischen Verfahrens konzentrieren; zudem sind erste Testmessungen von Isotopenverhältnissen $^{236}\text{U}/^{238}\text{U}$ in Tschernobyl-Proben geplant.

Literatur:

- [1] P.G. Schumann, B.A. Bushaw, K.D.A. Wendt, to be published

Spurenanalytische Bestimmung von ^{99}Tc mit einem Ti:Sa Lasersystem

K. Wies¹, N. Erdmann², G. Passler¹, N. Trautmann², K. Wendt¹

¹ Institut für Physik, ² Institut für Kernchemie
Johannes Gutenberg-Universität, D-55099 Mainz, Germany

^{99}Tc wird bei der Spaltung von ^{235}U mit hoher Ausbeute gebildet. Wegen der langen Halbwertszeit des Isomers $^{99\text{g}}\text{Tc}$ ($2,14 \times 10^5$ a) spielt das Verhalten von $^{99\text{g}}\text{Tc}$ in der Umwelt eine bedeutende Rolle [1]. Besonders bei der Untersuchung von möglichen Endlagerstätten für nukleare Abfälle ist es von großem Interesse, die Migration verschiedener Tc-Spezies in der Umwelt zu studieren [2]. In Deutschland wird zur Zeit Ton als Wirtsgestein auf seine Eignung für ein mögliches Endlager untersucht.

Um das Verhalten der Tc-Spezies über einen längeren Zeitraum und in Umweltproben zu untersuchen, ist die sensitive Bestimmung von $^{99\text{g}}\text{Tc}$ nötig. Die dafür eingesetzte Methode muss sehr empfindlich sein und eine hohe Elementselektivität aufweisen, um vorhandene Isobarenkontaminationen zu unterdrücken. In früheren Untersuchungen wurde gezeigt, dass die Resonanzions-Massenspektrometrie (RIMS) mit gepulsten Farbstofflasern für den Ultraspurennachweis von Technetium geeignet ist [3]. In einer Zusammenarbeit zwischen dem Institut für Physik und dem Institut für Kernchemie wurde im letzten Jahr der Einsatz eines modernen, wartungsarmen Ti:Sa Laser- systems [4] zum Nachweis von $^{99\text{g}}\text{Tc}$ in Verbindung mit einem Flugzeitmassenspektrometer (TOF-MS) erprobt.

Die resonante Anregung der $^{99\text{g}}\text{Tc}$ Atome erfolgt durch Wechselwirkung von drei Ti:Sa Laserstrahlen mit einem Atomstrahl, der durch Widerstandsheizen eines Rhenium-Filaments, auf dem atomares $^{99\text{g}}\text{Tc}$ elektrolytisch abgeschieden wurde, erzeugt wird. Experimentell konnte eine Abdampftemperatur von etwa 1800 K ermittelt werden.

Für die resonante Laserionisation wurde das in Abbildung 1a) dargestellte Anregungsschema verwendet. Durch Scannen des Lasers für den dritten Anregungsschritt konnte eine starke

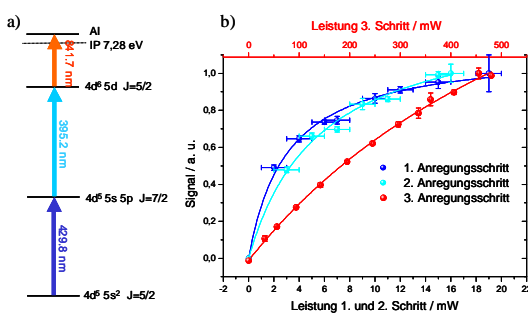


Abb. 1: a) Verwendetes Anregungsschema zur resonanten Anregung von $^{99\text{g}}\text{Tc}$ und b) experimentell bestimmte Sättigungskurven.

autoionisierende Resonanz gefunden werden. Für alle Schritte wurden die Sättigungsleistungen für typische experimentelle Bedingungen ermittelt, wie Abbildung 1b) zeigt. Für den ersten Schritt wurde eine Sättigungsleistung von 12 mW, für den zweiten Schritt von 22 mW und für den dritten Schritt von 3 W berechnet. Mit den zur Verfügung stehenden Leistungen können der erste Schritt vollständig und der zweite Schritt zu 80% gesättigt werden. Für den dritten Anregungsschritt können bis zu 1,5 W geliefert werden.

Die gefundene autoionisierende Resonanz zeigt eine starke Empfindlichkeit gegenüber elektrischen Feldern. Dies wurde detaillierter untersucht, da die Gesamteffizienz des Verfahrens dadurch entscheidend beeinflusst werden kann. Abbildung 2 zeigt die Struktur für verschiedene elektrische Feldstärken.

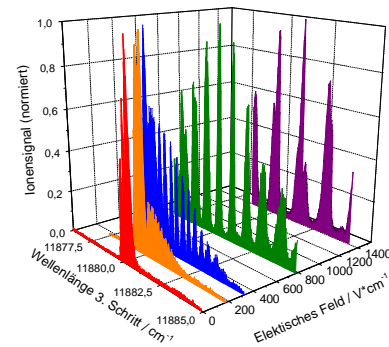


Abb. 2: Autoionisierender Zustand mit $\lambda_3 = 841,7$ nm bei verschiedenen elektrischen Feldstärken in der Ionisationsregion.

Die Gesamteffizienz des Verfahrens zur Bestimmung von $^{99\text{g}}\text{Tc}$ wurde zu 5×10^{-7} bestimmt.

Als nächstes soll eine alternatives Anregungsschema zur Verbesserung der Effizienz getestet, sowie die Methode zum Studium der Wechselwirkung von Tc mit Huminsäure und Kaolinit im Rahmen von Migrationsstudien unter Umweltbedingungen eingesetzt werden.

Literatur:

- [1] NEA, Actinide and Fission Product Partitioning and Transmutation: Status and Assessment Report (1999) http://www.nea.fr/html/trw/docs/neastatus99/complete_doc.pdf
- [2] A. Maes et al., Environ. Sci. Technol. 37, 747 (2003).
- [3] G. Passler et al., Kerntechnik 62, 85 (1997)
- [4] C. Grüning et al., Int. J. Mass Spectrom. 235, 171 (2004)

Complexation of ^{212}Pb with Humic Acids

A. Mansel¹, B. Kuczewski², H. Hummrich², N. Trautmann², J. V. Kratz², H. Kupsch¹

¹Institut für Interdisziplinäre Isotopenforschung, D-04318 Leipzig; ²Institut für Kernchemie, Universität Mainz, D-55099 Mainz

The complexation of Pb(II) with humic acids (HA) was studied at metal concentrations ranging from 1×10^{-9} up to 1×10^{-5} mol/l and at a constant humic acid concentration of 10 mg/l. For the first time, the radionuclide ^{212}Pb was used for these studies. The total Pb content of all solutions was controlled by ICP-MS. The natural purified Aldrich-HA and a synthetic HA (M42) were used at pH 5 and 6 [1, 2]. The indirect speciation - separation of the free metal ion and complexed metal ion - was performed with the anion-exchange resin Sephadex DEAE A-25 in batch experiments [3]. The stability constants were calculated by the metal-ion-charge-neutralization-model [4].

The short-lived radionuclide ^{212}Pb ($T_{1/2} = 10.64$ h) was isolated from the Th decay chain. A $^{228}\text{Th} / ^{220}\text{Rn} / ^{212}\text{Pb}$ - generator was used as illustrated in figure 1. $^{228}\text{Th}^{4+}$ (~500 kBq) was coprecipitated with Zr^{4+} and sodium stearate. The precipitate was filtered, washed and dried as a circular pellet. This was placed at the bottom of a titanium/polyethylene chamber. At the top of the chamber a Pt - foil closed the generator. A high voltage of 450 V was used between the titanium base and the Pt - foil. The ^{228}Th decay product ^{220}Rn escaped in the chamber from the precipitate by emanation. The ^{220}Rn decay product ^{212}Pb was electrodeposited on the Pt - foil for 10 - 20 hours (1 - 2 half lives of ^{212}Pb). The ^{212}Pb was dissolved by rinsing the Pt - foil three times with 100 μl 1 M HClO_4 for 10 min at room temperature. These three fractions were combined to the ^{212}Pb stock solution. The ^{212}Pb activity was measured with a Ge-detector at 239 keV. A comparison between the measurements of the foil before and after the dissolution gives a radiochemical yield of about 60 % for the stock solution. The lyophilized HA were dissolved with a few drops of diluted NaOH and these solutions were filled up with buffer to a stock solution of 1 g/l HA. In addition to the ^{212}Pb , known amounts of non-radioactive Pb (1×10^{-9} - 1×10^{-5} mol/l) were contacted with the HA. All Pb ion / HA solutions were buffered with 10^{-3} M MES at an ionic strength of 0.1 M NaClO_4 (pH 5 and 6) and were allowed to stand for 20 hours to reach chemical equilibrium. The total Pb concentrations were determined with ICP-MS (mass 208). The anion-exchange resin Sephadex DEAE A-25 was washed in batch with analytical-analogue solution until the supernatant had the same pH and conductivity as the analyte solution (Pb ion / HA). 200 - 400 mg of the resin were shaken 30 seconds with 4 ml of analyte solution and 2 ml of the supernatant and the activity in the original solution were measured by γ -spectrometry.

The determination of the non-radioactive Pb content of all ^{212}Pb / HA solutions by ICP-MS gave a Pb background of 9×10^{-9} mol/l in the solutions without addition of non-radioactive Pb, independend of the

HA used. This contamination with non-radioactive Pb is caused by the content in Pb of the chemicals (MES, NaClO_4 , NaOH and HClO_4 for pH adjustment). This Pb concentration was taken into consideration for the complexation experiments. The dependence of the complexation constant $\log \beta_{LC}$ on the total Pb concentration is shown in figure 2. There are no significant differences in the complexation constants between choosen pH or type of HA. We could not observe a significant increase in the complexation constant with decreasing Pb concentrations as it was previously determined for Np(V) [3]. Due to the contamination of the analytical solutions with non-radioactive Pb from the chemicals we could not reach the concentration range of 10^{-15} - 10^{-10} mol/l, as originally aimed in this work.

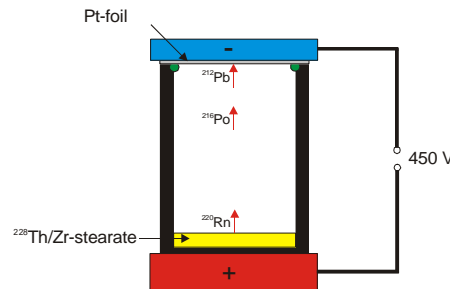


Figure 1: Schematic construction of a $^{228}\text{Th} / ^{220}\text{Rn} / ^{212}\text{Pb}$ - generator for the separation of carrier-free ^{212}Pb .

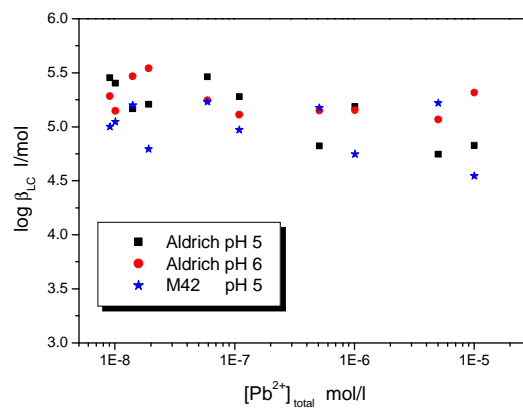


Figure 2: Dependence of the complexation constant $\log \beta_{LC}$ on the total Pb concentration; ^{212}Pb as radio-tracer.

- [1] S. Pompe et al., Radiochim. Acta **82**, 89 (1998)
- [2] A. Mansel et al., GDCh-Jahrestagung (2001)
- [3] A. Seibert et al., Radiochim. Acta **89**, 505 (2001)
- [4] J. I. Kim et al., Radiochim. Acta **73**; 5 (1996)

Interaction of Pu with Humic Substances

R. A. Buda, N. L. Banik, S. Bürger, B. Kuczewski, J. V. Kratz, N. Trautmann

Institut für Kernchemie, Johannes Gutenberg-Universität Mainz, Germany

For the risk assessment of plutonium being released into the environment in different ways, very precise knowledge on its interaction with natural groundwater is necessary. As this contains humic substances which form complexes with metal ions, complexed plutonium may be transported over long distances. Humic substances are natural polyelectrolytes with non-uniform structural and chemical characteristics. Mainly carboxylic and phenolic groups are responsible for the complexation behaviour of humic substances. The irregular nature of humic substances results in different approaches to explain their complexation with metal cations. However, all models agree in the view that pH and ionic strength are main factors which influence the complexation reaction of metal ions with humic substances [1].

The redox behaviour of plutonium in contact with fulvic acid was investigated. A mixture of all four oxidation states of plutonium, Pu(III) 5,1%; Pu(IV) 39,2%; Pu(V) 22,1%; Pu(VI) 33,6% at pH ≈ 0, $C_{Pu} \approx 60 \text{ } \mu\text{mol/l}$, was brought in contact with GoHy fulvic acid under atmospheric conditions (final solution pH ≈ 1). The redox behaviour was determined by CE-ICP-MS.

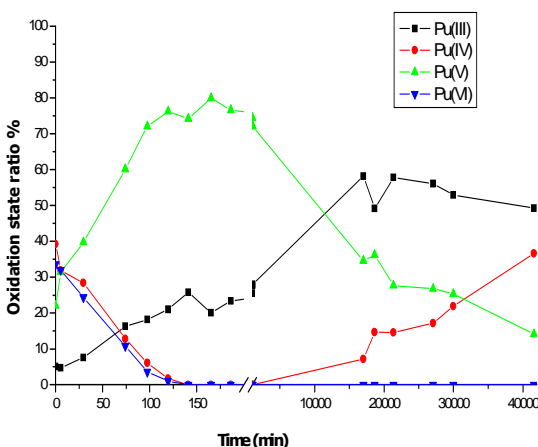


Fig.1 Redox behaviour of plutonium in contact with GoHy fulvic acid

Fig.1 shows that, after a long interaction time (28 days), the predominant oxidation states in solution are Pu(III) and Pu(IV). It must be mentioned that Fig.1 refers strictly to the free ions of plutonium in solution. There is no

knowledge about the behaviour of the complexed and colloidal plutonium in solution. Furthermore, the behaviour of Pu(III) in contact with Aldrich humic acid was investigated.

The determination of the oxidation state of the used Pu stock solution was performed by applying UV/VIS-spectrometry and CE-ICP-MS. The Pu(III) solution in different concentrations ($10^{-6} \text{ M}, 10^{-7} \text{ M}, 10^{-8} \text{ M}$), was brought in contact with Aldrich humic acid (0 – 25 mg/L) at pH = 5,5. Afterwards, the solutions were ultrafiltrated (filter pore size 1 kDalton), and the content of free plutonium in the filtrate was detected, using liquid scintillation counting (LSC). It was found that plutonium is complexed by Aldrich humic acid and reaches equilibrium in the course of one week. However, a strong adsorption process of plutonium by the contact surfaces was observed, yielding data with large uncertainties.

Therefore, the process of adsorption of Pu(III) by vessels and filters was investigated. The ultrafilter material, as well as the vials similar to the ones used in the earlier experiment, were brought in contact with Pu(III) at pH = 3, 4, and 5. The content of plutonium in solution was determined by LSC. The percentage of plutonium recovery after one day of contact showed that there was no plutonium adsorption on the vial walls. Instead there was a very strong adsorption on the filter material (60 – 70 % of plutonium adsorbed). Other trivalent ions like Am(III) and Cm(III) show no such effect. Unfortunately, no method that is sensitive enough, to determine the oxidation state of the plutonium in these solutions at these concentrations is available at this time. If an oxidation of Pu(III) to Pu(IV) would occur, this could make the observed strong adsorption plausible. As a consequence, the subsequent experiments will be performed in an inert gas atmosphere in order to maintain the plutonium ions in the Pu(III) state.

Furthermore, other methods will be used [2] in order to determine the complexation constant of Pu(III) with humic and fulvic acids over a pH range of 3 to 7.

References:

- [1] Ziechmann, H.: *Huminstoffe*. Verlag Chemie, Weinheim, 1980.
- [2] B. Kuczewski et al.; Institut für Kernchemie, Universität, Mainz, Jahresbericht 2004.

Limitation of the Ultrafiltration Method for the Determination of Complexation Constants of Pu(IV) with Humic Substances

N. L. Banik, R. A. Buda, S. Bürger, J. V. Kratz, B. Kuczewski, N. Trautmann
Institut für Kernchemie, Johannes Gutenberg-Universität, Mainz, Germany

Humic substances (HS) form strong complexes with heavy metals like plutonium. This behaviour can lead to an increase of the migration of the elements.

The complexation constants of Pu(IV) with Aldrich humic acid were determined at pH-values from 1.8 to 3.0 for varying humic acid (HA) concentrations (0, 1.0, 10, and 25 mg/L) [1]. Due to the precipitation of HA at pH < 3 [2] and thus a possible co-precipitation of Pu with HA, the complex formation studies with Pu(IV) were extended to pH > 3 using the ultrafiltration method.

As a first step, the recovery of plutonium(IV) after ultrafiltration in the absence of humic acid was investigated, i.e., the amount of adsorbed Pu on the filter and/or vessel material was determined. Pu(IV) was produced electrochemically and the oxidation state was confirmed by UV/VIS spectroscopy. A concentration of 4.15×10^{-7} M Pu was used at different pH-values (1.8, 2.5, 3.0, 3.8, and 4.8) with 0.1 M MES (2N-Morpholinoethane sulfonic acid) as buffer and NaClO₄ to fix the ionic strength at 0.1 M. The pH-value of the Pu(IV) solution was adjusted with 0.1 M NaOH or 0.1 M HClO₄. The Pu solutions were ultrafiltrated by using filters with different pore sizes (1, 3, 10 kDa) and the concentration of Pu in the filtrates was measured by liquid scintillation counting (LSC).

The percentage of plutonium recovery was calculated for the different pH-values (see Figure 1). The recovery is 85% at pH 1.8, 59% at pH 2.5, 48% at pH 3.0, 18% at pH 3.8, and 13% at pH 4.8. No differences were observed for the different filter pore sizes (1, 3, 10 kDa). Referring to the decreasing percentages of recovery for Pu(IV) at increasing pH, a determination of complexation constants with HS using the ultrafiltration method is not possible for higher pH-values without applying substantial corrections.

On the other hand, determining the complexation constants of Pu(IV) with HS for pH < 3 can lead to co-precipitation of Pu with HA due to the precipitation of HA at low pH-values yielding large uncertainties in the complexation constants [2].

Since fulvic acid is soluble in all pH ranges, it could be used for determining complexation constants at low pH-values, where adsorption effects on filter materials are almost negligible. However, ultrafiltration studies for Gorleben fulvic acid (FA) in absence and presence of different metal ions (Ca(II), La(III) and Zr(IV)) revealed that only 40 to 80% of FA was retained on the filter compared to 85% to 95% for HA [3]. Thus, the ultrafiltration method seems not be suitable to determine complexation constants of Pu(IV) with fulvic acid.

References:

- [1] N. L. Banik et al., Institut für Kernchemie, Universität Mainz, Annual Report, C10, (2003)
- [2] N. L. Banik et al., Institut für Kernchemie, Universität Mainz, Annual Report, (2004)
- [3] S. Bürger et al., Institut für Kernchemie, Universität Mainz, Annual Report, (2004)

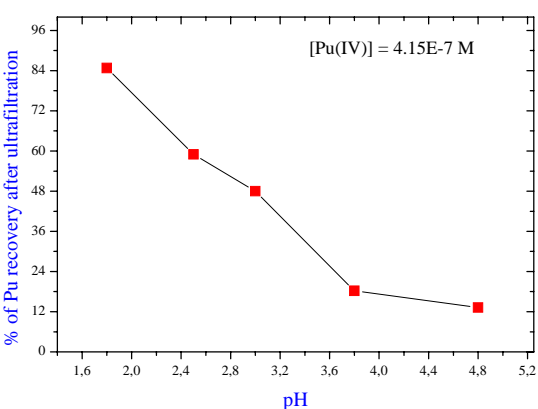


Figure 1: Percentage of plutonium recovery after ultrafiltration at varying pH-values (1 kDa filter pore size).

Precipitation of Aldrich Humic Acid in Dependence of pH

N. L. Banik, S. Bürger, J. V. Kratz, N. Trautmann

Institut für Kernchemie, Johannes Gutenberg-Universität, Mainz, Germany

Humic substances (HS) are the largest fraction of natural organic matter in environmental water sources. HS are naturally occurring materials and play an important role in the migration of radionuclides due to their complex formation. According to their solubility three fractions of HS are described: humic acid, fulvic acid, and humin. Humic acid (HA) which is soluble at pH-values ≥ 3 [1] is normally the major part of humic substances.

To predict the migration of plutonium, it is important to investigate the complexation constants $\log(\beta_{LC})$ of HA with plutonium. This was tried for Pu(IV) with Aldrich humic acid at pH 1.8 to 3.0 [2]. Due to the precipitation of the humic acid at these pH-values, the complexation constants may be influenced by the co-precipitation of Pu with humic acid. Therefore, a detailed understanding of the kinetics of precipitation of humic acid at low pH is necessary.

For this, Aldrich humic acid (AHA) was used at concentrations of 1, 10, and 25 mg/L. The influence of the pH-value on the precipitation of AHA at 1.8, 2.5, and 3.0 was studied by UV/VIS spectrometry (Carry50) by measuring the change of concentration of AHA in solution. The pH of the solution was checked regularly (Beckmann model-310 pH meter).

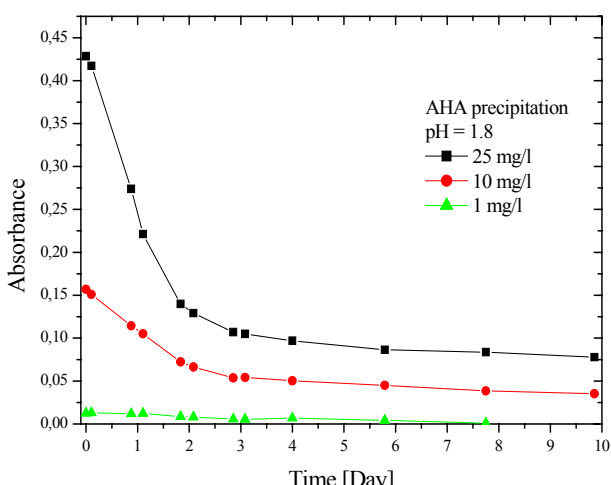


Figure 1: Precipitation of Aldrich humic acid for different concentrations (1, 10, and 25 mg/L) at pH 1.8 as a function of time

Figure 1 shows the precipitation of AHA at pH = 1.8 for three different humic acid concentrations (1, 10, and 25 mg/L). The concentration of AHA in solution decreases significantly with time. A precipitate of HA at the bottom of the cuvette is already observable by eye. A reduction of the AHA concentration in solution (original concentration 25 mg/L) of 80% at pH 1.8, 30% at pH 2.5 and almost 0% at pH 3.0 was found for the Aldrich humic acid after 240 h (see Figure 2).

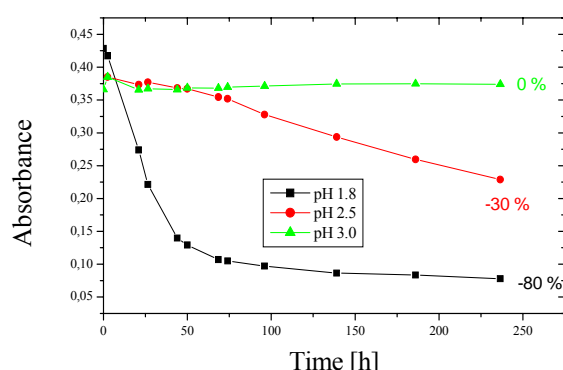


Figure 2: Decrease of AHA concentration in solution at different pH-values (1.8, 2.5, and 3.0) as a function of time (values in percent define the decrease after 10 d) for a starting AHA solution of 25 mg/L.

For the determination of the complexation constants $\log(\beta_{LC})$ of HA with plutonium(IV), a contact time of several days is necessary to achieve equilibrium [2]. At such a long contact time the Aldrich humic acid precipitates in a significant amount and co-precipitation of Pu(IV) with HA cannot be excluded, especially for pH = 1.8 and 2.5. Further studies have to be done at pH > 3 to exclude co-precipitation, but adsorption of Pu(IV) on vessel materials or filters, depending on the method, with increasing pH must be considered.

References:

- [1] G. R. Choppin, Radiochimica Acta, 44/45, 23 (1988)
- [2] N. L. Banik et al., Institut für Kernchemie, Universität Mainz, Annual Report, C10 (2003)

Untersuchungen zur Ultrafiltration von Huminsäure und Fulvinsäure für die Bestimmung von Komplexbildungskonstanten mit Metallionen

S. Bürger, N. L. Banik, J. V. Kratz, N. Trautmann

Institut für Kernchemie, Johannes Gutenberg-Universität Mainz, D-55099 Mainz, Germany

Huminstoffe entstehen durch die biologische Zersetzung von Biomasse und finden sich unter anderem in Böden und Grundwässern im ppm Konzentrationsbereich. Die löslichen Anteile der Huminstoffe, Huminsäure (HS) und Fulvinsäure (FS), sind starke Komplexbildner. Die Mobilisierung von Radionukliden, wie die bei der Endlagerung hochradioaktiver Abfälle relevanten Elemente Uran, Neptunium und Plutonium, kann durch die Komplexierung der Metallionen mit HS oder FS stark erhöht werden und zu einer Migration der Radionuklide führen [1].

Die Bestimmung der Komplexbildungskonstanten von Metallhuminsäurekomplexen kann durch Abtrennung der Humate von den nach der Komplexierung verbleibenden freien Metallionen mittels Ultrafiltration (UF) erfolgen und wurde für Pu(IV) in Kontakt mit Aldrich-HS bereits durchgeführt [2]. Neben der HS interessiert auch die Komplexierung mit FS. Dazu wurden Ultrafiltrationsexperimente (Porengröße 1 kDa) mit Gorleben-Fulvinsäure (GoHy-573) ($[FS] = 20$ und 50 mg/L) ohne Metallionen und in Kontakt mit Ca(II), La(III) und Zr(IV) (Konzentration ca. 10^{-4} mol/L, Kontaktzeit 1 Tag und 7 Tage) bei $pH \approx 6$ durchgeführt. Der Nachweis der FS erfolgte durch UV/Vis-Spektroskopie. Daraus wurde der Rückhalt an FS auf dem Filter nach UF ermittelt (siehe Abbildung 1). Zum Vergleich sind die Werte für HS angegeben, die experimentell auf die gleiche Weise bestimmt wurden.

Die Aldrich-Huminsäure wird zu 85 - 90% für $[HS] = 20$ mg/L und bis zu 95% für $[HS] = 50$ mg/L auf dem Filter zurückgehalten. Bei Zugabe von Metallionen nehmen die Werte in der Reihenfolge $Ca < La < Zr$ zu. Aufgrund dieses fast vollständigen Rückhalts ist die Methode der Ultrafiltration für die Bestimmung von Komplexbildungskonstanten mit HS geeignet. Im Gegensatz dazu werden für die Fulvinsäure nur Rückhaltewerte von 60 - 40% für $[FS] = 20$ mg/L und bis zu 80% für $[FS] = 50$ mg/L ermittelt. Bei Zugabe von Metallionen nehmen die Werte in gleicher Reihenfolge $Ca < La < Zr$ zu. Diese im Vergleich zur HS niedrigen Rückhaltewerte zeigen, dass die Methode der Ultrafiltration für die Bestimmung der Komplexbildungskonstanten mit FS wenig geeignet ist. Sowohl für FS also auch für HS wurde kein Unterschied in den Rückhaltewerten für Kontaktzeiten von 1 Tag oder 7 Tagen festgestellt.

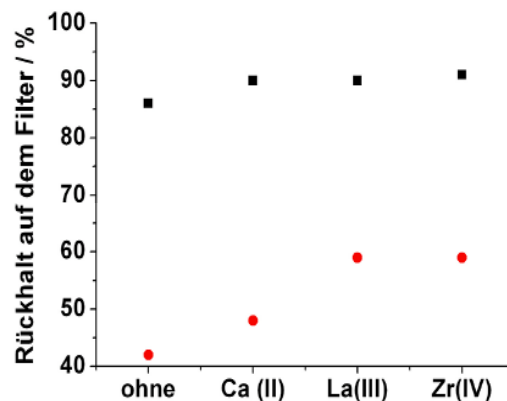


Abb. 1: Prozentualer Rückhalt der Huminsäure (Rechtecke) bzw. Fulvinsäure (rote Kreise) auf einem Filter mit 1 kDa Porengröße nach Ultrafiltration für 20 mg/L HS bzw. FS ohne und mit Zugabe von Metallionen (10^{-4} mol/L).

Diese Ergebnisse sind in Übereinstimmung mit experimentell bestimmten Daten für die Molekulargröße der Gorleben-FS von ca. 500 Da und Gorleben-HS von ca. 1000 Da (jeweils Maximum der Größenverteilungen) [3].

Zusammenfassend lässt sich sagen, dass mit der Ultrafiltration die Bestimmung von Komplexbildungskonstanten für Huminsäure mit Metallionen möglich ist, wohingegen für Fulvinsäure diese Methode ungeeignet erscheint.

Literatur:

- [1] Choppin, G. R. et al., Humics and radionuclide migration, *Radiochimica Acta* **44/45**, 23-28 (1988)
- [2] Banik, N. L. et al., Institut für Kernchemie, Universität Mainz, Jahresbericht C10 (2003)
- [3] Wolf, M. et al., Isolation and characterization of a new batch of Gohy-573 humic and fulvic acids, unveröffentlicht

Kopplung von Ionenstrahl-Sputtern und Resonanzionisationsmassenspektrometrie zur ortsaufgelösten Analyse von Actiniden

N. Erdmann¹, J.V. Kratz¹, N. Trautmann¹, G. Passler², P. Lievens³, R.E. Silverans³, E. Vandeweert³

¹ Institut für Kernchemie, Universität Mainz, D-55099 Mainz, Germany; ² Institut für Physik, Universität Mainz, D-55099 Mainz, Germany; ³ Laboratorium voor Vaste-Stoffysica en Magnetisme, K.U. Leuven, Celestijnenlaan 200D, B-3001 Leuven, Belgium

Micro-Partikel, die in hohen Konzentrationen Actiniden enthalten, sind von speziellem Interesse für „Nuclear Safeguards“ Analysen der IAEA und Euratom, zur Risikobewertung kontaminierten Gegenden, sowie für nukleare forensische Analysen. Ein Verfahren, welches sich in den letzten Jahren zur Routine-Methode für die Analyse solcher Partikel entwickelt hat, ist die Sekundärionenmassenspektrometrie (SIMS) [1]. Isobare Interferenzen (z.B. $^{238}\text{U}/^{238}\text{Pu}$, $^{241}\text{Pu}/^{241}\text{Am}$) stellen jedoch ein Problem dar.

Die Resonanzionisationsmassenspektrometrie (RIMS), die für Bulk-Analysen im Ultraspurenbereich bereits seit vielen Jahren erfolgreich eingesetzt wird [2], ist hoch-elementselektiv und sehr nachweisstark. Im Rahmen eines neuen, von der DFG geförderten Projekts soll ein kommerzielles TOF-SIMS Gerät (Fa. IONTOF) so umgebaut werden, dass es die Kopplung von Ionenstrahl-Sputtern und resonanter Nachionisation der gesputterten Neutralteilchen mit RIMS ermöglicht, wodurch das Isobarenproblem eliminiert wird.

Voruntersuchungen [3] wurden u.a. am Resonanzionisationsmassenspektrometer der K.U. Leuven, Belgien, [4] durchgeführt. Der Fokus der dort verfügbaren Ar-Ionenquelle ist mit $\varnothing = 3\text{mm}$ zu groß für die Einzelpartikelanalytik, jedoch lassen sich grundlegende Studien zu den gesputterten Neutralteilchen-Spezies durchführen. Die in den Partikeln nachzuweisenden Actiniden liegen typischerweise in oxidischer Form vor, beim Sputtern entstehen neben neutralen Atomen auch Oxid-Moleküle. Da für die selektive resonante Ionisation neutrale Atome erforderlich sind, ist es für einen effizienten Nachweis von Interesse, deren Anteil zu maximieren.

Als Modellelement wurde Uran eingesetzt. Mit U_3O_8 Partikeln wurde untersucht, wie Proben-Substrat und Proben-Vorbereitung das Verhältnis atomaren Urans zu Uranoxidmolekülen beeinflusst. Das atomare Uran wurde vom Grundzustand mittels 2-Schritt-resonanter Anregung mit $\lambda_1=324,614\text{ nm}$ und $\lambda_2=513,554\text{ nm}$ (Population eines autoionisierenden Zustands) ionisiert, während die Molekülionen nichtresonant erzeugt wurden, so dass nur ein qualitativer Vergleich der Signale möglich war. Bei kontinuierlichem Beschuss der Probe mit dem Ar-Ionenstrahl stellt sich nach ca. 15-30 min ein festes Verhältnis von Uran- zu Oxidionen ein. Es wurde beobachtet, dass bei Verwendung von Titan als Probenträger durch 10-minütiges

Aufheizen der Probe auf 800°C unter UHV Bedingungen das atomare Signal um ca. einen Faktor 10 gegenüber der nicht aufgeheizten Probe verbessert werden konnte.

Das verwendete TOF-SIMS Gerät ist in Abb. 1 gezeigt. Zum Sputtern wird eine Ga-Flüssigmetall-Ionenquelle eingesetzt, welche einen Fokus im sub- μm Bereich erlaubt. Der Ionenstrahl kann bis zu $500 \times 500\text{ }\mu\text{m}^2$ über die Probenoberfläche gerastert werden, um ortsaufgelöste Information zu erhalten. Die Ionen werden in einem Flugzeitmassenspektrometer nachgewiesen.

Zur resonanten Ionisation der gesputterten Neutralteilchen werden die Laserstrahlen von 3 durchstimmbaren Ti:Saphirlasern eingekoppelt. Diese 3-stufige Anregung und Ionisation lässt eine hohe Elementselektivität mit niedrigem Untergrund erwarten. Eine Besonderheit ist ferner die Tatsache, dass das verwendete Lasersystem hochrepetierend im kHz-Bereich arbeitet. Damit wird eine optimale Kopplung mit der Pulsfrequenz der Sputter-Ionenquelle möglich, wodurch sich kurze Meßzeiten ergeben.

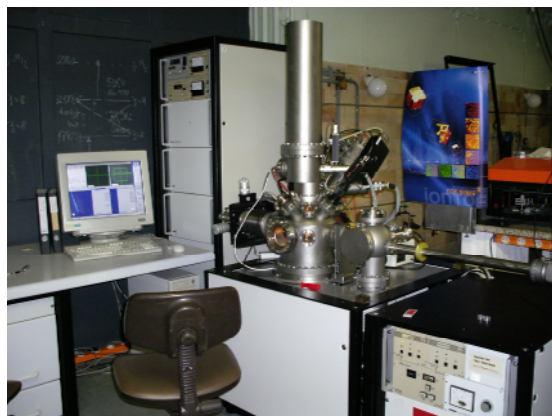


Abb. 1. Foto des TOF-SIMS Gerätes, welches durch Einkopplung von 3 durchstimmbaren Lasern für den RIMS-Betrieb umgebaut wird.

References

- [1] M Betti et al., *Anal. Chem.* **71**, 2616 (1999)
- [2] N. Trautmann et al., *Anal. Bioanal. Chem.* **378**, 348 (2004)
- [3] N. Erdmann et al., *Anal. Chem.* **75**, 3175 (2003)
- [4] E. Vandeweert et al., *Phys. Rev. B* **64**, 195417 (2001)

Spurenanalyse von gammastrahlenden Radionukliden in der bodennahen Luft

H. Keller, R. Heimann, B. Praast

Seit Beginn des Jahres 1994 werden die aerosol-partikelgetragenen Radionuklide aus der bodennahen Luft mittels einer großvolumigen Sammelapparatur ($\sim 100.000 \text{ m}^3/\text{Woche}$) auf Filtern abgeschieden, die wöchentlich gewechselt werden.

Nach dem Pressen der Filter können die gammastrahlenden Nuklide ohne weitere Probenvorbereitung direkt gemessen werden.

Nach einer Abklingzeit von etwa einer Stunde wurde zunächst eine Kurzzeitmessung mit einer Messzeit von 10 Stunden durchgeführt, um eventuell vorhandene kurzlebige Radionuklide nachweisen zu können. Aufgrund der hohen Aktivitäten der natürlichen Radionuklide lagen die Erkennungsgrenzen je nach Nuklid bei $1,2 \mu\text{Bq}/\text{m}^3$ für Nb-95 bis $380 \mu\text{Bq}/\text{m}^3$ für Te-132.

Bei der Langzeitmessung mit einer Messzeit von 60 Stunden wurden nach dem Zerfall der kurzlebigen natürlichen Radionuklide, abhängig von der Gesamtaktivität, die auf dem Filter abgeschieden wurde, folgende Erkennungsgrenzen erreicht:

Cs-137 :	$0,2 - 1,1 \mu\text{Bq}/\text{m}^3$
I-131 :	$0,8 - 1,4 \mu\text{Bq}/\text{m}^3$
Zr-95 :	$0,4 - 0,7 \mu\text{Bq}/\text{m}^3$

Der Grundpegel der Cs-137-Aktivitätskonzentration war im Vergleich zu den vergangenen Jahren unver-

ändert. Die natürlichen Radionuklide Be-7 und Na-22 werden durch Kernreaktionen (Spallation) in der Stratosphäre gebildet und gelangen durch Luftmassenaustausch in die bodennahe Luft. Die Werte der Be-7-Aktivitätskonzentrationen liegen wie schon in den vergangenen Jahren bei einigen mBq/m^3 , die des Na-22 bei maximal $1 \mu\text{Bq}/\text{m}^3$ (siehe Abb. 1).

Als mögliche Quellen der Cs-137-Kontamination in der bodennahen Luft kommen Resuspension, großräumiger Transport von Luftmassen aus Gebieten mit höherer Bodenkontamination und Austausch stratosphärischer Luftmassen in Frage [1]. Die Beiträge der einzelnen Quellen sind von den örtlichen meteorologischen Gegebenheiten und der Menge der infolge des Reaktorunfalls in Tschernobyl lokal deponierten Aktivität [2] abhängig.

[1] Hötzl H., Rosner G. und Winkler R.: Sources of Present Chernobyl-derived Caesium Concentrations in Surface Air and Deposition Samples, The Science of the Total Environment 119, 231-242, 1992

[2] Der Bundesminister für Umwelt, Naturschutz und Reaktorsicherheit (Hrsg.): Veröffentlichungen der Strahlenschutzkommision Band 7, Auswirkungen des Reaktorunfalls in Tschernobyl auf die Bundesrepublik Deutschland, 47, Gustav Fischer Verlag, Stuttgart, New York, 1987

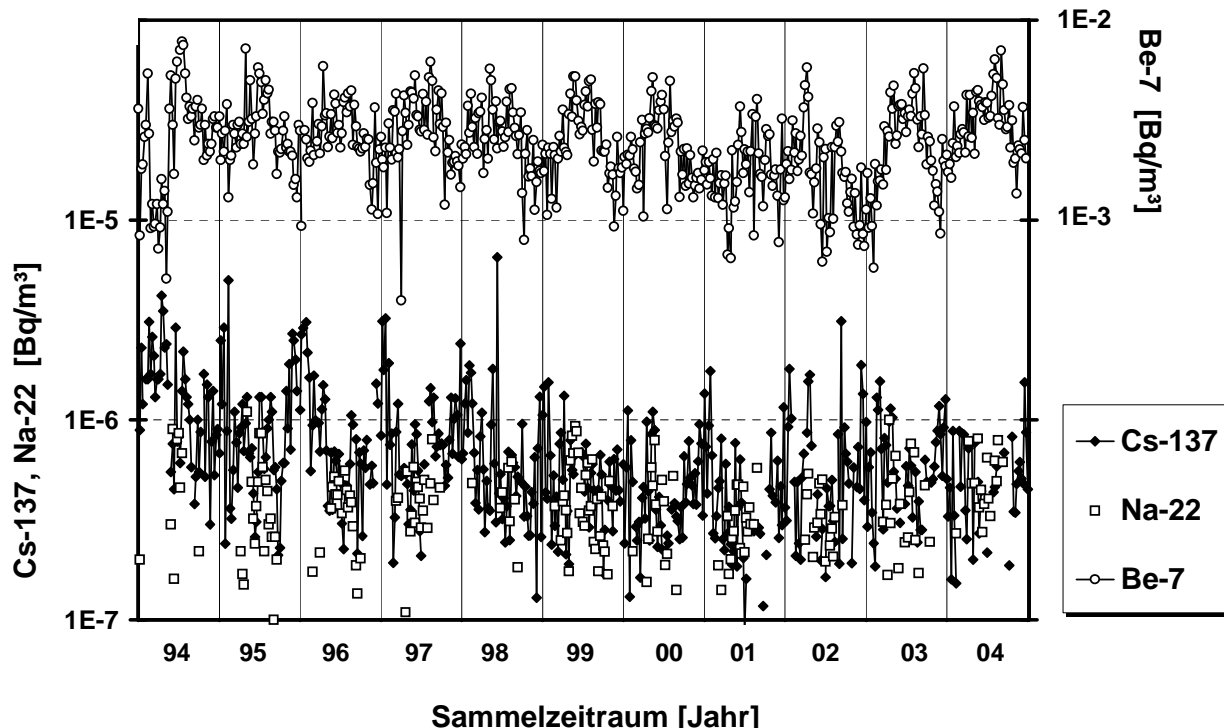


Abb.1 : Zeitlicher Verlauf der Wochenmittelwerte der Aktivitätskonzentrationen von Cs-137, Be-7 und Na-22 an der Messstation des Instituts für Kernchemie der Johannes Gutenberg-Universität Mainz in den Jahren 1994 bis 2004.

D. Technische Einrichtungen

- Betrieb des Forschungsreaktors TRIGA Mainz
- Personendosisüberwachung

D. Technical Facilities

- Operation of the research reactor TRIGA Mainz
- Personal dose monitoring

Betrieb des Forschungsreaktors TRIGA Mainz im Jahre 2004

N. Trautmann
Institut für Kernchemie, Universität Mainz

Der Forschungsreaktor TRIGA Mark II wurde auch im Jahre 2004 hauptsächlich im Dauerbetrieb mit 100 kW Leistung gefahren. Die Betriebsdaten des Reaktors sind in Tabelle 1 zusammengefaßt. Gegenüber 2003 sind bei den Betriebstagen und -stunden keine signifikanten Änderungen eingetreten. Dies gilt auch für die freigesetzte Energie und den Spaltstoffverbrauch, der 2004 bei 4,3 g U-235 lag. Seit Inbetriebnahme des TRIGA Mainz im August 1965 sind 161,5 g U-235 abgebrannt worden. Der Kern des Mainzer Reaktors ist seit Februar 2002 mit 75 Brennelementen beladen.

In Tabelle 2 ist die Zahl der Bestrahlungen in den verschiedenen Bestrahlungspositionen aufgeführt. Am häufigsten wurde das Bestrahlungskarussell genutzt, was hauptsächlich mit den neutronenaktivierungsanalytischen Untersuchungen zusammenhängt.

Im Zentralen Bestrahlungsrohr und in den Strahlrohren wurden auch 2004 wieder zahlreiche Proben bestrahlt, wobei in den Strahlrohren vor allem spaltbare Materialien eingesetzt wurden.

In Zusammenarbeit mit der TU München (Physik Department E18) und dem Institut für Physik der Universität Mainz ist an Strahlrohr C eine Apparatur zur Erzeugung ultrakalter Neutronen (UCN) aufgebaut worden. Der Kryoteil konnte Ende 2004 erfolgreich getestet werden.

Das Spektrum der Reaktornutzer (Tabelle 3) ist bei den externen Bestrahlern gegenüber 2003 fast unverändert.

Im Jahre 2004 besichtigten 496 Personen den Reaktor (Tabelle 4), wobei etwa 80 Stunden für Führungen und Erläuterungen der Forschungsarbeiten am hiesigen Institut aufgewandt wurden.

Tabelle 1: Betriebsdaten des Reaktors

Betriebsdaten	von 1965 bis 1999	2000	2001	2002	2003	2004	insgesamt
Betriebstage	6651	175	169	185	192	188	7560
Betriebsstunden	33741	867	829	927	850	918	38132
Impulse	14500	102	45	79	94	112	14932
davon Reaktivität bis 1,25 \$	326	1	2	4	2	4	339
1,50 \$	11395	88	38	62	83	82	11748
1,75 \$	228	2	2	1	3	4	240
2,00 \$	2551	11	3	12	6	22	2605
Freigesetzte Energie (MWh)	2709,6	78,9	77,7	80,6	76,5	82,2	3105,5
davon im Dauerbetrieb	2675,2	78,6	77,6	80,5	76,2	82,0	3070,1
im Impulsbetrieb	34,4	0,3	0,1	0,1	0,2	0,2	35,3
Spaltstoffverbrauch [g U-235]	141,0	4,1	4,0	4,2	3,9	4,3	161,5

Tabelle 2: Zahl der Bestrahlungen in den verschiedenen Bestrahlungspositionen des Reaktors

Bestrahlungsposition	von 1965 bis 1999	2000	2001	2002	2003	2004	insgesamt
Bestrahlungskarussell	48983	1339	1233	1469	1946	1505	56475
Rohrpost 1, 2 und 3	61700	298	310	478	81	22	62889
Schnelle Rohrpostanlagen	134453	301	226	84	110	61	135235
Strahlrohre	9875	77	11	77	115	121	10276
Zentrales Bestrahlungsrohr	2379	78	137	34	55	61	2744
Reaktortank (auf dem Kern)	1236	4	--	--	--	--	1240
Thermische Säule	563	--	--	--	--	--	563
alle Bestrahlungspositionen	259189	2097	1917	2142	2307	1770	269422

Tabelle 3: Benutzer des Reaktors im Jahre 2004

	Zahl der Bestrahlungen
Universität Mainz	
Institut für Kernchemie	955
Externe Bestrahlung	
Max-Planck-Institut für Chemie Mainz	20
Gesellschaft für Schwerionenforschung Darmstadt	20
Universität Köln	14
Universität Marburg	8
TU München	4
Bergakademie Freiberg	582
Institut für Interdisziplinäre Isotopenforschung Leipzig	2
Gabelmann & Lerch Analytik GmbH Mainz	1
Framatome ANP Karlstein	155
BASF Ludwigshafen	9
	<hr/>
	insgesamt: 1770
	<hr/> <hr/> <hr/>
	Vorjahr: 2307

Tabelle 4: Besucher des Reaktors im Jahre 2004

Datum	Besucher/Anlass	Anzahl
15.01.2004	Chir. Abtlg. St. Josef Krankenhaus Rüdesheim	15
28.01.2004	MTRA-Schule Mainz	10
05.02.2004	Gymnasium an der Stadmauer Bad Kreuznach	23
11.02.2004	Tag der offnen Tür	71
25.02.2004	Theresianum Mainz	14
26.02.2004	Goethe-Gymnasium Bad Ems	10
11.03.2004	Martin-Niemöller-Schule Wiesbaden	10
15.03.2004	Fachkundekurs „Strahlenschutz für Schulen“	38
23.04.2004	BBS Technik I Ludwigshafen	26
26.05.2004	Gymnasium Philippinum Weilburg	25
30.06.2004	Krankenpflegeschule Uniklinik Mainz	18
14.07.2004	GfA Bad Kreuznach	21
15.07.2004	Ortsverband Deutscher Hausfrauenbund Mainz	20
28.07.2004	Institut für Physik, Univ. Mainz	4
04.08.2004	Institut für Zoologie, Univ. Mainz	13
05.08.2004	Universität Valencia	12
11.08.2004	Institut für Phys. Chemie, Univ. Mainz	4
26.08.2004	Institut für Org. + Anorg. Chemie, Univ. Mainz	16
27.08.2004	Inst. für Anorg. + Analyt. Chemie, Univ. Mainz	20
09.09.2004	Grundkurs im Strahlenschutz	15
21.09.2004	Bund-Länder Ausschuss Forschungsreaktoren	11
04.10.2004	Fachkundekurs „Strahlenschutz an Schulen“	14
14.10.2004	Personalrat der Joh. Gutenberg-Univ. Mainz	9
11.11.2004	Krankenpflegeschule am Universitätsklinikum	14
26.11.2004	Präsidialamt Univ. Mainz	13
30.11.2004	BISS-Programm	14
08.12.2004	FH Trier UC Birkenfeld	21
16.12.2004	Techn. Gymnasium Mainz	15
		<hr/>
		insgesamt: 496
		<hr/> <hr/>

Personendosisüberwachung

B. Praast, I. Onasch

Ergebnisse der amtlichen Personendosisüberwachung in den Jahren 1994 bis 2004 (Monatsdosen in mSv). Die untere Nachweisgrenze der Personendosis bei monatlicher Auswertung beträgt 0,1 mSv.

Anzahl der ausgewerteten Personendosimeter														
1994		1995		1996		1997		1998		1999		2000		
1035	1026	1056	1000	1028	957	866	954	934	862	903	2001	2002	2003	2004

Anzahl der Monatsdosen $\geq 0,1$ mSv																					
1994		1995		1996		1997		1998		1999		2000		2001		2002		2003		2004	
1	0,4	6	0,2	1	1,4	1	0,8	3	>0,8	5	>1,0	4	>1,0	4	>1,0	3	>1,0	2	>1,0	-	>1,0
4	0,2			7	0,2	9	0,6	4	0,8	4	1,0	2	1,0	21*	$\leq 1,0$	18*	$\leq 1,0$	33*	$\leq 1,0$	67*	$\leq 1,0$
						9	0,4	4	0,6	3	0,8	7	0,8	19*	$\leq 0,8$	18*	$\leq 0,8$	26*	$\leq 0,8$	66*	$\leq 0,8$
						24	0,2	13	0,4	2	0,6	6	0,6	15*	$\leq 0,6$	18*	$\leq 0,6$	24*	$\leq 0,6$	66*	$\leq 0,6$
								27	0,2	6	0,4	6	0,4	12*	$\leq 0,4$	16*	$\leq 0,4$	22*	$\leq 0,4$	64*	$\leq 0,4$
									17	0,2	11	0,2	8	0,2	10	0,2	16	0,1	51	0,1	

*: kumulative Angaben

Von im Mittel 74 überwachten Personen erhielten 57 Jahresdosen, die sämtlich unterhalb der Nachweisgrenze ($< 0,1$ mSv / Monat) lagen. 17 Personen erhielten monatliche Dosen $\geq 0,1$ mSv.

E. Veröffentlichungen, Vorträge, Lehrveranstaltungen

- Diplomarbeiten und Dissertationen
- Veröffentlichungen und Vorträge
- Vorträge in den Seminaren des Instituts
- Beiträge der Dozenten des Instituts zu den Lehrveranstaltungen des Fachbereichs sowie zur Weiterbildung

E. Publications and Teaching Activities

- Diploma theses and dissertations
- Publications in journals and contributions to conferences
- Guest contributions to the seminars of the institute
- Contributions of the staff to lectures and lab-courses of the Department of Chemistry and Pharmacy and to professional training in health physics

Dissertationen

Comagic Slobodan

Synthese und radioaktive Markierung potentieller PET- bzw. SPECT-Liganden zur Quantifizierung und Visualisierung der pankreatischen β -Zell-Masse

Kautzsch, Thomas

Gamma-Spektroskopie an neutronenreichen Silber-Isotopen

Kuczewski, Bernhard

Trennung der Oxidationsstufen des Plutoniums mit CE-ICP-MS und Untersuchung des Redoxverhaltens von Plutonium im Grundwasser

Wängler, Björn

Synthese, ^{11}C - und ^{18}F -Markierung und Evaluierung von Repaglinid-Derivaten zur Quantifizierung der pankreatischen β -Zell-Masse in vivo mittels PET

Veröffentlichungen und Vorträge der Mitarbeiter der berichterstattenden Arbeitsgruppen

Veröffentlichungen

- S. Amayri, T. Arnold, T. Reich, H. Foerstendorf, G. Geipel, G. Bernhard, A. Massanek
Spectroscopic characterization of the uranium carbonate andersonite $\text{Na}_2\text{Ca}[\text{UO}_2(\text{CO}_3)_3] \bullet 6\text{H}_2\text{O}$
Environ. Sci. Technol. **38**, 6032 (2004)
- S. Amayri, T. Arnold, H. Foerstendorf, G. Geipel, G. Bernhard
Spectroscopic characterization of synthetic becquerelite, $\text{Ca}[(\text{UO}_2)_6\text{O}_4(\text{OH})_6] \bullet 8\text{H}_2\text{O}$, and swartzite, $\text{CaMg}[\text{UO}_2(\text{CO}_3)_3] \bullet 12\text{H}_2\text{O}$
Canadian Mineral. **42**, 953 (2004)
- O. Arndt, I. Dillmann, M. Hannawald, S. Hennrich, P. Hoff, U. Köster, K.-L. Kratz, B. Pfeiffer, J.M. Shergur, W.B. Walters, L. Weissman, A. Wöhr, and the ISOLDE IS333, IS378 and IS393 Collaborations
Beta-Delayed Neutron Measurements of r-Process Isotopes in the ^{132}Sn Region
EPJ, in print
- H. Backe, A. Dretzke, R. Horn, T. Kolb, W. Lauth, R. Repnow, M. Sewitz, N. Trautmann
Ion Mobility Measurements and Ion Chemical Reaction Studies at Heavy Elements in a Buffer Gas Cell
Hyperfine Interactions, im Druck
- St. Bürger, R.A. Buda, H. Geckes, G. Huber, J.V. Kratz, P. Kunz, C. Lierse von Gostomski, G. Passler, A. Remmert, N. Trautmann
Isotope Selective Ultratrace Analysis of Plutonium for Environmental Studies by Laser Mass Spectrometry
J. Environm. Radioactivity, eingereicht
- N. Christlieb, T.C. Beers, P.S. Barklem, M. Bessell, V. Hill, J. Holmberg, A.J. Korn, B. Marsteller, L. Mashonkina, Y.-Z. Qian, S. Rossi, G.J. Wasserburg, F.-J. Zickgraf, K.-L. Kratz, B. Nordström, B. Pfeiffer, J. Rhee, and S.G. Ryan
The Hamburg/ESO R-process Enhanced Star Survey (HERES)
I. Project description, and discovery of two stars with strong enhancements of neutron-capture elements
A&A **428**, 1027 (2004)
- K. Eberhardt, M. Schädel, E. Schimpf, P. Thörle, N. Trautmann
Preparation of Targets by Electrodeposition for Heavy Element Studies
Nucl. Instr. Meth. Phys. Res. A **521**, 208 (2004)
- K. Eberhardt, N. Trautmann
Neutron Activation Analysis at the TRIGA Mark II Research Reactor of the University of Mainz
In: IAEA-Compendium on Purpose-Designed Research Reactor Facilities, im Druck
- A. El-Taher, A. Nossair, A.H. Azzam, K.-L. Kratz, A.S. Abdel-Halim
Determination of traces of Uranium and Thorium in some Egyptian environmental matrices by instrumental neutron activation analysis
Environment Protection Engineering **30/1-2**, 19 (2004)
- H.W. Gäggeler, W. Brüchle, Ch.E. Düllmann, R. Dressler, K. Eberhardt, B. Eichler, R. Eichler, C.M. Folden, T.N. Ginter, F. Glans, K.E. Gregorich, F. Hauessler, D.C. Hoffman, E. Jäger, D.T. Jost, U.W. Kirbach, J.V. Kratz, H. Nitsche, J.B. Patin, V. Pershina, D. Piguet, Z. Qin, U. Rieth, M. Schädel, E. Schimpf, B. Schausten, S. Soverna, R. Sudowe, P. Thörle, N. Trautmann, A. Türler, A. Vahle, P.A. Wilk, G. Wirth, A.B. Yakushev, A. von Zweidorff
Chemical and Nuclear Studies of Hassium and Element 112
Nucl. Phys. A **734**, 208 (2004)
- H. Geissel, Yu.A. Litvinov, F. Attalah, K. Beckert, P. Beller, F. Bosch, D. Boutin, T. Fästermann, M. Falch, B. Franzke, M. Hausmann, M. Hellström, E. Kaza, Th. Kerscher, O. Klepper, H.-J. Kluge, C. Kozhuharov, K.-L. Kratz, S.A. Litvinov, K.E.G. Löbner, L. Maier, M. Matos, G. Münzenberg, F. Nolden, Yu.N. Novikov, T. Ohtsubo, A. Ostrowski, Z. Patyk, B. Pfeiffer, M. Portillo, T. Radon, C. Scheidenberger, V. Shishkin, J. Stadtmann, M. Steck, D.J. Viera, H. Weick, M. Winkler, H. Wollnik, T. Yamaguchi
New Results with Stored Exotic Nuclei at Relativistic Energies
Ibid.
Nucl. Phys. A **746**, 150c (2004)

S. Grévy, J.C. Angélique, P. Baumann, C. Borcea, A. Buta, G. Canel, W.N. Catford, S. Courtin, J.M. Daugas, F. de Oliveira, P. Dessagne, Z. Dlouhy, A. Knipper, K.-L. Kratz, F.R. Lecolley, J.L. Lecouey, G. Lhersonneau, M. Lewitowicz, E. Liénard, S. Lukyanov, F. Maréchal, C. Miehé, J. Mrazek, F. Negoita, N.A. Orr, D. Pantelica, Y. Penionzhkovich, J. Péter, B. Pfeiffer, S. Pietri, E. Poirier, O. Sorlin, M. Stanoiu, I. Stefan, C. Stodel, and C. Timis
Beta-decay half-lives at the $N = 28$ shell closure
Phys. Lett. B594, 252 (2004)

S. Grévy, J.C. Angélique, P. Baumann, C. Borcea, A. Buta, G. Canel, W.N. Catford, S. Courtin, J.M. Daugas, F. de Oliveira, P. Dessagne, Z. Dlouhy, A. Knipper, K.-L. Kratz, F.R. Lecolley, J.L. Lecouey, G. Lhersonneau, M. Lewitowicz, E. Liénard, S. Lukyanov, F. Maréchal, C. Miehé, J. Mrazek, F. Negoita, N.A. Orr, D. Pantelica, Y. Penionzhkovich, J. Péter, B. Pfeiffer, S. Pietri, E. Poirier, O. Sorlin, M. Stanoiu, I. Stefan, C. Stodel and C. Timis
Beta-decay studies at the $N=28$ shell closure: indications for a weakening of the spin-orbit force far from stability?
ibid.
Nucl. Phys. A746, 145c (2004)

C. Grüning, G. Huber, P. Klopp, J.V. Kratz, P. Kunz, G. Passler, N. Trautmann, A. Waldek, K. Wendt
Resonance Ionization Mass Spectrometry for Ultratrace Analysis of Plutonium with a New Solid State Laser System
Int. J. Mass Spectrometry 235, 171 (2004)

H. Haba, K. Tsukada, M. Asai, A. Toyoshima, K. Akiyama, I. Nishinaka, M. Hirata, T. Yaita, S. Ichikawa, Y. Nagame, K. Yasuda, Y. Miyamoto, T. Kaneko, S. Goto, S. Ono, T. Hirai, H. Kudo, M. Shigekawa, A. Shinohara, Y. Oura, H. Nakahara, K. Sueki, H. Kikunaga, N. Kinoshita, N. Tsuruga, A. Yokoyama, M. Sakama, S. Enomoto, M. Schädel, W. Brüchle, J.V. Kratz
Fluoride Complexation of Element 104, Rutherfordium
J. Am. Chem. Soc. 126, 5219 (2004)

P.T. Hosmer, R.R.C. Clement, A. Estrade, S.N. Liddick, P.F. Mantica, W.F. Mueller, F. Montes, A.C. Morton, M. Ouellette, E. Pellegrini, P. Santi, H. Schatz, M. Steiner, A. Stoltz, B.E. Tomlin, O. Arndt, K.-L. Kratz, B. Pfeiffer, W.B. Walters, P. Reeder, A. Aprahamian and A. Wöhr
Beta-decay studies of neutron rich nickel isotopes

First Argonne/MSU/INT/RIA Workshop The r-Process: The Astrophysical Origin of the Heavy Elements and Related Rare Isotope Accelerator Physics, Seattle, USA, Jan. 8 - 10 2004;
World Scientific, 30 – 33 (2004)

S. Ilievski, T. Aumann, K. Boretzky, Th.W. Elze, H. Emling, A. Grünschloß, J. Holeczek, R. Holzmann, C. Kozuharov, J.V. Kratz, R. Kulessa, A. Leistenschneider, E. Lubkiewicz, T. Ohtsuki, P. Reiter, H. Simon, K. Stelzer, J. Stroth, K. Süßer, E. Wajda, W. Walus
Evidence for Multiphonon Giant Resonances in Electromagnetic Fission of ^{238}U
Phys. Rev. Lett. 92, 112502 (2004)

M. Jennewein, A. Schmidt, A.F. Novgorodov, S.M. Qaim, F. Rösch
A No-carrier-added $^{72}\text{Se}/^{72}\text{As}$ Radionuclide Generator Based on Distillation.
Radiochim. Acta 92, 245 (2004)

M. Jennewein, S.M. Qaim, A. Hermanne, E. Tsyanov, N. Slavine, S. Seliounine, P.A. Antich, P. Kulkarni, P.E. Thorpe, R.P. Mason, F. Rösch
A New Method for the Radiochemical Separation of Arsenic Isotopes from Reactor and Cyclotron Irradiated Germanium Oxide Targets
Appl. Rad. Isot., 2005, submitted

B. Kaina, U. Mühlhausen, A. Piee-Staffa, M. Christmann, R. Garcia Boy, F. Rösch, R. Schirrmacher
Inhibition of $\text{O}^6\text{-methylguanine-DNA Methyltransferase (MGMT)}$ by Glucose-conjugated Inhibitors: Comparison with Non-conjugated Inhibitors and Effect on Fotemustine and Temozolamide-induced Cell Death
J. Pharmacol. Exptl. Therap. 311, 585 (2004)

T. Kautzsch, A. Wöhr, W.B. Walters, K.-L. Kratz, B. Pfeiffer, M. Hannawald, J.M. Shergur, O. Arndt, S. Hennrich, S. Falahat, T. Griesel, O. Keller, A. Aprahamian, B.A. Brown, P.F. Mantica, M.A. Stoyer, H.L. Ravn, and the ISOLDE IS333 and Rochester CHICO/Gammashpere Collaborations
Decay Spectroscopy of Very Neutron-Rich Silver Isotopes
EPJ, in print

U. Köster, O. Arndt, U. Bergmann, R. Catherall, J. Cederkäll, I. Dillmann, M. Dubois, F. Durantel, L. Fraile, S. Franchoo, G. Gaubert, L. Gaudefroy, O. Hallmann, C. Hurt-Equilbec, B. Jacquot, P. Jardin, K.-L. Kratz, N. Lecesne, R. Leroy, A. Lopez, L. Maunoury, J.Y. Pacquet,

B. Pfeiffer, M.G. Saint-Laurent, C. Stodel, A.C.C. Villari and L. Weissman
ISOL beams of neutron-rich oxygen isotopes at ISOLDE and SPIRAL
EPJ, in print

U. Köster, G. Auböck, U.C. Bergmann, R. Catherall, J. Cederkäll, L.M. Fraile, S. Franchoo, H. Fynbo, U. Georg, A. Joinet, O.C. Jonsson, J. Lettry, K. Peräjärvi, L. Weissman, O. Bajeat, R. Borcea, C. Bourgeois, C. Donzaud, M. Ducourtieux, S. Essabaa, D. Guillemaud-Mueller, F. Hosni, F. Ibrahim, C. Lau, H. Lefort, J. Obert, O. Perru, J.C. Poitier, B. Roussiére, B. Pfeiffer, E. Fioretti, G. Lhersonneau, G. Prete, L. Stroe, L. Tecchio, C.A.A. Diget, H. Jeppesen, K. Riisager, H. Gausemel, E. Hagebø, D. Ridikas
Fission Yield Measurements with the ISOL Method
First Argonne/MSU/INT/RIA Workshop The r -Process: The Astrophysical Origin of the Heavy Elements and Related Rare Isotope Accelerator Physics, Seattle, USA, Jan. 8 - 10 2004;
World Scientific, 83 – 91 (2004)

J.V. Kratz, N. Trautmann, G. Huber, G. Passler, K. Wendt
Laser Mass Spectrometry
Analytical applications of nuclear techniques, International Atomic Energy Agency, Vienna, ISBN 92-0-114703-1, 33 (2004)

K.-L. Kratz, B. Pfeiffer, S. Hennrich, and A. Wöhr
R-Process Isotopes in the ^{132}Sn Region
Fourth Int. Conf. on Exotic Nuclei and Atomic Masses - ENAM04, September 12 - 16, 2004, Callaway Gardens, Pine Mountain, Georgia, USA;
EPJ, in print

A. Kronenberg, P.K. Mohapatra, J.V. Kratz, G. Pfrepper, R. Pfrepper
Anion-exchange behavior of Mo and W as Homologs of Sg (Element 106) in HCl and HNO_3 as well as in Mixed HCl-HF and HNO_3 -HF
Radiochim. Acta 92, 395 (2004)

A. Kronenberg, K. Eberhardt, J.V. Kratz, P.K. Mohapatra, A. Nähler, P. Thörle, W. Brüchle, M. Schädel, A. Türler
On-line Anion Exchange of Rutherfordium in HF/ HNO_3 and HF Solutions
Radiochim. Acta 92, 379 (2004)

P. Kunz, G. Huber, G. Passler, N. Trautmann
Efficient Three-step, Two-color Ionization of Plutonium Using a Resonance Enhanced 2-Photon Transition into an Autoionizing State
Eur. Phys. J. D29, 183 (2004)

P. Kunz, G. Huber, G. Passler, N. Trautmann, K. Wendt
Resonance Ionization Mass Spectrometry (RIMS) with Pulsed and cw-Lasers on Plutonium
Hyperfine Interactions, eingereicht

C.M. Marquardt, A. Seibert, R. ARtinger, M. A. Denecke, B. Kuczewski, D. Schild, Th. Fanghänel
The Redox Behaviour of Plutonium in Humic rich Groundwater
Radiochim. Acta 92, 617 (2004)

J. Maul, T. Berg, K. Eberhardt, I. Hoog, G. Huber, S. Karpuk, G. Passler, I. Strachnov, N. Trautmann, K. Wendt
A Laser Desorption / Resonance Enhanced Photoionisation TOF-System for the Spatially Resolved Trace Analysis of Elements
Nucl. Instr. Meth. Phys. Res. B226, 644 (2004)

E. Mauerhofer, K. Zhernosekov, F. Rösch
Limiting Transport Properties and Hydratation Numbers of Actinyl Ions in Pure Water
Radiochim. Acta 92, 5 (2004)

M. Merroun, J. Raff, A. Rossberg, C. Hennig, T. Reich, S. Selenska-Pobell
Interaction of U(VI) with bacterial strains isolated from uranium mining piles: Spectroscopic and microscopic studies
Geochim. Cosmochim. Acta 68, A499 Suppl. S (2004)

C. Nociforo, R. Palit, P. Adrich, T. Aumann, K. Boretzky, D. Cortina-Gil, U. Datta Pramanik, Th.W. Elze, H. Emling, H. Geissel, M. Hellström, N. Iwasa, K.L. Jones, J.V. Kratz, R. Kulessa, Le Hong Khiem, A. Leistenschneider, G. Münenberg, P. Reiter, C. Scheidenberger, H. Scheit, H. Simon, K. Sümerer, S. Typel, E. Wajda, W. Walus, H. Weick
Coulomb Breakup of Neutron-Rich Oxygen Isotopes
in: The Labyrinth in Nuclear Structure, A. Bracco and C.A. Kalfas (eds.), American Institute of Physics 701, 174 (2004)

R. Palit, P. Adrich, T. Aumann, K. Boretzky, D. Cortina, U. Datta Pramanik, Th.W. Elze, H. Emling, M. Fallot, H. Geissel, M. Hellström, K.L. Jones, L.H. Khiem, J.V. Kratz, R. Kulessa, Y. Leifels, A. Leistenschneider, G. Münenberg, C. Nociforo, P. Reiter, H. Simon, K. Sümerer, W. Walus

Dipole Excitations of Neutron-proton Asymmetric Nuclei
Nucl. Phys. A731, 235-248 (2004)

I.V. Panov, B. Pfeiffer, K.-L. Kratz, E. Kolbe, T. Rauscher, F.-K. Thielemann
Fission Barriers: How do they affect the r-Process?
Workshop Neutrinos and Neutrons in Astrophysics, 15 - 16 September 2003, and Seminar on Fission "Pont d'Oye V", 16 - 19 September 2003; Pont d'Oye, Habay-la-Neuve, Belgium
World Scientific Publishing, 3-12 (2004)

B. Pfeiffer, K.-L. Kratz
Neutron-induced nucleosynthesis in the r-process
Workshop Neutrinos and Neutrons in Astrophysics, 15 - 16 September 2003, and Seminar on Fission "Pont d'Oye V", 16 - 19 September 2003; Pont d'Oye, Habay-la-Neuve, Belgium
World Scientific Publishing, 29-36 (2004)

F. Rösch, E. Forssell-Aronsson.
Radio-lanthanides in Nuclear Medicine
in: Metal Ions and Their Complexes in Medication. A. Sigel, H. Sigel, Eds. M. Dekker, Inc., New York & Basel, Vol. 42. p. 77-108 (2004)

F. Rösch
Radionuklid-Generatorsysteme für die PET
Der Nuklearmediziner 27, 226 (2004)

S. Sachs, K. Schmeide, V. Brendler, A. Krepelova, J. Mibus, G. Geipel, T. Reich, K.H. Heise, G. Bernhard
Investigation of the Complexation and the Migration of Actinides and Non-radioactive Substances with Humic Acid Under Geogenic Conditions – Complexation of Humic Acid with Actinides in the Oxidation State IV (Th, U, Np)
Wissenschaftliche Berichte, Forschungszentrum Karlsruhe FZKA 6999 19 (2004)

H. Schatz, P. Hosmer, A. Aprahamian, O. Arndt, R.R.C. Clement, A. Estrade, K.-L. Kratz, P.F. Mantica, W.F. Mueller, F. Montes, C. Morton, M. Ouellette, E. Pellegrini, B. Pfeiffer, P. Reeder, P. Santi, M. Steiner, A. Stolz, B.E. Tomlin, W.B. Walters, A. Wöhr
First half-life measurement of the doubly-magic r-process nucleus ⁷⁸Ni
EPJ, in print

R. Schirrmacher, S. Comagic, E. Schirrmacher, F. Rösch
Synthesis of a Technetium-99m Labeled L-Tyrosine Derivative with the *fac*-^{99m}Tc(I)(CO)₃-core for Imaging Cancer
J. Label. Compd. Radiopharm. 47, 477 (2004)

G. Schmidt
Are high-temperature fractionations in the solar nebula preserved in highly siderophile element systematics of the Earth's mantle?
Meteoritics and Planetary 39, 1995 (2004)

G. Schmidt
Cosmochemical fractionations and/or astrophysical effects in planetary materials?
In: Workshop on Chondrites and Protoplanetary Disk, Nov. 8-11, Kaua'i Hawai'i (2004)

G. Schmidt
Highly fractionated materials from the Inner Solar System: evidence from the Earth
In: Workshop on Chondrites and Protoplanetary Disk, Nov. 8-11, Kaua'i Hawai'i (2004)

A. Schmitz, C.-Y. Shiue, Q. Feng, G.G. Shiue, S. Deng, M.T. Pourdehnad R. Schirrmacher, M. Vatamanuk, N. Doliba, F. Matschinsky, B. Wolf, F. Rösch, A. Naji, A.A. Alavi
Synthesis and Evaluation of Fluorine-18 Labeled Glyburide Analogs as Beta-cell Imaging Agents
Nucl. Med. Biol. 31, 483 (2004)

M. Schreckenberger, S. Hägele, T. Siessmeier, H.G. Buchholz, H. Armbrust-Henrich, F. Rösch, P. Bartenstein, T. Vogt
The Dopamine D₂-receptor Ligand F-18 Desmethoxyfallypride is an Appropriate PET Tracer for the Differential Diagnosis of Parkinsonism
Eur. J. Nucl. Med. Mol. Imaging 31, 1128 (2004)

O. Stetzer, M. Betti, J. van Geel, N. Erdmann, J.V. Kratz, R. Schenkel, N. Trautmann
Determination of the U-235 Content in Uranium Oxide Particles by Fission Track Analysis
Nucl. Instr. Meth. Phys. Res. A525, 582 (2004)

A. Stolz, A. Estrade, A.D. Davies, T.N. Ginter, P.T. Hosmer, E. Kwan, S.N. Lidick, P.F. Mantica, T.J. Mertzimekis, F.A. Montes, D.J. Morrissey, A.C. Morton, M. Oullette, E. Pellegrini, P. Santi, H. Schatz, M. Steiner, A.E. Stuchberry, B.E. Tomlin, W.B. Walters, A. Wöhr, O. Arndt, K.-L. Kratz, B. Pfeiffer, P. Reeder
Radioactive Ion Beams in the Region of ¹⁰⁰Sn and ⁷⁸Ni at the NSCL

Sixth Int. Conf. on *Radioactive Nuclear Beams (RNB6)*, Sept. 22 -26, 2003, Argonne, Illinois, USA
Nucl. Phys. A746 54c (2004)

F.-K. Thielemann, D. Argast, D. Mocelj, T. Rauscher, J.J. Cowan, K.-L. Kratz, B. Pfeiffer
The r-Process in Supernovae
First Argonne/MSU/INT/RIA Workshop The r-Process: The Astrophysical Origin of the Heavy Elements and Related Rare Isotope Accelerator Physics, Seattle, USA, Jan. 8 - 10 2004;
World Scientific, 1 – 10 (2004)

N. Trautmann, G. Passler, K.D.A. Wendt
Ultratrace Analysis and Isotope Ratio Measurements of Long-lived Radioisotopes by Resonance Ionization Mass Spectrometry (RIMS)
Anal. Bioanal. Chem. 378, 348 (2004)

I. Vernaleken, T. Siessmeier, H.-G. Buchholz, S. Härtter, Ch. Hiemke, P. Stoeter, F. Rösch, P. Bartenstein, G. Gründer
High Striatal Occupancy of D₂-like Dopamine Receptors by Amisulpride in Brain of Schizophrenic Patients: Implications for Atypical Antipsychotic Mechanism of Action
Int. J. Neuropsychopharmacol. 7/4, 421 (2004)

B. Wängler, S. Schneider, O. Thews, E. Schirrmacher, S. Comagic, P. Feilen, C. Schwanstecher, M. Schwanstecher, C.-Y. Shiue, A. Alavi, S. Höhnemann, M. Piel, F. Rösch, R. Schirrmacher
Synthesis and Evaluation of (S)-2-(2-[¹⁸F]fluoroethoxy)-4-([3-methyl-1-(2-piperidin-1-yl-phenyl)-butyl-carbamoyl]-methyl)-benzoic acid ([¹⁸F]repaglinide): A Promising Radioligand for Quantification of Pancreatic Beta-cell Mass with Positron Emission Tomography (PET)
Nucl. Med. Biol. 31, 639 (2004)

L. Weissman, O. Arndt, U. Bergmann, J. Cederkall, I. Dillmann, O. Hallmann, L. Fraile, S. Franschoo, L. Gaudefroy, U. Köster, K.-L. Kratz, A. F. Lisetskiy, B. Pfeiffer, S. Tavor
Beta-decay of ²⁶Ne
Phys. Rev. C70, (2004)

L. Weissman, O. Arndt, U. Bergmann, A. Brown, R. Catheral, J. Cederkall, I. Dillmann, O. Hallmann, L. Fraile, S. Franschoo, U. Köster, K.-L. Kratz, L. Gaudefroy, B. Pfeiffer, O. Sorlin, and ISOLDE collaboration
Beta-decay of ⁴⁷Ar
Phys. Rev. C70, 024304 (2004)

K. Wendt, N. Trautmann
Recent Developments in Isotope Ratio Measurements by Resonance Ionization Mass Spectrometry
Int. J. Mass Spectrometry, im Druck

E.F. Worden, J. Blaise, M. Fred, N. Trautmann, J.-F. Wyart
Spectra and Electronic Structures of Free Actinide Atoms and Ions
in: The Chemistry of the Actinide and Transactinide Elements, 3rd Edition (J.J. Katz, L.R. Morss, N. Edelstein, J. Fuger, eds.), Kluwer Academic Publishers, im Druck

A. von Zweidorff, R. Angert, W. Brüchle, S. Bürger, K. Eberhardt, R. Eichler, H. Hummrich, E. Jäger, H.-O. Kling, J.V. Kratz, B. Kuczewski, G. Langrock, M. Mendel, U. Rieth, M. Schädel, B. Schausten, E. Schimpf, P. Thörle, N. Trautmann, K. Tsukada, N. Wiehl, G. Wirth
Evidence for the formation of sodium hassate(VIII)
Radiochim. Acta 92, 855 (2004)

Vorträge+

Seattle, USA: First Argonne/MSU/INT/RIA Workshop The r-Process:The Astrophysical Origin of the Heavy Elements and Related Rare Isotope Accelerator Physics, 8. – 10.01.2004

I. Dillmann

Decay experiments in the ^{132}Sn region

H. Geissel, F. Attallah, K. Beckert, P. Beller, F. Bosch, D. Boutin, M. Falch, T. Faestermann, B. Franczak, B. Franzke, M. Hausmann, M. Hellström, E. Kaza, Th. Kerscher, O. Klepper, H.-J. Kluge, C. Kozhuharov, K.-L. Kratz, K.E.G. Löbner, Yu.A. Litvinov, M. Matos, L. Maier, G. Münzenberg, F. Nolden, Yu.N. Novikov, T. Ohtsubo, A.N. Ostrowski, Z. Patyk, B. Pfeiffer, M. Portillo, T. Radon, H. Schatz, C. Scheidenberger, J. Stadelmann, M. Steck, K. Süümmerer, D. Vieira, H. Weick, M. Winkler, H. Wollnik, T. Yamaguchi
Mass and Lifetime Measurements of Stored Exotic Nuclei at Relativistic Energies

K.-L. Kratz

The r-Process: Nuclear Data Needs

Orsay, Frankreich : Seminaire de la Division de Recherche, 02.02.2004

K.-L. Kratz

R-Process Nucleosynthesis and Th-U Cosmochronometry

Salzburg, Österreich: HPCE2004, 17th International Symposium on Microscale Separation and Capillary Electrophoresis, 08.-12.02.2004

B. Kuczewski, H. Geckeis, J.V. Kratz, C.M. Marquardt, A. Seibert, N. Trautmann
Separation of Plutonium and Neptunium Species by CE-ICP-MS

A. Seibert, B. Kuczewski, C.M. Marquardt
CE-ICP-MS: A tool to determine oxidation state species of plutonium added to ground waters

Mainz: Tag der Offenen Tür, Vortragsreihe zur Hirnforschung: Kopfarbeit – Dem Denken und Fühlen auf der Spur, 11.02.2004

F. Rösch

Dem Gehirn beim Arbeiten zusehen

Marburg: GDCh-Kolloquium des Fachbereichs Chemie, 11.02.2004

N. Trautmann*

Ultraspurenanalytik langlebiger Radionuklide mit Lasermassenspektrometrie

Darmstadt: NUSTAR Annual Meeting, 19.-21.02.2004

K.-L. Kratz

Perspectives of Nuclear Astrophysics at GSI

Frankfurt: Frankfurter Bürgerstiftung zum 125. Geburtstag von Otto Hahn, 08.03.2004

G. Herrmann*

Geschichte der Kernspaltung - eine Entdeckung auf Umwegen

Köln: DPG Nuclear Physics Spring Meeting, 08.-12.03.2004

P. Adrich for the S221 collaboration

Coulomb breakup of nuclei in the ^{132}Sn region

Th. Aumann for the R3B collaboration

Perspectives for Scattering Experiments with Relativistic Radioactive Beams at the Future Super-FRS at GSI

E. Kaza, F. Attallah, K. Beckert, P. Beller, F. Bosch, D. Boutin, T. Faestermann, B. Franczak, B. Franzke, H. Geissel, M. Hausmann, M. Hellström, O. Klepper, H.-J. Kluge, C. Kozhuharov, K.-L. Kratz, Y. Litvinov, L. Maier, M. Matos, G. Münzenberg, F. Nolden, Y. Novikov, A.N. Ostrowski, T. Ohtsubo, A. Ozawa, B. Pfeiffer, M. Portillo, C. Scheidenberger, J. Stadelmann, T. Suzuki, K. Süümmerer, D. Vieira, H. Weick, M. Winkler, H. Wollnik, and T. Yamaguchi

Schottky mass measurements of neutron-rich nuclides between lead and uranium

Yu.A. Litvinov, H. Geissel, M. Matos, Yu.N. Novikov, Z. Patyk, T. Radon, C. Scheidenberger, F. Attallah, K. Beckert, P. Beller, F. Bosch, D. Boutin, T. Buervenich, M. Falch, T. Faestermann, B. Franzke, M. Hausmann, E. Kaza, T. Kerscher, O. Klepper, H.-J. Kluge, C. Kozhuharov, K.-L. Kratz, S.A. Litvinov, K.E.G. Löbner, G. Münzenberg, L. Maier, F. Nolden, T. Ohtsubo, A. Ostrowski, A. Ozawa, B. Pfeiffer, M. Portillo, J. Stadelmann, K. Suzuki, M. Steck, S. Typel, D. Vieira, H. Weick, M. Winkler, H. Wollnik, and T. Yamaguchi

New results from direct mass measurements at GSI

+ Vortragender unterstrichen, falls nicht an erster Stelle aufgeführt

* auf Einladung

B. Pfeiffer, K. Farouqi, and K.-L. Kratz
Isotopic abundance ratios in ultra-metal-poor
Halo stars

Russbach, Österreich: 1st VISTARS Workshop
on Nuclear Astrophysics, 14.-19.03.2004

O. Arndt, I. Dillmann, K.-L. Kratz, A. Ostrowski,
B. Pfeiffer, A. Wöhr
Very neutron-rich isotopes at the $A \approx 130$ re-
gion

K. Farouqi
Astrophysical conditions for an r-process in the
high-entropy bubble scenario

K.-L. Kratz
Nuclear data needs for explosive nucleosyn-
thesis

K.-L. Kratz
R-process

B. Pfeiffer
Nuclear Astrophysics: History of Nucleosynthe-
sis up to B^2FH

B. Pfeiffer
R-process cosmochronometer

Flachau, Österreich: Second n_TOF Winter
School, 22.-26.03.2004

K.-L. Kratz
R-process nucleosynthesis and Th-U-
cosmochronometry

München: 68. Physikertagung und AMOP-
Frühjahrstagung, 22.-26.03.2004

S. Bürger, R. Buda, H. Geckeis, G. Huber, J.V.
Kratz, G. Passler, N. Trautmann
Empfindliche Plutoniumbestimmung in Sicker-
wasserproben von Granitgestein

A. Dretzke, R. Horn, H. Backe, K. Eberhardt, S.
Fritzsche, R.G. Haire, T. Kolb, W. Lauth, M.
Sewitz, P. Thörle, N. Trautmann
Optische Spektroskopie an Fermium ($Z = 100$)

Ch. Geppert, P. Schumann, K. Wies, K.
Wendt, N. Trautmann, E. Denk, T. Walczyk
Anwendungen der RIMS für ^{41}Ca Tracerstu-
dien zu biomedizinischen Fragestellungen

P. Kunz, G. Huber, G. Passler, N. Trautmann
Efficient Three-Step, Two-Color Ionization of
Plutonium Using a Resonance Enhanced 2-
Photon Transition into an Autoionizing State

J. Maul, K. Eberhardt, G. Huber, S. Karpuk, G.
Passler, I. Strachnov, N. Trautmann, K. Wendt
Bimodal Velocity Distribution of Neutral Atoms
Released from Laser Ablation

P. Schumann, S.F. Boulyga, G. Passler, N.
Trautmann, K.D.A. Wendt
Hochauflösende Resonanzionisationsspektro-
skopie an Uran-Isotopen für den Nachweis von
Uran-236

I. Strachnov, K. Eberhardt, G. Huber, S. Kar-
puk, N. Kotovski, J. Maul, G. Passler, M.C.
Roca, N. Trautmann, K. Wendt
Spatially Resolved Ultra Trace Analysis of
Elements Using Laser Desorption and Reso-
nance Enhanced Photoionisation

Ringberg: 12th Workshop on Nuclear Astro-
physics, 22.-27.03.2004

K.-L. Kratz, W. Böhmer, C. Freiburghaus, P.
Möller, B. Pfeiffer, T. Rauscher, F.-K. Thiele-
mann
The EK-1-4-1 story

Mainz: Volkshochschule, 23.03.04

B. Pfeiffer
Kosmische Strahlung – Boten aus dem Weltall

Karlsruhe: International Workshop on Sorption
Processes at Oxide and Carbonate Mineral
Water Interfaces SOPRO, 25.-26.03.2004

S. Amayri, J. Drebert, T. Reich
EXAFS Investigation of Uranium(VI) Adsorp-
tion on Kaolinite

Anaheim, USA: 227th ACS National Meeting,
Division of Nuclear Chemistry and Technolgy,
28.03.-01.04.2004

S. Amayri, T. Reich*, T. Arnold, G. Geipel, G.
Bernhard
Spectroscopic characterization of alkaline earth
uranyl carbonates
Abstract of papers of the American Chemical
Society, 227 U77 149-NUCL (2004)

T. Reich, S. Amayri, J. Drebert
Uranium Sorption on Kaolinite
Abstract of papers of the American Chemical
Society, 227 U98 16-NUCL (2004)

Jülich: Fortbildungsseminar des Forschungszentrums Jülich zu speziellen Fragen im Strahlenschutz, 14.04.2004

N. Trautmann*

Isotopenselektive Ultraspurenanalyse von langlebigen Radionukliden mit laserresonanter Ionisations-Massenspektrometrie (RIMS)

Rostock: 42. Jahrestagung der Deutschen Gesellschaft für Nuklearmedizin und SGNM/SSMN: 5th Annual Congress, 21.24.04.2004

H.G. Buchholz, Y. Zhou, I.B. Vernaleken, C. Landvogt, T. Siessmeier, F. Rösch, P. Bartenstein
Vergleich parparametrischer Methoden für die Quantifizierung von D2-Dopamin-Rezeptorliganden unterschiedlicher Affinität

H.G. Buchholz, T. Siessmeier, C. Landvogt, M. Piel, R. Schirrmacher, M. Schreckenberger, P. Bartenstein
Normalisierung von D2-Dopamin-Rezeptorligandenbildern mit SPM unter Verwendung eines ligandenspezifischen Templates

M. Jennewein, O. Bergner, S.M. Qaim, P.P. Antich, P.E. Thorpe, R.P. Mason, F. Rösch
Nca As-77 and As-74 Triiodide as new Synthons for Antibody Labelling and First in vivo Imaging

C. Landvogt, I. Vernaleken, T. Siessmeier, H.G. Buchholz, F. Rösch, G. Gründer, P. Bartenstein
Welche Eigenschaften machen Clozapin „atypisch“: eine PET-Studie mit ¹⁸F-Fallyprid

E. Schirrmacher, C. Beck, R. Schirrmacher, F. Rösch, N. Trautmann, W. Mier
Synthesis of a Tyr3-Octreotide Conjugated Clos-Carborane: A Potenial Compound for Boron Neutron Capture Therapy

T. Siessmeier, H.G. Buchholz, G. Hendriksen, H.J. Wester, F. Rösch, M. Schreckenberger, P. Bartenstein
Vergleich unterschiedlicher Quantifizierungsmethoden für den unspezifischen Opiatrezeptorliganden ¹⁸F-Fluori-Ethyl-Diprenorphin

T. Siessmeier, G. Gründer, P. Bartenstein, A. Heinz, H.G. Buchholz, R. Schirrmacher, Y. Kumakura
Das Verlangen nach Alkohol korreliert mit der striatalen Dopaminrezeptorbinding und Dopaminspeicherkapazität

Mainz: Tagung der Arbeitsgemeinschaft der Betreiber von Forschungsreaktoren (AFR), 27.-28.04.2004

K. Eberhardt, N. Trautmann
Der Forschungsreaktor TRIGA Mainz

Turin, Italien: Advances in Nuclear Medicine Seminar, 28.04.04

M. Jennewein
Somatostatin Receptor Imaging with ⁶⁸Ga-DOTATOC and Radioactive Arsenic Isotopes for Antibody-Labelling and Imaging

M. Piel
PET and Radiopharmaceutical Chemistry for Tumor Metabolism and -physiology and Routine Diagnosis

Denver, USA: Annual APS April Meeting, 01.-04.05.2004

K.-L. Kratz
[B2.001] The r-Process and Nuclear Structure near the Dripline

J. Shergur, A. Wöhr, W.B. Walters, K.-L. Kratz, O. Arndt, A. Brown, I. Dillmann, P. Hoff, U. Köster, B. Pfeiffer
[L10.006] Determination of Low-Spin Levels in ^{134,135}Sb via Decay of ¹³⁵Sn

Berlin: Medizinisch wissenschaftliches Symposium - Europatag, 05.05.2004

F. Rösch
Molecular Imaging – Biochemische Ansätze der PET

Saarbrücken: BMWA-Workshop „Migration von Actiniden im System Ton, Huminstoff, Aquifer“, 11. und 12.05.2004

S. Amayri, J. Drebert, S. Boulyga, T. Reich
EXAFS-Untersuchungen zur Sorption von U(VI) an Kaolinit

S. Bürger, R. Buda, H. Geckes, G. Huber, J.V. Kratz, P. Kunz, G. Passler, N. Trautmann
Empfindliche Plutoniumbestimmung in Umweltproben mit Lasermassenspektrometrie

B. Kuczewski
Speziationsuntersuchungen am Plutonium

Orsay, Frankreich: Workshop TANDEM-ALTO, 17.-18.05.2004

K.-L. Kratz
R-process with ALTO

Athen, Griechenland: COSTD18, Working Group 2004, 20.-22.05.2004

H. Mäcke, M. Jennewein, H. Zhang, J. Chen, F. Rösch, J.C. Reubi
Simultaneous Evaluation of DOTA-Bombesin Derivatives Using the Cocktail Approach

A.F. Novgorodov, D.V. Filosofov, K.P. Zhernosekov, A. Korobeinikov, N.A. Lebedev, N.A. Korolev, G.-J. Beyer, F. Rösch, and the ISOLDE Collaboration

Isolation of Lanthanide and Hafnium Radioisotopes from a Massive Ta-target Irradiated with 1 GeV Protons

K. Zhernosekov, N.A. Korolev, D.V. Filosofov, A.F. Novgorodov, F. Rösch
Non-Invasive Analysis of the Chemical Status of ^{111}In -Labelled Compounds Using 1-PAC and Potential Application for Radiolanthandies

Genf, Schweiz: Workshop on Physics with a Multi-MW Proton Source, 25.-27.05.2004

K.-L. Kratz
Astrophysics with RIB

Kopenhagen, Dänemark: 14th Annual Goldschmidt Conference, 05.-11.06.2004

M. Merroun, J. Raff, A. Rossberg, C. Hennig, T. Reich, S. Selenska-Pobell
Interaction of U(VI) with Bacterial Strains Isolated from Uranium Mining Piles: Spectroscopic and Microscopic Studies

Bochum: Physikalisches Kolloquium, Ruhr-Universität Bochum, 7.6.2004

K.-L. Kratz
Entstehung der schweren Elemente im r-Prozess

Philadelphia, USA: 51st Annual Meeting of the Society of Nuclear Medicine, 19.-23.06.2004

B. Wängler, R. Schirrmacher, S. Schneider, C.Y. Shiue, F. Rösch, A.A. Alavi
Synthesis and Evaluation of (S)-2-(2-[^{18}F]Fluoroethoxy)-4-([3-Methyl-1-(2-Piperidin-1-YL-Phenyl)-Butyl-Carbamoyl]-Methyl)-Benzoc Acid ([^{18}F]Repaglinide): A Potential Radioligand for Quantification of Pancreatic Beta-Cell Mass With Positron Emission Tomography (PET)

Yale, USA: 14th Conference on Solid State Dosimetry (SSD14), 27.06.-02.07.2004

B. Burgkhardt, P. Bilski, M. Budzanowski, R. Böttger, K. Eberhardt, G. Hampel, P. Olko, S. Scheloske, A. Straubing
Application of Different TL-Detectors for the Dosimetry of the Photon Component in BNCT

Göteborg, Schweden: Int. Nuclear Physics Conference - INPC2004, 27.06.-02.07.2004

P. Hosmer, O. Arndt, R.R.C. Clement, A. Estrade, K.-L. Kratz, P.F. Mantica, W.F. Mueller, F. Montes, C. Morton, M. Ouellette, E. Pellegrini, B. Pfeiffer, P. Reeder, P. Santi, H. Schatz, M. Steiner, A. Stolz, B.E. Tomlin, W.B. Walters, A. Wöhr
First half-life measurement of the doubly-magic r-process nucleus ^{78}Ni

K.-L. Kratz for the Mainz - Maryland - Notre Dame - Oslo - ISOLDE Collaboration
The r-process and nuclear structure in the ^{132}Sn region

Petershof, Russland: Int. Symp. on Exotic Nuclei - EXON2004, 5.-12.07.2004

M. Matos, Yu. N. Novikov, K. Beckert, P. Beller, F. Bosch, D. Boutin, T. Faestermann, B. Franczak, B. Franzke, H. Geissel, M. Hausmann, E. Kaza, O. Klepper, H.-J. Kluge, C. Kozuharov, K.-L. Kratz, Yu. A. Litvinov, L. Maier, G. Münzenberg, F. Nolden, T. Ohtsubo, A.N. Ostrowski, Z. Patyk, B. Pfeiffer, M. Portillo, C. Scheidenberger, J. Stadtmann, M. Steck, D. Vieira, H. Weick, M. Winkler, H. Wollnik, T. Yamaguchi
Direct Mass Measurements of Short-Lived Neutron-Rich Fission Fragments at the FRS-ESR Facility at GSI

Vancouver, Canada: "The Eighth International Symposium on Nuclei in the Cosmos NIC VIII", 19.-23.07.2004

K. Farouqi, C. Freiburghaus, K.-L. Kratz, B. Pfeiffer, T. Rauscher and F.-K. Thielemann
Astrophysical conditions for an r-process in the high-entropy wind scenario of type II supernovae

F. Montes, H. Schatz, A. Aprahamian, O. Arndt, A. Estrade, K.-L. Kratz, S.N. Liddick, P.F. Mantica, W.F. Mueller, P. Hosmer, A.C. Morton, M. Ouellette, E. Pellegrini, B. Pfeiffer, P. Reeder, P. Santi, A. Stolz, B.E. Tomlin, W.B. Walters, A. Wöhr
Beta-decay studies close to the N=82 r-process path

H. Schatz, R.R.C. Clement, A. Estrade, P. Hosmer, P.F. Mantica, F. Montes, C. Morton, W.F. Mueller, M. Ouellette, E. Pellegrini, P. Santi, M. Steiner, A. Stoltz, B.E. Tomlin, O. Arndt, K.-L. Kratz, B. Pfeiffer, P. Reeder, W.B. Walters, A. Aprahamian, A. Wöhr
Experiments with radioactive beams of r-process nuclei

Santa Fe, New Mexico, USA: Chemical Enrichment of the Early Universe, 09.-13.08.2004

K.-L. Kratz
R-Process Data

Philadelphia, USA: 228th National ACS Meeting, 22.-26.08.2004

J. Shergur, W.B. Walters, K.-L. Kratz, and A. Wöhr,
Using Laser Resonance Ionization to Enhance Selectivity in the Production of Neutron-Rich Sn Nuclei

Darmstadt: 3rd Workshop on Recoil Separator for Superheavy Element Chemistry, 27.08.2004

H. Hummrich, J.V. Kratz
Electrochemical Deposition – a Tool for the Investigation of Superheavy Element Chemistry?

J.P. Omtvedt and the SISAK collaboration
Liquid Phase Chemistry with SISAK Using Preseparated Activity

Aachen: 6th International Conference on Nuclear and Radiochemistry (NRC-6), 29.08.-03.09.2004

S. Anderson, K. Eberhardt, C. Ekberg, J.O. Liljenzin, M. Nilsson, G. Skarnemark
Determination of Stability Constants of Lanthanide Nitrate Complex Formation Using a Solvent Extraction Technique

K. Eberhardt, S. Andersson, C. Ekberg, B. Horn, J.V. Kratz, A. Müller, M. Nilsson, G. Skarnemark, N. Trautmann
MicroSISAK – A New Device for Fast and Continuous Liquid-Liquid-Extractions on a Microliter Scale

G. Herrmann*
Ein Jahrhundert Kern- und Radiochemie – Von Marie Curie bis zu den superschweren Elementen

H. Hummrich, J.V. Kratz
Electrochemical Deposition – a Tool for the Investigation of Superheavy Element Chemistry?

M. Jennewein, S. Maus, S.M. Qaim, F. Rösch
A New ⁷²Se/⁷²As Radionuclide Generator Based on Solid Phase Extraction

J.V. Kratz
Status and Future Developments of the Aqueous Heavy-element Chemistry

B. Kuczewski, C.M. Marquardt, A. Seibert, H. Geckes, J.V. Kratz, N. Trautmann
Separation of Plutonium and Neptunium Species by CE-ICP-MS and Application to Natural Groundwater Samples

E. Mauerhofer, K. Zhernosekov, F. Rösch
Limiting Transport Properties of Actinide Ions in Pure Water

A. Seibert, C.M. Marquardt, J.V. Kratz, N. Trautmann, Th. Fanghänel
Humate Complexation of Neptunium (V)

S. Soverna, W. Brüchle, R. Dressler, Ch.E. Düllmann, K. Eberhardt, B. Eichler, R. Eichler, Ch.M. Folden, H.W. Gäggeler, K.E. Gregorich, F. Haeussler, E. Jäger, J.V. Kratz, H. Nitsche, D. Piguet, Z. Qin, U. Rieth, M. Schädel, B. Schausten, E. Schimpf, N. Trautmann, P. Thörle, A. Türler, P.A. Wilk, G. Wirth, A.B. Yakushev, A. von Zweidorff
Attempt to Chemically Characterize Element 112

N. Trautmann*
Ultratrace Analysis of Long-lived Radionuclides by Laser Mass Spectrometry (RIMS)

A. von Zweidorff, R. Angert, W. Brüchle, S. Bürger, K. Eberhardt, R. Eichler, H. Hummrich, E. Jäger, R. Jera, H.-O. Kling, J.V. Kratz, U. Krille, B. Kuczewski, G. Langrock, G. Lehr, M. Mendel, A. Nähler, A. Peil, V. Pershina, U. Rieth, M. Schädel, B. Schaustem, E. Schimpf, H.-J. Schött, E. Stiel, P. Thörle, N. Trautmann, K. Tsukada, N. Wiehl, G. Wirth
Final Result of the CALLISTO-Experiment: Formation of Sodium Hassate (VIII)

K.P. Zhernosekov, E. Mauerhofer, D.V. Filosofov, N.A. Korolov, A.F. Novgorodov, F. Rösch
Complex Formation of In(III) with D-gluconate and Glycolate in Neutral Aqueous Perchlorate Solutions in Wide Range of pH

Helsinki, Finland: Annual Congress of the EANM, 05.09.-08.09.2004

M. Jennewein, A. Constantinescu, O. Bergner, M. Lewis, D. Zhao, N. Slavine, S. Selioline, S. O'Kelly, S. Maus, S.M. Qaim, E. Tsyganov, P.P. Antich, F. Rösch, R.P. Mason, P.E. Thorpe
Molecular Imaging of the Vascular Targeting Antibody Vatuximab® in Rat Prostate Cancer

C. Landvogt, G. Gründer, I. Vernaleken, H.G. Buchholz, T. Siessmeier, F. Rösch, P. Barthenstein
Beyond The Striatum: The Extrastriatal Binding Characteristics of Clozapine. A PET Study with [¹⁸F]Fallypride in Schizophrenic Patients

Wien, Österreich: 2nd World TRIGA Users Conference, 15.-18.09.2004

K. Eberhardt, N. Trautmann
Operation Experience and Research Activities at the TRIGA Mainz

Berkeley, USA: 3rd Workshop on Speciation, Techniques, and Facilities for Radioactive Materials at Synchrotron Light Sources, 14.-16.09.2004

T. Reich, S. Amayri, J. Drebert
EXAFS Study of Uranium(VI) Sorption on Kaolinite

Bornheim-Walberberg: 12. Arbeitstreffen der AG Radiochemie/Radiopharmazie der DGN, 23.-25.09.2004

M. Jennewein, P. Thorpe, R.P. Mason, A. Hermann, F. Rösch
Neue Strategien zur Antikörpermarkierung mit nca As-Isotopen und erste in vitro/in vivo Evaluierungen

U. Mühlhausen, R. Schirrmacher, M. Piel, B. Kaina, F. Rösch
Synthese, Radioiodierung und Evaluierung von neuen MGMT-Inhibitoren und ihren Glucosekonjugaten

A Coruña, Spanien: Workshop COST D18 „Lanthanide Chemistry for Diagnosis and Therapy”, 23.-25.09.2004

K.P. Zhernosekov, D.V. Filosofov, N.A. Korolev, A.F. Novgorodov, F. Rösch
Non-invasive 1-PAC Determination of Indium and Lanthanides Complex Formation Relevant to Molecular Imaging and Endoradiotherapy

D.V. Filosofov, N.A. Korolev, K. Zhernosekov, A.F. Novgorodov, F. Rösch
Gamma-Gamma Perturbed Angular Correlation Techniques for the Determination of Physical-Chemical Properties of Radiolanthanide Species

Santa Fe, NM, USA: Nuclear Data for Science and Technology Conference - ND2004, 26.09.-01.10. 2004

T. Fukahori, A.V. Ignatyuk, F.G. Kondev, K.-L. Kratz, V. McLane, A.L. Nichols, A. Nouri, O. Schwerer, A.A. Sonzogni, D.F. Winchell
Data Dissemination and International Collaborations

K.-L. Kratz, A.N. Ostrowski and B. Pfeiffer
Nuclear Physics Data Relevant to R-Process Nucleosynthesis

Berlin: 2. Workshop "Nano-Carrier für die medizinische Anwendung in Diagnostik und Therapie", 27.09.2004

F. Rösch
Octreotid als Vektor zum Targeting neuroendokriner Tumore

Ludwigshafen: Seminar der Abteilung GVC der Firma BASF, 29.09.2004

K. Eberhardt*
Aufbau und Nutzung des Forschungsreaktors TRIGA Mainz

Heidelberg: Workshop des Projektverbundes "Migration von Actiniden im System Ton, Huminstoff, Aquifer", 12.-13.10.2004

B. Kuczewski
Neue Ergebnisse zur Wechselwirkung von Plutonium mit Humin- und Fulvinsäure

T. Reich, S. Amayri, J. Drebert
Erste Untersuchungen zur Sorption von Neptunium an Kaolinit

Boston, USA: Eleventh World Congress on Neutron Capture Therapie (ISNTC-11), 11.-15.10.2004

G. Hampel, A. Lizon Aguilar, R. Behrendt, W. Bernnat, K. Eberhardt, D. Nigg, C. Wemple
Dose Calculations with SERA fort he Application of BNCT at the TRIGA Mainz

Argonne, USA: International Conference on Laser Probing „LAP 2004“, 19.-23.10.2004

H. Backe, A. Dretzke, R. Horn, T. Kolb, P. Kunz, W. Lauth, M. Sewtz, P. Schwamb, K. Eberhardt, P. Thörle, N. Trautmann, G. Passler, S. Fritzsche, R.G. Haire
Optical Spectroscopy of the Element Fermium

N. Erdmann, J.V. Kratz, N. Trautmann, J. Bastiaansen, Ü. Lievens, R.E. Silverans, F. Vervaecke, E. Vandeweert
Resonance Ionization Mass Spectrometry of Uranium Sputtered from Uranium Particles

P. Kunz, N. Erdmann, G. Huber, J.V. Kratz, G. Passler, N. Trautmann, K. Wendt
Efficient and Selective Ionization of Plutonium Using Pulsed and cw-Lasers with Three-Step, Three-Color and Three-Step, Two-Color Excitation

I. Strachnow, J. Maul, K. Eberhardt, G. Huber, S. Karpuk, G. Passler, M.C. Roca-Sais, N. Trautmann, K. Wendt
A Laser Desorption/Resonance Enhanced Photoionization TOF-System for the Spatially Resolved Trace Analysis of Elements

K. Wendt, K. Blaum, Ch. Geppert, A. Schmitt, P. Schumann, N. Trautmann, B.A. Bushaw
High Resolution Resonance Ionization for Spectroscopy and Elemental Ultra Trace Analysis: from ^{41}Ca to ^{236}U

K. Wies, N. Erdmann, N. Trautmann, G. Passler, K. Wendt
Spectroscopy of ^{99}Tc with a Ti:Sa Laser System

Argonne, USA: The 9th International Conference and Workshop on Post Ionization Techniques in Surface Analysis “PITS9”, 17.-20.10.2004

K. Wendt, K. Blaum, Ch. Geppert, A. Schmitt, P. Schumann, N. Trautmann, B.A. Bushaw
High Resolution Resonance Ionization for Spectroscopy and Elemental Ultra Trace Analysis: from ^{41}Ca to ^{236}U

Monte-Carlo, Monaco: International Conference on Isotopes in Environmental Studies – Aquatic Forum 2004, 25.-29.10.2004

S. Bürger, R. Buda, H. Geckes, G. Huber, J.V. Kratz, P. Kunz, Ch. Lierse von Gostomski, G. Passler, A. Remmert, N. Trautmann
Isotope Selective Ultratrace Analysis of Plutonium for Environmental Studies by Laser Mass Spectrometry

Leipzig: 5. Leipziger Kolloquium "Radionuklid-anwendung zur Gesunderhaltung des Menschen, 27.10.2004

N. Trautmann*
Wechselwirkung von Plutonium mit Huminstoffen unter geogenen Bedingungen

Chicago, IL, USA: 2004 Fall Meeting of Division of Nuclear Physics, American Physical Society, 27.-30.10.2004

P. Hosmer, R.R.C. Clement, A. Estrade, S.N. Liddick, F. Montes, M. Ouellette, E. Pellegrini, H. Schatz, A. Aprahamian, O. Arndt, K.-L. Kratz, B. Pfeiffer, P.F. Mantica, B.E. Tomlin, A.C. Morton, W.F. Mueller, P. Santi, M. Steiner, A. Stolz, P. Reeder, W.B. Walters, A. Wöhr
First half-life measurements of the doubly-magic r-process nucleus ^{78}Ni

F. Montes, A. Estrade, P. Hosmer, S.N. Liddick, P.F. Mantica, A.C. Morton, W.F. Mueller, M. Ouellette, E. Pellegrini, P. Santi, H. Schatz, A. Stolz, B.E. Tomlin, O. Arndt, K.-L. Kratz, B. Pfeiffer, P. Reeder, W.B. Walters, A. Aprahamian, A. Wöhr
Beta-decay studies close to the N=82 r-process path

St. Louis, USA: 37th Annual Meeting & Scientific Exposition, 29.10.-01.11.2004

T. Odenwald, E. Ritz, F. Rösch, F. Schäfer, C.P. Schmitt
The Calcimimetic R568 Lowers Blood Pressure but not Total Body Sodium Content in Rats

East Lansing, Michigan, USA: Special Seminar on the Occasion of Peter Möller's 60th birthday, 02.11.04

K.-L. Kratz
20 years of research in nuclear/astro physics with Peter Möller

Mainz: PharmaForum 2004, 02.11.2004

F. Rösch
Radioaktive Markierung neuer Wirkstoffe und Arzneimittel zur nichtinvasiven und quantitativen Evaluierung (Tier und Mensch)

Tübingen: Radiopharmazeutisches Seminar, 04.11.2004

M. Piel
Systematische Untersuchungen zur Markierung mit 2-Brom-[^{18}F]fluorethan ([^{18}F]BFE) und 2-[^{18}F]Fluorethyltosylat ([^{18}F]FETos)

Bad Münster am Stein-Ebernburg: GRK-Seminar „Elementspeziation“, 04.-05.11.2004

N.L. Banik
Speciation of Pu(IV) with Humic Acids

R. Buda
Speciation of Pu(III) with Humic Acids

S. Bürger
Speziation der leichten Actiniden mit CE-ICP-MS und CE-RIMS

Erlangen: Pharmazeutisch-Chemisches Kolloquium des Emil Fischer Centrums, Institut für Pharmazie und Lebensmittelchemie, Friedrich-Alexander Universität Erlangen-Nürnberg, 18.11.2004

F. Rösch*
Synthese und ^{18}F -Markierung D2-selektiver Liganden und ihre Anwendung in der Psychiatrischen Forschung

Mainz: 4. Mainzer Symposium über Spurenanalytik, 26.11.2004

S. Amayri, J. Drebert, T. Reich
Structure of Uranium(VI) Surface Complexes on Kaolinite

T. Reich, S. Amayri, J. Drebert, S. Boulyga
Speziation von Uran bei der Sorption an Kaolinit mittels EXAFS-Spektroskopie

Dresden: ROBL-Radiochemie Workshop, Institut für Radiochemie, Forschungszentrum Rosendorf, 13.12.2004

T. Reich, S. Amayri, J. Drebert, A. Jermolajev, Ta. Reich
Ergebnisse einer EXAFS-Machbarkeitsstudie zur Sorption von Neptunium(V) an Kaolinit

R3B-Collaboration:

T. Aumann¹, Ch.-O. Bacri², J. Benlliure³, M. Bentley⁴, M. Böhmer⁵, M.J.G. Borge⁶, W. Catford⁷, M. Chartier⁸, L.V. Chulkov^{9,1}, D. Cortina-Gil³, D. Cullen¹⁰, A. Dael¹¹, J.-E. Ducret¹¹, H. Emling¹, L.M. Fraile⁶, S. Freeman¹⁰, M. Freer¹², J. Friesen⁵, H.O.U. Fynbo¹³, B. Gastineau¹¹, H. Geissel^{1,14}, B. Gelletly⁷, R. Gernhäuser⁵, J. Hoffmann¹, B. Jonson¹⁵, M. Kajetanowicz¹⁶, O. Kiselev¹⁷, K. Korcyl¹⁶, A. Krasznahorkay¹⁸, J.V. Kratz¹⁷, R. Krücken⁵, R. Kulessa¹⁶, N. Kurz¹, R.C. Lemon¹⁹, W. Mittig²⁰, G. Münzenberg^{1,21}, T. Nilsson²², G. Nyman¹⁵, P. Regan⁷, P. Reiter²³, K. Riisager¹³, P. Roussel-Chomaz²⁰, K.-H. Schmidt¹, G. Schrieder²², B.M. Sherrill²⁴, H. Simon^{1,22}, J. Simpson⁷, K. Süßer¹, O. Tengblad⁶, V. Vysotsky¹¹, A. Wagner²⁵, P. Walker⁷, D. Warner¹⁹, H. Weick¹, and M. Winkler^{1,14}

¹Gesellschaft für Schwerionenforschung (GSI), D-64291 Darmstadt

²IN2P3/IPN Orsay, F-91406 Orsay, France

³Universidad de Santiago de Compostela, 15706, Santiago de Compostela, Spain

⁴University of Keele, Staffordshire ST5 5BG, UK

⁵Physik Department, TU München, D-85747 Garching, München

⁶Intituto de Estructura de la Materia, CSIC, E-28006 Madrid, Spain

⁷Department of Physics, University of Surrey, Guildford, GU2 5XH, UK

⁸Department of Physics, University of Liverpool, Liverpool L69 7ZE, UK

⁹RRC Kurchatov Institute, RU-123182 Moscow, Russia

¹⁰University of Manchester, Manchester, M13 9 PL, UK

¹¹CEA, Saclay, F-91191 Gif-sur Yvette, France

¹²University of Birmingham, Edgbaston, Birmingham, B15 2TT, UK

¹³Inst. Pf Üphys. And Astronomy, Univ. of Aarhus, DK-8000 Aarhus, Denmark

¹⁴II. Physikalisches Institut, Universität Giessen, D-35392 Giessen

¹⁵Chalmers Tekniska Högskola, SE-41296 Göteborg, Sweden

¹⁶Fizyki, Uniwersytet Jagellonski, PL-30059 Krakow, Poland

¹⁷Institut für Kernchemie, Johannes Gutenberg Universität, D-55099 Mainz

¹⁸Institute of Nuclear Research (ATOMKI), H-4001 Debrecen, Hungary

¹⁹CLRC Daresbury, Warrington, Cheshire, WA4 4AD, UK

²⁰GANIL, BP 5027, 14021 Caen Cedex 5, France

²¹Institut für Physik, Johannes Gutenberg-Universität Mainz, D-55099 Mainz

²²Institut für Kernphysik, TU Darmstadt, D-64289 Darmstadt

²³Institut für Kernphysik, Universität zu Köln, D-50937 Köln

²⁴NSCL, Michigan State University, East Lansing, Michigan 48824, USA

²⁵Forschungszentrum Rossendorf, D-01314 Dresden

S221-Collaboration:

P. Adrich^{1,2}, T. Aumann¹, K. Boretzky³, D. Cortina-Gil⁴, U. Datta Pramanik¹, TH.W. Elze⁵, H. Emling¹, M. Fallot¹, H. Geissel¹, M. Hellström¹, K.L. Jones¹, A. Klimkiewicz^{1,2}, J.V. Kratz³, R. Kulessa², Y. Leifels¹, C. Nociforo³, R. Palit⁵, H. Simon⁶, G. Surowka², K. Süßer¹, and W. Walus²

¹Gesellschaft für Schwerionenforschung (GSI), D-64291 Darmstadt

²Instytut Fizyki, Uniwersytet Jagielloński, PL-30-059 Kraków, Poland

³Institut für Kernchemie, Johannes Gutenberg-Universität, D-55099 Mainz

⁴Universidad de Santiago de Compostela, 15706, Santiago de Compostela, Spain

⁵IKF, Johann Wolfgang Goethe Universität, D-60486 Frankfurt

⁶Institut für Kernphysik, Technische Universität, D-64289 Darmstadt

Vorträge
im Seminar für Kern- und Radiochemie und
im Seminar über aktuelle Themen aus Kosmochemie und Astrophysik*

*Gemeinsames Seminar mit
U. Ott, Max-Planck-Institut für Chemie (Otto-Hahn-Institut)
und G. Münzenberg, Institut für Physik, Mainz

- | | |
|---|--|
| D. Ackermann (GSI Darmstadt)
<i>Elementsynthesis in the Lab - Production and Structure of Superheavy Nuclei</i> | R. Gellert (MPI Mainz)
<i>APXS - Aufbau, Kalibrierung und Datenreduktion</i> |
| T. Aumann (GSI, Darmstadt)
<i>Untersuchungen von exotischen Kernen mit hochenergetischen Sekundärstrahlen</i> | G. Getahun (Univ. Mainz)
<i>Migration, Komplexierung sowie Sorptions mechanismen von Lanthaniden</i> |
| T. Bastian (Nuklarchemie, Köln)
<i>Kosmogene Nuklide in Marsmeteoriten: Analyse und Modellierung</i> | W. Hammer (Univ. Stuttgart)
<i>Schlüsselreaktionen in der Sternentwicklung und Nukleosynthese</i> |
| C. Beck (Univ. Mainz)
<i>Syntese von Tyr³-Octreotat-kunjugierten Corclustern für die Bor-Neutronen-Eifang-Therapie</i> | D. Hezel (Universität Köln)
<i>Die Bildung von SiO₂ im frühen Sonnensystem</i> |
| F. Brohl (Univ. Mainz)
<i>Markierung von DOTA bzw. DTPA-Octreotid mit den radioaktiven Nukliden 111-In und 172-Lu; (mit anschließend Internalisierungsexperimenten an exokrinen Tumorzellen)</i> | M. Hjorth-Jensen (University of Oslo, CERN-ISOLDE)
<i>Shell model approaches and effective interactions for weakly bound systems</i> |
| L. De Smet, (Universität Gent)
<i>(n,p)- and (n,a)-reactions on ²⁶Al and ³⁶Cl an their astrophysical relevance</i> | J. Hopp (Universität Heidelberg)
<i>Edelgas-Isotope als Indikatoren für Wechselwirkungen und Prozesse im Erdmantel</i> |
| Yu-Shin Ding (Brookhaven National Laboratory, USA)
<i>PET Imaging of Neurochemistry in Living Systems</i> | P. Hosmer u. F. Montes (MSU)
<i>Beta-decay, Neutrons, and NERO at the NSCL, MSU</i> |
| N. Edelstein (Lawrence Berkeley National Laboratory)
<i>Octahedral Complexes of f-Elements: Is the Metal Ion – Ligand Bond Length Shorter in the Excited d-State?</i> | A. Jacobs (MPI für Neurologische Forschung, Köln)
<i>Gezeilte Entwicklung von Vektoren und Radiotracern für die Molekulare Bildgebung</i> |
| M. Fehr (ETH Zürich)
<i>Tellurium isotopes and their applications in cosmochemistry and geochemistry</i> | M. Jung (Universität Mainz)
<i>Edelgasalter des Eukriten DAG 380</i> |
| D. Frekers (Universität Münster)
<i>Facets for the (d,²He) charge exchange reaction: from few-body physics to astrophysics to double beta-decay</i> | B. Kaina (Universität Mainz)
<i>Alkytransferase und Alkytransferase-Inhibitoren in Drug- Resistenz und Tumorthерапie</i> |
| J. Fritz (Humboldt-Universität Berlin)
<i>Aufbruch vom Mars: Stosswellenmetamorphose der Marsmeteorite</i> | G. Korschinek (TU München)
<i>Supernovaproduziertes ⁶⁰Fe in terrestrischen Proben: Nachweis und mögliche Korrelationen</i> |
| | G. Kurat (Naturhistorisches Museum, Wien)
<i>D'Orbigny: ein Achondrit erinnert sich an Unerwartetes</i> |
| | W. Kutschera (Universität Wien)
<i>Das Problem der exakten Datierung des minoischen Vulkanausbruchs auf Santorini</i> |

- A. Mengoni (n_TOF, CERN)
Nuclear Astrophysics with Neutrons at CERN n_TOF
- M. Merroun (Forschungszentrum Rossendorf)
Interaction of uranium with bacterial strains isolated from uranium contaminated environments: microscopic and spectroscopic
- G.-J. Meyer (Medizinische Hochschule Hannover)
Gewinnung von Ga-68 zur Markierung von Peptiden im nanomolaren Massstab aus Ge-68/Ga-68 Generatoren
- S. Mostefaoui (MPI Chemie, Mainz)
In-situ evidence for live ^{60}Fe in the early solar system
- T. Nilsson (CERN-ISOLDE, Genf)
Post-accelerated radioactive beams at CERN_ISOLDE first physics output and future perspectives
- W. Nörthershäuser (GSI, Darmstadt)
Elektronischer Lauschangriff auf Kerne - Laserspektroskopische Bestimmung von Ladungsradien an der Neutronen-Dripline
- E. Pernicka (Archäometrie, Bergakademie Freiberg)
Untersuchungen der Himmelsscheibe von Nebra
- T. Posch (Universität Wien)
Circumstellar oxide dust grains: An IR-spectroscopic approach
- C. Scheidenberger (GSI, Darmstadt)
Experimente zu Grundzustand- und Zerfallseigenschaften hochgeladener Ionen mit gespeicherten exotischen Nukliden
- A. Schrattenholz (ProteoSys AG, Mainz)
Proteomics: How to control highly dynamic patterns of millions of molecules and interpret changes correctly?
- S. Schwenzer (MPI, Mainz)
Marsmeteore: Edelgase in Mineralseparaten, Gesamtgesteinen und terrestrischen Karbonaten
- E. Strub (Hahn-Meitner-Institut, Berlin)
Elastic Recoil Detection Analysis (ERDA) am Ionenstrahlabor des Hahn-Meitner-Instituts- mit der Schwerionenkanone auf der Jagd nach neuen Materialien
- K. Süümmerer (GSI, Darmstadt)
High-energy Coulomb dissociation as a tool for nuclear astrophysics
- S. Szidat (Universität Bern)
Ermittlung von Emissionsquellen kohlenstoffhaltiger Partikel in Aerosolen mittels C-14
- C. Walther (Forschungszentrum Karlsruhe)
Untersuchungen zur Kolloidbildung tetravalenter Actiniden mit laserspektroskopischen Methoden (Habilitationsvortrag)
- B. Wierczinski (Inst. f. Radiochemie, TU München)
Bestimmung der kinetischen Stabilität von Metallkomplexen mit FISRE (Free-Ion Selektive Radiotracer Extraction): Beispiele für Anwendungen in Radiopharmazie und Actinidenchemie
- A. Wittig (Strahlenklinik Essen)
Bor-Neutronen-Einfang-Therapie – Ein langer Weg vom Reaktor zum Patienten
- A. Wöhr (University of Notre Dame, USA)
 Q_β Messung des N-Z rp-Prozess "waiting-point" Kernes ^{68}Se und seine astrophysikalische Bedeutung
- J. Zipfel (MPI Mainz)
APXS - Ergebnisse von Gusev-Krater und Meridiani Planum auf Mars

Beiträge der Dozenten des Instituts zu den Lehrveranstaltungen des Fachbereichs Chemie und Pharmazie (SS 04 und WS 04/05)
sowie zur Weiterbildung

Vorlesungen, Seminare, Kurse und Praktika in Kernchemie:

Einführung in die Kernchemie (mit Übungen)	J.V. Kratz
Kernreaktionen	J.V. Kratz
Chemie und Kernchemie der schwersten Elemente	J.V. Kratz
Radiopharmazeutische Chemie	F. Rösch
Einführung in die Astrophysik	K.-L. Kratz
(Astro-) Physikalische Anwendungen radioaktiver Ionenstrahlen	K.-L. Kratz A.N. Ostrowski
Radioaktive Ionenstrahlen in (astro-) physikalischer Anwendung	K.-L. Kratz
Bildung der schweren Elemente im Universum	K.-L. Kratz
Einführung in die Kosmochemie	U. Ott
Geo- und Kosmochemie der Edelgase	U. Ott
Anwendung der Neutronenaktivierung in den Geowissenschaften	G. Schmidt
Überblick über die Lagerstätten I: Erze	G. Schmidt
Übungen zur Petrologie der Magmatite	G. Schmidt
Übungen Phasenpetrologie	G. Schmidt
Anwendung von Lasern in der Spurenanalytik	C. Walther
Modul Kernchemie I	J.V. Kratz K.-L. Kratz T. Reich F. Rösch N. Trautmann K. Eberhardt
Modul Kernchemie II	J.V. Kratz K.-L. Kratz T. Reich F. Rösch
Modul Radiopharmazeutische Chemie I	F. Rösch G. Dannhardt M. Piel
Modul Radiopharmazeutische Chemie II	F. Rösch M. Piel

Seminar über laufende Arbeiten im Institut für Kernchemie	J.V. Kratz K.-L. Kratz T. Reich F. Rösch
Seminar für Kern- und Radiochemie	J.V. Kratz K.-L. Kratz T. Reich F. Rösch
Seminar über aktuelle Themen aus der Kosmochemie und Astrophysik	K.-L. Kratz G. Münzenberg U. Ott
Kernchemisches Praktikum I (25 Teilnehmer)	J.V. Kratz K.-L. Kratz T. Reich F. Rösch
Kernchemisches Praktikum II (17 Teilnehmer)	J.V. Kratz K.-L. Kratz T. Reich F. Rösch
Seminar des IAK PET-Forschung	R. Schirrmacher M. Jansen M. Raabe
Grundkurs im Strahlenschutz zum Erwerb der Fachkunde nach § 29 Strahlenschutzverordnung (16 Teilnehmer)	H. Keller J.V. Kratz F. Rösch N. Trautmann sowie weitere Referenten
Kurs Fachkunde im Strahlenschutz für Lehramtskandidaten der Chemie und Physik (unter Mitwirkung des Ministeriums für Umwelt und Forsten, Mainz) (54 Teilnehmer)	K. Eberhardt H. Keller G. Roos S. Schön E.R. Schmidt N. Trautmann
Reaktorpraktikum (16 Teilnehmer)	N. Trautmann K. Eberhardt

Mitwirkung an Diplomprüfungen, in denen Kernchemie als viertes Fach gewählt wurde:
16 Prüfungen

Mitwirkung an Promotionen, in denen Kernchemie als Haupt- oder Nebenfach gewählt wurde:
11 Prüfungen

Lehrveranstaltungen in Chemie:

Vorlesung Chemie für Physiker, Geologen und Mineralogen I T. Reich
(mit Übungen)

Vorlesung Chemie für Physiker, Geologen und Mineralogen II T. Reich
(mit Übungen)

Allgemeines anorganisch-chemisches Praktikum für Geologen und Mineralogen (13 Teilnehmer)

T. Reich
U. Mühlhausen
sowie weitere Assistenten

Allgemeines anorganisch-chemisches Praktikum für Physiker und Meteorologen (7 Teilnehmer)

K.-L. Kratz
U. Mühlhausen
sowie weitere Assistenten

Vordiplom in Physik (Fach: Chemie):

46 Prüfungen

Vordiplom in Geologie-Paläontologie (Fach: Chemie):

3 Prüfungen

Vordiplom in Mineralogie (Fach: Chemie):